

Dissertation
submitted to the
Combined Faculties of the Natural Sciences and Mathematics
of the Ruperto-Carola-University of Heidelberg. Germany
for the degree of
Doctor of Natural Sciences

Put forward by

Stefan, Maier

born in: Rheinfelden

Oral examination: December 05, 2011

Effect of electron-phonon interaction
in nanostructures
and ultracold quantum gases

Referees:

Prof. Andreas Komnik
Prof. Manfred Salmhofer

Elektron-Phonon Wechselwirkung in Nanostrukturen und ultrakalten Quantengasen:

Die vorliegende Arbeit untersucht den Effekt der Elektron-Phonon Wechselwirkung in zwei Klassen von mesoskopischen Systemen. Die erste Klasse umfasst molekulare Quantenpunkte. Sie gelten als gute Kandidaten für zukünftige Transistoren auf der Nanoskala. Mittels der Ladungstransferstatistik (*full counting statistics*, FCS) wird der elektrische Transport für verschiedene Modelle eines molekularen Transistors charakterisiert. Das Hauptaugenmerk dieser Arbeit liegt dabei einerseits auf Systemen mit starker Elektron-Phonon Wechselwirkung und andererseits auf Modellen mit stark korrelierten Zuleitungen in Form von Tomonaga-Luttinger Flüssigkeiten. Basierend auf einem erweiterten Keldysh Formalismus werden verschiedene perturbative und nichtperturbative Methoden zur Berechnung der FCS erarbeitet. Die Analogie zu Mehrniveausystemen wird anhand eines Doppel-Quantenpunkt Modells diskutiert. Die zweite Klasse umfasst das BEC-Polaron Problem. Hierbei wird die Analogie von Verunreinigungen in Bose-Einstein Kondensaten mit Elektronen in einem Kristallgitter ausgenutzt. Mittels Pfadintegral Monte Carlo Simulationen, Variationsrechnung und perturbativen Methoden wird das effektive Fröhlich Modell untersucht. Die formale Ähnlichkeit zur Cherenkov-Strahlung wird erläutert.

Effect of electron-phonon interaction in nanostructures and ultracold quantum gases:

The subject of this thesis is the effect of electron-phonon interaction in two classes of mesoscopic systems. The first class includes molecular quantum dots. They are believed to be good candidates for future realizations of transistors on the nanoscale. Using the concept of full counting statistics (FCS), the charge transfer for several models is characterized. On the one hand, the main focus of this work lies on systems with rather strong electron-phonon interactions, on the other hand, it lies on models with strongly correlated electrodes described by Tomonaga-Luttinger liquids. Based on a generalized Keldysh formalism, perturbative and non-perturbative methods have been provided to calculate the FCS. Using double quantum dot models, the analogy with multi-level systems is discussed. The second class contains the BEC polaron problem. The BEC polaron is based on the analogy of immersed quantum gases with electrons in crystal lattices. Using imaginary-time path integral Monte Carlo methods, variational principles and perturbation theory, the effective Fröhlich model is investigated. The similarity to the emission of Cherenkov radiation is discussed.

Contents

| | |
|--|-----------|
| 1. Introduction | 3 |
| 1.0.1. Electron-phonon interaction in quantum impurity systems | 4 |
| 1.0.2. The BEC polaron | 4 |
| 1.0.3. Contents of this thesis | 5 |
| 2. Transport characteristics of quantum impurity models coupled to bosonic degrees of freedom | 7 |
| 2.1. Quantum transport theory and full counting statistics | 7 |
| 2.1.1. Field theoretical implementation of the full counting statistics | 8 |
| 2.1.2. The FCS of the resonant level model | 10 |
| 2.2. Strongly coupled Holstein polaron | 15 |
| 2.2.1. The model and the Lang-Firsov transformation | 16 |
| 2.2.2. Perturbative approach | 20 |
| 2.2.3. Resummation schemes for the Holstein model | 22 |
| 2.2.4. Results and discussion | 27 |
| 2.3. Effects of e-ph interaction in the IRLM | 28 |
| 2.3.1. The model and its Toulouse point | 30 |
| 2.3.2. Full counting statistics in absence of e-ph coupling | 33 |
| 2.3.3. Keldysh functions of the impurity site | 35 |
| 2.3.4. The resonant case | 37 |
| 2.3.5. The off-resonant case | 42 |
| 2.3.6. Results and discussion | 47 |
| 2.4. Double quantum dot interferometer | 47 |
| 2.4.1. Double quantum dot spin valve | 50 |
| 2.4.2. Spin-valve for finite temperature | 51 |
| 2.4.3. Effect of electron-electron interactions | 52 |
| 2.4.4. Results and discussion | 55 |
| 3. Impurities in ultracold quantum gases: the BEC polaron problem | 57 |
| 3.1. The BEC polaron problem | 57 |
| 3.2. Polaron mass, radius and Bragg spectroscopy | 62 |
| 3.3. BEC polaron: perturbative approach | 63 |
| 3.4. Imaginary time path integral Monte Carlo simulation | 67 |
| 3.4.1. Monte Carlo integration, Markov processes and importance sampling | 68 |
| 3.4.2. Error analysis and correlations | 70 |
| 3.4.3. Analytical continuation and Padé approximants | 71 |
| 3.4.4. QMC simulation for the BEC polaron | 72 |
| 3.4.5. Test of the Monte Carlo simulation | 74 |
| 3.4.6. Results and discussion for interacting systems | 76 |
| 3.5. Variational principle for the BEC polaron | 77 |

| | |
|--|------------|
| 3.6. Cherenkov radiation in ultracold binary mixtures | 79 |
| 3.6.1. Cherenkov radiation and critical velocity | 80 |
| 3.6.2. Experimental fingerprint of Cherenkov radiation | 83 |
| 4. Conclusions and outlook | 85 |
| A. Non-equilibrium formalism for quantum impurity systems | 91 |
| A.1. Non-equilibrium Green's functions: The Keldysh-Schwinger formalism | 91 |
| A.2. Important Keldysh functions | 95 |
| A.2.1. Keldysh function of the electronic leads | 95 |
| A.2.2. Keldysh function for the quantum dot | 96 |
| A.2.3. Keldysh function of the bosonic degree of freedom | 97 |
| A.3. Functional integral formalism for the resonant level model | 97 |
| A.4. Polarization loop for the TLL | 100 |
| A.5. Functional integral treatment of the double quantum dot | 101 |
| B. BEC polaron: partition functions and Green's functions | 107 |
| B.1. Matsubara Green's functions for a harmonically confined particle | 107 |
| B.2. Variational principle: partition function and Matsubara Green's functions | 108 |
| Bibliography | 109 |

1. Introduction

Wer kann was Dummes,
wer was Kluges denken,
Das nicht die Vorwelt schon gedacht?

(J.W. von Goethe, Faust II)

Historically, solid state theory aimed at a universal description of matter in its condensed form. Quantum theory together with quantum statistical physics proved to provide the common framework to address the most basic properties of solids, for example their mechanical, electric, magnetic and thermal properties. During the last couples of decades, based on these foundations, theorists continuously developed the very fruitful field of quantum many-particle physics. Without doubt, one of the most important accomplishments is the notion of quantum field theory. Its rapid development and broad acceptance certainly was supported by the close relation to a similar development in high energy physics.

Often, solids are described by spatially periodic structures, a.k.a. lattices, which are assumed to be formed by atoms. The electrons belonging to these atoms can play several roles. For example, there are electrons forming directional bonds (σ -bonds) with each other. These electrons strongly participate in forming the lattice and are often strongly localized. Other electrons might only be loosely bound to their atom. These electrons can move quasi-freely through the solid and experience the lattice as a periodic potential. Bloch identified the wave-like nature of these electrons and introduced the concept of band structure. Assuming a static background, however, only leads to a partial description of a real solid. Dynamical distortions of the lattice, i.e. lattice vibrations, account for many important properties like the propagation of sound or the formation of Cooper pairs in a conventional superconductor. It is one of the biggest advantages of quantum many-body theory to provide the concept of phonons, i.e. quantized lattice vibrations. Basically, phonons are described by bosonic quasiparticles interacting with electrons or other phonons.

These days, there are still plenty of aspects involving electron-phonon interaction not fully understood by theorists and experimentalists. It is highly recommended to look for systems where the effect of electron-phonon interaction can be observed in absence of other sources of distortion. Very interesting are mesoscopic systems, like molecular transistors: here, atoms, molecules or larger clusters are coupled to electrodes. Due to their simple structure, their vibrational degrees of freedom are much easier to describe than phonons in the bulk of a solid. This defines a very controlled system to observe the effects of electron-phonon coupling to the transport of electrons. It is a great advantage that well-established manufacturing techniques like lithography and molecular beam epitaxy can be used to implement these kinds of systems on-chip.

In contrast, ultracold quantum gases belong to the cleanest and best manageable quantum many-body systems. The control of the scattering properties of the atoms via Feshbach resonances offers the opportunity to continuously drive a system from weak to very strong particle-particle interaction. Interestingly, one is also able to tune a system from repulsive to attractive interactions. This allows

for the observation of the famous BEC-BCS crossover. In this sense, experiments using cold quantum gases are superior to most experiments in solids. Mixtures of two or more species of atoms leads to interesting new features. One of them is the formation of the BEC polaron in a two-component mixture where one species is a minority, i.e. represents impurities. It turns out that this system can be described similar to the polaron system in solids, i.e. by a Fröhlich Hamiltonian. Here, the advantage is again the control over the coupling constants, which allows for arbitrary tuning of the electron-phonon interaction strength.

1.0.1. Electron-phonon interaction in quantum impurity systems

Carbon nanotubes are ideal candidates to build nanoscale devices. For example, a single carbon nanotube is a simple and important realization of a quantum wire, i.e. a one-dimensional electronic device. One-dimensional systems per se are very interesting: electron-electron interaction leads to the formation of a highly correlated system, the so-called Tomonaga-Luttinger liquid. Impurities in carbon nanotubes can be used to build even smaller systems: 0-dimensional quantum dots. A quantum dot embedded in a nanotube is a good candidate for a molecular transistor with very distinct vibrational modes. The basic electronic properties of molecular transistors can be captured by quantum impurity models with internal vibrational degrees of freedom.

In experiments, the easiest way to obtain information about the nature of charge transport in mesoscopic devices is measuring the electric conductance and current. However, these quantities provide by no means a complete characterization. For example, the current-current correlation, i.e. the noise, in general reveals information which is not present in the current or the conductance: using the famous Schottky formula $S = qI$ allows for a determination of the quasiparticle charge q of the participating particles by measuring the current I and the noise S .

Therefore, it is very useful to have a method at hand to address higher order current-current (charge-charge) correlation functions: the full counting statistics. By definition, the full counting statistics is the probability distribution function to transfer a certain amount of charge during a fixed measurement time.

1.0.2. The BEC polaron

Mixtures of ultracold quantum gases are excellent candidates for immersed quantum systems. The high degree of control of its scattering properties allows an investigation of many interesting effects: for example, mixing/de-mixing phenomena can be investigated by tuning the inter-species scattering from the attractive regime to the repulsive one.

A two-component mixtures where the concentration of one species is small compared to the other one can be treated as a quantum impurity system: the majority species provides a background BEC in which the impurities are embedded. It turns out that the inter-species scattering can be described by the coupling of the impurities to the Bogoliubov modes of the background BEC. The effective model for this kind of coupling is the Fröhlich Hamiltonian. Therefore, impurities in BEC's can be thought of as an analog to electrons in a crystal lattice interacting with phonons. This analogy allows us to simulate the effects of electron-phonon interactions in a very clean and very controlled setup.

It is well known from solid state physics, that systems with strong electron-phonon interaction tend to form polarons as quasiparticles. However, the transition from weak to strong coupling itself is hardly accessible in solid state experiments. It is believed that experiments with ultracold atoms can bridge this gap.

1.0.3. Contents of this thesis

As previously mentioned, this work consists of two parts: first, the effect of electron-phonon coupling in quantum impurity systems and, secondly, the BEC polaron problem. This is reflected in the structure of the presentation.

In chapter 2 we investigate the effect of electron-phonon interaction in quantum dots. First, we give a short introduction into the concepts of quantum transport theory in mesoscopic systems. Especially, the very useful full counting statistics is formulated in a quantum field theoretical framework. Secondly, we introduce the Anderson-Holstein model. Based on the Lang-Firsov (polaron) transformation, we develop approximation schemes to handle the Anderson-Holstein model in the strong coupling regime. We provide expressions for the various approximation schemes, discuss the physical implications and compare the results with numerical data from the literature. Thirdly, we introduce a quantum dot capacitively and tunneling coupled to correlated electrodes, i.e. Tomonaga-Luttinger liquids. Using bosonization techniques and the notion of the Toulouse point, this model can be mapped to the Majorana resonant level model which describes the propagation of collective excitations, i.e. plasmons. We equip this system with an additional bosonic degree of freedom to study the effect of phonons on transport of collective excitations. An important aspect occurring in systems including electron-phonon effects can be understood in multi-level structures. For a better understanding, we investigate transport properties in double quantum dot structures in the last section of this chapter. The existence of sharp anti-resonances in these setups allows for interesting applications. We propose a setup based on double quantum dots in parallel arrangement to generate highly spin-polarized currents. We show that our setup is robust against external influences like finite temperature and electron-electron interactions.

In chapter 3 we study the BEC polaron. In the first paragraph, we give a microscopic model of the two-component mixture and map it to the Fröhlich polaron. Secondly, we discuss several observables like the polaron radius and the density-density correlation function (together with a very brief introduction to Bragg spectroscopy). Thirdly, we provide a perturbative treatment of the BEC polaron. In the fourth section, we introduce an imaginary time path integral Monte Carlo simulation technique to give a numerically exact solution to the BEC polaron (described by the Fröhlich model). In the fifth section, the Jensen-Feynman variational principle is applied. In the sixth section, we adapt the concept of Cherenkov radiation to the BEC polaron problem.

We close this thesis by a discussion and an outlook. The results are published in [Dahlhaus et al. \[2010\]](#), [Maier and Komnik \[2010\]](#), [Maier et al. \[2011\]](#). The article [Maier and Komnik](#) is in preparation.

2. Transport characteristics of quantum impurity models coupled to bosonic degrees of freedom

The noise is the signal

(Rolf Landauer)

This chapter is devoted to quantum transport theory in quantum impurity systems. The main focus is the effect of electron-phonon interaction on the charge transfer statistics. In the first section, we introduce the concept of the full counting statistics (FCS). The subsequent section deals with the local Holstein model in the strong coupling regime. The third section focuses on a weakly coupled phonon in the Majorana resonant level model. The fourth section introduces double quantum dot systems to illustrate the phenomenon of interference in multi-level systems. The chapter ends with a discussion. Appendix A gives a short introduction to the non-equilibrium Green's functions formalism employed here and provides all necessary details on various important Keldysh functions for quantum impurity systems.

2.1. Quantum transport theory and full counting statistics

The understanding of quantum transport processes is highly important from theoretical, experimental and practical aspects. Tunneling experiments like scanning tunneling microscopy can reveal a lot of information about a sample which is hardly accessible by other methods. For example, the local density of states of a high-Tc superconductor and hence the spatially resolved gap function can be probed (Pan et al. [2001]). However, we are more interested in transport in nanostructures, e.g. transport through molecular quantum dots (Park et al. [2000, 2002], Smit et al. [2002], Yu and Natelson [2004], Yu et al. [2004]). The model those systems have in common is a mesoscopic system with internal degrees of freedom which is coupled to electronic leads (see fig.2.1). Applying a source-drain voltage V_{SD} across the contacts induces a current flowing through the molecule. Via an attached gate electrode, the electronic level structure of the quantum dot can be varied. The question arising is how the transport processes can be characterized.

In state-of-the-art experiments in mesoscopic physics, transport quantities like the linear conductance, differential conductance or the current are easily accessible. More challenging are current fluctuations. But they can reveal information about the nature of the participating quasiparticles which are not accessible by other methods. This, for example, is expressed by the famous Schottky formula, $S = qI$, which connects the current I and the quasiparticle charge q to the current noise S . Using this relation, de-Picciotto and colleagues (de Picciotto et al. [1997]) find strong evidence

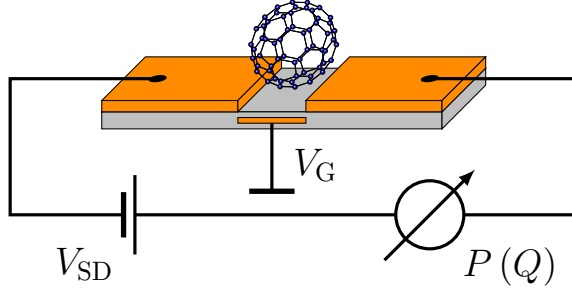


Figure 2.1.: Molecular quantum dot: A molecular quantum dot (here a C_{60} molecule) is placed between two metallic leads. An applied source-drain voltage V_{SD} across the contacts induces transport processes through the quantum dot. The molecular island can be probed via measuring the transport characteristics, i.e the full counting statistics $P(Q)$. An attached gate electrode allows to alter the electronic level structure of the quantum dot.

for charge $e/5$ quasiparticles and Saminadayar and colleagues ([Saminadayar et al. \[1997\]](#)) for charge $e/3$ quasiparticles in fractional quantum Hall samples.

Differential conductance, current and current noise have something in common: they all can be derived from the full counting statistics. Before we proceed by introducing the concept of the full counting statistics, a remark about the system of units we employ is in order. Unless stated otherwise, we use units with $\hbar = e = k_B = 1$ throughout this chapter.

2.1.1. Field theoretical implementation of the full counting statistics

Charge transfer can best be described in a probabilistic framework: the charge transfer statistics $P(Q)$ is defined as the probability to transport an amount of charge Q during a measuring time \mathcal{T} . From a theoretical point of view, the Fourier transformation of $P(Q)$,

$$\chi(\lambda) = \sum_Q e^{i\lambda Q} P(Q) \quad (2.1)$$

is much more suitable. The logarithm of this quantity, the cumulant generating function (CGF), produces the cumulants (irreducible moments) of the probability distribution,

$$\langle\langle Q^n \rangle\rangle = i^n \frac{\partial^n}{\partial \lambda^n} \Big|_{\lambda=0} \ln \chi(\lambda). \quad (2.2)$$

The first cumulant is directly related to the current, $\langle\langle Q \rangle\rangle = \sum_Q Q P(Q) = \mathcal{T}I$ and the second cumulant to the noise, $\langle\langle Q^2 \rangle\rangle = \mathcal{T}S$ where $S = \frac{1}{2} \int dt \langle\langle I(t) I(0) + I(0) I(t) \rangle\rangle$. In [fig. 2.2](#), the graphical meaning of the cumulants is depicted.

The foundation of the full counting statistics for fermionic systems have been laid by Levitov and Lesovik in the milestone article ([Levitov and Lesovik \[1993\]](#)). Later on, there was a substantial extension and a more detailed discussion by Levitov, Lesovik and Lee ([Levitov et al. \[1996\]](#)). Nazarov ([Nazarov \[1999\]](#)) adapted the full counting statistics to the Keldysh-Schwinger formalism. These early approaches have one thing in common: they use a fictitious measurement device to define the

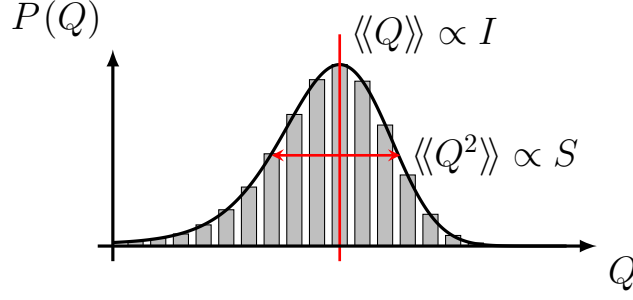


Figure 2.2.: Charge transfer statistics $P(Q)$.

FCS. In the work by [Nazarov and Kindermann \[2003\]](#), the authors succeeded in reformulating the problem in a more formal way without referring to a fictitious detector.

In the following, we give a field theoretical description of the charge transfer statistics. We begin by writing down the Hamiltonian of the model,

$$H = H_{\text{leads}}[\psi_\alpha] + H_{\text{M}}[d_l, \phi_\kappa] + H_{\text{T}} + W_{\text{M}}. \quad (2.3)$$

H_{leads} is the lead contribution which may include interactions/correlations and is described by field operators ψ_α . α is a multi-index which, for example, labels lead number, spin species or channel. The mesoscopic island is defined by a Hamiltonian H_{M} consisting of a set of discrete levels with associated creation and annihilation operators d_l^\dagger , d_l and continua (for example a heat bath) described by field operators ϕ_κ . There is a redundancy in this description: the components ϕ_κ can also be thought of as a contribution to H_{leads} , too. But from an experimental point of view, this kind of separation is meaningful. The tunneling Hamiltonian H_{T} can be split up in two contributions,

$$H_{\text{T}} = T_+ + T_- \quad (2.4)$$

where

$$T_- = \sum_{\alpha, l} \gamma_{\alpha l} d_l^\dagger \psi_\alpha(x_\alpha) + \sum_{\alpha, \kappa} \gamma'_{\alpha \kappa} \phi_\kappa^\dagger(y_\kappa) \psi_\alpha(x'_\alpha) \quad (2.5)$$

$$T_+ = \sum_{\alpha, l} \gamma_{\alpha l}^* \psi_\alpha^\dagger(x_\alpha) d_l + \sum_{\alpha, \kappa} \gamma'^*_{\alpha \kappa} \psi_\alpha^\dagger(x'_\alpha) \phi_\kappa(y_\kappa). \quad (2.6)$$

T_- populates the mesoscopic island and T_+ depopulates it. The parameters x_α , x'_α and y_κ are the coordinates where the tunneling takes place. W_{M} describes capacitive interactions between leads and the island. Interactions including particle exchange are not allowed in this contribution. In our case, we are always dealing with a system initially (in the distant past) in a state

$$\rho(-\infty) = \bigotimes_{\alpha} \rho_{\alpha} \bigotimes_{\kappa} \rho_{\text{M}, \kappa} \bigotimes_{l} \rho_l \quad (2.7)$$

where the densities of the lead operators are given by grand canonical ensembles with chemical potentials μ_α and $\mu_{\text{M}, \kappa}$. We define the charge operator Q_α by

$$Q_\alpha = \int dx \psi_\alpha^\dagger(x) \psi_\alpha(x). \quad (2.8)$$

Due to particle conservation, one can easily verify the commutation relations,

$$[Q_\alpha, H_{\text{leads}}] = [Q_\alpha, H_{\text{M}}] = [Q_\alpha, W_{\text{M}}] = 0. \quad (2.9)$$

The commutators involving the tunneling Hamiltonian are

$$[rQ_\alpha, T_-]_1 := [rQ_\alpha, T_-] = r \sum_\iota \gamma_{\alpha\iota} d_\iota^\dagger \psi_\alpha(x_\alpha) + r \sum_\kappa \gamma'_{\alpha\kappa} \phi_\kappa^\dagger(y_\kappa) \psi_\alpha(x'_\alpha), \quad (2.10)$$

$$[rQ_\alpha, T_+]_1 := [rQ_\alpha, T_+] = -r \sum_\iota \gamma_{\alpha\iota}^* \psi_\alpha^\dagger(x_\alpha) d_\iota - r \sum_\kappa \gamma'_{\alpha\kappa}^* \psi_\alpha^\dagger(x'_\alpha) \phi_\kappa(y_\kappa). \quad (2.11)$$

Similarly, the nested commutators $[A, B]_n := [A, [A, B]_{n-1}]$ can be calculated,

$$[rQ_\alpha, T_-]_n = r^n \sum_\iota \gamma_{\alpha\iota} d_\iota^\dagger \psi_\alpha(x_\alpha) + r^n \sum_\kappa \gamma'_{\alpha\kappa} \phi_\kappa^\dagger(y_\kappa) \psi_\alpha(x'_\alpha), \quad (2.12)$$

$$[rQ_\alpha, T_+]_n = (-r)^n \sum_\iota \gamma_{\alpha\iota}^* \psi_\alpha^\dagger(x_\alpha) d_\iota + (-r)^n \sum_\kappa \gamma'_{\alpha\kappa}^* \psi_\alpha^\dagger(x'_\alpha) \phi_\kappa(y_\kappa). \quad (2.13)$$

The full counting statistics can be introduced by

$$\begin{aligned} \chi(\{\lambda_\alpha\}) &= \text{Tr} \rho e^{i \sum_\alpha \lambda_\alpha Q_\alpha(\mathcal{T})} = \text{Tr} \rho e^{i \sum_\alpha \frac{\lambda_\alpha Q_\alpha}{2}} \\ &\times \exp \left[i \mathcal{T} e^{-i \sum_\alpha \frac{\lambda_\alpha Q_\alpha}{2}} H e^{i \sum_\alpha \frac{\lambda_\alpha Q_\alpha}{2}} \right] \exp \left[-i \mathcal{T} e^{i \sum_\alpha \frac{\lambda_\alpha Q_\alpha}{2}} H e^{-i \sum_\alpha \frac{\lambda_\alpha Q_\alpha}{2}} \right] e^{-i \sum_\alpha \frac{\lambda_\alpha Q_\alpha}{2}} \quad (2.14) \\ &= \text{Tr} \rho e^{i \sum_\alpha \frac{\lambda_\alpha Q_\alpha}{2}} e^{i H_\lambda \mathcal{T}} e^{-i H_{-\lambda} \mathcal{T}} e^{i \sum_\alpha \frac{\lambda_\alpha Q_\alpha}{2}}, \end{aligned}$$

where in the last equation the operator $H_\lambda = e^{i \sum_\alpha \frac{\lambda_\alpha Q_\alpha}{2}} H e^{-i \sum_\alpha \frac{\lambda_\alpha Q_\alpha}{2}}$ was introduced. Defining Keldysh time dependent counting fields $\lambda_\alpha(\tau)$,

$$\lambda_\alpha(\tau) = \Theta(\tau) \Theta(\mathcal{T} - \tau) \begin{pmatrix} \lambda_{\alpha^+} = -\lambda & \tau \in \mathcal{C}^+ \\ \lambda_{\alpha^-} = \lambda & \tau \in \mathcal{C}^- \end{pmatrix} \quad (2.15)$$

one can rewrite eq. (2.14) using the non-equilibrium Keldysh formalism (see Appendix A.1)

$$\chi(\{\lambda_\alpha\}) = \left\langle T_{\mathcal{C}} \left[e^{-i \int_{\mathcal{C}} d\tau H_\lambda(\tau)} \right] \right\rangle. \quad (2.16)$$

Using the commutator relations above, one obtains

$$H_\lambda = H_{\text{leads}} + H_{\text{M}} + W_{\text{M}} + T_\lambda, \quad (2.17)$$

where

$$T_\lambda = T_{\lambda,-} + T_{\lambda,+}, \quad (2.18)$$

with

$$T_{\lambda,-} = \sum_{\alpha,\iota} e^{i \frac{\lambda_\alpha}{2}} \gamma_{\alpha\iota} d_\iota^\dagger \psi_\alpha(x_\alpha) + \sum_{\alpha,\kappa} e^{i \frac{\lambda_\alpha}{2}} \gamma'_{\alpha\kappa} \phi_\kappa^\dagger(y_\kappa) \psi_\alpha(x'_\alpha), \quad (2.19)$$

$$T_{\lambda,+} = \sum_{\alpha,\iota} e^{-i \frac{\lambda_\alpha}{2}} \gamma_{\alpha\iota}^* \psi_\alpha^\dagger(x_\alpha) d_\iota + \sum_{\alpha,\kappa} e^{-i \frac{\lambda_\alpha}{2}} \gamma'_{\alpha\kappa}^* \psi_\alpha^\dagger(x'_\alpha) \phi_\kappa(y_\kappa). \quad (2.20)$$

2.1.2. The FCS of the resonant level model

In order to demonstrate the power of the FCS formalism, we determine the CGF for the exactly solvable resonant level model. In principle, there are two different ways to calculate the CGF. The first method is based on a current-like expansion of the CGF (see Gogolin and Komnik [2006]) and

is presented in this section. The second one is a functional integral approach and is presented in appendix A.3.

There is another more educational reason to look at the resonant level model: we can introduce and motivate the common assumptions of quantum transport theory in nanostructures. We begin by providing a physical picture of the resonant level model. The most simple setup one could have in mind is sketched in fig. 2.1: there are two metallic leads which are both tunneling coupled to a tiny island, for example a buckyball. Ignoring the internal degrees of freedom of the island, it can be described by a quantum dot, which is nothing more than a discrete ensemble of energy levels which can be occupied by charge carriers. The energy levels can be tuned with an attached gate electrode and an applied bias voltage to the leads allows for a current to flow through the system. As a first approximation, one can assume the quantum dot and the electronic leads to be non-interacting. In this case, we can model the electrodes by simple Fermi liquids which are held at different chemical potentials $\mu_{L,R}$,

$$H_{\text{leads}} = \sum_{m=L,R} \sum_k (\epsilon_{m,k} - \mu_m) c_{m,k}^\dagger c_{m,k} \quad (2.21)$$

where $\epsilon_{m,k}$ are the energy-momentum dispersion relations for free electrons¹ and $c_{m,k}^\dagger, c_{m,k}$ are creation and annihilation operators for particles with momentum k . The quantum dot can be described by a single energy level,

$$H_M = \Delta_0 d^\dagger d \quad (2.22)$$

where Δ_0 is the energy of the level and d^\dagger, d are the creation and annihilation operators of the dot level. In real devices, a quantum dot of course consists of more than one energy level. However, assuming the quantum dot to be sufficiently small, the level spacing can be rather large compared to the other energy scales of the system. In these kinds of systems, tunneling effectively involves a single energy level only². We did not include a spin degree of freedom of the particles. To justify this, we can think of an applied magnetic field lifting the spin degeneracy. As long as we are not interested in the Kondo effect, i.e. do not approach the Kondo temperature, we can safely neglect onsite interactions or treat them perturbatively. In order to describe tunneling, we have to introduce field operators for the electronic leads. So far, we have not discussed the role of the spatial dimension of the leads. As long as we are dealing with spatially localized, structureless tunneling events, i.e. s-wave scattering processes, the universal low-energy behaviour can be described by one-dimensional field theories, see Ludwig and Affleck [1994] for more details on this subject. Indeed, these assumptions are quite reasonable and often met in experiments³. In fig. 2.3, we sketched the mentioned mapping to a one-dimensional system. Now, we can define the field operators for the

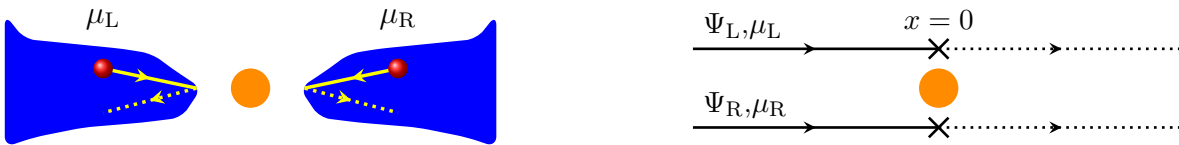


Figure 2.3.: The panel to the left shows the typical geometry of tunneling events in real experiments. The right panel shows the mapping to an effective 1D low energy field theory. Here, tunneling is described as scattering processes on a impurity.

¹In interacting systems, we have to think of quasiparticles rather than bare electrons.

²Additionally, one has to assume a sufficiently small bias voltage.

³The tunneling probability is exponentially suppressed by the width of the tunneling barrier. Therefore, tunneling naturally occurs from within a small region in the lead.

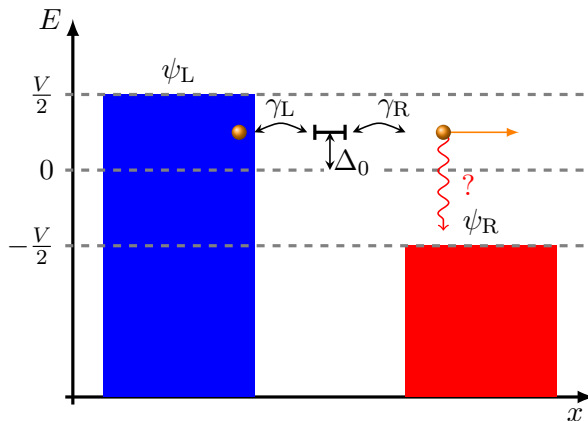


Figure 2.4.: Energy scales in the resonant level model. An electron tunnels from the left lead through the quantum dot to the right lead.

leads,

$$\psi_m(x) = \int \frac{dk}{2\pi} e^{ikx} c_{m,k} \quad (2.23)$$

and formulate the Hamiltonian for the tunneling processes,

$$H_T = \sum_{m=L,R} \left[\gamma_m d^\dagger \psi_m(x=0) + \text{H.c.} \right], \quad (2.24)$$

where γ_m are the tunneling amplitudes. In fig. 2.4, we depicted the energy scales of the system (at temperature $T = 0$) and sketched a single tunneling process. There is an obstacle in the picture of non-interacting leads: what happens with the excess energy? Without interactions there is no reason for relaxation. The mechanism of relaxation and the existence of a steady state is an interesting and ongoing area of research of its own (see for example [Doyon and Andrei \[2006\]](#)). We circumvent the problem of relaxation by assuming the leads to be of infinite length. In this case, the problem of the excess energy does not arise. Electrons with higher energy just vanish into infinity and never come back. In the following, we omit the $x = 0$ statement in the tunneling operator.

In order to calculate the CGF, we need the λ -dependent tunneling operator,

$$T_\lambda = \sum_{m=L,R=\pm} \left[\gamma_m e^{im\lambda/4} d^\dagger \psi_m + \text{H.c.} \right] \quad (2.25)$$

where we have introduced the counting fields in a symmetric way: electrons are counted twofold. Once when they are tunneling from the left lead to the dot, and a second time when they are tunneling from the dot to the right lead. Therefore, we have the coefficient $1/4$ in front of the counting field instead of $1/2$ as in the previous expressions (see eq. (2.20)). The notation $m = L, R = \pm$ is self-explanatory. Tunneling processes from the left lead to the dot $d^\dagger \psi_L$ have to be counted with a positive sign, i.e. $m = L = +$. However, tunneling processes from the right lead to the dot $d^\dagger \psi_R$ have to be counted with a negative sign and therefore $m = R = -$.

The current-like expansion is based on the fact that the counting field $\lambda(t)$ is a constant on each

branch of the Keldysh contour. With this in mind, we can use eq. (2.16) to find the CGF

$$\begin{aligned}
 \ln \chi(\lambda_-, \lambda_+) &= \frac{1}{\chi(\lambda_-, \lambda_+)} \int d\lambda_- \frac{\delta \langle T_C e^{-i \int_C dt T_\lambda(t)} \rangle}{\delta \lambda(t_-)} \\
 &= \frac{-i}{\chi(\lambda_-, \lambda_+)} \int d\lambda_- \int_{C_-} dt_- \left\langle T_C \left[\frac{\delta T_\lambda}{\delta \lambda(t_-)} e^{-i \int_C dt T_\lambda(t)} \right] \right\rangle \\
 &= -i \int d\lambda_- \int_{C_-} dt_- \left\langle \frac{\delta T_\lambda}{\delta \lambda(t_-)} \right\rangle_\lambda
 \end{aligned} \tag{2.26}$$

where in the last equation we have introduced the λ -dependent expectation value,

$$\langle \cdot \rangle_\lambda := \frac{\langle \cdot \rangle}{\chi(\lambda_-, \lambda_+)}, \tag{2.27}$$

where the expectation values $\langle \cdot \rangle$ have to be calculated with respect to $H = H_{\text{leads}} + H_M + T_\lambda$. The occurrence of $\chi(t_-, t_+)$ in the denominator is crucial. Otherwise, unconnected diagrams do not necessarily cancel⁴. The functional derivative on the r.h.s of eq. (2.26) can now be rewritten to

$$\left\langle \frac{\delta T_\lambda}{\delta \lambda(t_-)} \right\rangle_\lambda = \frac{i}{4} \sum_{m=L,R=\pm} m \left\langle T_C \left[\gamma_m e^{im\lambda_-/4} d^\dagger(t_-) \psi_m(t_-) - \text{H.c.} \right] \right\rangle_\lambda. \tag{2.28}$$

Next, it is convenient to introduce counting field-dependent Keldysh Green's functions,

$$G_{md}(t-t') = -i \left\langle T_C \psi_m(t) d^\dagger(t') \right\rangle_\lambda \tag{2.29}$$

$$G_{dm}(t-t') = -i \left\langle T_C d(t) \psi_m^\dagger(t') \right\rangle_\lambda \tag{2.30}$$

and rewrite the eq. (2.28) to

$$\begin{aligned}
 \left\langle \frac{\delta T_\lambda}{\delta \lambda(t_-)} \right\rangle_\lambda &= \frac{1}{4} \sum_{m=L,R=\pm} m \left[\gamma_m e^{im\lambda_-/4} G_{md}^{--}(t_-, t_-) - \gamma_m^* e^{-im\lambda_-/4} G_{dm}^{--}(t_-, t_-) \right] \\
 &= \frac{1}{4} \sum_{m=L,R=\pm} m \int \frac{d\omega}{2\pi} \left[\gamma_m e^{im\lambda_-/4} G_{md}^{--}(\omega) - \gamma_m^* e^{-im\lambda_-/4} G_{dm}^{--}(\omega) \right].
 \end{aligned} \tag{2.31}$$

In the last equation, we have introduced the Fourier transformation of the Keldysh functions. Unless stated otherwise, the Fourier transform of a Keldysh Green's function is always a 2×2 matrix in Keldysh space. The mixed Green's functions can be expressed in terms of the Keldysh function of the quantum dot only,

$$D(t-t') = -i \left\langle T_C d(t) d^\dagger(t') \right\rangle_\lambda. \tag{2.32}$$

One easily finds the relations

$$G_{md}(t-t') = \gamma_m^* \int_C d\tau g_m(t, \tau) D(\tau, t') e^{im\lambda(\tau)/4} \tag{2.33}$$

$$G_{dm}(t-t') = \gamma_m \int_C d\tau D(t, \tau) g_m(\tau, t') e^{-im\lambda(\tau)/4} \tag{2.34}$$

⁴Usually, the Keldysh formalism has a built-in cancellation of unconnected diagrams. This stems from the fact that the Keldysh partition function is always unity. But this is no longer true in the presence of contour-dependent counting fields.

which, in Fourier space, transform to the matrix equations for Keldysh matrices,

$$G_{md}(\omega) = g_m(\omega) \hat{\gamma}_m^* D(\omega) \quad (2.35)$$

$$G_{dm}(\omega) = D(\omega) \hat{\gamma}_m g_m(\omega) \quad (2.36)$$

where $\hat{\gamma}_m$ are the matrices,

$$\hat{\gamma}_m = \gamma_m \begin{pmatrix} e^{im\lambda_-/4} & 0 \\ 0 & -e^{im\lambda_+/4} \end{pmatrix} \quad (2.37)$$

and $g_m(t-t') = -i \langle T_C \psi_m(t) \psi_m^\dagger(t') \rangle_0$ are the Keldysh functions of the isolated leads which are calculated and listed in appendix A.2.1. Putting everything together we find

$$\left\langle \frac{\delta T_\lambda}{\delta \lambda(t_-)} \right\rangle_\lambda = \sum_{m=L,R=\pm} \frac{m |\gamma_m|^2}{4} \int \frac{d\omega}{2\pi} \left[g_m^{+-}(\omega) D^{-+}(\omega) e^{-im\lambda/2} - g_m^{-+}(\omega) D^{+-}(\omega) e^{im\lambda/2} \right], \quad (2.38)$$

with the definition $\lambda = (\lambda_- - \lambda_+)/2$. Eq. (2.38) can be thought of as an extension of the Meir-Wingreen formula (Meir and Wingreen [1992]) of the current for the CGF. Later on, we will argue that this formula even holds for an interacting quantum dot. In case of the non-interacting resonant level model, we can find an exact expression for the Keldysh function D of the quantum dot by solving the Dyson equation,

$$D(\omega) = d_0(\omega) + d_0(\omega) \Sigma_T(\omega) D(\omega) \quad (2.39)$$

which is a purely algebraic (matrix-) equation. d_0 is the Keldysh function of the isolated dot level (see appendix A.2.2), $d_0(t-t') = -i \langle T_C d(t) d^\dagger(t') \rangle_0$ and Σ_T the self-energy due to tunneling given by

$$\Sigma_T(\omega) = \sum_{m=L,R=\pm} \hat{\gamma}_m g_m(\omega) \hat{\gamma}_m^*. \quad (2.40)$$

It is now a simple exercise to obtain

$$D(\omega) = \frac{1}{\det D^{-1}} \begin{pmatrix} (\omega - \Delta_0) + i(\Gamma_L n_L + \Gamma_R n_R - 1) & i\Gamma \left(e^{\frac{i\lambda}{2}} \Gamma_L n_L + e^{-\frac{i\lambda}{2}} \Gamma_R n_R \right) \\ i \left[e^{-\frac{i\lambda}{2}} \Gamma_L (n_L - 1) + e^{\frac{i\lambda}{2}} \Gamma_R (n_R - 1) \right] & -(\omega - \Delta_0) + i(\Gamma_L n_L + \Gamma_R n_R - 1) \end{pmatrix}, \quad (2.41)$$

with the determinant

$$\det D^{-1} = (\omega - \Delta_0)^2 + \Gamma^2 + 4\Gamma_L \Gamma_R \left[\left(e^{i\lambda} - 1 \right) n_L (1 - n_R) + \left(e^{-i\lambda} - 1 \right) n_R (1 - n_L) \right], \quad (2.42)$$

the hybridization parameters, $\Gamma_m = \pi \rho_{0m} \gamma_m^2$, $\Gamma = \Gamma_L + \Gamma_R$, where ρ_{0m} is the density of states of lead m near the Fermi edge. $n_m(\omega)$ denotes the Fermi distribution function with chemical potential μ_m . Putting everything together, one finds

$$\left\langle \frac{\delta T_\lambda}{\delta \lambda(t_-)} \right\rangle_\lambda = i \int \frac{d\omega}{2\pi} \frac{\partial}{\partial \lambda_-} \ln \det D^{-1}(\omega). \quad (2.43)$$

Now, the remaining integrals in eq. (2.26) are trivial. The time integration reproduces the measurement time \mathcal{T} and the λ_- integration produces the logarithm of $\det D^{-1}$ up to proper normalization. The normalization can easily be restored using $\chi(0) = 1$. The CGF then takes the form,

$$\ln \chi(\lambda) = \mathcal{T} \int \frac{d\omega}{2\pi} \ln \left\{ 1 + T(\omega) \left[\left(e^{i\lambda} - 1 \right) n_L (1 - n_R) + \left(e^{-i\lambda} - 1 \right) n_R (1 - n_L) \right] \right\} \quad (2.44)$$

which is the well known Levitov-Lesovik formula (Levitov et al. [1996]) with transmission coefficient $T(\omega)$ of the resonant level model,

$$T(\omega) = \frac{4\Gamma_L\Gamma_R}{(\omega - \Delta_0)^2 + \Gamma^2}. \quad (2.45)$$

The current through the resonant level model is obtained by

$$I = -\frac{i}{\mathcal{T}} \frac{d \ln \chi(\lambda)}{d\lambda} \Big|_{\lambda=0} = \int \frac{d\omega}{2\pi} T(\omega) (n_L - n_R) \quad (2.46)$$

which is well known from the Meir-Wingreen formula. The current noise is given by

$$S = \frac{(-i)^2}{\mathcal{T}} \frac{d^2 \ln \chi(\lambda)}{d\lambda^2} \Big|_{\lambda=0} = \int \frac{d\omega}{2\pi} T(\omega) \left[n_L(1 - n_R) + n_R(1 - n_L) - T(\omega)(n_L - n_R)^2 \right] \quad (2.47)$$

which in case of zero temperature and $\mu_L > \mu_R$ simplifies to

$$S = \int \frac{d\omega}{2\pi} T(\omega) [1 - T(\omega)] (n_L - n_R). \quad (2.48)$$

In case of a small bias voltage $V = \mu_L - \mu_R$, one recovers the linear response result

$$S = T\left(\frac{\mu_L + \mu_R}{2}\right) \left[1 - T\left(\frac{\mu_L + \mu_R}{2}\right) \right] V. \quad (2.49)$$

In case of a symmetrically applied voltage $\mu_R = -\mu_L = -V/2$ this further simplifies to $S = T(0)[1 - T(0)]$, i.e. only the transmission coefficient for small energies is relevant.

2.2. Strongly coupled Holstein polaron

The fundamental building blocks of modern day microelectronics are transistors based on conventional silicon n-p junctions or for low-noise applications, two dimensional electron gases at the interface of semiconductor heterostructures. Typical structures in these kinds of systems are of the size of several 10 nm (state-of-the-art is the 22 nm technology). Atom and molecule based electronic circuits can, in principle, improve this limit by at least one order of magnitude. As an example, one can build a small island – a quantum dot – in a carbon nanotube via mechanical deformations (for example via an STM) at two distinct points (see fig. 2.5). Effectively, the quantum dot is a zero dimensional system and its electronic degrees of freedom can be described by a set of discrete energy levels. Using a gate electrode, the position of the electronic levels can be shifted. Depending on this position, an applied voltage across the nanotube can lead to a current of different magnitude.

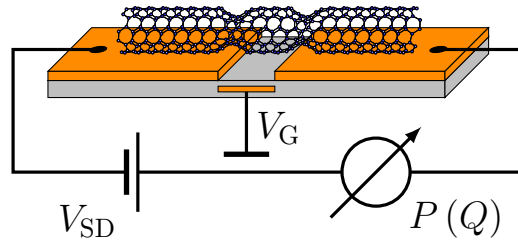


Figure 2.5.: Quantum dot embedded in a suspended carbon nanotube.

For molecular circuits, however, this picture is often oversimplified. For example, charging of the molecule can lead to substantial structural deformation of the molecule itself. This leads to a coupling of the conformational or vibrational degrees of freedom to the electronic ones. In this section, we focus on quantum dots with a rather strong electron-phonon coupling. Recent experiments (Leturcq et al. [2009]) have shown that this is indeed the case in quantum dots embedded in carbon nanotubes.

The Anderson-Holstein model (AHM, see Anderson [1961], Holstein [1959]) is able to describe quantum impurities in the presence of vibrational degrees of freedom. In its full extent, the AHM captures a huge variety of physical phenomena. Its physical properties depend on several energy scales, e.g., temperature, charging energy, hybridization energy, level spacing, and electron-phonon interaction strength. These define many interesting and physically distinct regimes in parameter space. We are mainly interested in the effect of electron-phonon interactions on the charge transport through a contacted molecule. The model can therefore be simplified to contain a single electronic level (thus neglecting the spin degree of freedom as well as the charging energy) linearly coupled to a local (Holstein) phonon, i.e., a bosonic oscillator degree of freedom with a single frequency. Even this simplified model offers rich physics. The conductance and the nonlinear I-V characteristic of such a system can be approached by a number of methods, such as diagrammatic Monte Carlo (diagMC) schemes (Mühlbacher and Rabani [2008]), rate equations (Koch and von Oppen [2005], Leturcq et al. [2009]), perturbation theory (de la Vega et al. [2006], Flensberg [2003], Galperin et al. [2006], Riwar and Schmidt [2009]) and $P(E)$ theory (Kast et al. [2011]).

Its full counting statistics (FCS) are well understood in the limit of weak electron-phonon coupling (Avriller and Levy Yeyati [2009], Haupt et al. [2009], Schmidt and Komnik [2009]) as well as in situations where rate equations apply (Avriller [2011], Dong et al. [2009], Koch and von Oppen [2005]). We would like to extend these results and present a calculation of the FCS beyond these limits. The model of our interest consists of electrodes as well as the quantum dot made of a single carbon nanotube subject to a bias voltage V (see fig. 2.5). The electronic level structure of the quantum dot can be tuned by an additional backgate. The nanotube can be of such a geometry that the relevance of the purely electronic interactions is negligible. Because of its simple structure, the vibrational modes of such a quantum dot are well understood (see Mariani and von Oppen [2009]). The model we employ is fairly general. Depending on the parameter regime, it also allows the description of transport through molecules contacted using mechanically controlled break junctions (Djukic et al. [2005], Smit et al. [2002]) and STM tips (Qiu et al. [2004], Stipe et al. [1998]) as well as in nanoelectromechanical setups (Knobel and Andrew [2003]).

2.2.1. The model and the Lang-Firsov transformation

The starting point of our calculation is the Hamiltonian of the Anderson-Holstein model,

$$H = H_0 + H_T + H_{e-ph}. \quad (2.50)$$

The contribution H_0 describes the uncoupled degrees of freedom, i.e. the electrodes, the single electronic level of the quantum dot and the bosonic mode,

$$H_0 = H_{\text{leads}}[\psi_L, \psi_R] + \Delta_0 d^\dagger d + \Omega B^\dagger B. \quad (2.51)$$

The electrodes are described by non-interacting spinless electron field operators $\psi_{L,R}(x)$ which are held at chemical potentials $\mu_{L,R}$. This is achieved by a source-drain voltage $V = \mu_L - \mu_R$. In many

cases, assuming spinless particles is not a severe constraint. For example, in systems with sufficiently strong magnetic fields, this can be a valid assumption⁵. In case of non-interacting electrons, all the necessary information of H_{leads} is encoded in the local tunneling density of states $\rho(\omega)$. For reasons of simplicity, we work in the wide flat band limit $\rho(\omega) = \rho_0$, which corresponds to free fermions with linear dispersion and infinite bandwidth. However, any other shape of $\rho(\omega)$ can be treated in the same way. The second contribution in eq. (2.51) describes the single electronic level of the quantum dot with bare energy Δ_0 and associated creation and annihilation operators d^\dagger , d . The last term in H_0 comes from the vibrational degree of freedom which is given by a single phonon with frequency Ω and creation and annihilation operators B^\dagger , B . As long as the vibrational modes of the molecular quantum dot in question are energetically well separated, the assumption of a single Einstein mode is quite reasonable. Tunneling of electrons from the leads to the quantum dot and back is described by H_T ,

$$H_T = \sum_{\alpha=L,R} \gamma_\alpha \left[d^\dagger \psi_\alpha(x=0) + \text{H.c.} \right] \quad (2.52)$$

where γ_α are the tunneling amplitudes, which can be assumed to be real. Only in case of interference experiments where multiple paths are possible (for example in a double quantum dot setup in parallel arrangement), the phases can not be gauged away. In the following we assume a symmetric coupling to both of the leads, $\gamma_L = \gamma_R = \gamma$. This substantially simplifies the expressions. An asymmetric coupling requires only small adjustments, however, the notation becomes significantly more complicated. As usual, we omit the $x = 0$ statement in the following. In order to calculate the CGF, we need the λ -dependent tunneling operator,

$$T_\lambda = \gamma \sum_{m=L,R=\pm} e^{im\lambda/4} \left[d^\dagger \psi_m + \text{H.c.} \right]. \quad (2.53)$$

The last contribution of the Hamiltonian (2.50) is the electron-phonon interaction

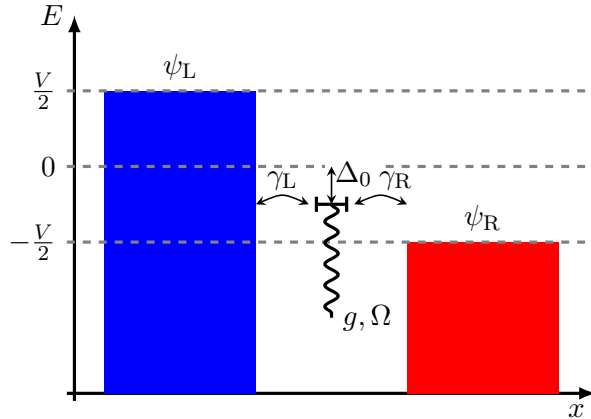


Figure 2.6.: Energy scales of the Anderson-Holstein model with a bosonic degree of freedom.

$$H_{\text{e-ph}} = g d^\dagger d (B^\dagger + B). \quad (2.54)$$

It couples the occupation of the dot, $n = d^\dagger d$, to the displacement of a harmonic oscillator $Q \sim B^\dagger + B$ with a coupling strength g . In the strong coupling regime, it turns out to be convenient to

⁵Due to Zeeman splitting, one spin species is shifted out of resonance.

calculate the full counting statistics via the current-like expression,

$$\ln \chi(\lambda_-, \lambda_+) = -i \int d\lambda_- \int_{\mathcal{C}_-} dt_- \left\langle \frac{\delta T_\lambda}{\delta \lambda(t_-)} \right\rangle_\lambda. \quad (2.55)$$

Obviously, the derivative on the r.h.s. of eq. (2.55) can be expressed via Keldysh Green's functions in exactly the same fashion as in the case of the non-interacting resonant level model (see eq. (2.31)),

$$\left\langle \frac{\delta T_\lambda}{\delta \lambda(t_-)} \right\rangle_\lambda = \frac{\gamma}{4} \sum_{m=L,R=\pm} m \int \frac{d\omega}{2\pi} \left[e^{im\lambda_-/4} G_{md}^{--}(\omega) - e^{-im\lambda_-/4} G_{dm}^{--}(\omega) \right] \quad (2.56)$$

where the expectation values in the definition of the Keldysh functions have to be evaluated with respect to the operator $H = H_0 + T_\lambda + H_{e\text{-ph}}$. In presence of arbitrary interactions, it is in general not possible to express G_{md}, G_{dm} in terms of g_m and D , only. However, if the interaction is localized on the quantum dot, eq. (2.34) still holds. This can easily be verified using functional integration techniques (see appendix A.3). Therefore, again we obtain eq. (2.38),

$$\left\langle \frac{\delta T_\lambda}{\delta \lambda(t_-)} \right\rangle_\lambda = \sum_{m=L,R=\pm} \frac{m\gamma^2}{4} \int \frac{d\omega}{2\pi} \left[g_m^{+-}(\omega) D^{-+}(\omega) e^{-im\lambda/2} - g_m^{-+}(\omega) D^{+-}(\omega) e^{im\lambda/2} \right]. \quad (2.57)$$

We proceed by applying a Lang-Firsov (polaron) transformation (Lang and Firsov [1963]) $U = \exp[\alpha d^\dagger d (B^\dagger - B)]$ to our system,

$$U H_0 U^\dagger = H_{\text{leads}} + (\Delta_0 + \alpha^2 \Omega) d^\dagger d + \Omega B^\dagger B - \alpha \Omega d^\dagger d (B^\dagger + B) \quad (2.58)$$

$$U T_\lambda U^\dagger = \gamma \sum_{m=L,R=\pm} \left[e^{im\lambda/4} e^{-\alpha(B^\dagger - B)} d^\dagger \psi_m + \text{H.c.} \right] \quad (2.59)$$

$$U H_{e\text{-ph}} U^\dagger = g d^\dagger d (B^\dagger + B) - 2\alpha g d^\dagger d. \quad (2.60)$$

Apart of being real, there is no other constraint for the parameter α . However, there is a convenient value, $\alpha = g/\Omega$. In this case, we have

$$H_\lambda = H_{\text{leads}} + \Delta D^\dagger D + \Omega B^\dagger B + T'_\lambda \quad (2.61)$$

$$T'_\lambda = \gamma \sum_{m=L,R=\pm} \left[e^{im\lambda/4} D^\dagger \psi_m + \text{H.c.} \right]. \quad (2.62)$$

We have introduced the shifted dot level energy $\Delta = \Delta_0 - g^2/\Omega$, also known as polaron shift, and the dressed dot operator, $D := X d := e^{g(B^\dagger - B)/\Omega} d$. The operator $X = e^{g(B^\dagger - B)/\Omega}$ is the phonon cloud operator. The physical picture behind this transformed system is simple: tunneling of an electron from the lead to the dot or vice versa excites/de-excites a phonon cloud on the quantum dot. It is not difficult to verify that eq. (2.57) maintains its structure under the polaron transformation. One has just to replace the Keldysh function of the bare quantum dot by the Keldysh function of the dressed quantum dot,

$$D(t, t') = -i \left\langle T_C D(t) D^\dagger(t') \right\rangle_\lambda = -i \left\langle T_C d(t) d^\dagger(t') X(t) X^\dagger(t') \right\rangle_\lambda. \quad (2.63)$$

Unfortunately, the expansion of the dressed Keldysh function with respect to the tunneling amplitude γ is much more involved than for bare particles,

$$D(t, t') = \sum_{n=0}^{\infty} \gamma^{2n} D^{(2n)}(t, t') \quad (2.64)$$

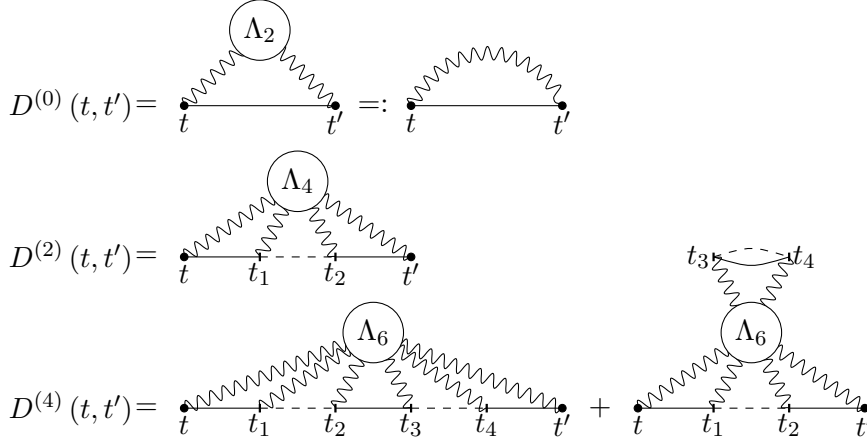


Figure 2.7.: Feynman diagrams of the contributions $D^{(0)}$, $D^{(2)}$ and $D^{(4)}$. The solid lines denote the free propagators of the quantum dot d_0 and the dashed lines the free propagators of the electric contacts, $g_{L,R}$. The vertex functions Λ_{2n} connect each time variables with each other. Internal time integrals t_i are integrated over.

where $D^{(2n)}(t, t')$ denotes the set of all Feynman diagrams to $2n$ th order in the tunneling amplitude. The basic ingredient to the expansion (2.64) is the Keldysh time ordered expectation value of the phonon cloud operator X ,

$$\Lambda_{2n}(t_1, \dots, t_{2n}) := \left\langle T_C X(t_1) X^\dagger(t_2) \dots X(t_{2n-1}) X^\dagger(t_{2n}) \right\rangle_0 \quad (2.65)$$

where the expectation value has to be evaluated with respect to UH_0U^\dagger . Because of the exponential structure of the operator X , we will refer to the function Λ_{2n} as vertex function according to the usual notation in string or conformal field theory. Because we are dealing with free bosons B^\dagger, B , expectation values of exponentials can easily be calculated using the prescription (see for example von Delft and Schoeller [1998] and references therein)

$$\left\langle e^{\alpha B + \beta B^\dagger} \right\rangle = e^{\langle [\alpha B + \beta B^\dagger]^2 / 2 \rangle}. \quad (2.66)$$

We obtain for the vertex functions of the bosons,

$$\Lambda_{2n}(t_1, \dots, t_{2n}) = \prod_{i < j}^{2n} [\Lambda(t_i - t_j)]^{\sigma_{ij}} \quad (2.67)$$

where we defined $\sigma_{ij} = (-1)^{i-j+1}$ and $\Lambda(t - t')$ is defined on the Keldysh contour by

$$\Lambda(t - t') = \left\{ \Lambda^{kl}(t - t') \right\}_{k,l=\pm} = \begin{pmatrix} \kappa(|t - t'|) & \kappa(t' - t) \\ \kappa(t - t') & \kappa(-|t - t'|) \end{pmatrix}. \quad (2.68)$$

$\kappa(t)$ is given by

$$\kappa(t) = \exp \left\{ - (g^2 / \Omega^2) [(e^{i\Omega t} - 1) n_B + (e^{-i\Omega t} - 1) (n_B - 1)] \right\}. \quad (2.69)$$

We introduced the uncoupled phonon occupation number $n_B = \langle B^\dagger B \rangle_0$ which accounts for the initial occupation of the harmonic oscillator states. Basically, we can distinguish two different scenarios. First, the molecule is coupled to a thermal environment (see for example Mitra et al. [2004]). For example, this can be the coupling of the molecule to the substrate or the backgate.

In this case, n_B is a temperature dependent distribution function. Then, it is often a good choice to assume a Bose distribution function $n_B = 1/(e^{-\Omega/T} - 1)$. Alternatively, one can consider a completely 'frozen' system at $T = 0$. Then n_B is simply zero.

The function $\kappa(t)$ can be subdivided in processes involving excitation/de-excitation of n phonons. In case of $T = 0$, one obtains

$$\kappa(t) = \exp\left[\left(\frac{g}{\Omega}\right)^2 (e^{-i\Omega t} - 1)\right] = e^{-\left(\frac{g}{\Omega}\right)^2} \sum_{n=0}^{\infty} \frac{1}{n!} \left(\frac{g}{\Omega}\right)^{2n} e^{-in\Omega t}. \quad (2.70)$$

In case of finite temperature, the calculation is more involved. First, we rewrite $\kappa(t)$ as an exponential of trigonometric functions,

$$\kappa(t) = e^{-\left(\frac{g}{\Omega}\right)^2 (2n_B+1)} e^{-\left(\frac{g}{\Omega}\right)^2 [(2n_B-1)\cos(\Omega t) + i\sin(\Omega t)]}. \quad (2.71)$$

Using the Jacobi-Anger expansion (see [Watson \[1996\]](#)) one finds,

$$\kappa(t) = e^{-\left(\frac{g}{\Omega}\right)^2 (2n_B+1)} \sum_{n,m=-\infty}^{\infty} I_n \left[-\left(\frac{g}{\Omega}\right)^2 (2n_B-1)\right] J_m \left[-\left(\frac{g}{\Omega}\right)^2\right] e^{i\Omega(n+m)t} \quad (2.72)$$

where J_n are the Bessel functions of the first kind and I_n the modified Bessel functions of the first kind. Using addition theorems for Bessel functions (Graf's generalization of Neumann's formula, see [Watson \[1996\]](#)) one obtains after a lengthy calculation,

$$\kappa(t) = e^{-\left(\frac{g}{\Omega}\right)^2 (2n_B+1)} \sum_{n=-\infty}^{\infty} I_n \left[2\left(\frac{g}{\Omega}\right)^2 \sqrt{n_B(n_B+1)}\right] e^{n\Omega/2T} e^{-n\Omega t}. \quad (2.73)$$

This expression was previously derived by Mahan in the context of the spectral function of the independent boson model ([Mahan \[2000\]](#)). The main difference between the $T = 0$ and finite temperature case, is the range of summation. The implication for transport processes is obvious: in case of zero temperature we have $n \geq 0$, i.e. phonons can only be emitted. In case of finite temperature phonons can be emitted and absorbed during tunneling events.

2.2.2. Perturbative approach

To leading order, the Keldysh function of the dressed quantum dot is given by

$$D^{(0)}(t-t') = d_0(t-t') \Lambda(t-t'). \quad (2.74)$$

In leading order calculation, the electrons are tunneling, or in our case, the polarons are tunneling through the junctions one by one without 'knowing' about each other. Then, the CGF (eq. (2.57)) is given by

$$\ln \chi(\lambda) = \mathcal{T} |\gamma|^2 \sum_{m=L,R=\pm} \int \frac{d\omega}{2\pi} \left[g_m^{+-}(\omega) D^{(0)-+}(\omega) e^{-im\lambda/2} + g_m^{-+}(\omega) D^{(0)+-}(\omega) e^{im\lambda/2} \right]. \quad (2.75)$$

Therefore, we only need the off-diagonal components of $D^{(0)}$,

$$D^{(0)k\bar{k}}(\omega) = \int \frac{dy}{2\pi} d_0^{k\bar{k}}(y) \Lambda^{k\bar{k}}(\omega-y) = 2\pi i (n_d - 1 - k) \Lambda^{k\bar{k}}(\omega - \Delta) \quad (2.76)$$

where n_d is the occupation number of the uncoupled bare quantum dot, i.e. $n_d = \langle d^\dagger d \rangle_0$. In case of zero temperature, we have

$$\Lambda^{k\bar{k}}(\omega) = 2\pi e^{-(\frac{g}{\Omega})^2} \sum_{n=0}^{\infty} \frac{1}{n!} \left(\frac{g}{\Omega}\right)^{2n} \delta(\omega - kn\Omega) \quad (2.77)$$

and therefore

$$\begin{aligned} \ln \chi(\lambda) = i\mathcal{T} |\gamma|^2 e^{-(\frac{g}{\Omega})^2} \sum_{m=L,R=\pm} \sum_{n=0}^{\infty} \frac{1}{n!} \left(\frac{g}{\Omega}\right)^{2n} & \left[n_d g_m^{+-} (-n\Omega + \Delta) e^{-im\lambda/2} \right. \\ & \left. + (n_d - 1) g_m^{-+} (n\Omega + \Delta) e^{im\lambda/2} \right]. \end{aligned} \quad (2.78)$$

The current can now be calculated as usual by performing a differentiation of the CGF w.r.t. λ ,

$$\begin{aligned} I = \frac{\Gamma}{2} e^{-(\frac{g}{\Omega})^2} \sum_{n=0}^{\infty} \frac{1}{n!} \left(\frac{g}{\Omega}\right)^{2n} & \left\{ n_d [n_L (-n\Omega + \Delta) - n_R (-n\Omega + \Delta)] \right. \\ & \left. - (n_d - 1) [n_L (n\Omega + \Delta) - n_R (n\Omega + \Delta)] \right\}. \end{aligned} \quad (2.79)$$

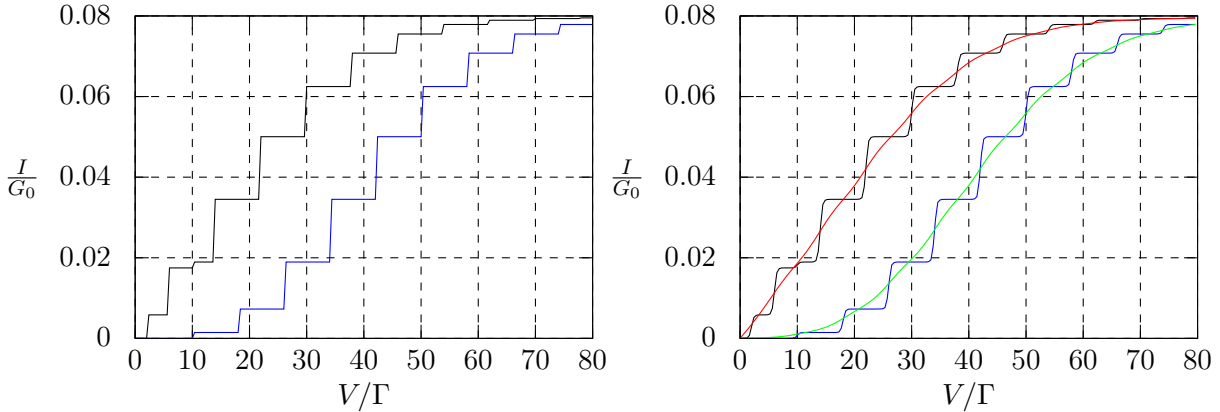


Figure 2.8.: Current in the leading order tunneling regime. **Left panel:** The parameters are $\Delta/\Gamma = -5$, $\Omega/\Gamma = 4$ and $g/\Gamma = 8$. For the black curve, the dot occupation number $n_d = 0$ and, for the blue curve, $n_d = 1$. The temperature is zero. **Right panel:** The parameters are the same as for the left panel except for the temperature. The black and blue curves show the current at temperature $T/\Gamma = 0.1$ and the red and green curves at temperature $T/\Gamma = 1$.

The current for finite temperature can be obtained in complete analogy,

$$\begin{aligned} I = \frac{\Gamma}{2} e^{-(\frac{g}{\Omega})^2 (2n_B + 1)} \sum_{n=-\infty}^{\infty} I_n & \left[2 \left(\frac{g}{\Omega}\right)^2 \sqrt{n_B (n_B + 1)} \right] e^{n\Omega/2T} \\ & \times \left\{ n_d [n_L (-n\Omega + \Delta) - n_R (-n\Omega + \Delta)] - (n_d - 1) [n_L (n\Omega + \Delta) - n_R (n\Omega + \Delta)] \right\}. \end{aligned} \quad (2.80)$$

In fig. 2.8, we have plotted the current for zero and finite temperature for uncoupled dot occupation numbers $n_d = 0$ and $n_d = 1$. In case of a non-interacting resonant level model, none of the transport quantities depend on n_B . This is especially true for the leading order corrections. However, coupling

a phonon sufficiently strong to the quantum dot completely changes the situation. For the noise at $T = 0$, one obtains

$$S = \frac{\Gamma}{4} e^{-\left(\frac{g}{\Omega}\right)^2} \sum_{n=0}^{\infty} \frac{1}{n!} \left(\frac{g}{\Omega}\right)^{2n} \left\{ n_d [2 - n_L (-n\Omega + \Delta) - n_R (-n\Omega + \Delta)] \right. \\ \left. - (n_d - 1) [n_L (n\Omega + \Delta) + n_R (n\Omega + \Delta)] \right\} \quad (2.81)$$

and for finite temperature

$$S = \frac{\Gamma}{4} e^{-\left(\frac{g}{\Omega}\right)^2 (2n_B + 1)} \sum_{n=-\infty}^{\infty} I_n \left[2 \left(\frac{g}{\Omega}\right)^2 \sqrt{n_B (n_B + 1)} \right] e^{n\Omega/2T} \\ \times \left\{ 2 - n_d [n_L (-n\Omega + \Delta) - n_R (-n\Omega + \Delta)] - (n_d - 1) [n_L (n\Omega + \Delta) + n_R (n\Omega + \Delta)] \right\}. \quad (2.82)$$

However, these results are not trustworthy. The reason is the following: in the leading order correction the quantum dot does not really contain information about its coupling to the leads. The occupation of the dot is adjusted in higher orders of the expansion. But there is a severe problem in calculating higher order diagrams: they are all singular. This is very well known from the singular expansion of the resonant level model. A method to work around this problem is summing up an infinite subset of diagrams. This ensures a proper hybridization of the quantum dot with the leads.

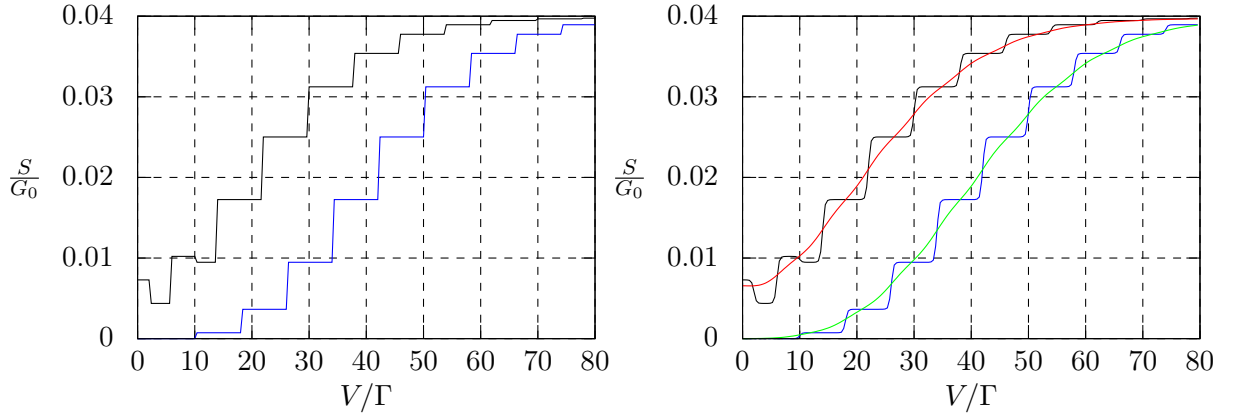


Figure 2.9.: Noise in the leading order tunneling regime. **Left panel:** The parameters are $\Delta/\Gamma = -5$, $\Omega/\Gamma = 4$ and $g/\Gamma = 8$. For the black curve, the dot occupation number $n_d = 0$ and, for the blue curve, $n_d = 1$. The temperature is zero. **Right panel:** The parameters are the same as for the left panel except for the temperature. The black and blue curves show the noise at temperature $T/\Gamma = 0.1$ and the red and green curves at temperature $T/\Gamma = 1$.

2.2.3. Resummation schemes for the Holstein model

In this section, we present physically motivated approximation schemes to cure the divergences in the tunneling expansion. We begin with the single particle approximation (SPA) which is similar to the current calculation in Braig and Flensberg [2003] or the noise calculations in Tahir and

MacKinnon [2010]. In this approximation the Keldysh propagator of the quantum dot is given by the expression,

$$D^{\text{SPA}}(t, t') = \begin{array}{c} \textcircled{\Lambda} \\ \text{---} \end{array} + \begin{array}{c} \textcircled{\Lambda} \\ \text{---} \end{array} + \dots \quad (2.83)$$

where the solid lines denote the free quantum dot Keldysh functions d_0 and the dashed lines the free leads Keldysh functions $g_{L,R}$. This kind of approximation is expected to be reasonable in systems where electronic tunneling processes are fast compared to the atomic rearrangement of the quantum dot (molecule). Or more precisely for $\Gamma/g \geq 1$. In frequency space, D^{SPA} is given as the convolution of the vertex function Λ with the quantum dot Keldysh function $D^{(0)}$ exact in tunneling, and hence,

$$D^{\text{SPA},k\bar{k}}(\omega) = \int \frac{dy}{2\pi} D^{(0),k\bar{k}}(y) \Lambda^{k\bar{k}}(\omega - y) = \sum_{n=-\infty}^{\infty} f_n D^{(0),k\bar{k}}(\omega - kn\Omega) \quad (2.84)$$

where the coefficients f_n are

$$f_n = \begin{cases} \Theta(n) e^{-\left(\frac{g}{\Omega}\right)^2} \frac{1}{n!} \left(\frac{g}{\Omega}\right)^{2n} & T = 0 \\ e^{-\left(\frac{g}{\Omega}\right)^2 (2n_B+1)} I_n \left[2 \left(\frac{g}{\Omega}\right)^2 \sqrt{n_B(n_B+1)} \right] e^{n\Omega/2T} & T \neq 0 \end{cases} \quad (2.85)$$

This approximation is conserving in the sense, that the spectral function $A(\omega) = -2\text{Im} D^{\text{SPA},R}(\omega)$ is properly normalized. $D^{\text{SPA},R}$ is the retarded Green's function $D^{\text{SPA},R}(\omega) = D^{\text{SPA},--}(\omega) - D^{\text{SPA},-+}(\omega)$. Therefore, one needs to know at least the imaginary part of one off-diagonal component of the quantum dot's Keldysh function. The $(--)$ component of the vertex function is

$$\Lambda^{--}(\omega) = \sum_{n=-\infty}^{\infty} f_n \left[\pi \delta(\omega - n\Omega) + \pi \delta(\omega + n\Omega) + i\mathcal{P} \frac{1}{\omega + n\Omega} - i\mathcal{P} \frac{1}{\omega - n\Omega} \right]. \quad (2.86)$$

The principal value part does not affect the normalization property of the spectral function, because we have

$$\text{Im} \int \frac{dy}{2\pi} D^{(0),--}(y) \left[\mathcal{P} \frac{i}{\omega - y + n\Omega} - \mathcal{P} \frac{i}{\omega - y - n\Omega} \right] = \frac{2\Gamma(\omega - \Delta)n\Omega}{\left[(\omega - \Delta)^2 + \Gamma^2 + \Omega^2 \right]^2 + 4\Gamma^2(n\Omega)^2} \quad (2.87)$$

which is odd with respect to $(\omega - \Delta)$. Hence,

$$\int d\omega A(\omega) = 2\pi \sum_n f_n = 2\pi. \quad (2.88)$$

In case of zero temperature, $\sum_n f_n = 1$ is obvious. For finite temperature, one again has to use the Jacobi-Anger relation for the modified Bessel functions. For the CGF, one finds

$$\begin{aligned}
 \ln \chi(\lambda) = & \mathcal{T} \sum_n f_n \int \frac{d\omega}{2\pi} \left\{ \left[n_L^+ (n_L - 1) - (n_L^- - 1) n_L - n_R^+ (n_R - 1) - (n_R^- - 1) n_R \right] \right. \\
 & \times \frac{T(\omega)}{\sqrt{\mathcal{E}(\omega)}} \tan^{-1} \left[\frac{T(\omega) (\mathcal{F}_{\lambda+} - \mathcal{F}_{\lambda-}) - (n_L - n_R) T(\omega) + 1}{\sqrt{\mathcal{E}(\omega)}} \right] \\
 & + \frac{1}{2} \left(\frac{n_L^- - 1}{n_L - 1} + \frac{n_R^+}{n_R} \right) \left\{ -\frac{i\lambda}{2} + \left[\frac{T(\omega)}{\sqrt{\mathcal{E}(\omega)}} [n_L (1 - n_R) + n_R (1 - n_L)] - \frac{1}{\sqrt{\mathcal{E}(\omega)}} \right] \right. \\
 & \times \tan^{-1} \left[\frac{T(\omega) (\mathcal{F}_{\lambda+} - \mathcal{F}_{\lambda-}) - (n_L - n_R) T(\omega) + 1}{\sqrt{\mathcal{E}(\omega)}} \right] + \frac{1}{2} \ln(1 + T(\omega) \mathcal{F}_{\lambda+}) \left. \right\} \\
 & + \left(\frac{n_R^- - 1}{n_R - 1} + \frac{n_L^+}{n_L} \right) \left\{ \frac{i\lambda}{2} + \left[\frac{T(\omega)}{\sqrt{\mathcal{E}(\omega)}} [n_L (1 - n_R) + n_R (1 - n_L)] - \frac{1}{\sqrt{\mathcal{E}(\omega)}} \right] \right. \\
 & \times \tan^{-1} \left[\frac{T(\omega) (\mathcal{F}_{\lambda+} + \mathcal{F}_{\lambda-}) + (n_L - n_R) T(\omega) + 1}{\sqrt{\mathcal{E}(\omega)}} \right] + \frac{1}{2} \ln(1 + T(\omega) \mathcal{F}_{\lambda+}) \left. \right\} \left. \right\} \quad (2.89)
 \end{aligned}$$

where $T(\omega)$ is the transmission coefficient of the resonant level model,

$$T(\omega) = \frac{\Gamma^2}{(\omega - \Delta)^2 + \Gamma^2}, \quad (2.90)$$

$n_{L,R}^\pm$ are shifted Fermi distribution functions,

$$n_{L,R}^\pm(\omega) = n_{L,R}(\omega \pm n\Omega), \quad (2.91)$$

the abbreviation $\mathcal{F}_{\lambda\pm}$,

$$\mathcal{F}_{\lambda\pm} = (e^{i\lambda} - 1) n_L (1 - n_R) + (e^{-i\lambda} - 1) n_R (1 - n_L) \quad (2.92)$$

and $\mathcal{E}(\omega)$,

$$\mathcal{E}(\omega) = T^2(\omega) (n_L - n_R)^2 - 2T(\omega) [n_L (1 - n_R) + n_R (1 - n_L)] + 1. \quad (2.93)$$

Although, the occurrence of the fractions n_m^\pm/n_m might indicate divergences in the case of zero temperature, $T \rightarrow 0$, all cumulants are well defined. For example, one obtains for the current

$$I = \sum_n f_n \int \frac{d\omega}{2\pi} \frac{1}{2} T(\omega) [2(n_L^+ - n_R^+) + (n_L + n_R)(n_L^- - n_L^+ - n_R^- + n_R^+)] \quad (2.94)$$

and for the noise

$$\begin{aligned}
 S = \sum_n f_n \int \frac{d\omega}{2\pi} \frac{1}{2} \left\{ T(\omega) [n_L^+ (1 - n_R) + n_R^+ (1 - n_L) + n_R (1 - n_L^-) + n_L (1 - n_R^-)] \right. \\
 \left. - T^2(\omega) (n_L - n_R) [2(n_L^+ - n_R^+) + (n_L + n_R)(n_L^- - n_L^+ - n_R^- + n_R^+)] \right\}. \quad (2.95)
 \end{aligned}$$

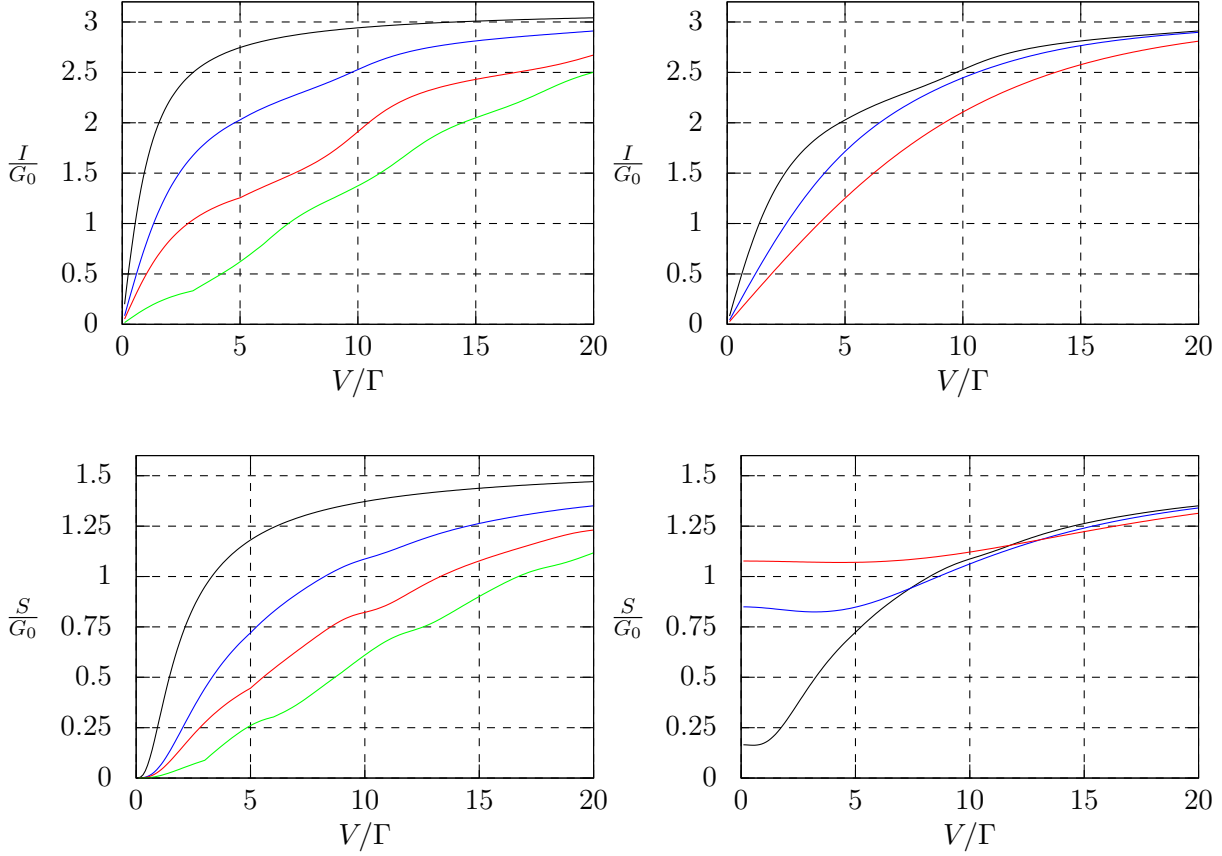


Figure 2.10.: Current and noise in the single particle approximation. **Left panels:** The dot level energy is fixed to $\Delta/\Gamma = 0$ and the temperature is $T = 0$. The other parameters are $g/\Gamma = 0$ for the black curves, $g/\Gamma = 2, \Omega/\Gamma = 5$ for the blue curves, $g/\Gamma = 4, \Omega/\Gamma = 5$ for the red curves and $g/\Gamma = 4, \Omega/\Gamma = 3$ for the green curves. **Right panels:** The dot level energy is fixed to $\Delta/\Gamma = 0$, $g/\Gamma = 2$ and $\Omega/\Gamma = 5$. The temperature is varied from $T/\Gamma = 0.1, 1, 2$ (black, blue and red curves).

In fig. 2.10, current and noise are depicted for several electron-phonon interaction strengths and temperatures. Increasing interaction strengths leads to more pronounced step-like features in current and noise when crossing multiples of the phonon resonance frequency. Also, the unitary limits of current and noise are approached much slower than in the non-interacting case. Temperature leads to a smearing out of the step-like features as expected. In the noise one observes a finite offset in the noise for voltages $V \rightarrow 0$ which is due to thermal (Johnson-Nyquist) noise.

In the opposite limit $g/\Gamma > 1$ we propose the polaron tunneling approximation (PTA) to be a valid approximation. It is based on the assumption, that tunneling always leads to a complete phonon cloud excitation or de-excitation, i.e. an electron drags its phonon-cloud with it. In terms of Feynman diagrams, this approximation is represented by

$$D^{\text{PTA}}(t, t') = \text{diagram 1} + \text{diagram 2} + \text{diagram 3} + \dots \quad (2.96)$$

The diagrams represent Feynman diagrams for the polaron tunneling approximation. The first diagram shows a solid line from t to t' with a wavy line (phonon) loop labeled Λ above it. The second diagram shows a solid line from t to t_1 , a dashed line from t_1 to t_2 , and a solid line from t_2 to t' , with a wavy line loop labeled Λ above the solid line from t to t_1 . The third diagram is similar but with the wavy line loop labeled Λ above the solid line from t_2 to t' .

where the solid lines denote the free quantum dot propagator d_0 and the dashed lines the free leads Keldysh functions g_m . This series can be rewritten in a Dyson equation,

$$D^{\text{PTA}}(\omega) = D^{(0)}(\omega) + D^{(0)}(\omega) \Sigma_{\text{T}}(\omega) D^{\text{PTA}}(\omega) \quad (2.97)$$

with the λ -dependent self-energy due to tunneling

$$\Sigma_T = \sum_{m=L,R=\pm} \hat{\gamma}_m g_m(\omega) \hat{\gamma}_m^* \quad (2.98)$$

with

$$\hat{\gamma}_m = \gamma \begin{pmatrix} e^{im\lambda-/4} & 0 \\ 0 & -e^{im\lambda+/4} \end{pmatrix}. \quad (2.99)$$

Hence, one obtains for the quantum dot Keldysh function,

$$D^{\text{PTA}}(\omega) = \frac{1}{\det \mathcal{D}_\lambda^{-1}} \begin{pmatrix} \sum_n \frac{f_n}{\omega - \Delta + n\Omega} + i\Gamma(n_L + n_R - 1) & i\Gamma(e^{i\lambda/2}n_L + e^{-i\lambda/2}n_R) \\ i\Gamma[e^{-i\lambda/2}(n_L - 1) + e^{i\lambda/2}(n_R - 1)] & \sum_n \frac{-f_n}{\omega - \Delta + n\Omega} + i\Gamma(n_L + n_R - 1) \end{pmatrix} \quad (2.100)$$

with

$$\det \mathcal{D}_\lambda^{-1} = \left[\sum_n \frac{f_n}{\omega - \Delta + n\Omega} \right]^{-2} + \Gamma^2(1 + \mathcal{F}_{\lambda+}). \quad (2.101)$$

Therefore, the derivative of the tunneling operator is

$$\left\langle \frac{\delta T_\lambda}{\delta \lambda(t_-)} \right\rangle_\lambda = i \int \frac{d\omega}{2\pi} \ln \det \mathcal{D}_\lambda^{-1}(\omega) \quad (2.102)$$

and hence the CGF

$$\ln \chi(\lambda) = \mathcal{T} \int \frac{d\omega}{2\pi} \ln [1 + T^{\text{PTA}}(\omega) \mathcal{F}_{\lambda+}] \quad (2.103)$$

with effective transmission coefficient

$$T^{\text{PTA}}(\omega) = \frac{\Gamma^2}{\left[\sum_n \frac{f_n}{\omega - \Delta + n\Omega} \right]^{-2} + \Gamma^2}. \quad (2.104)$$

The transmission coefficient is made up of a sequence of peaks at the energies $N\Omega$ for $T = 0$ or $\mathbb{Z}\Omega$ for $T > 0$ and it is properly normalized (see fig. 2.11). To get a rough estimate of the width of the peaks, one can assume a Lorentzian shape. This leads to peaks of widths $2\Gamma e^{-(g/\Omega)^2} (g/\Omega)^{2n} / n!$ in case of zero temperature or $2\Gamma e^{-(g/\Omega)^2(2n_B+1)} I_n \left[2(g/\Omega)^2 \sqrt{n_B(n_B+1)} \right]$ in case of $T > 0$. The maximum peak width must not be the one at $n = 0$. In fact, the maximum peak width can be found approximately at $n \approx (g/\Omega)^2$. In case of $T = 0$ this is obvious. In case of finite temperature, the situation is slightly different. Together with the polaron shift, this leads to the well known Franck-Condon blockade (Koch and von Oppen [2005]): The current in a system with strong-electron phonon interaction is strongly suppressed for small voltages compared to the non-interacting quantum dot. It is possible to have perfect transmission as well as zero transmission. This is due to the special structure of $T^{\text{PTA}}(\omega)$, which is equivalent to the transmission coefficient of a sequence of electronic levels in parallel arrangement with energies $\Delta + n\Omega$. This is a consequence of the PTA, because every single electron tunneling event through the system takes away its polaron cloud and leaves the dot exactly in the same state as before the tunneling event. Hence, the resonance condition is given by $\omega = n\Omega$. The anti-resonance emerges due to an interference effect similarly to

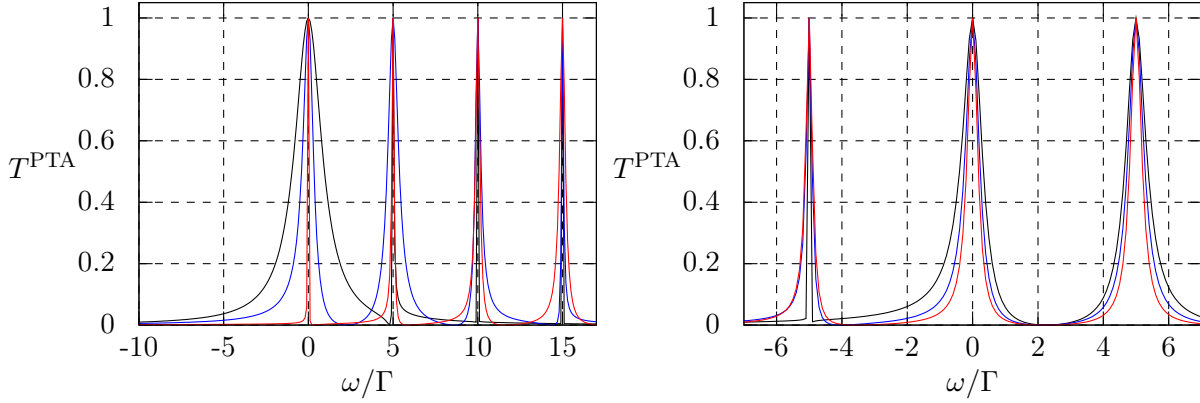


Figure 2.11.: Transmission coefficient in the PTA approximation. **Left panel:** The parameters are temperature $T/\Gamma = 0$, dot level energy $\Delta/\Gamma = 0$ and phonon energy $\Omega/\Gamma = 5$. The electron-phonon coupling constant is varied from $g/\Gamma = 1, 5, 10$ (black, blue and red curve). **Right panel:** The parameters are $\Delta/\Gamma = 0$, $\Omega/\Gamma = 5$ and $g/\Gamma = 5$. The temperature is varied from $T/\Gamma = 1, 5, 10$ (black, blue, red).

the double-dot setup described later on. Current and noise can be obtained via derivatives of the CGF with respect to λ . In fig. 2.12, current and noise are depicted for several interaction strengths and temperatures. The step-like features due to the phonon-resonances are clearly observable. Increasing the electron-phonon coupling constant leads to a more pronounced formation of the single steps. The noise reveals an additional plateau as a novel feature. Again, for zero voltages thermal noise is observed.

2.2.4. Results and discussion

Finally, we would like to compare our approximation schemes to numerical data. Unfortunately, there are not many numerically exact methods available dealing with non-equilibrium quantum impurity systems with vibrational degrees of freedom. In fig. 2.13, we compare our approximation schemes to the numerically exact data taken from Mühlbacher and Rabani [2008]. For reasonably small g/Ω the single particle approximation agrees well with the numerical MC data. For increasing g/Ω the steps in the $I-V$ due to the phonon resonance become steeper which is not accounted for in the single particle approximation. However, the polaron tunneling approximation is able to describe this behaviour quite well. In case of large voltages, both the single particle approximation and the polaron tunneling approximation tend to deviate from the numerical data. This is due to the finite bandwidth of the diagrammatic Monte Carlo simulation which was set to 20Γ . In agreement with Migdals theorem (Migdal [1958]), vertex corrections seem to play a secondary role at least in the current. To the best of our knowledge, there are up to date no numerically exact data available for higher cumulants like the noise. It remains a future task to investigate the role of vertex corrections in higher cumulants.

In conclusion, we developed an approach to calculate the FCS of the Holstein polaron dot in a strong-coupling regime. Using a polaron tunneling approximation, we derived an analytical Levitov-Lesovik formula for the cumulant generating function with an effective, properly normalized transmission coefficient. Our approach yields predictions for zero temperature as well as for arbitrary temperatures, where the phonon is assumed to be thermally equilibrated. The results of these section are

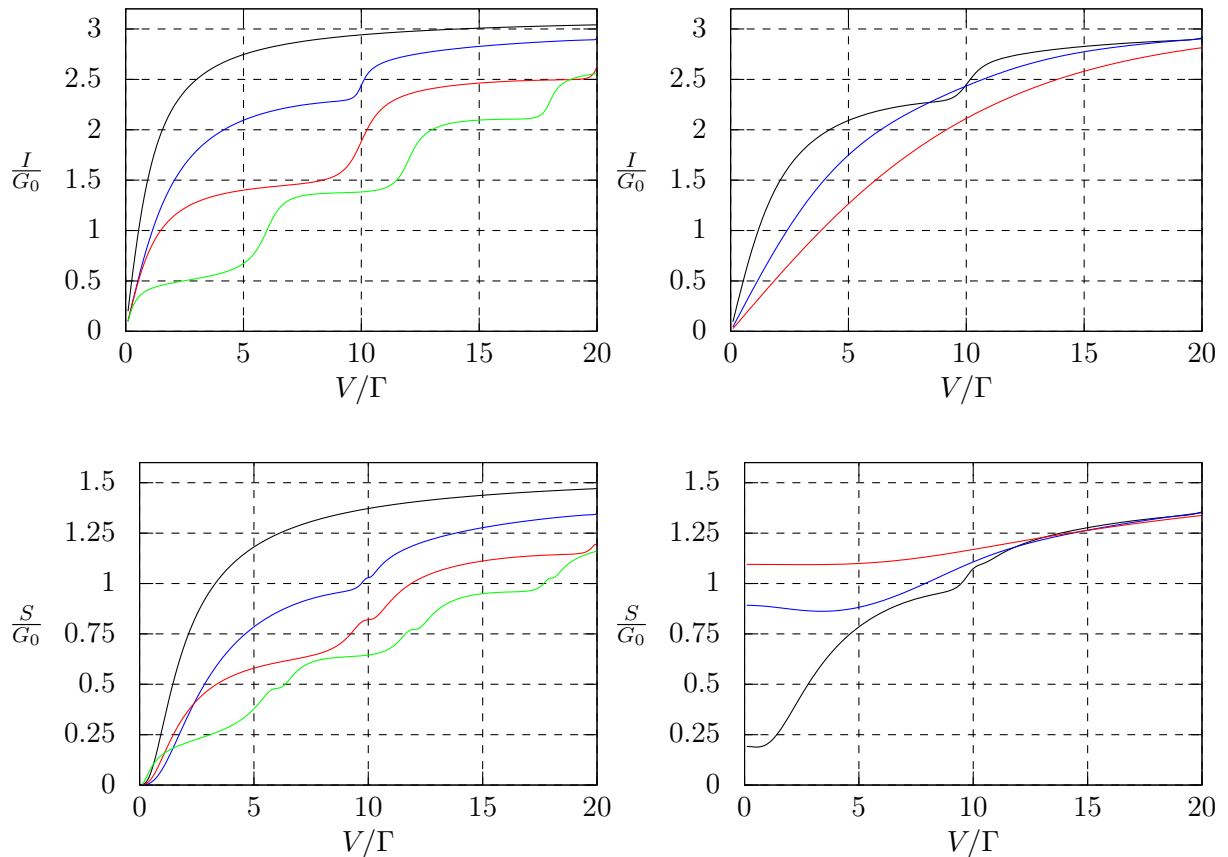


Figure 2.12.: Current and noise in the polaron tunneling approximation. **Left panels:** The dot level energy is fixed to $\Delta/\Gamma = 0$ and the temperature is $T = 0$. The other parameters are $g/\Gamma = 0$ for the black curves, $g/\Gamma = 2, \Omega/\Gamma = 5$ for the blue curves, $g/\Gamma = 4, \Omega/\Gamma = 5$ for the red curves and $g/\Gamma = 4, \Omega/\Gamma = 3$ for the green curves. **Right panels:** The dot level energy is fixed to $\Delta/\Gamma = 0$, $g/\Gamma = 2$ and $\Omega/\Gamma = 5$. The temperature is varied from $T/\Gamma = 0.1, 1, 2$ (black, blue and red curves).

published in [Maier et al. \[2011\]](#).

2.3. Effects of electron-phonon interaction in the interacting resonant level model

In the previous section, we mainly focused on quantum dots with internal degrees of freedom coupled to non-interacting metallic leads. In this paragraph we incorporate interactions in the reservoirs and an additional capacitive coupling between leads and quantum dot. It is well known that for a certain parameter constellation – the so called Toulouse limit – the transmission properties of such systems show a rather surprising dependency on the position of the electronic dot level. The system at resonance shows perfect transmission for small energies. An arbitrarily small detuning of the dot level position, however, leads to a complete blocking of the system. We are asking the question how electron-phonon interaction modifies this situation.

Probably one of the most prominent features of electron-phonon interaction in quantum impurity models is the different behavior of the conductance which can grow or decline as soon as the applied

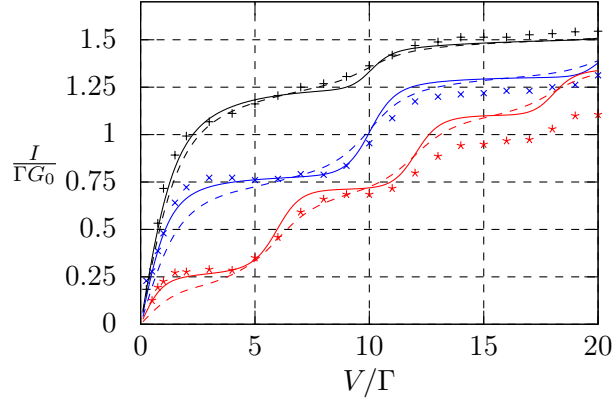


Figure 2.13.: Comparison of approximation schemes with diagrammatic Monte Carlo data. The solid lines represent the polaron tunneling approximation, the dashed lines represent the single particle approximation and the plot markers the diagrammatic Monte Carlo simulation results (Mühlbacher and Rabani [2008]). The dot level energy is fixed to $\Delta = 0$ and the temperature is set to $T/\Gamma = 0.2$. The other parameters are $g/\Gamma = 2, \Omega/\Gamma = 5$ black set, $g/\Gamma = 4, \Omega/\Gamma = 5$ blue set and $g/\Gamma = 4, \Omega/\Gamma = 3$ red set. The Monte Carlo method uses a finite bandwidth of 20Γ and a slightly different definition of the hybridization Γ .

voltage gets larger than the phonon frequency (Avriller and Levy Yeyati [2009], de la Vega et al. [2006], Egger and Gogolin [2008], Haupt et al. [2009], Mii et al. [2003], Paulsson et al. [2005], Schmidt and Komnik [2009]). This phenomenon can be understood as follows: at zero temperature and voltage the vibrational degrees of freedom can be safely assumed to be frozen out and one effectively deals with the (noninteracting) resonant level with some energy Δ_0 . The spectral function of the quantum dot is a single Lorentzian of some width Γ (which is related to the hybridization of the dot level with the electrode) centered around Δ_0 . For the large initial transmittance of the system, Δ_0 should lie in between the chemical potentials of the contacting electrodes. On the opposite, for small transmittance, Δ_0 is well below/above the chemical potentials. The system is virtually insulating at $|\Delta_0| \gg \Gamma$ because then the spectral weight around the chemical potentials position, which is necessary for transmission, is very small. When the phonon gets excited its spectral function is known to develop equidistant sidebands (Braig and Flensberg [2003]). The central peak at Δ_0 persists but, due to spectral weight redistribution, its height diminishes. Therefore, the initially large transmission drops as soon as the vibrational degrees of freedom can be excited. On the contrary, due to the finite spectral weight in the sidebands the conductance grows for the out-of-resonance Δ_0 . It turns out that, in general, the crossover from enhanced to suppressed transmission does not correspond to any universal parameter constellation apart from the limiting cases of large/small Δ_0 (see Egger and Gogolin [2008], Schmidt and Komnik [2009]).

Thus far, only few authors have considered the properties of such systems in case of interacting electrodes (Fehske et al. [2008], Takei et al. [2005]). While in Takei et al. [2005] the high-temperature regime of molecules contacted by interacting electrodes is discussed, Fehske et al. [2008] contains a numerical treatment of the problem in equilibrium. Given the small dimensions of the corresponding devices, it is very likely that the electrodes might in fact possess genuine one-dimensional geometry as far as the electronic degrees of freedom are concerned. Alternatively, one might conceive a device contacted, e.g. by armchair carbon nanotubes, which are known to host one-dimensional electrons. In these situations one deals with the Tomonaga-Luttinger liquids (TLLs, see Egger and Gogolin [1997], Kane et al. [1997]) instead of conventional Fermi liquids. Their most prominent feature is the power-law singularity of the local density of states in the vicinity of the Fermi edge. Among

other things, it results in complete suppression of transmission in presence of impurities in the low energy sectors leading to the zero-bias anomaly (Furusaki and Nagaosa [1993], Kane and Fisher [1992]). As a result, the transmission through a featureless quantum dot coupled to two TLLs vanishes toward small voltages and low temperatures (Furusaki [1998], Kane and Fisher [1992], Komnik and Gogolin [2003b], Nazarov and Glazman [2003], Polyakov and Gornyi [2003]). The only exception is the perfect resonant setup when $\Delta_0 = 0$ and hybridizations with both electrodes are equal to each other. Thus, contrary to the noninteracting electrodes, when the dot transmission can smoothly interpolate between perfect and zero transmission, in the TLL setup, only two low-energy transmission regimes are possible: either zero or unity. Applying the above line of reasoning, one might conclude that in the former case, the current through the system starts to flow only after the voltage gets larger than the phonon frequency. In the opposite case, one would expect that the conductance of an initially perfectly transmitting dot would rapidly decrease above the threshold set by the phonon frequency. In the following, we are aiming at an understanding of transport properties of such a setup and want to quantify this heuristic picture. In order to proceed, one needs a model which can equally well describe the off-resonant as well as the perfectly transmitting case.

2.3.1. The model and its Toulouse point

The system can be described by the Hamiltonian

$$H = H_0 + H_T + H_C + H_{e-ph} \quad (2.105)$$

where the single contributions are

$$H_0 = H_{\text{leads}}[\psi_L, \psi_R] + \Delta_0 d^\dagger d + \Omega B^\dagger B \quad (2.106)$$

describing the leads, the single dot level with dot level energy Δ_0 and a phonon with frequency Ω . ψ_L, ψ_R are the field operators of the leads, d the annihilation operator of the quantum dot level and B the annihilation operator of the phonon mode. The Hamiltonian of the leads, H_{leads} is described later in the framework of bosonization (see Fabrizio and Gogolin [1995], Gogolin et al. [1998], Kane and Fisher [1992]). H_T describes the tunneling processes from the leads to the dot and vice versa,

$$H_T = \sum_{\alpha=L,R} \gamma_\alpha \psi_\alpha^\dagger(0) d + \text{H.c.}, \quad (2.107)$$

with the tunneling amplitudes γ_R, γ_L . The electrostatic interaction H_C is given by

$$H_C = U_C d^\dagger d \sum_{\alpha=L,R} \psi_\alpha^\dagger(0) \psi_\alpha(0) \quad (2.108)$$

with interaction strength U_C . The electron-phonon interaction is modeled via

$$H_{e-ph} = g d^\dagger d (B^\dagger + B) \quad (2.109)$$

with electron-phonon coupling strength g . As usual, a source-drain voltage is applied across the junction in a symmetric way, i.e. $\mu_L = -\mu_R = V/2$. In fig. 2.14, the occurring energy scales of the model are depicted. In order to calculate the full counting statistics, the tunneling Hamiltonian has to be equipped with counting fields,

$$T_\lambda = \sum_{\alpha=L,R=\pm} \gamma_\alpha e^{i\alpha\frac{\lambda}{4}} \psi_\alpha^\dagger(0) d + \text{H.c.} \quad (2.110)$$

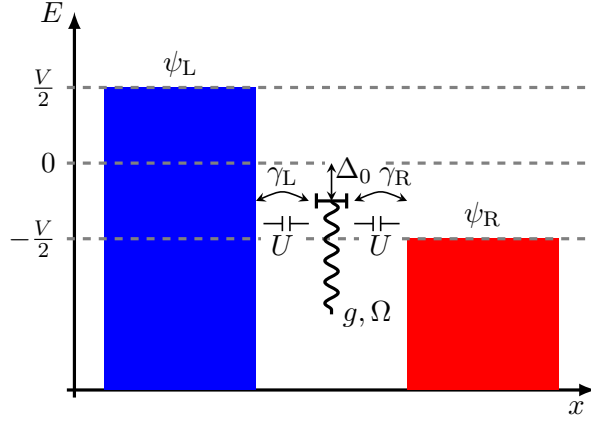


Figure 2.14.: Energy scales of the interacting resonant level model with bosonic degree of freedom.

where we have used the sum convention as before, $\alpha \in \{L = +1, R = -1\}$. Using bosonization procedure (see Gogolin et al. [1998]),

$$\psi_\alpha(x) = \frac{\eta_\alpha}{\sqrt{2\pi a_0}} e^{i\phi_\alpha(x)/K} \quad (2.111)$$

where K is the usual Luttinger parameter, $K = 1/\sqrt{1 + \frac{U}{\pi v_F}}$, η_α a Klein factor to ensure fermionic anti-commutation relations with the dot level operator and a_0 the lattice constant of an underlying lattice model. U is the bare electron-electron interaction strength in the leads. The bosonic field $\phi(x)$ describes the slow varying component of the local electron density, i.e. plasmons. We have chosen units where the renormalized Fermi velocity v is unity $v = v_F/K = 1$. Instead of referring to an underlying lattice spacing, i.e. including a momentum cut-off, we could have used normal ordering to express the fermionic fields in terms of bosons. Both procedures, however, are equivalent. Using eq. (2.111) and an analogous expression for the local density (see Gogolin et al. [1998]),

$$\rho_\alpha(x) = \psi_\alpha^\dagger(x) \psi_\alpha(x) = \frac{\partial_x \phi_\alpha(x)}{2\pi\sqrt{K}} \quad (2.112)$$

together with the spin representation of the dot level operator,

$$S_x = \frac{d + d^\dagger}{2}, \quad S_y = i\frac{d - d^\dagger}{2}, \quad S_z = d^\dagger d - \frac{1}{2} \quad (2.113)$$

we can associate bosonized counterparts for the single contributions of the Hamiltonian in eq. (2.105). For the free Hamiltonian, one finds

$$H_0 = H_{\text{leads}}[\phi_L, \phi_R] + \Delta_0 S_z + \Omega B^\dagger B \quad (2.114)$$

with

$$H_{\text{leads}}[\phi_L, \phi_R] = \frac{1}{4\pi} \sum_{\alpha=L,R} \int dx [\partial_x \phi_\alpha(x)]^2 + \frac{V}{2} \int dx [\rho_L(x) - \rho_R(x)] \quad (2.115)$$

where V is the symmetrically applied source-drain voltage. The tunneling contribution transforms to

$$T_\lambda = \sum_{\alpha=L,R=\pm} \left[\frac{\gamma_\alpha \eta_\alpha}{\sqrt{2\pi a_0}} e^{i\alpha \frac{\lambda}{4}} e^{-i\phi_\alpha(0)/K} S_- + S_+ \frac{\gamma_\alpha^* \eta_\alpha}{\sqrt{2\pi a_0}} e^{-i\alpha \frac{\lambda}{4}} e^{i\phi_\alpha(0)/K} \right] \quad (2.116)$$

where we have introduced the ladder operators $S_{\pm} = S_x \pm iS_y = d^{\dagger}, d$. The capacitive contribution resembles the S_z to density coupling term in the Kondo Hamiltonian,

$$H_C = \frac{U_C}{2\pi\sqrt{K}} S_z \sum_{\alpha=L,R} \partial_x \Big|_{x=0} \phi_{\alpha}(x). \quad (2.117)$$

For the electron-phonon interaction, we find

$$H_{e-ph} = gS_z (B + B^{\dagger}). \quad (2.118)$$

We disregarded constant shifts in energy which do not affect transport properties. Using even/odd fields, $\phi_{\pm} = \frac{\phi_L \pm \phi_R}{\sqrt{2}}$ and the Emery-Kivelson rotation ([Emery and Kivelson \[1992\]](#)),

$$U_{EK} = \exp \left[i \frac{S_z \phi_+(0)}{\sqrt{2K}} \right] \quad (2.119)$$

the transformed Hamiltonian $U_{EK} H U_{EK}^{\dagger}$ is given by

$$H_0 + H_C + H_{e-ph} \rightarrow H_0 + H_{e-ph} + \left[\frac{U_C}{\pi\sqrt{2K}} - \sqrt{\frac{2}{K}} \right] S_z \partial_x \Big|_{x=0} \phi_-(x) \quad (2.120)$$

and

$$T_{\lambda} \rightarrow \sum_{\alpha=L,R=\pm} \left[\frac{\gamma_{\alpha} \eta_{\alpha}}{\sqrt{2\pi a_0}} e^{i\alpha \frac{\lambda}{4}} e^{-i\alpha \phi_-(0)/\sqrt{2K}} S_{-} + S_{+} \frac{\gamma_{\alpha}^* \eta_{\alpha}}{\sqrt{2\pi a_0}} e^{-i\alpha \frac{\lambda}{4}} e^{i\alpha \phi_-(0)/\sqrt{2K}} \right]. \quad (2.121)$$

Here, we can already draw some interesting conclusions. First, odd/even channel ϕ_{\pm} completely decouple. The dynamics of the even channel ϕ_+ even in presence of interactions is trivial. Therefore, it does not affect the transport properties and will be neglected in the following. Secondly, for $U_C = 2\pi$, the particle-particle interaction contribution in eq. (2.120) vanishes. Thirdly, if additionally $K = 1/2$ holds, the refermionized model is quadratic up to the electron-phonon interaction. This point in parameter space is one of the Toulouse points ([Schiller and Hershfield \[1998\]](#)) and are extremely rare. In the following, we will always assume to be in the Toulouse limit. But first we like to clarify, why Toulouse points besides of being a benchmark for numerical calculations are extremely useful. Deviations from $U_C = 2\pi$ leads to corrections which are in the sense of renormalization group irrelevant ([Komnik and Gogolin \[2003a\]](#)). In the low energy regime (temperature smaller than the Kondo temperature $D e^{-1/\Gamma a_0}$, D bandwidth, Γ hybridization) these corrections are negligible. Detuning of $K = 1/2$ is much more involved. Increasing the bare particle-particle interaction U i.e. decreasing K in general leads to completely different behaviour. However, decreasing the bare interaction, i.e. $1/2 < K < 1$ leaves the basic properties intact. Perturbation theory in the fashion of [Weiss et al. \[1995\]](#) is then applicable.

Refermionization of the bosonic field $\psi_- \propto \frac{1}{\sqrt{2\pi a_0}} e^{i\phi_-}$, using Majorana representation of quantum dot and field operators

$$d = \frac{a + ib}{\sqrt{2}}, \quad \psi_- = \frac{\xi + i\eta}{\sqrt{2}} \quad (2.122)$$

and introducing new tunneling couplings $\gamma_{\pm} = \gamma_L \pm \gamma_R$ lead to

$$H = H_{\text{leads}}[\xi, \eta] + iab \left[\Delta_0 + g (B + B^{\dagger}) \right] + \Omega B^{\dagger} B + T_{\lambda} \quad (2.123)$$

with

$$H_{\text{leads}}[\xi, \eta] = \int dx [\xi(x) \partial_x \xi(x) + \eta(x) \partial_x \eta(x) + V \xi(x) \eta(x)] \quad (2.124)$$

and

$$T_\lambda = i\gamma_- \left[a\eta \cos\left(\frac{\lambda}{2}\right) - a\xi \sin\left(\frac{\lambda}{2}\right) \right] - i\gamma_+ \left[b\xi \cos\left(\frac{\lambda}{2}\right) + b\eta \sin\left(\frac{\lambda}{2}\right) \right] \quad (2.125)$$

which is known as the Majorana resonant level model (MRLM) with an additional electron-phonon coupling. In contrast to the IRLM we started with, the MRLM seems only to depend on the voltage V instead of $V/2$.

2.3.2. Full counting statistics in absence of e-ph coupling

In order to calculate the transport characteristics of the IRLM one first needs the Keldysh functions for the isolated subsystems,

$$g_{\alpha\beta}(t-t') = -i \langle T_C \alpha(t) \beta(t') \rangle \quad (2.126)$$

$$d_{fh}(t-t') = -i \langle T_C f(t) h(t') \rangle \quad (2.127)$$

where $\alpha, \beta \in \{\xi, \eta\}$ and $f, h \in \{a, b\}$. We start with the Keldysh functions of the reservoirs⁶. This can be achieved by reducing the calculation to the calculation of Keldysh functions of non-interacting fermions with chemical potential $\mu = V$ (see eq. (2.124)),

$$H_{\text{leads}}[\psi_-] = \int dx \left[\psi_-^\dagger(x) i\partial_x \psi_-(x) + V \psi_-^\dagger(x) \psi_-(x) \right]. \quad (2.128)$$

Using eq. (2.122), the homogeneous Keldysh functions $g_{\alpha\alpha}$ ($\alpha \in \{\xi, \eta\}$) can be rewritten,

$$g_{\alpha\alpha}(t-t') = -\frac{i}{2} \left[\langle T_C \psi_-^\dagger(t) \psi_-(t') \rangle + \langle T_C \psi_-(t) \psi_-^\dagger(t') \rangle \right] = \frac{1}{2} [g(t-t') - g(t'-t)] \quad (2.129)$$

where g was calculated in eq. (A.36) with chemical potential $\mu = V$ and density of states at the Fermi edge $\rho_0 = 1/2\pi$. Therefore, the homogeneous Green's functions in Fourier space are (Komnik and Gogolin [2003b])

$$g_{\xi\xi}(\omega) = g_{\eta\eta}(\omega) = \frac{i}{2} \begin{pmatrix} n_L + n_R - 1 & n_L + n_R \\ n_L + n_R - 2 & n_L + n_R - 1 \end{pmatrix} \quad (2.130)$$

with $n_L(\omega) = n_F(\omega - V)$ and $n_R(\omega) = n_F(\omega + V)$ where we have used the relation $n_F(-\omega, \mu) = 1 - n_F(\omega, -\mu)$ of the Fermi-Dirac distribution function. The inhomogeneous/mixed Keldysh function of the leads can analogously be calculated:

$$g_{\xi\eta}(t-t') = -g_{\eta\xi}(t-t') = \frac{i}{2} [g(t-t') + g(t'-t)] \quad (2.131)$$

or in Fourier space

$$g_{\xi\eta}(\omega) = -g_{\eta\xi}(\omega) = -\frac{n_L - n_R}{2} \begin{pmatrix} 1 & 1 \\ 1 & 1 \end{pmatrix}. \quad (2.132)$$

⁶As usual, we are only interested in the behaviour near the impurity site, $x = 0$.

The next step is the calculation of the impurity Keldysh functions. We proceed as before and start with the homogeneous one,

$$d_{ff}(t-t') = -\frac{i}{2} \left[\langle T_C d(t) d^\dagger(t') \rangle + \langle T_C d^\dagger(t) d(t') \rangle \right] = \frac{1}{2} [d(t-t') - d(t'-t)] \quad (2.133)$$

which, in energy space takes the form,

$$d_{aa}(\omega) = d_{bb}(\omega) = \frac{\omega}{\omega^2 - \Delta_0^2} \begin{pmatrix} 1 & 0 \\ 0 & -1 \end{pmatrix} \quad (2.134)$$

and similarly, for the mixed Greens functions,

$$d_{ab}(t-t') = -d_{ba}(t-t') = \frac{i}{2} [d(t-t') - d(t'-t)] \quad (2.135)$$

resp. in Fourier space

$$d_{ab}(\omega) = -d_{ba}(\omega) = -\frac{i\Delta_0}{\omega^2 - \Delta_0^2} \begin{pmatrix} 1 & 0 \\ 0 & -1 \end{pmatrix}. \quad (2.136)$$

Again, we are using the functional integral formalism to calculate the full counting statistics for the unperturbed system. The Keldysh action is $S = S_0 + S_T[\lambda]$ where the free contribution is

$$S_0 = \int \frac{d\omega}{2\pi} \left[\Psi_{\xi\eta}^\dagger(\omega) \mathfrak{g}_{\xi\eta}^{-1}(\omega) \Psi_{\xi\eta}(\omega) + \mathbf{c}_{ab}^\dagger(\omega) \mathfrak{d}_{ab}^{-1}(\omega) \mathbf{c}_{ab}(\omega) \right] \quad (2.137)$$

and the contribution due to tunneling

$$S_T[\lambda] = \int \frac{d\omega}{2\pi} \mathbf{c}_{ab}^\dagger(\omega) \Gamma_\lambda \Psi_{\xi\eta}(\omega). \quad (2.138)$$

We have introduced the combined Majorana Keldysh vectors $\Psi_{\xi\eta} = (\xi_-, \xi_+, \eta_-, \eta_+)$ and $\mathbf{c}_{ab} = (a_-, a_+, b_-, b_+)$, the 4×4 Keldysh matrices

$$\mathfrak{g}_{\xi\eta} = \begin{pmatrix} g_{\xi\xi} & g_{\xi\eta} \\ g_{\eta\xi} & g_{\eta\eta} \end{pmatrix} \quad \mathfrak{d}_{ab} = \begin{pmatrix} d_{aa} & d_{ab} \\ d_{ba} & d_{bb} \end{pmatrix} \quad (2.139)$$

and

$$\Gamma_\lambda = i \begin{pmatrix} -\gamma_- \sin\left(\frac{\lambda_-}{2}\right) & 0 & \gamma_- \cos\left(\frac{\lambda_-}{2}\right) & 0 \\ 0 & \gamma_- \sin\left(\frac{\lambda_+}{2}\right) & 0 & -\gamma_- \cos\left(\frac{\lambda_+}{2}\right) \\ -\gamma_+ \cos\left(\frac{\lambda_-}{2}\right) & 0 & -\gamma_+ \sin\left(\frac{\lambda_-}{2}\right) & 0 \\ 0 & \gamma_+ \cos\left(\frac{\lambda_+}{2}\right) & 0 & \gamma_+ \sin\left(\frac{\lambda_+}{2}\right) \end{pmatrix}. \quad (2.140)$$

As before in the resonant level model (appendix A.3), the cumulant generating function is given by

$$\ln \chi(\lambda) = \ln \frac{\mathcal{Z}[\lambda]}{\mathcal{Z}[\lambda=0]}, \quad (2.141)$$

where $\mathcal{Z}[\lambda]$ is the Keldysh partition function (Kamenev and Levchenko [2009])

$$\mathcal{Z}[\lambda] = \int \mathcal{D}[\Psi_{\xi\eta}, \mathbf{c}_{ab}] e^{-S_0 - S_T[\lambda]}. \quad (2.142)$$

The path integral of the lead degrees of freedom can easily be performed by introducing auxiliary fields $\Psi'_{\xi\eta}$,

$$\Psi_{\xi\eta}(\omega) = -\frac{1}{2}\mathfrak{g}_{\xi\eta}(\omega)\mathbf{\Gamma}_\lambda^\top\mathbf{c}_{ab} + \Psi'_{\xi\eta}(\omega), \quad \Psi_{\xi\eta}^\top(\omega) = -\frac{1}{2}\mathbf{c}_{ab}^\top\mathbf{\Gamma}_\lambda\mathfrak{g}_{\xi\eta}(\omega) + \Psi_{\xi\eta}'^\top(\omega). \quad (2.143)$$

The Keldysh action transforms to

$$S = \int \frac{d\omega}{2\pi} \left\{ \mathbf{c}_{ab}^\top \left[\mathfrak{d}_{ab}^{-1}(\omega) + \frac{1}{4}\mathbf{\Gamma}_\lambda\mathfrak{g}_{\xi\eta}(\omega)\mathbf{\Gamma}_\lambda^\top \right] \mathbf{c}_{ab} + \Psi_{\xi\eta}'^\top(\omega)\mathfrak{g}_{\xi\eta}^{-1}(\omega)\Psi'_{\xi\eta}(\omega) \right\}. \quad (2.144)$$

Integrating out the remaining fields yields the CGF

$$\ln \chi(\lambda) = \ln \prod_{\omega} \frac{\det \left[\mathfrak{d}_{ab}^{-1}(\omega) + \frac{1}{4}\mathbf{\Gamma}_\lambda\mathfrak{g}_{\xi\eta}(\omega)\mathbf{\Gamma}_\lambda^\top \right] \Big|_{\lambda_- = -\lambda_+ = \lambda/2}}{\det \left[\mathfrak{d}_{ab}^{-1}(\omega) + \frac{1}{4}\mathbf{\Gamma}_\lambda\mathfrak{g}_{\xi\eta}(\omega)\mathbf{\Gamma}_\lambda^\top \right] \Big|_{\lambda_- = \lambda_+ = 0}} \quad (2.145)$$

$$= \mathcal{T} \int \frac{d\omega}{2\pi} \frac{\det \left[\mathfrak{d}_{ab}^{-1}(\omega) + \frac{1}{4}\mathbf{\Gamma}_\lambda\mathfrak{g}_{\xi\eta}(\omega)\mathbf{\Gamma}_\lambda^\top \right] \Big|_{\lambda_- = -\lambda_+ = \lambda/2}}{\det \left[\mathfrak{d}_{ab}^{-1}(\omega) + \frac{1}{4}\mathbf{\Gamma}_\lambda\mathfrak{g}_{\xi\eta}(\omega)\mathbf{\Gamma}_\lambda^\top \right] \Big|_{\lambda_- = \lambda_+ = 0}} \quad (2.146)$$

where in the last line we performed the continuum limit. The result again has Levitov-Lesovik form,

$$\ln \chi(\lambda) = \mathcal{T} \int \frac{d\omega}{2\pi} \ln \left\{ 1 + T(\omega) \left[\left(e^{i\lambda} - 1 \right) n_L (1 - n_R) + \left(e^{-i\lambda} - 1 \right) n_R (1 - n_L) \right] \right\} \quad (2.147)$$

with transmission coefficient (Komnik and Gogolin [2003b])

$$T(\omega) = \frac{4E^2\gamma^2}{(E^2 + \beta_+^2)(E^2 + \beta_-^2) + 2\gamma^2(E^2 + \beta_+\beta_-) + \gamma^4} \quad (2.148)$$

where we have defined

$$E = \Delta_0^2 - \omega^2, \quad \beta_{\pm} = \frac{(1 - 2\alpha)\Delta_0 \pm \omega}{2}, \quad \gamma = \omega\sqrt{\alpha(1 - \alpha)}, \quad \alpha = \frac{\gamma_L^2}{\gamma_L^2 + \gamma_R^2} \quad (2.149)$$

and all energies are measured in units of $\Gamma = \gamma_L^2 + \gamma_R^2$. The quantity α describes the asymmetry of the tunneling coupling. In case of $\gamma_L = \gamma_R$, i.e. $\alpha = 1/2$, the transmission coefficient resembles the simple form

$$T(\omega) = \frac{\omega^2}{(\Delta_0^2 - \omega^2)^2 + \Gamma^2\omega^2} \quad (2.150)$$

with hybridization $\Gamma = \gamma_R^2/2$. The low energy behaviour of the transmission coefficient of the system is fundamentally different for the resonant and off-resonant case. The first one is completely transparent, i.e. $T(0) = 1, \Delta_0 = 0$ and the latter one is completely opaque, i.e. $T(0) = 0, \Delta_0 \neq 0$. In fig. 2.15, the transmission coefficient is depicted for several values of detuning Δ_0 .

2.3.3. Keldysh functions of the impurity site

In this section, we provide the Keldysh function of the quantum dot which are exact in tunneling. The calculation is straightforward. Using eq. (2.144), one can immediately identify the Dyson equation

$$\mathbf{D}_{ab}(\omega) = \left[\mathfrak{d}_{ab}^{-1}(\omega) + \frac{1}{4}\mathbf{\Gamma}_\lambda\mathfrak{g}_{\xi\eta}(\omega)\mathbf{\Gamma}_\lambda^\top \right]^{-1} = \left[\mathfrak{d}_{ab}^{-1}(\omega) - \mathbf{\Sigma}_T(\omega) \right]^{-1} \quad (2.151)$$

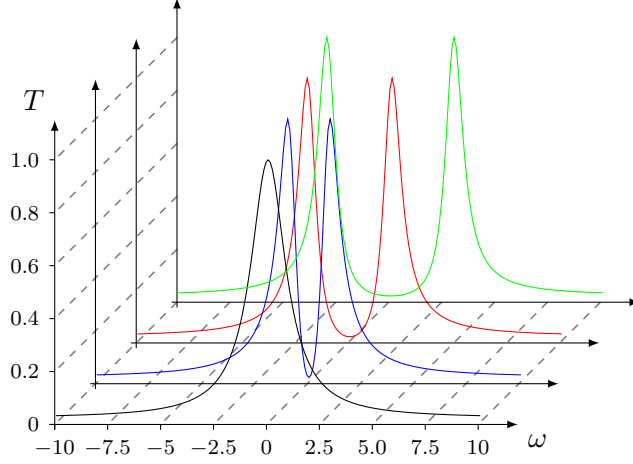


Figure 2.15.: Transmission coefficient of the interacting resonant level in the Toulouse limit. The dot level position is varied from $\Delta_0/\Gamma = 0, 1, 2, 3$ (black, blue, red, green).

where Σ_T is the self energy due to tunneling. The homogeneous and mixed Keldysh functions of the quantum dot exact in tunneling can then be identified as components of the 4×4 Keldysh matrix \mathbf{D}_{ab} ,

$$\mathbf{D}_{ab} = \begin{pmatrix} D_{aa} & D_{ab} \\ D_{ba} & D_{bb} \end{pmatrix}. \quad (2.152)$$

In the following we will restrict ourselves to the symmetric case, i.e. $\gamma_- = 0$. In general, the calculation can be done for the asymmetric case. However, the results are quite lengthy and less universal. For the homogeneous Majorana a -channel we find

$$\begin{aligned} \mathcal{D}_\lambda D_{aa}^{--}(\omega) &= -i\Gamma\Delta_0^2(n_L + n_R - 1) + \omega(\omega^2 - \Delta_0^2) + \omega\Gamma^2(1 + \mathcal{F}_{\lambda+}) \\ \mathcal{D}_\lambda D_{aa}^{-+}(\omega) &= -\Gamma\Delta_0^2[i(n_L + n_R)\cos(\lambda/2) - (n_L - n_R)\sin(\lambda/2)] \\ \mathcal{D}_\lambda D_{aa}^{+-}(\omega) &= -\Gamma\Delta_0^2[i(n_L + n_R - 2)\cos(\lambda/2) + (n_L - n_R)\sin(\lambda/2)] \\ \mathcal{D}_\lambda D_{aa}^{++}(\omega) &= -i\Gamma\Delta_0^2(n_L + n_R - 1) - \omega(\omega^2 - \Delta_0^2) - \omega\Gamma^2(1 + \mathcal{F}_{\lambda+}) \end{aligned} \quad (2.153)$$

with

$$\mathcal{F}_{\lambda\pm} = (e^{i\lambda} - 1)n_L(1 - n_R) \pm (e^{-i\lambda} - 1)n_R(1 - n_L) \quad (2.154)$$

$$\mathcal{D}_\lambda = \mathcal{D}_0 + \omega^2\Gamma^2\mathcal{F}_{\lambda-} \quad (2.155)$$

$$\mathcal{D}_0 = (\omega^2 - \Delta_0^2)^2 + \omega^2\Gamma^2 \quad (2.156)$$

and for the Majorana b -channel

$$\begin{aligned} \mathcal{D}_\lambda D_{bb}^{--}(\omega) &= -i\Gamma\omega^2(n_L + n_R - 1) + \omega(\omega^2 - \Delta_0^2) \\ \mathcal{D}_\lambda D_{bb}^{-+}(\omega) &= -\Gamma\omega^2[i(n_L + n_R)\cos(\lambda/2) - (n_L - n_R)\sin(\lambda/2)] \\ \mathcal{D}_\lambda D_{bb}^{+-}(\omega) &= -\Gamma\omega^2[i(n_L + n_R - 2)\cos(\lambda/2) + (n_L - n_R)\sin(\lambda/2)] \\ \mathcal{D}_\lambda D_{bb}^{++}(\omega) &= -i\Gamma\omega^2(n_L + n_R - 1) - \omega(\omega^2 - \Delta_0^2). \end{aligned} \quad (2.157)$$

The Keldysh functions for the mixed channels are

$$\begin{aligned} \mathcal{D}_\lambda D_{ab}^{--}(\omega) &= -\omega\Gamma\Delta_0(n_L + n_R - 1) - i\Delta_0(\omega^2 - \Delta_0^2) \\ \mathcal{D}_\lambda D_{ab}^{-+}(\omega) &= -\omega\Gamma\Delta_0[(n_L + n_R)\cos(\lambda/2) + i(n_L - n_R)\sin(\lambda/2)] \\ \mathcal{D}_\lambda D_{ab}^{+-}(\omega) &= -\omega\Gamma\Delta_0[(n_L + n_R - 2)\cos(\lambda/2) - i(n_L - n_R)\sin(\lambda/2)] \\ \mathcal{D}_\lambda D_{ab}^{++}(\omega) &= -\omega\Gamma\Delta_0(n_L + n_R - 1) + i\Delta_0(\omega^2 - \Delta_0^2) \end{aligned} \quad (2.158)$$

and obviously $D_{ab} = -D_{ba}$.

2.3.4. The resonant case

In this section, we discuss the effect of electron-phonon interaction on the full counting statistics at resonance, i.e. $\Delta_0 = 0$. In this case, the mixed Keldysh functions are identically zero, $D_{ab} = 0$. The homogeneous Keldysh functions for the Majorana a -channel become diagonal and counting field independent,

$$D_{aa}(\omega) = \begin{pmatrix} \frac{1}{\omega} & 0 \\ 0 & -\frac{1}{\omega} \end{pmatrix} \quad (2.159)$$

and the Majorana b -channel

$$\begin{aligned} [\omega^2 + \Gamma^2 (1 + \mathcal{F}_{\lambda-})] D_{bb}^{--}(\omega) &= -i\Gamma (n_L + n_R - 1) + \omega \\ [\omega^2 + \Gamma^2 (1 + \mathcal{F}_{\lambda-})] D_{bb}^{+-}(\omega) &= -\Gamma [i(n_L + n_R) \cos(\lambda/2) - (n_L - n_R) \sin(\lambda/2)] \\ [\omega^2 + \Gamma^2 (1 + \mathcal{F}_{\lambda-})] D_{bb}^{+0}(\omega) &= -\Gamma [i(n_L + n_R - 2) \cos(\lambda/2) + (n_L - n_R) \sin(\lambda/2)] \\ [\omega^2 + \Gamma^2 (1 + \mathcal{F}_{\lambda-})] D_{bb}^{++}(\omega) &= -i\Gamma (n_L + n_R - 1) - \omega. \end{aligned} \quad (2.160)$$

The full counting statistics including interaction can be calculated via

$$\chi(\lambda) = \left\langle e^{-i(ig) \int_C d\tau a(\tau)b(\tau)[B(\tau)+B^\dagger(\tau)]} \right\rangle \quad (2.161)$$

$$= \chi_0(\lambda) \left\langle e^{-i(ig) \int_C d\tau a(\tau)b(\tau)[B(\tau)+B^\dagger(\tau)]} \right\rangle_\lambda \quad (2.162)$$

where the expectation value in the first line $\langle \cdot \rangle$ has to be calculated with respect to the Hamiltonian eq. (2.123) in absence of interactions, $g = 0$ and in the second line, the usual λ -expectation value has been introduced. $\chi_0(\lambda)$ denotes the full counting statistics in absence of interactions which was calculated in the previous section. The leading order correction to the CGF, $\ln \chi'(\lambda)$ can then be

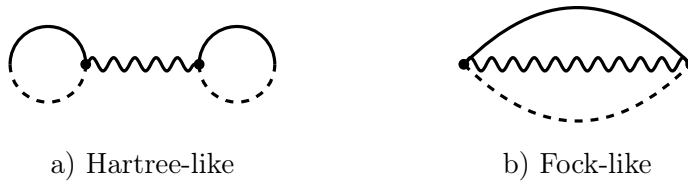


Figure 2.16.: Leading order Feynman diagrams. Solid lines — represent D_{aa} propagators, dashed lines - - - - D_{bb} propagators, mixed lines - · - · - D_{ab} propagators and wavy lines phonon propagators.

obtained with the linked-cluster expansion,

$$\ln \chi'(\lambda) = \ln \chi'_H(\lambda) + \ln \chi'_F(\lambda) \quad (2.163)$$

where the Hartree-like contribution (see Fig. 2.16) is

$$\ln \chi'_H = -i \frac{g^2}{2} \sum_{k,l=\pm} (kl) \int dt_1 dt_2 b_0^{kl}(t_1 - t_2) D_{ab}^{kk}(-k0^+) D_{ab}^{ll}(-l0^+) \quad (2.164)$$

which identically vanishes in the resonant case, and the Fock-like contribution,

$$\ln \chi'_F = \mathcal{T} \frac{g^2}{2} \sum_{k,l=\pm} (kl) \int \frac{d\omega}{2\pi} b_0^{kl}(\omega) \pi^{kl}(\omega) \quad (2.165)$$

where we have introduced the polarization loop π^{kl}

$$\pi^{kl}(\omega) = -i \int \frac{dy}{2\pi} \left[D_{ab}^{kl}(y) D_{ab}^{lk}(\omega+y) - D_{aa}^{kl}(y) D_{bb}^{lk}(\omega+y) \right]. \quad (2.166)$$

b_0 is the phonon Keldysh function calculated in eq. (A.45),

$$\begin{aligned} b_0(\omega) &= \sum_{\alpha=\pm} \begin{pmatrix} \frac{1}{\alpha\omega - \Omega + i\eta} & \frac{\alpha}{\omega + \Omega + i\alpha\eta} \\ \frac{\alpha}{\omega - \Omega + i\alpha\eta} & \frac{1}{\alpha\omega + \Omega + i\eta} \end{pmatrix} \\ &= \sum_{\alpha=\pm} \begin{pmatrix} \mathcal{P} \frac{1}{\alpha\omega - \Omega} & 0 \\ 0 & \mathcal{P} \frac{1}{\alpha\omega + \Omega} \end{pmatrix} + i\pi \sum_{\alpha=\pm} \begin{pmatrix} \delta(\alpha\omega - \Omega) & \delta(\omega + \Omega) \\ \delta(\omega - \Omega) & \delta(\alpha\omega + \Omega) \end{pmatrix} \end{aligned} \quad (2.167)$$

where η is an infinitesimal. For the polarization loop one obtains

$$\begin{aligned} \pi^{kl}(\omega) &= -\frac{i\delta_{kl}}{2\pi} \left[\frac{ik\Gamma}{\omega^2 + \Gamma^2} \ln \left(\frac{V^2 - \omega^2}{V^2 + \Gamma^2} \right)^2 - \frac{2 \tan^{-1}(V/\Gamma) - \omega \tanh^{-1}[2\omega V/(\omega^2 + V^2)]}{\omega^2 + \Gamma^2} \right. \\ &\quad \left. + \frac{2e^{i\lambda/2} \tan^{-1}(Ve^{-i\lambda/2}/\Gamma) - \omega \tanh^{-1}[2\omega V/(\omega^2 + V^2)]}{\omega^2 + \Gamma^2 + \Gamma^2(e^{i\lambda} - 1)} + \frac{\pi\Gamma}{\omega^2 + \Gamma^2} \right]. \end{aligned} \quad (2.168)$$

We do not have to deal with the λ -independent contribution because it does not affect transport properties. Because of the symmetry in the Keldysh indices, the remaining integration including the phonon propagator becomes trivial: the principal parts cancel each other and we are left with the singular part. The leading order correction to the CGF is

$$\ln \chi'(\lambda) = -\frac{\mathcal{T}g^2 e^{-i\lambda/2} \Gamma \tan^{-1}(e^{-i\lambda} V/\Gamma) - \Omega \tanh^{-1}(V/\Omega)}{2\pi (\Gamma^2 + \Omega^2 + \Gamma^2(e^{i\lambda} - 1))}. \quad (2.169)$$

Remarkably, even at zero temperature, there is no sharp threshold in any cumulant which is usually found in phonon-affected transport for uncorrelated leads. Those are usually originated in the onset of inelastic tunneling processes, i.e. electrons gain/loss of energy Ω during tunneling between the leads for $V > \Omega$. In case of the MRLM at resonance, one can barely think of individual/dressed particles participating in the transport processes. Moreover, the Majorana fermions describe collective excitations in the Tomonaga-Luttinger liquid aka kinks/antikinks. The leading order correction of the current I' for an example are,

$$I' = \frac{g^2 \Gamma^2}{2\pi} \left[\frac{V}{(V^2 + \Gamma^2)(\Gamma^2 + \Omega^2)} + \frac{(\Gamma^2 - \Omega^2) \tan^{-1}(V/\Gamma) - 2\Gamma\Omega \tanh^{-1}(V/\Omega)}{\Gamma(\Gamma^2 + \Omega^2)^2} \right]. \quad (2.170)$$

One can easily verify that the corrections are purely negative in agreement with phonon enhanced backscattering of an initially⁷ perfectly transmitting channel. Especially, this is reflected in the low voltage behaviour of the current,

$$I' = -\frac{g^2 \Gamma}{\pi \Omega^2} \left(\frac{V}{\Gamma} \right)^3 + \mathcal{O} \left(\frac{V}{\Gamma} \right)^5. \quad (2.171)$$

⁷more precisely, perfect transmitting in absence of electron-phonon interactions

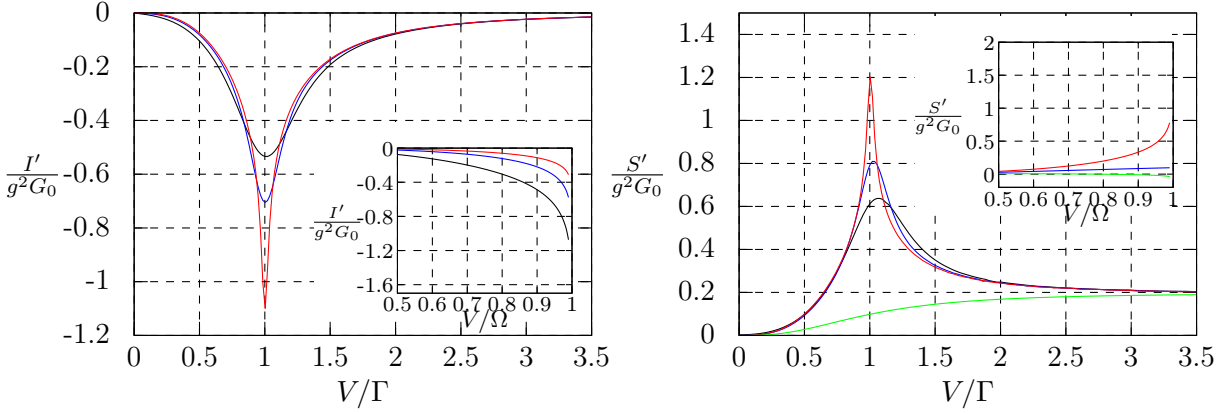


Figure 2.17.: Leading order corrections to current and noise. **Left panel:** The main graph depicts finite temperature corrections to the current in the resonant case $\Delta_0 = 0$. The parameters are $\Omega/\Gamma = 1$ and $T/\Gamma = 0.1, 0.05$ and 0.01 (black, blue and red lines). The inset shows the correction to the current for zero temperature for $\Gamma/\Omega = 1, 2$, and 3 (black, blue and red lines). **Right panel:** Finite temperature corrections to the noise on resonance. The parameters are $\Omega/\Gamma = 1$ and $T/\Gamma = 0.1, 0.05, 0.01$ and 0 (black, blue, red and green lines). The inset show the correction to the shot noise for zero temperature for plotting parameters $\Gamma/\Omega = 0.5, 1, 2$ and 3 .

In case of $V \rightarrow \Omega$ all cumulants logarithmically diverge at zero temperature. Finite temperature results are best accessible in building the cumulants first, i.e. performing the derivatives with respect to λ , and calculating the integrals afterwards. In case of the current one finds,

$$I' = -\frac{\Gamma}{4} \frac{\partial}{\partial \Gamma} \left\{ \frac{2\pi\Gamma}{\Gamma^2 + \Omega^2} \frac{\sinh(V/T)}{\cos(\Gamma/T) + \cosh(V/T)} + \sum_{k,l=\pm} \frac{(kl)}{\Gamma^2 + \Omega^2} \left[i\Gamma\psi\left(\frac{1}{2} + \frac{k\Gamma - iV}{2\pi T}\right) + \Omega\psi\left(\frac{1}{2} + i\frac{k\Omega - lV}{2\pi T}\right) \right] \right\} \quad (2.172)$$

where ψ denotes the Digamma function. Explicit expressions for higher cumulants become much more involved and lengthy. Therefore, it is recommended to perform the integration numerically.

The current and noise corrections in case of finite temperatures show a typical resonance shape (see fig. 2.17). To cure the singular behaviour for zero temperature, we performed an RPA-like resummation of a certain subset of diverging diagrams. To achieve this, we choose the current-like expression for the cumulant generating function (see eq. (2.26)),

$$\ln \chi(\lambda_-, \lambda_+) = -i \int d\lambda_- \int_{c_-} dt_- \left\langle \frac{\delta T_\lambda}{\delta \lambda(t_-)} \right\rangle_\lambda. \quad (2.173)$$

There are some advantages of this kind of approach. First of all, current-like expressions appear to be more natural in the context of quantum transport theory. Secondly, approximation schemes can be applied directly on the level of a single Keldysh function. This makes the verification of conservation rules much simpler.

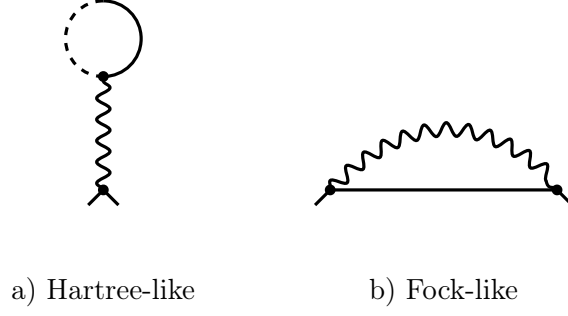


Figure 2.18.: Self energy contributions in leading order due to electron-phonon interaction. Solid lines ——— represent D_{aa} propagators, mixed lines - - - D_{ab} propagators and wavy lines phonon propagators

The derivative of T_λ in eq. (2.173) can quite easily be expressed in terms of Keldysh functions,

$$\begin{aligned} \left\langle \frac{\delta T_\lambda}{\delta \lambda(t_-)} \right\rangle_\lambda &= \frac{\gamma_+}{2} \left[\langle b(t_-) \xi(t_-) \rangle_\lambda \sin\left(\frac{\lambda_-}{2}\right) + \langle b(t_-) \eta(t_-) \rangle_\lambda \cos\left(\frac{\lambda_-}{2}\right) \right] \\ &= i \frac{\gamma_+}{2} \left[G_{b\xi}^{--}(t_-, t_- + 0^+) \sin\left(\frac{\lambda_-}{2}\right) + G_{b\eta}^{--}(t_-, t_- + 0^+) \cos\left(\frac{\lambda_-}{2}\right) \right]. \end{aligned} \quad (2.174)$$

Below, we will omit the infinitesimal 0^+ as long as it is not necessary to ensure convergence. Taking into account that the electron-phonon interaction is localized on the quantum dot, the mixed Keldysh function can be expressed in terms of the homogeneous Keldysh function D_{bb} (which is exact in interaction) and free leads Green's functions $g_{\alpha\beta}$, $\alpha, \beta \in \{\eta, \xi\}$ only,

$$G_{b\xi}^{--}(\omega) = \gamma_+ \sum_{k=\pm} (-k) D_{bb}^{-k}(\omega) \left[g_{\xi\xi}^{k-}(\omega) \cos\left(\frac{\lambda_k}{2}\right) - g_{\xi\eta}^{k-}(\omega) \sin\left(\frac{\lambda_k}{2}\right) \right] \quad (2.175)$$

$$G_{b\eta}^{--}(\omega) = \gamma_+ \sum_{k=\pm} (-k) D_{bb}^{-k}(\omega) \left[g_{\eta\xi}^{k-}(\omega) \cos\left(\frac{\lambda_k}{2}\right) - g_{\eta\eta}^{k-}(\omega) \sin\left(\frac{\lambda_k}{2}\right) \right]. \quad (2.176)$$

Putting all together and taking into account the symmetry of the Keldysh functions, one finds

$$\frac{\delta \langle T_\lambda \rangle_\lambda}{\delta \lambda(t_-)} = -\gamma_+^2 \int \frac{d\omega}{2\pi} \left\{ D_{bb}^{--} g_{\eta\xi}^{--} - D_{bb}^{+-} \left[g_{\eta\eta}^{+-} \sin\left(\frac{\lambda_- - \lambda_+}{2}\right) + g_{\eta\xi}^{+-} \cos\left(\frac{\lambda_- - \lambda_+}{2}\right) \right] \right\}. \quad (2.177)$$

Therefore, the knowledge of the exact Keldysh function D_{bb} enables us to determine the full counting statistics of our system.

An RPA-approximation of D_{bb} can be obtained via solving the Dyson equation,

$$D_{bb}^{\text{RPA}}(t) = D_{bb}^0(t) + \int dt_1 dt_2 D_{bb}^0(t-t_1) [\Sigma_{\text{H}}(t_1-t_2) + \Sigma_{\text{F}}(t_1-t_2)] D_{bb}^{\text{RPA}}(t_2) \quad (2.178)$$

where D_{bb}^0 denote the homogeneous Keldysh function for the Majorana a -channel exact in tunneling but without electron-phonon interactions, see eq. (2.157). In the following, we will omit the superscript "0" to keep notation simple. The Hartree type of self-energy is given by

$$\Sigma_{\text{H}}(t-t') = -ig^2 b_0(t-t') D_{ab}(t') \quad (2.179)$$

which of course is zero in the resonant case. The Fock type is given by

$$\Sigma_{\text{F}}(t-t') = -ig^2 b_0(t-t') D_{aa}(t'-t). \quad (2.180)$$

The Dyson equation above can be solved by Fourier transformation,

$$D_{bb}^{\text{RPA}}(\omega) = [D_{bb}^{-1}(\omega) - \sigma_3 \Sigma_{\text{F}}(\omega) \sigma_3]^{-1} \quad (2.181)$$

where the self energy in Fourier space is

$$\Sigma_{\text{F}}^{kk}(\omega) = \frac{k}{2} \left(\frac{1}{\omega + k\Omega + i\eta} + \frac{1}{\omega - k\Omega - i\eta} \right) \quad (2.182)$$

Putting all together, one finds after a lengthy calculation for the CGF

$$\ln \chi(\lambda) = \mathcal{T} \int \frac{d\omega}{2\pi} \ln \left[1 + T(\omega) (e^{i\lambda} - 1) (n_{\text{L}} - n_{\text{R}}) \right] \quad (2.183)$$

with effective transmission coefficient

$$T(\omega) = \frac{\Gamma^2 (\omega^2 - \Omega^2)^2}{g^4 \omega^2 - 2g^2 \omega^2 (\omega^2 - \Omega^2) + (\omega^2 + \Gamma^2) (\omega^2 - \Omega^2)^2}. \quad (2.184)$$

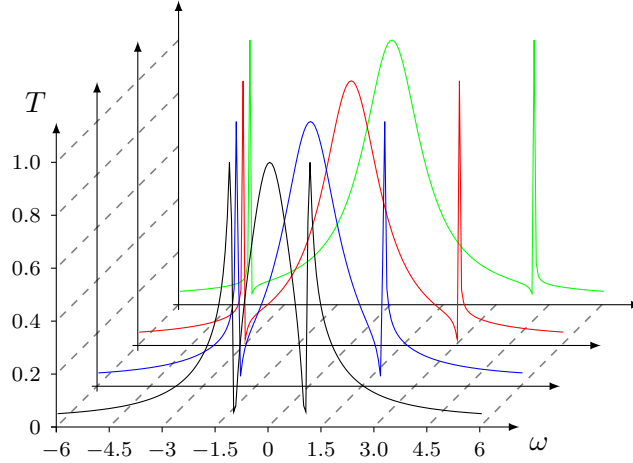


Figure 2.19.: Effective transmission coefficient of the interacting resonant level in the Toulouse limit coupled to a bosonic degree of freedom. The electron-phonon coupling parameter is set to $g/\Gamma = 0.5$. The frequency of the phonon is varied from $\Omega/\Gamma = 1, 2, 3, 4$ (black, blue, red, green).

In fig. 2.19, the effective transmission coefficient is depicted for several phonon frequencies Ω . There are three maxima (perfect transmission) at $\omega = 0, \pm \sqrt{g^2 + \Omega^2}$ and two minima at $\omega = \pm \Omega$. From the diagrammatic structure one can identify the involved transport processes. The phonon mode is (de)excited at every single tunneling vertex. That means that the incoming fermion which is not the original physical electron but rather a collective excitation subject to fermionic statistics tunnels into the dot exciting the phonon and deexcites the latter upon leaving the dot. This is only the case when the (de)excitation time scales are much shorter than the fermion dwelling time on the dot. Neglecting the processes of higher orders we then obtain one of the necessary conditions for the validity of our approach: $g \gg \Gamma$.

In fig. 2.20, current and noise are depicted for several electron-phonon coupling strengths. One observes that for small voltages the current increases nearly linear. For voltages near Ω one finds a plateau, e.g., the current enhancement is suppressed by the electron-phonon interaction. This

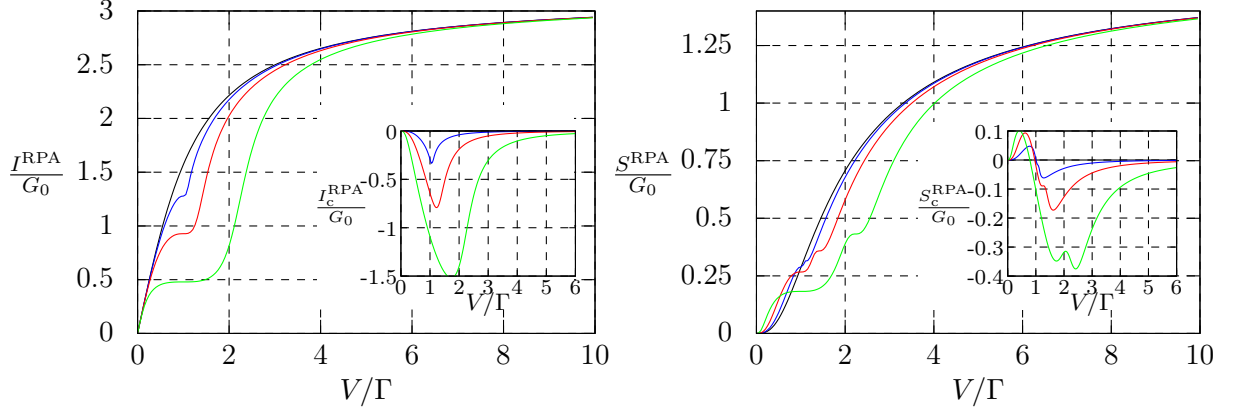


Figure 2.20.: RPA-approximation of current and shot noise. **Left panel:** The main graph depicts the full current in the resonant case $\Delta_0 = 0$ and zero temperature. The parameters are $\Omega/\Gamma = 1$ and $g/\Gamma = 0, 0.5, 1$ and 2 (black, blue, red and green lines). The inset shows the correction to the current ($I_c^{\text{RPA}} = I_c^{\text{RPA}} - I_c^{\text{RPA}}|_{g=0}$) for the same set of parameters and color coding. **Right panel:** Noise in resonance and at zero temperature. The parameters and color coding are the same as for the left panel. The correction to the noise is defined by $S_c^{\text{RPA}} = S_c^{\text{RPA}} - S_c^{\text{RPA}}|_{g=0}$.

feature does not occur exactly at $V = \Omega$. One finds that the maximal reduction in the current is at $V = \Omega\sqrt{1 + g^2/2\Omega^2}$ or if one assumes $\Omega \gg g$, $V \approx \Omega + g^2/4\Omega$. This kind of a shift by g^2 is one normally produced by a polaron transformation. Similar features can be observed in the noise. Interestingly, the correction to the noise changes sign for high voltages.

2.3.5. The off-resonant case

In this section, we are interested in the case of finite detuning $\Delta_0 \neq 0$. For this case, we have to calculate the Hartree (see e.q. (2.164)) as well as the Fock contribution (see e.q. (2.165)). Again, we are interested in the case of zero temperature. First, we have to transform the Keldysh functions for the homogeneous and mixed channel to a more suitable form. Using $n_L^2 = n_L$, $n_R^2 = n_R$ and $n_L n_R = n_R$ and

$$\mathcal{F}_{\lambda+} = \mathcal{F}_{\lambda-} = (e^{i\lambda} - 1) (n_L - n_R) \quad (2.185)$$

$$\mathcal{D}_\lambda = (\omega^2 - \Delta_0)^2 + \omega^2 \Gamma^2 \left[1 + (e^{i\lambda} - 1) (n_L - n_R) \right]. \quad (2.186)$$

we find the very interesting relation,

$$\mathcal{D}_\lambda = \left\{ \omega^2 - \Delta^2 + i\omega\Gamma \left[1 + (e^{i\lambda/2} - 1) (n_L - n_R) \right] \right\} \left\{ \omega^2 - \Delta^2 - i\omega\Gamma \left[1 + (e^{i\lambda/2} - 1) (n_L - n_R) \right] \right\} \quad (2.187)$$

which we extensively use to reduce the degree of the polynomial in the denominators of the Keldysh functions. For the diagonal components of the Majorana a -channel's Keldysh function we find,

$$\begin{aligned}
 D_{aa}^{kk} &= \left[\frac{\Delta_0^2 (n_L + n_R - 1)}{2\omega} - ik \frac{\Gamma}{2} \right] \left(\sum_{\pm} \frac{\pm 1}{\omega^2 - \Delta_0^2 \pm i\omega\Gamma} \right) - k \frac{\omega}{2} \left(\sum_{\pm} \frac{1}{\omega^2 - \Delta_0^2 \pm i\omega\Gamma} \right) \\
 &\quad - k \frac{\omega (n_L - n_R)}{2} \left[\sum_{\pm} \left(\frac{1}{\omega^2 - \Delta_0^2 \pm i\omega\Gamma e^{i\lambda/2}} - \frac{1}{\omega^2 - \Delta_0^2 \pm i\omega\Gamma} \right) \right] \\
 &\quad - ik \frac{\Gamma (n_L - n_R)}{2} \left[\sum_{\pm} \left(\frac{\pm e^{i\lambda/2}}{\omega^2 - \Delta_0^2 \pm i\omega\Gamma e^{i\lambda/2}} - \frac{\pm 1}{\omega^2 - \Delta_0^2 \pm i\omega\Gamma} \right) \right]
 \end{aligned} \tag{2.188}$$

and for the off-diagonal components

$$D_{aa}^{-+} = \frac{\Delta_0^2 (n_L - n_R)}{2\omega} \left(\sum_{\pm} \frac{\pm 1}{\omega^2 - \Delta_0^2 \pm i\omega\Gamma e^{i\lambda/2}} \right) + \frac{\Delta_0^2}{\omega} n_R \left[\sum_{\pm} \frac{\pm \cos(\lambda/2)}{\omega^2 - \Delta_0^2 \pm i\omega\Gamma} \right] \tag{2.189}$$

$$D_{aa}^{+-} = -\frac{\Delta_0^2 (n_L - n_R)}{2\omega} \left(\sum_{\pm} \frac{\pm 1}{\omega^2 - \Delta_0^2 \pm i\omega\Gamma e^{i\lambda/2}} \right) + \frac{\Delta_0^2}{\omega} (n_L - 1) \left[\sum_{\pm} \frac{\pm \cos(\lambda/2)}{\omega^2 - \Delta_0^2 \pm i\omega\Gamma} \right]. \tag{2.190}$$

All the components are of course well behaved for $\omega \rightarrow 0$ as long as $\Delta_0 \neq 0$. The Keldysh functions for the Majorana b -channel are slightly less involved,

$$\begin{aligned}
 D_{bb}^{kk} &= \frac{\omega (n_L + n_R - 1)}{2} \left(\sum_{\pm} \frac{\pm 1}{\omega^2 - \Delta_0^2 \pm i\omega\Gamma} \right) - k \frac{\omega}{2} \left(\sum_{\pm} \frac{1}{\omega^2 - \Delta_0^2 \pm i\omega\Gamma} \right) \\
 &\quad - k \frac{\omega (n_L - n_R)}{2} \left[\sum_{\pm} \left(\frac{1}{\omega^2 - \Delta_0^2 \pm i\omega\Gamma e^{i\lambda/2}} - \frac{1}{\omega^2 - \Delta_0^2 \pm i\omega\Gamma} \right) \right]
 \end{aligned} \tag{2.191}$$

and

$$D_{bb}^{-+} = \frac{\omega (n_L - n_R)}{2} \left(\sum_{\pm} \frac{\pm 1}{\omega^2 - \Delta_0^2 \pm i\omega\Gamma e^{i\lambda/2}} \right) + \omega n_R \left[\sum_{\pm} \frac{\pm \cos(\lambda/2)}{\omega^2 - \Delta_0^2 \pm i\omega\Gamma} \right] \tag{2.192}$$

$$D_{bb}^{+-} = -\frac{\omega (n_L - n_R)}{2} \left(\sum_{\pm} \frac{\pm 1}{\omega^2 - \Delta_0^2 \pm i\omega\Gamma e^{i\lambda/2}} \right) + \omega (n_L - 1) \left[\sum_{\pm} \frac{\pm \cos(\lambda/2)}{\omega^2 - \Delta_0^2 \pm i\omega\Gamma} \right]. \tag{2.193}$$

For the mixed channels one finds,

$$\begin{aligned}
 D_{ab}^{kk} &= -\frac{i\Delta_0 (n_L + n_R - 1)}{2} \left(\sum_{\pm} \frac{\pm 1}{\omega^2 - \Delta_0^2 \pm i\omega\Gamma} \right) + k \frac{i\Delta_0}{2} \left(\sum_{\pm} \frac{1}{\omega^2 - \Delta_0^2 \pm i\omega\Gamma} \right) \\
 &\quad + k \frac{i\Delta_0 (n_L - n_R)}{2} \left[\sum_{\pm} \left(\frac{1}{\omega^2 - \Delta_0^2 \pm i\omega\Gamma e^{i\lambda/2}} - \frac{1}{\omega^2 - \Delta_0^2 \pm i\omega\Gamma} \right) \right]
 \end{aligned} \tag{2.194}$$

and

$$D_{ab}^{-+} = -\frac{i\Delta_0 (n_L - n_R)}{2} \left(\sum_{\pm} \frac{\pm 1}{\omega^2 - \Delta_0^2 \pm i\omega\Gamma e^{i\lambda/2}} \right) - i\Delta_0 n_R \left[\sum_{\pm} \frac{\pm \cos(\lambda/2)}{\omega^2 - \Delta_0^2 \pm i\omega\Gamma} \right] \tag{2.195}$$

$$D_{ab}^{+-} = \frac{i\Delta_0 (n_L - n_R)}{2} \left(\sum_{\pm} \frac{\pm 1}{\omega^2 - \Delta_0^2 \pm i\omega\Gamma e^{i\lambda/2}} \right) - i\Delta_0 (n_L - 1) \left[\sum_{\pm} \frac{\pm \cos(\lambda/2)}{\omega^2 - \Delta_0^2 \pm i\omega\Gamma} \right]. \tag{2.196}$$

Next, we have to determine the polarization loop, e.q. (2.166). But first, we introduce the new quantities π_{\perp}^{kl} and π_{\parallel}^{kl} (Majorana polarization bubbles) to simplify notation,

$$\pi_{\perp}^{kl}(\omega) = -i \int \frac{dy}{2\pi} D_{ab}^{kl}(y) D_{ab}^{lk}(\omega + y) \quad (2.197)$$

and

$$\pi_{\parallel}^{kl}(\omega) = -i \int \frac{dy}{2\pi} D_{aa}^{kl}(y) D_{bb}^{lk}(\omega + y). \quad (2.198)$$

We begin with the orthogonal component, π_{\perp}^{kl} , where we only need to consider λ -dependent contributions. For the diagonal components, we find

$$\begin{aligned} \pi_{\perp}^{kk} = \frac{-i\Delta_0^2}{8\pi} \sum_{m,n=\pm} \left\{ - \left[\Upsilon_{m,n}^{\lambda,0}(V-\omega) - \Upsilon_{m,n}^{\lambda,0}(-V-\omega) + \Upsilon_{m,n}^{0,\lambda}(V) - \Upsilon_{m,n}^{0,\lambda}(-V) \right] \right. \\ + mk\sigma(\omega)\theta(|\omega|-2V) \left[\Upsilon_{m,n}^{\lambda,0}(V-\omega) - \Upsilon_{m,n}^{\lambda,0}(-V-\omega) \right] \\ + mk\theta(2V-|\omega|) \left[\Upsilon_{m,n}^{\lambda,0}(-\sigma(\omega)V) - \Upsilon_{m,n}^{\lambda,0}(-\sigma(\omega)V-\omega) \right] \\ - \sigma(\omega)\theta(2V-|\omega|) \left[\Upsilon_{m,n}^{\lambda,0}(-\sigma(\omega)V) - \Upsilon_{m,n}^{\lambda,\lambda}(-\sigma(\omega)V) + \Upsilon_{m,n}^{0,\lambda}(-\sigma(\omega)V) \right. \\ \left. + \Upsilon_{m,n}^{\lambda,\lambda}(\sigma(\omega)V-\omega) - \Upsilon_{m,n}^{0,\lambda}(\sigma(\omega)V-\omega) - \Upsilon_{m,n}^{\lambda,0}(\sigma(\omega)V-\omega) \right] \\ - nk\sigma(\omega)\theta(|\omega|-2V) \left[\Upsilon_{m,n}^{0,\lambda}(V) - \Upsilon_{m,n}^{0,\lambda}(-V) \right] \\ \left. - nk\theta(2V-|\omega|) \left[\Upsilon_{m,n}^{0,\lambda}(\sigma(\omega)V) - \Upsilon_{m,n}^{0,\lambda}(\sigma(\omega)V-\omega) \right] \right\}. \end{aligned} \quad (2.199)$$

The occurrence of the θ -functions indicates, that there might be inelastic contributions. $\sigma(\omega)$ denotes the sign of ω , i.e. $\sigma(\omega) = \text{sgn}(\omega)$. We have introduced the quantity $\Upsilon_{m,n}^{\lambda,\nu}(y)$ which is due to its lengthy form is listed in appendix A.4 eq. (A.74). In case of the off-diagonal components we can use the obvious identity $\pi_{\perp}^{-+}(y) = \pi_{\perp}^{+-}(-y)$. Therefore, it is enough to calculate only one of them,

$$\begin{aligned} \pi_{\perp}^{-+} = \frac{-i\Delta_0^2}{8\pi} \sum_{m,n=\pm} (mn) \left\{ 4 \cos^2(\lambda/2) \theta(\omega-2V) \left[\Upsilon_{m,n}^{0,0}(-V) - \Upsilon_{m,n}^{0,0}(V-\omega) \right] \right. \\ + \sigma(\omega)\theta(2V-|\omega|) \left[\Upsilon_{m,n}^{\lambda,\lambda}(\sigma(\omega)V-\omega) - \Upsilon_{m,n}^{\lambda,\lambda}(-\sigma(\omega)V) \right] \\ + 2 \cos(\lambda/2) \theta(\omega)\theta(2V-\omega) \left[\Upsilon_{m,n}^{0,\lambda}(V) - \Upsilon_{m,n}^{0,\lambda}(V-\omega) \right] \\ + 2 \cos(\lambda/2) \theta(\omega-2V) \left[\Upsilon_{m,n}^{0,\lambda}(V) - \Upsilon_{m,n}^{0,\lambda}(-V) \right] \\ + 2 \cos(\lambda/2) \theta(\omega)\theta(2V-\omega) \left[\Upsilon_{m,n}^{\lambda,0}(-V) - \Upsilon_{m,n}^{\lambda,0}(-V-\omega) \right] \\ \left. + 2 \cos(\lambda/2) \theta(\omega-2V) \left[\Upsilon_{m,n}^{\lambda,0}(V-\omega) - \Upsilon_{m,n}^{\lambda,0}(-V-\omega) \right] \right\}. \end{aligned} \quad (2.200)$$

The parallel polarization loop is more involved than the orthogonal one. Again, we begin with the diagonal components,

$$\begin{aligned}
 \pi_{\parallel}^{kk} = & \frac{-i}{8\pi} \sum_{m,n=\pm} \left\{ \Upsilon_{3,m,n}^{0,\lambda}(V) - \Upsilon_{3,m,n}^{0,\lambda}(-V) + im\Gamma e^{\frac{i\lambda}{2}} \left[\Upsilon_{2,m,n}^{0,\lambda}(V) - \Upsilon_{2,m,n}^{0,\lambda}(-V) \right] \right. \\
 & + im\Gamma \left[\Upsilon_{2,m,n}^{\lambda,0}(V - \omega) - \Upsilon_{2,m,n}^{\lambda,0}(-V - \omega) \right] + \left[\Upsilon_{3,m,n}^{\lambda,0}(V - \omega) - \Upsilon_{3,m,n}^{\lambda,0}(-V - \omega) \right] \\
 & - km\Delta_0^2 \sigma(\omega) \theta(|\omega| - 2V) \left[\Upsilon_{1,m,n}^{\lambda,0}(V - \omega) - \Upsilon_{1,m,n}^{\lambda,0}(-V - \omega) \right] \\
 & - km\Delta_0^2 \theta(2V - |\omega|) \left[\Upsilon_{1,m,n}^{\lambda,0}(-\sigma(\omega)V) - \Upsilon_{1,m,n}^{\lambda,0}(-\sigma(\omega)V - \omega) \right] \\
 & + \sigma(\omega) \theta(2V - |\omega|) \left[\Upsilon_{3,m,n}^{\lambda,\lambda}(\sigma(\omega)V - \omega) - \Upsilon_{3,m,n}^{\lambda,\lambda}(-\sigma(\omega)V) \right. \\
 & \left. - \Upsilon_{3,m,n}^{\lambda,0}(\sigma(\omega)V - \omega) + \Upsilon_{3,m,n}^{\lambda,0}(-\sigma(\omega)V) - \Upsilon_{3,m,n}^{0,\lambda}(\sigma(\omega)V - \omega) + \Upsilon_{3,m,n}^{0,\lambda}(-\sigma(\omega)V) \right] \\
 & + im\Gamma \sigma(\omega) \theta(2V - |\omega|) \left[e^{\frac{i\lambda}{2}} \Upsilon_{2,m,n}^{\lambda,\lambda}(\sigma(\omega)V - \omega) - e^{\frac{i\lambda}{2}} \Upsilon_{2,m,n}^{\lambda,\lambda}(-\sigma(\omega)V) \right. \\
 & \left. - \Upsilon_{2,m,n}^{\lambda,0}(\sigma(\omega)V - \omega) + \Upsilon_{2,m,n}^{\lambda,0}(-\sigma(\omega)V) - \Upsilon_{2,m,n}^{0,\lambda}(\sigma(\omega)V - \omega) + \Upsilon_{2,m,n}^{0,\lambda}(-\sigma(\omega)V) \right] \\
 & + kn\sigma(\omega) \theta(|\omega| - 2V) \left[\Upsilon_{3,m,n}^{0,\lambda}(V) - \Upsilon_{3,m,n}^{0,\lambda}(-V) \right] \\
 & + kn\theta(2V - |\omega|) \left[\Upsilon_{3,m,n}^{0,\lambda}(\sigma(\omega)V) - \Upsilon_{3,m,n}^{0,\lambda}(\sigma(\omega)V - \omega) \right] \\
 & + ik\Gamma(mn) \theta(|\omega| - 2V) e^{\frac{i\lambda}{2}} \left[\Upsilon_{2,m,n}^{0,\lambda}(V) - \Upsilon_{2,m,n}^{0,\lambda}(-V) \right] \\
 & \left. + ik\Gamma(mn) \theta(2V - |\omega|) e^{\frac{i\lambda}{2}} \left[\Upsilon_{2,m,n}^{0,\lambda}(\sigma(\omega)V) - \Upsilon_{2,m,n}^{0,\lambda}(\sigma(\omega)V - \omega) \right] \right\}
 \end{aligned} \tag{2.201}$$

where we have introduced the quantities $\Upsilon_{i,m,n}^{\lambda,\nu}(y)$, $i = 1, 2, 3$ which are listed in appendix A.4 eq. (A.76) to (A.78). The off-diagonal components are

$$\begin{aligned}
 \pi_{\parallel}^{+-} = & \frac{-i\Delta_0^2}{8} \sum_{m,n=\pm} (mn) \left\{ -\sigma(\omega) \theta(2V - |\omega|) \left[\Upsilon_{1,m,n}^{\lambda,\lambda}(-\sigma(\omega)V - \omega) - \Upsilon_{1,m,n}^{\lambda,\lambda}(-\sigma(\omega)V) \right] \right. \\
 & - 4 \cos^2(\lambda/2) \theta(-2V - \omega) \left[\Upsilon_{1,m,n}^{0,0}(-V - \omega) - \Upsilon_{1,m,n}^{0,0}(V) \right] \\
 & - 2 \cos(\lambda/2) \theta(-\omega) \theta(\omega + 2V) \left[\Upsilon_{1,m,n}^{0,\lambda}(-V - \omega) - \Upsilon_{1,m,n}^{0,\lambda}(-V) \right] \\
 & - 2 \cos(\lambda/2) \theta(-2V - \omega) \left[\Upsilon_{1,m,n}^{0,\lambda}(V) - \Upsilon_{1,m,n}^{0,\lambda}(-V) \right] \\
 & - 2 \cos(\lambda/2) \theta(-2V - \omega) \left[\Upsilon_{1,m,n}^{\lambda,0}(V - \omega) - \Upsilon_{1,m,n}^{\lambda,0}(-V - \omega) \right] \\
 & \left. - 2 \cos(\lambda/2) \theta(-\omega) \theta(2V + \omega) \left[\Upsilon_{1,m,n}^{\lambda,0}(V - \omega) - \Upsilon_{1,m,n}^{\lambda,0}(V) \right] \right\}
 \end{aligned} \tag{2.202}$$

and

$$\begin{aligned}
 \pi_{\parallel}^{+-} = \frac{-i\Delta_0^2}{8} \sum_{m,n=\pm} (mn) & \left\{ -\sigma(\omega) \theta(2V - |\omega|) \left[\Upsilon_{1,m,n}^{\lambda,\lambda}(-\sigma(\omega)V - \omega) - \Upsilon_{1,m,n}^{\lambda,\lambda}(-\sigma(\omega)V) \right] \right. \\
 & - 4 \cos^2(\lambda/2) \theta(\omega - 2V) \left[\Upsilon_{1,m,n}^{0,0}(-V) - \Upsilon_{1,m,n}^{0,0}(V - \omega) \right] \\
 & - 2 \cos(\lambda/2) \theta(\omega) \theta(2V - \omega) \left[\Upsilon_{1,m,n}^{0,\lambda}(V) - \Upsilon_{1,m,n}^{0,\lambda}(V - \omega) \right] \\
 & - 2 \cos(\lambda/2) \theta(-2V + \omega) \left[\Upsilon_{1,m,n}^{0,\lambda}(V) - \Upsilon_{1,m,n}^{0,\lambda}(-V) \right] \\
 & - 2 \cos(\lambda/2) \theta(\omega) \theta(2V - \omega) \left[\Upsilon_{1,m,n}^{\lambda,0}(-V) - \Upsilon_{1,m,n}^{\lambda,0}(-V - \omega) \right] \\
 & \left. - 2 \cos(\lambda/2) \theta(\omega - 2V) \left[\Upsilon_{1,m,n}^{\lambda,0}(V - \omega) - \Upsilon_{1,m,n}^{\lambda,0}(-V - \omega) \right] \right\}. \tag{2.203}
 \end{aligned}$$

In order to calculate the Fock-type corrections to the CGF, the polarization loop has to be integrated together with the bare Keldysh phonon propagator. In case of off-diagonal components, this integration is trivial, because the phonon Keldysh functions are just δ -functions. In case of the diagonal contributions, we can split the phonon propagator in its singular and principal value parts. The contribution coming from the principal value part is best done numerically. We do not provide an explicit expression for the Fock-like corrections to the CGF because of the very demanding structure of its constituents. The Hartree-like correction to the CGF is much easier to evaluate. Basically, one needs the mixed Keldysh function D_{ab} at times $\pm 0^+$,

$$\begin{aligned}
 D_{ab}^{kk}(-k0^+) = \frac{i\Delta_0}{\pi\sqrt{\Gamma^2 - 4\Delta_0^2}} & \left[k - \sum_{\pm} \pm \tan^{-1} \left(\frac{2V \pm i\Gamma}{\sqrt{\Gamma^2 - 4\Delta_0^2}} \right) - k \sum_{\pm} \tan^{-1} \left(\frac{2V \pm i\Gamma}{\sqrt{\Gamma^2 - 4\Delta_0^2}} \right) \right] \\
 & + k \sum_{\pm} \left[\frac{i\Delta_0}{\pi\sqrt{\Gamma^2 e^{i\lambda} - 4\Delta_0^2}} \tan^{-1} \left(\frac{2V \pm i\Gamma e^{i\lambda/2}}{\sqrt{\Gamma^2 e^{i\lambda} - 4\Delta_0^2}} \right) \right], \tag{2.204}
 \end{aligned}$$

and for the off-diagonal components,

$$D_{ab}^{-+}(0^+) = D_{ab}^{+-}(-0^+) = \frac{i\Delta_0}{\pi\sqrt{\Gamma^2 - 4\Delta_0^2}} \cos(\lambda/2) \sum_{\pm} \tan^{-1} \left(\frac{\pm 2V + i\Gamma}{\sqrt{\Gamma^2 - 4\Delta_0^2}} \right). \tag{2.205}$$

In fig. 2.21, we have depicted the leading order current correction for several parameter constellations. We decided to choose the parameters in such a way, that features coming from elastic and inelastic processes are distinguishable. In case of small voltages, a peak like structure is observed. Its position and width is independent of the phonon frequency. Its height, however, depends on Ω ; the higher Ω the smaller the peak. The dot level detuning Δ influences both the position and the height of the peak (left panel, fig. 2.21). For voltages approaching the phonon frequency, a double-steplike feature is observed. This is a clear sign of inelastic processes⁸. The occurrence of the double-step can be explained by the double peak like structure of the transmission coefficient. The width of the steps is of the order of Δ . In contrast to the resonant case, the corrections are purely positive. This is in agreement with the picture of phonon assisted tunneling for a weakly conducting system. In fig. 2.22 the leading order corrections to the noise is depicted. The features are similar to those in the current.

⁸One has to be careful with this kind of interpretation, because we are dealing with complex, collective excitations in the TLL, i.e. kinks/anti-kinks, instead of single particle excitations.

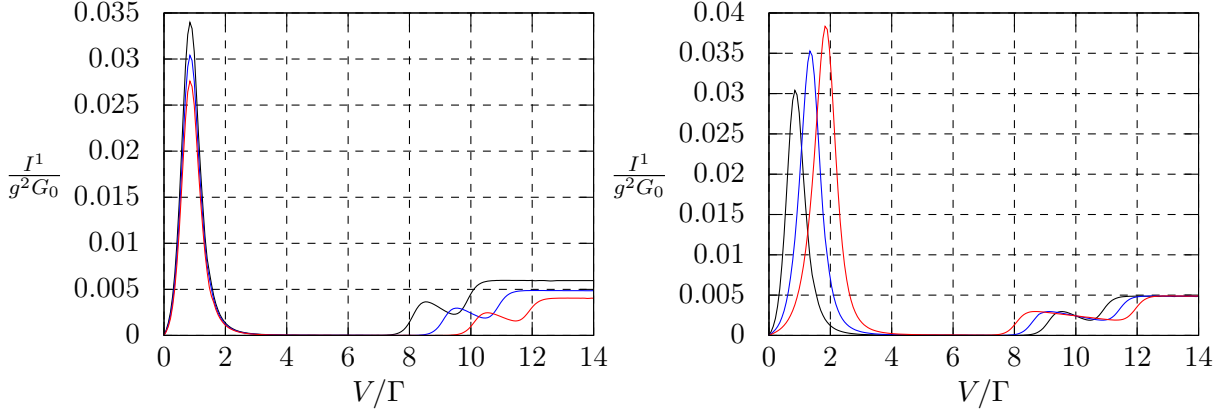


Figure 2.21.: Leading order current correction. **Left panel:** current correction in leading order for zero temperature, $T = 0$ and dot level detuning $\Delta/\Gamma = 1$. The phonon frequency is varied from $\Omega/\Gamma = 9, 10, 11$ (black, blue and red curve). **Right panel:** the parameters are $T = 0$ and $\Omega/\Gamma = 10$. The dot level detuning is varied from $\Delta/\Gamma = 1, 1.5, 2$ (black, blue and red curve).

2.3.6. Results and discussion

To conclude, we investigated the interacting resonant level model in presence of a harmonic degree of freedom coupled to the quantum dot. We observe that in the resonant case, where the system is initially perfectly transmitting, finite electron-phonon coupling leads to negative corrections to the current. In the zero-temperature limit we identified a strongly non-perturbative regime where the current correction is log divergent and performed an RPA-like resummation of divergent diagram contributions, which turned out to produce a plateaulike feature in the full current-voltage characteristics of the system. We believe that this behavior is generic in all setups with TLL electrodes also beyond the chosen parameter constellation. Single-wall carbon nanotubes SWCNTs, are known to be typical realizations of the Tomonaga-Luttinger liquid electronic state (see for example [Bockrath et al. \[1999\]](#), [Egger and Gogolin \[1997\]](#), [Kane et al. \[1997\]](#), [Yao et al. \[1999\]](#)). Therefore we expect the above strong conductance suppression phenomenon to be observable in experiments on molecular quantum dots coupled to SWCNTs. In the opposite off-resonant case, when the system without the phonon has zero conductance, we observe conductance enhancement due to electron-phonon interaction. For voltages comparable to phonon frequency we find a double-steplike feature in the lowest order perturbation expansion in electron-phonon coupling. Contrary to the resonant case no singularities are observed. The results of this section are published in [Maier and Komnik \[2010\]](#).

2.4. Double quantum dot interferometer

In this section, we focus on double quantum dot systems. Although we do not consider effects of electron-phonon coupling, there is a striking similarity to the previous models: the existence of a sharp anti-resonance in the transmission properties.

The Hamiltonian of our model is given by

$$H = H_{\text{leads}}[\psi_{L,\sigma}, \psi_{R,\sigma}] + H_{\text{QD}} + H_{\text{T}} + H_{\text{C}} \quad (2.206)$$

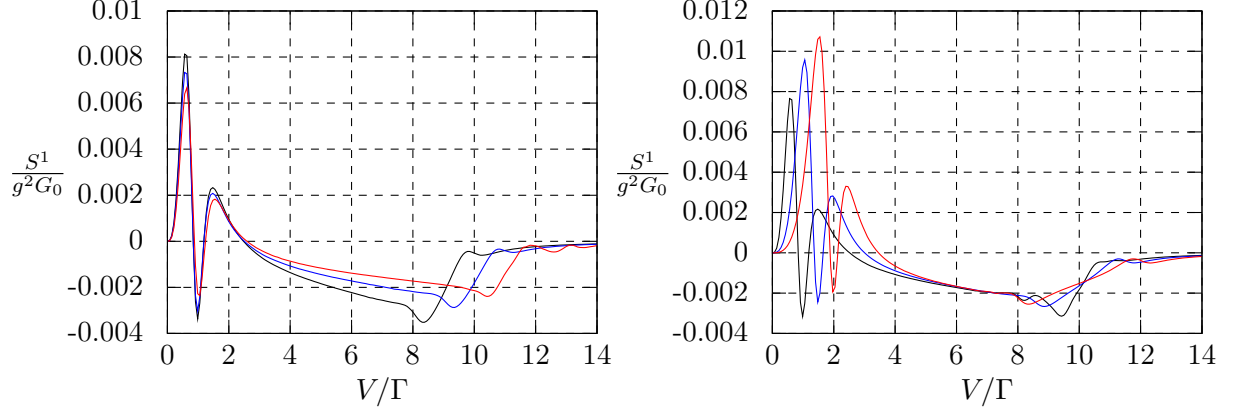


Figure 2.22.: Leading order correction to the noise. **Left panel:** noise correction in leading order for zero temperature, $T = 0$ and dot level detuning $\Delta/\Gamma = 1$. The phonon frequency is varied from $\Omega/\Gamma = 9, 10, 11$ (black, blue and red curve). **Right panel:** the parameters are $T = 0$ and $\Omega/\Gamma = 10$. The dot level detuning is varied from $\Delta/\Gamma = 1, 1.5, 2$ (black, blue and red curve).

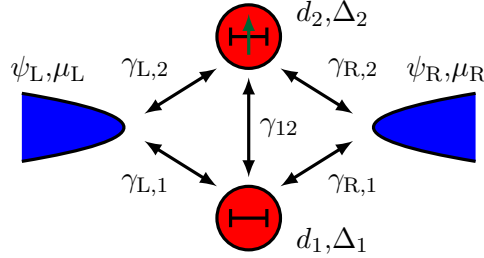


Figure 2.23.: Schematics of the double quantum dot interferometer.

where $H_{\text{leads}}[\psi_{L,\sigma}, \psi_{R,\sigma}]$ describes the free leads and is, up to an additional spin degree of freedom, the same as for the resonant level model. $\psi_{m,\sigma}^\dagger, \psi_{m,\sigma}$ describe of course the creation and annihilation of a particle in lead m with spin σ . The contacts are held at different chemical potentials $\mu_{L,R}$ with $\mu_L - \mu_R = V$. The free quantum dots are modeled by,

$$H_{\text{QD}} = \sum_{\substack{i=1,2 \\ \sigma=\uparrow,\downarrow}} (\Delta_i + h_i \mu_B g \sigma / 2) d_{i,\sigma}^\dagger d_{i,\sigma} + \sum_{\sigma} \left(\gamma_{12} d_{1,\sigma}^\dagger d_{2,\sigma} + \gamma_{12}^* d_{2,\sigma}^\dagger d_{1,\sigma} \right) \quad (2.207)$$

where Δ_i ($i = 1, 2$) are the energies of the dot levels and h_i are magnetic fields on the quantum dots and γ_{12} is a hopping amplitude describing hopping from quantum dot 1 to quantum dot 2 and vice versa. μ_B is Bohr's magneton and g is the Landé factor. $d_{i,\sigma}^\dagger, d_{i,\sigma}$ are the creation and annihilation operators for the single dot levels with spin σ . H_T is the tunneling Hamiltonian,

$$H_T = \sum_{m=L,R} \sum_{\substack{i=1,2 \\ \sigma=\uparrow,\downarrow}} \left(\gamma_{m,i} d_{i,\sigma}^\dagger \psi_{m,\sigma} + \text{H.c.} \right) \quad (2.208)$$

where $\gamma_{m,i}$ are the tunneling amplitudes for tunneling from lead m to quantum dot i . In fig. 2.23, the tunneling couplings of the double quantum dot are depicted. The interaction Hamiltonian is

$$H_C = \sum_{i=1,2} U_i n_{i,\sigma} n_{i,-\sigma} + \sum_{\sigma=\uparrow,\downarrow} (V_{\parallel} n_{1,\sigma} n_{2,\sigma} + V_{\perp} n_{1,\sigma} n_{2,-\sigma}) \quad (2.209)$$

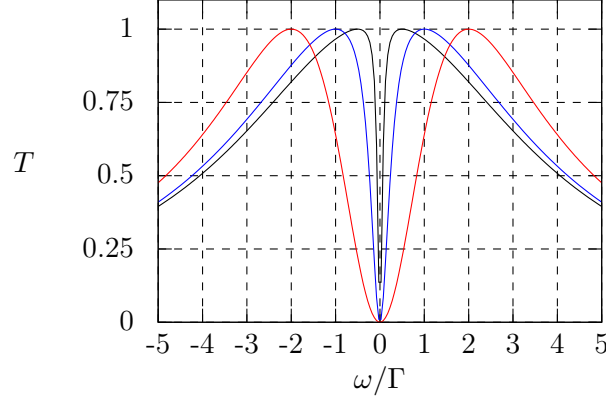


Figure 2.24.: Anti-resonance in the transmission coefficient. The parameters are $\gamma_{12} = 0$, $h = 0$ and $\gamma_{m,i} = \gamma$. The detuning $\Delta_1 = -\Delta_2 = \Delta$ is varied $\Delta/\Gamma = 0.5, 1, 2$ (black, blue, red).

where U_i is the onsite interaction strength and V_{\parallel}, V_{\perp} are the inter-dot interaction strengths. The effects of V_{\parallel} and V_{\perp} have been perturbatively investigated in Dahlhaus [2009]. Therefore, we only refer the results therein and focus on the effect of the onsite interaction, i.e. we set $V_{\parallel} = V_{\perp} = 0$. The λ -dependent tunneling operator is obtained in the usual way,

$$T_{\lambda} = \sum_{m=L,R} \sum_{\substack{i=1,2 \\ \sigma=\uparrow,\downarrow}} \left(e^{im\lambda/4} \gamma_{m,i} d_{i,\sigma}^{\dagger} \psi_{m,\sigma} + \text{H.c.} \right). \quad (2.210)$$

Again, the non-interacting system can best be solved using functional integration. The details to the calculations can be found in appendix A.5. The transmission coefficient for an arbitrary parameter constellation is quite cumbersome. We argued that a generic feature of the transmission coefficient is the occurrence of anti-resonances which can be arbitrarily sharp. Only for very symmetric parameter constellations the absence of the anti-resonance is observable. We are interested in the case $\Delta_1 = -\Delta_2 = \Delta$, $h_i = 0$, $\gamma_{m,i} = \gamma$ and $\gamma_{12} = 0$. In this case, one finds for the transmission coefficient the very appealing form

$$T(\omega) = \frac{4\Gamma^2}{4\Gamma^2 + [1/(\omega - \Delta) + 1/(\omega + \Delta)]^{-2}} = \frac{\Gamma}{\sqrt{4\Gamma^2 - \Delta^2}} \left(\frac{\Omega_+^2}{\omega^2 + \Omega_+^2} - \frac{\Omega_-^2}{\omega^2 + \Omega_-^2} \right) \quad (2.211)$$

with $\Omega_{\pm} = 2\Gamma \pm \sqrt{4\Gamma^2 - \Delta^2}$ and hybridization $\Gamma = \pi\rho_0\gamma^2$ in the wide flat band limit. To ensure the root in Ω_{\pm} to be real, we have the additional constraint $2\Gamma > \Delta$.⁹ The meaning of the decomposition in eq. (2.211) is obvious: there is a resonance (positive Lorentzian) of width $2\Omega_+$ and an anti-resonance (negative Lorentzian) of width $2\Omega_-$. Again, we point out that there is no artificial fine tuning involved. From an experimental point of view, the coupling strengths and the position of the dot level energies can be well controlled. The transmission coefficient eq. (2.211) is quite similar to the transmission coefficient of the Holstein polaron in the PTA approximation, eq. (2.104). This assures our previous interpretation of the PTA approximation: the strongly coupled phonon effectively appears as a set of energy levels with level spacing Ω individually coupled to the leads.. The interesting fact about the anti-resonance is its width. In principle, it can be arbitrarily small. In case of small detuning of the dots, i.e. $\Delta/\Gamma \ll 1$ we have approximately $\Omega_+ \approx 2\Gamma - \frac{\Delta^2}{4\Gamma}$ and

⁹This additional constraint is only necessary for this kind of representation of the transmission coefficient. Of course, there is a anti-resonance for $2\Gamma < \Delta$, too.

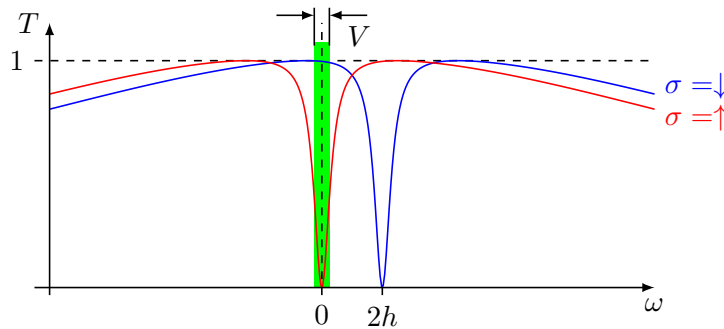


Figure 2.25.: Operating mode of the double quantum dot spin valve. Using an in-plane magnetic field h , the resonance peak of one spin species is aligned with the anti-resonance dip of the other species. We have assumed, that the quantum dots are gated in such a way, that the transmission of one species is resonant, i.e. in between the voltage window (green area).

$\Omega_- \approx \frac{\Delta^2}{4\Gamma}$. In fig. 2.24, the anti-resonance is depicted for several detunings Δ . The control via the gate voltage allows for interesting applications. We propose to use double quantum dot structures to build spin valves.

From a theoretical point of view, a single quantum dot is enough to produce spin-polarized currents. The idea is simple: a magnetic field applied to the quantum dot shifts the energy level of one distinct spin species out of resonance. Via appropriate gating the second spin species can be kept at resonance. The problem, however, comes from the energy scales. In conventional GaAs-based heterostructures the level splitting is of the order of 0.025 meV/T and typical hybridization energies Γ ranging between 0.1 and 10 meV (see Cronenwett et al. [1998], Goldhaber-Gordon et al. [1998], Schmid et al. [1998]). In order to have a substantial current, one needs a contact transparency Γ as large as possible. Then, however, huge magnetic fields are necessary to achieve a high degree of spin polarization. In these setups, a compromise has always to be arranged between intensity of current and spin-polarization quality. Spin valves based on anti-resonances (see Dahlhaus et al. [2010]) in double quantum dot structures are not afflicted by this optimization problem.

2.4.1. Double quantum dot spin valve

The operating mode of the double quantum dot spin valve is similar to the single quantum dot one. But instead of using the Zeeman splitting to shift one spin species out of resonance, the Zeeman splitting is used to align the resonance peak of one spin species with the anti-resonance dip of the other one (see fig. 2.25). The transmission coefficient of the different spin species in presence of a magnetic field h is given by

$$T_\sigma(\omega) = T(\omega + \sigma h), \quad (2.212)$$

where we have redefined the magnetic field $h = \mu_B g h / 2$. In order to keep one spin species, say σ , in resonance, we have to apply an appropriate gate voltage, i.e. we have to shift $\Delta = \Delta + \sigma h$. Effectively, this can be described by introducing the quantities $h_\pm = 0, -2h$ where $h_+ = 0$ denotes the spin species which is blocked and $h_- = -2h$ the spin species which is transmitted. To define a measure for the efficiency of the double quantum dot spin valve we introduce the spin polarized

currents,

$$I_{\pm} = G_0 \int d\omega T(\omega + h_{\pm}) [n_L(\omega) - n_R(\omega)], \quad (2.213)$$

where $G_0 = e^2/h$ is the conductance quantum and $n_{L,R}(\omega) = n_F(\omega \mp V/2)$ are Fermi distribution functions of the leads. From this we may draw predictions for the universal linear response regime, where the linear conductance is a fundamental quantity. We define it for the distinct spin species by

$$G_{\pm} = \lim_{V \rightarrow 0} \frac{I_{\pm}(V)}{V}. \quad (2.214)$$

Then, the efficiency of our spin valve can be measured by the spin filtering quality factor q defined by

$$q = \left| \frac{G_+ - G_-}{G_+ + G_-} \right|. \quad (2.215)$$

A quality factor of $q = 1$ then indicates perfect spin filtering and $q = 0$ the flow of a totally unpolarized current. For an experimental application, effects of several perturbations have to be considered. We have already argued that deviations from the symmetrically tunneling coupled system does in general not destroy the anti-resonance. Another important issue is the role of temperature or the role of interactions which we would like to discuss next.

2.4.2. Spin-valve for finite temperature

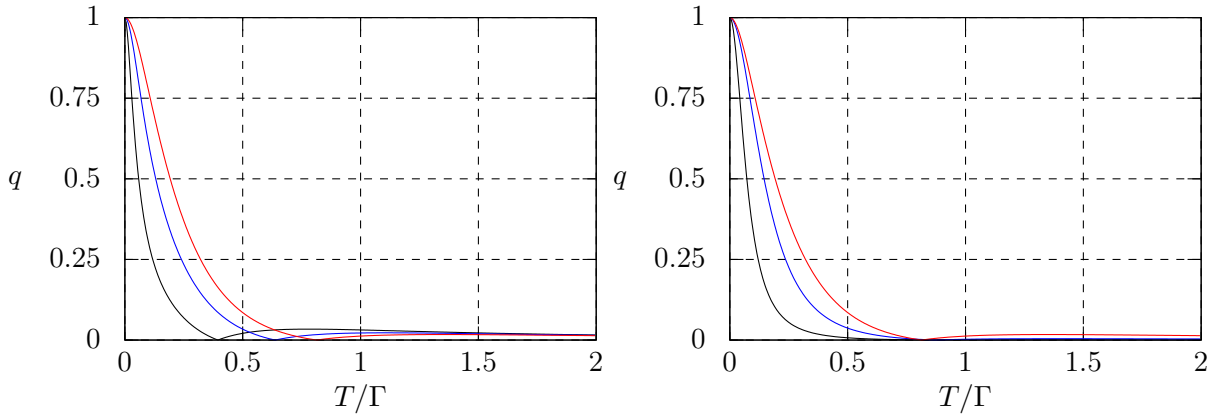


Figure 2.26.: Temperature dependence of the quality factor. The **left graph** depicts the quality factor for fixed magnetic field $h/\Gamma = 0.5$ as a function of temperature for several dot level detunings $\Delta/\Gamma = 0.5, 0.75, 0.95$ (black, blue and red). The graph to the **right** shows the quality factor for fixed dot level detuning $\Delta/\Gamma = 0.95$ and several magnetic fields $h/\Gamma = 0.1, 0.25, 0.5$ (black, blue and red).

In the non-interacting case, the effect of the temperature on the quality factor has its origin in the temperature dependence of the Fermi distribution functions in eq. (2.213). Because of the Lorentzian structure of the transmission coefficient in eq. (2.211), an analytical expression of the spin-polarized currents can be obtained. We find

$$I_{\pm} = \frac{2i\Gamma}{\sqrt{4\Gamma^2 - \Delta^2}} \sum_{l,m,n=\pm} (mn) \Omega_m \psi \left(\frac{1}{2} + \frac{ilh_{\pm} - inV/2 + \Omega_m}{2\pi T} \right) \quad (2.216)$$

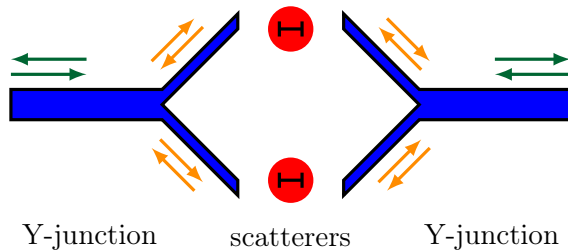


Figure 2.27.: Scattering matrix approach for the spin valve. In terms of scattering and transfer matrices, the double quantum dot system can be decomposed into three regions. Two Y-junctions describing how the modes from the leads (green arrows) are distributed among the arms of the interferometer (orange arrows) and a scattering region given by the scattering matrices of the quantum dots.

where ψ is the Digamma function. The linear conductance can then be found by an expansion of the ψ functions with respect to the voltage V . This leads to

$$G_{\pm} = \frac{2\Gamma}{\sqrt{4\Gamma^2 - \Delta^2}} \sum_{m,n=\pm} \frac{m\Omega_m}{2\pi T} \psi' \left(\frac{1}{2} + \frac{inh_{\pm} + \Omega_m}{2\pi T} \right), \quad (2.217)$$

where ψ' is the first derivative of the ψ function. In fig. 2.26, q is depicted as a function of temperature for several dot level energies Δ and several magnetic fields h . The important observation is, that for temperatures realized in experiments, the efficiency is nearly perfect. Typical values for the temperature are of the order of several 10 mK and therefore $T/\Gamma \lll 1$.

2.4.3. Effect of electron-electron interactions

It is known, that resonance and anti-resonance features can be quite robust with respect to interactions (see for example Breyel [2010], Meden and Marquardt [2006]). In principle, the effect of electron-electron interactions in quantum dot devices can be rather strong. Under certain circumstances, it can also lead to the Kondo effect. However, for sufficiently large quantum dots or sufficiently high temperatures (higher than the Kondo temperature), the effect of electron-electron interactions can be treated perturbatively. For a quantum dot system where tunneling is exactly accounted for, there are no divergences in the perturbative expansion in the electron-electron interaction.

In this section we consider the effect of onsite interactions to the spin valve setup. Instead of using Keldysh Green's function methods, we employ an approach based on scattering matrices which is more suitable to calculate effective transmission coefficients. In order to proceed, we decompose our spin valve setup into three regions: a left Y-junction, a middle scattering region and a right Y-junction, see fig. 2.27. Details to this kind of decomposition of similar interferometer geometries can be found in Büttiker et al. [1984], Kubala and König [2003]. The Y-junctions are described by scattering matrices S_Y defined by

$$(\beta_1, \beta_2, \beta_3) = S_Y (\alpha_1, \alpha_2, \alpha_3) \quad (2.218)$$

i.e. it describes how the incoming modes α_i are scattered into outgoing modes β_i . In case of

symmetric Y-junctions, there are no free parameters in the S_Y matrix (Nayak et al. [1999]),

$$S_Y = \begin{pmatrix} 1/3 & 2/3 & 2/3 \\ 2/3 & 1/3 & -2/3 \\ 2/3 & -2/3 & 1/3 \end{pmatrix}. \quad (2.219)$$

The respective scattering matrix of the quantum dots is given by

$$S_i = \begin{pmatrix} r_i & t_i^* \\ t_i & r_i^* \end{pmatrix} \quad (2.220)$$

where t_i are the transmission amplitudes of the quantum dots and r_i the reflection amplitudes. In case of a non-interacting system, one trivially has

$$t_i = \frac{-i\Gamma}{\omega - \Delta_i - i\Gamma} \quad (2.221)$$

$$r_i = \frac{\omega - \Delta_i}{\omega - \Delta_i - i\Gamma}. \quad (2.222)$$

Using the scattering matrix above, one finds after a lengthy but straightforward calculation for the transmission coefficient

$$T(\omega) = 4 \left| \frac{t_1 t_2 r_1^* - t_1^* t_2 r_2 - t_1 t_2 r_1^* + t_1^* t_2^* r_2}{t_1 t_2 - t_1^* t_2^* - t_2^* r_1 - t_1^* r_2 + t_1^* r_2^*} \right|^2. \quad (2.223)$$

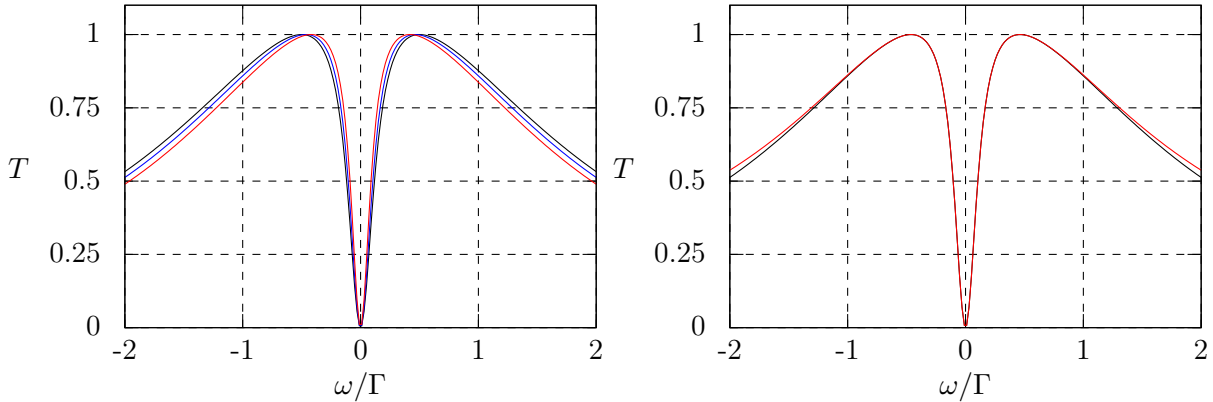


Figure 2.28.: Effective transmission coefficient for the spin valve including onsite interactions. The **left graph** depicts the effective transmission coefficient for dot level detuning $\Delta/\Gamma = 0.5$ and self energy corrections linear in ω and second order U/π . The bare interaction strength is $U/\Gamma = 0, 1, 1.5$ (black, blue and red). The graph to the **right** compares the effective model for corrections to the self energy linear in ω (black curve) with the effective model including up to order ω^2 into the self energy (red curve). The bare interaction strength in this case is $U/\Gamma = 1$ and the dot level energy $\Delta/\Gamma = 0.5$.

Following Hecht et al. [2009] and Bruder et al. [1996] the transmission amplitudes can be expressed in terms of the retarded Green's functions of the scattering region, i.e. the hybridized quantum dots D_i^R . It possesses the representation (Yamada [1975b]),

$$D_{i,\sigma}^R(\omega) = \frac{1}{\omega - \Delta_i - \text{Re} \Sigma_{i,\sigma}^R(\omega) + i \left[\Gamma - \text{Im} \Sigma_{i,\sigma}^R(\omega) \right]} \quad (2.224)$$

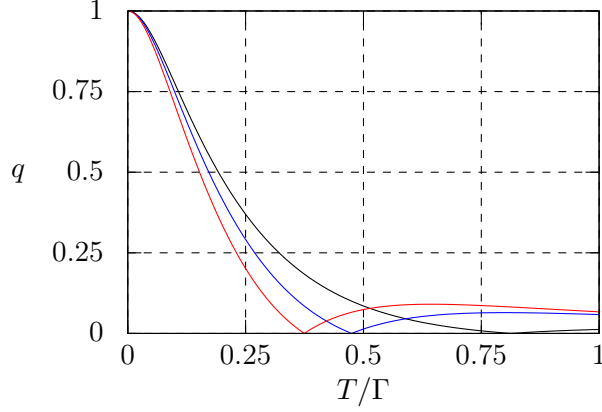


Figure 2.29.: Temperature dependence of the double quantum dot spin valve including onsite interactions. The magnetic field is fixed to $h/\Gamma = 0.95$ and the dot level detuning to $\Delta/\Gamma = 0.95$. The onsite interaction strength is varied $U/\Gamma = 0, 1, 1.5$ (black, blue and red).

where $\Sigma_i^R(\omega)$ is the self-energy due to onsite interaction. For the spin valve, it is sufficient to know the self-energy around $\omega = 0$. There are quite good approximations around for $\Sigma^R(\omega)$ of the Anderson model (Horvatić and Zlatić [1980], Yamada [1975a], Yosida and Yamada [1970, 1975], Zlatić and Horvatić [1983]). In leading order of ω , the correction to the real part is (Oguri [2001]),

$$\text{Re } \Sigma_{i,\sigma}^R(\omega) = \chi_{i,c}(\Delta_i + U/2) + \sigma h \chi_{i,s} + \left(1 - \frac{\chi_{i,c} - \chi_{i,s}}{2}\right) \omega + \dots \quad (2.225)$$

where $\chi_{i,c/s}$ are the static charge/spin susceptibilities and are known for arbitrary U from the Bethe ansatz (Zlatić and Horvatić [1983]). $(\Delta_i + U/2)$ is the electron-hole symmetry breaking field. We conclude, that up to a shift of the dot level energies, $\delta\Delta_i = \text{Re } \Sigma_{i,\sigma}^R(0)$ the anti-resonance survives. In principle, the same quality of spin polarization is achievable. The width of the anti-resonance is affected by the imaginary part of the self-energy. The leading order correction to the width is ω^2 , which is obvious since it is responsible for the dissipative part (inelastic processes). One finds for the transmission coefficient

$$T(\omega) = \frac{4\Gamma^2}{4\Gamma^2 + \left[\frac{1}{\omega(\chi_{1,c} - \chi_{1,s})/2 - (\Delta_1 + \delta\Delta_1)} + \frac{1}{\omega(\chi_{2,c} - \chi_{2,s})/2 - (\Delta_2 + \delta\Delta_2)} \right]^{-2}}. \quad (2.226)$$

For small onsite interactions U , we can use an expansion for the susceptibilities (Horvatić and Zlatić [1980]) and rewrite the transmission coefficient again as a sum of two Lorentzians. One just has to rescale the widths $\Omega_{\pm} \rightarrow \Omega_{\pm}/\alpha$ with $\alpha = \frac{U^2}{2\pi^2\Gamma^2} \left[3 - \frac{\pi^2}{4} + \left(\frac{25}{3} - \frac{3\pi^2}{4} \right) \frac{\Delta^2}{\Gamma^2} \right]$. In fig. 2.28, the transmission coefficient is plotted for several interaction strengths and the effect of higher order corrections in ω is included. One observes a reduced width of the anti-resonance. However, it remains perfect, i.e. zero transmission is accomplished. The effect of higher order corrections in ω is less pronounced in the anti-resonance itself. Deviations are observed in the tails of the transmission coefficient. In fig. 2.29, we depicted the temperature dependent quality factor of the interacting spin valve. Again, quality remains nearly perfect for temperatures achieved in experiments.

The effect of inter-dot interaction was investigated in Dahlhaus [2009] and details can be found therein. We only refer to some results. In fig. 2.30, the effect of the inter-dot interaction is depicted

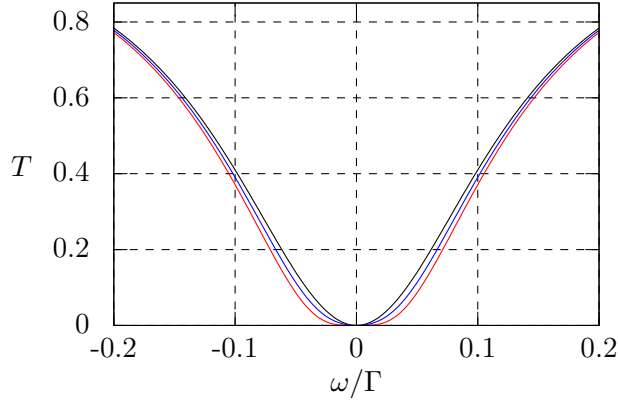


Figure 2.30.: Effective transmission coefficient of the spin valve including inter-dot interactions. The dot level energy is fixed to $\hbar/\Gamma = 0.95$ and the dot level detuning to $\Delta/\Gamma = 0.5$. The interaction strength $V_{\perp}/\Gamma = V_{\parallel}/\Gamma = 0, 0.05, 0.01$ is varied (black, blue and red).

for several interaction strengths. The tendencies are opposite as compared to the case of onsite interactions. An increase of the interaction leads to a broadening of the anti-resonance. We have only depicted the transmission coefficient for very small perturbations. This has two reasons: first, the results are purely perturbative and secondly, in experiments inter-dot interactions are usually quite small, i.e. negligible.

2.4.4. Results and discussion

We have proposed a novel device for spin-polarized current generation and detection based on double quantum dot structures. The key feature of its operating mode is the generic existence of sharp and tunable anti-resonances in the transmission coefficient of these kinds of interferometer geometries. We have introduced a quality factor to measure the efficiency of spin filtering. We have demonstrated the robustness of our spin valve against intrinsic and extrinsic factors such as temperature, asymmetry and interactions. We expect that our spin valve can be implemented in state-of-the-art double quantum dot devices as presented in [Holleitner et al. \[2001\]](#) and [Wilhelm et al. \[2002\]](#). The results of this section are published in [Dahlhaus et al. \[2010\]](#).

3. Impurities in ultracold quantum gases: the BEC polaron problem

In the last couple of years, the field of cold atom physics influenced the condensed matter community like no other discipline. The rapidly increased gain of control of cold atom systems opened a new field to test models and ideas originally coming from solid state theory. There are barely other systems where external potentials and interaction parameters can be tuned that precisely and over such a wide range of magnitude like in cold quantum gases. We are interested in Bose-Einstein condensates (BEC's) interspersed with impurities (Bosons or Fermions) or mixtures of cold quantum gases (Bose/Bose- or Bose/Fermi mixtures). These kinds of setups are very similar to problems in solid state theory involving electron-phonon coupling.

This chapter is organized as follows: first, we introduce a general description of BEC's with impurities and demonstrate how they can be mapped on various models from solid state theory. In the second section, observable quantities like the polaron mass, the polaron radius and the density-density correlation function are introduced. Thirdly, we study the problem with a perturbative approach. The subsequent section examines the polaron problem with Quantum Monte Carlo (QMC) methods. In the fifth section the Jensen-Feynman variational principle is applied to the BEC polaron. The sixth part is dedicated to Cherenkov radiation in mixtures of cold quantum gases. A discussion concludes this chapter. Details not included in the main text can be found in appendix B.

3.1. The BEC polaron problem

In this section we build up the basic framework of the BEC polaron theory. We do not intend to give a theoretical description of the phenomenon of Bose-Einstein condensation itself, neither do we comment on experimental methods to create and control Bose-Einstein condensates. There are plenty of excellent textbooks (Leggett [2006], Pethick and Smith [2008], Pitaevskii and Stringari [2003], Stoof et al. [2009]) and various review articles (Bloch et al. [2008], Chin et al. [2010], Dalfovo et al. [1999], Morsch and Oberthaler [2006]) giving broad and detailed introductions into these subjects. Here, we focus on the description of mixtures of ultracold quantum gases instead.

After the first experimental realization of a BEC (Anderson et al. [1995], Bradley et al. [1997], Davis et al. [1995]), the investigation of mixtures of quantum gases naturally arose. Early experiments with mixtures consisting of two different kinds of bosons (Myatt et al. [1997]) showed, that via sympathetic cooling a two-component BEC can be created by only cooling one boson species. Using crude approximations like Thomas-Fermi (Ho and Shenoy [1996]) or Hartree-Fock approximation (Esry et al. [1997]), these kinds of experiments can be understood quite easily. Shortly after first predictions concerning Bose-Fermi mixtures have been made (phase diagram, mixing-demixing properties by Mølmer [1998], limitation of sympathetic cooling by Timmermans and Côté [1998])

and only a couple of years later, the first Bose-Fermi mixtures have been realized experimentally by [Truscott et al. \[2001\]](#) and [Schreck et al. \[2001\]](#).

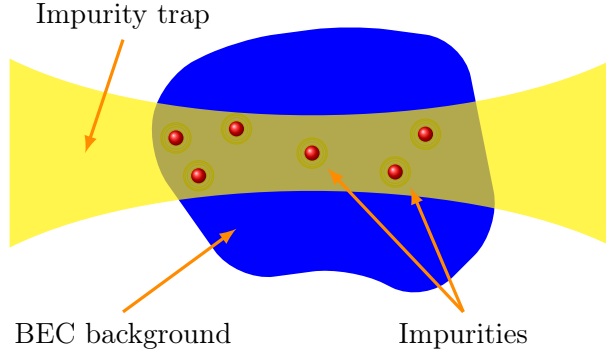


Figure 3.1.: Sketch of the BEC polaron setup.

In the following, we will closely follow the works of [Tempere et al. \[2009\]](#) and [Novikov and Ovchinnikov \[2010\]](#). A microscopic model for impurities in BEC is given by the Hamiltonian,

$$H = H_B + H_I + H_{I-B}. \quad (3.1)$$

The bosons are described by

$$H_B = \frac{-1}{2m_B} \int d^3\mathbf{r} \Phi^\dagger(\mathbf{r}) (\nabla^2 - \mu) \Phi(\mathbf{r}) + \frac{1}{2} \int d^3\mathbf{r} d^3\mathbf{r}' \rho_B(\mathbf{r}) V_B(\mathbf{r} - \mathbf{r}') \rho_B(\mathbf{r}') \quad (3.2)$$

where Φ , Φ^\dagger are field operators describing a homogeneous Bose gas, $\rho_B = \Phi^\dagger \Phi$ is the boson density, m_B is the mass of the bosons, μ is the chemical potential and V_B is a contact interaction,

$$V_B(\mathbf{r}) = g_{BB} \delta(\mathbf{r}). \quad (3.3)$$

Via the Lippmann-Schwinger equation, the parameter g_{BB} of the pseudopotential can be linked to the experimentally accessible s-wave scattering length α_{BB} ,

$$g_{BB} = \frac{4\pi\alpha_{BB}}{m_B}. \quad (3.4)$$

Assuming a homogeneous Bose gas is not really a severe constraint. In experiments, two traps are used, one for the BEC and another for the impurities. Therefore, the impurities can be placed inside the BEC far away from the boundaries. The contribution H_I in eq. (3.1) describes the impurities,

$$H_I = \frac{-1}{2m_I} \int d^3\mathbf{r} \Psi^\dagger(\mathbf{r}) \nabla^2 \Psi(\mathbf{r}) + \int d^3\mathbf{r} V_{\text{ext}}(\mathbf{r}) \Psi^\dagger(\mathbf{r}) \Psi(\mathbf{r}) \quad (3.5)$$

where Ψ , Ψ^\dagger are field operators which may be fermions or bosons, m_I is the mass of the impurities and V_{ext} is an external potential, for example, a trap potential for the impurities. The impurity-boson interaction is described by a density-density interaction,

$$H_{I-B} = \int d^3\mathbf{r} d^3\mathbf{r}' \rho_I(\mathbf{r}) V_{I-B}(\mathbf{r} - \mathbf{r}') \rho_B(\mathbf{r}'), \quad (3.6)$$

where $\rho_I = \Psi^\dagger \Psi$ and V_{I-B} again is a contact interaction,

$$V_{I-B}(\mathbf{r}) = g_{IB} \delta(\mathbf{r}). \quad (3.7)$$

The pseudopotential parameter g_{IB} can be related to the s-wave scattering length α_{IB} for BEC-impurity scattering,

$$g_{\text{IB}} = \frac{2\pi\alpha_{\text{IB}}}{m'} \quad (3.8)$$

where m' is the reduced mass, $m'^{-1} = m_{\text{B}}^{-1} + m_{\text{I}}^{-1}$. Before proceeding, a little remark about the s-wave scattering approach is in order. This kind of approximation is valid, if the thermal de Broglie wavelength $\lambda_{\text{T}} = \sqrt{\frac{2\pi\beta}{m}}$ (m is the reduced mass of the two scattering particles) is large compared to the range of the interatomic interactions. In this case, the particles only sense the low momentum behaviour of the true interaction potential (see for example [Stoof et al. \[2009\]](#)).

Using the momentum representation of the bosonic fields,

$$\Phi(\mathbf{r}) = \frac{1}{\sqrt{V}} \sum_{\mathbf{k}} a_{\mathbf{k}} e^{i\mathbf{k}\mathbf{r}} \quad (3.9)$$

where V is the volume of the BEC the Hamiltonian H_{B} transforms to

$$H_{\text{B}} = \sum_{\mathbf{k}} E_{\mathbf{k}} a_{\mathbf{k}}^{\dagger} a_{\mathbf{k}} + \frac{g_{\text{BB}}V}{2} \sum_{\mathbf{q}} \rho_{\text{B}}(\mathbf{q}) \rho_{\text{B}}(-\mathbf{q}) \quad (3.10)$$

with

$$\rho_{\text{B}}(\mathbf{q}) = \frac{1}{V} \sum_{\mathbf{k}} a_{\mathbf{k}+\mathbf{q}}^{\dagger} a_{\mathbf{k}}, \quad (3.11)$$

and

$$E_{\mathbf{k}} = \frac{\mathbf{k}^2}{2m_{\text{B}}} - \mu. \quad (3.12)$$

Similarly, the impurity sector can be rewritten to

$$H_{\text{I-B}} = g_{\text{IB}}V \sum_{\mathbf{q}} \rho_{\text{I}}(\mathbf{q}) \rho_{\text{B}}(-\mathbf{q}). \quad (3.13)$$

We are interested in a dilute Bose gas, i.e. we use Bogoliubov's prescription and replace the operators for zero momentum by a c -number, $a_0 = \sqrt{N}$ where N is the number of bosons and keep only terms quadratic in $a_{\mathbf{k}}$, $a_{\mathbf{k}}^{\dagger}$ for $\mathbf{k} \neq 0$. Details of the calculation can be found in [Pitaevskii and Stringari \[2003\]](#). After some algebra one obtains

$$H_{\text{B}} = \frac{g_{\text{BB}}N^2}{2V} + \sum_{\mathbf{k}} E_{\mathbf{k}} a_{\mathbf{k}}^{\dagger} a_{\mathbf{k}} + \frac{g_{\text{BB}}n}{2} \sum_{\mathbf{k} \neq 0} \left(2a_{\mathbf{k}}^{\dagger} a_{\mathbf{k}} + a_{\mathbf{k}}^{\dagger} a_{-\mathbf{k}}^{\dagger} + a_{\mathbf{k}} a_{-\mathbf{k}} + \frac{g_{\text{BB}}nm_{\text{I}}}{\mathbf{k}^2} \right) \quad (3.14)$$

and

$$H_{\text{I-B}} = g_{\text{IB}}N + g_{\text{IB}}\sqrt{N} \sum_{\mathbf{k} \neq 0} \rho_{\text{I}}(\mathbf{k}) \left(a_{\mathbf{k}} + a_{-\mathbf{k}}^{\dagger} \right) \quad (3.15)$$

where n is the density of the condensate, $n = \frac{N}{V}$. Using standard Bogoliubov rotation, the Hamiltonians can be diagonalized,

$$H_{\text{B}} = E_{\text{GP}} + \sum_{\mathbf{k} \neq 0} \epsilon_{\mathbf{k}} b_{\mathbf{k}}^{\dagger} b_{\mathbf{k}} + \sum_{\mathbf{k} \neq 0} \frac{g_{\text{BB}}nm_{\text{I}}}{\mathbf{k}^2} \quad (3.16)$$

$$H_{\text{I-B}} = g_{\text{IB}}N + g_{\text{IB}} \sum_{\mathbf{k} \neq 0} \sqrt{\frac{\xi_{\mathbf{k}}N}{\epsilon_{\mathbf{k}}}} \rho_{\text{I}}(\mathbf{k}) \left(b_{\mathbf{k}} + b_{-\mathbf{k}}^{\dagger} \right) \quad (3.17)$$

where $b_{\mathbf{k}}, b_{\mathbf{k}}^\dagger$ annihilate or create Bogoliubov excitations, E_{GP} is the Gross-Pitaevskii energy,

$$E_{\text{GP}} = N\epsilon_0 + \frac{g_{\text{BB}}N^2}{2V} + \frac{g_{\text{BB}}}{2} \sum_{\mathbf{k} \neq 0} n, \quad (3.18)$$

$\xi_{\mathbf{k}}$ the free particle energy $\xi_{\mathbf{k}} = \frac{\mathbf{k}^2}{2m_{\text{B}}}$ and $\epsilon_{\mathbf{k}}$ the Bogoliubov spectra,

$$\epsilon_{\mathbf{k}} = \sqrt{\xi_{\mathbf{k}}(\xi_{\mathbf{k}} + 2g_{\text{BB}}n)} = ck\sqrt{1 + \frac{(\xi k)^2}{2}}. \quad (3.19)$$

In eq. (3.19), we have introduced the sound velocity $c := \frac{k_c}{2m_{\text{B}}} := \frac{\sqrt{16\pi n \alpha_{\text{BB}}}}{2m_{\text{B}}}$ of the condensate, where k_c is the inverse coherence length, and the healing length $\xi := 1/\sqrt{8\pi n \alpha_{\text{BB}}}$. Omitting constant shifts in energy, one finds

$$H_{\text{B}} = \sum_{\mathbf{k}} E_{\mathbf{k}} b_{\mathbf{k}}^\dagger b_{\mathbf{k}} \quad (3.20)$$

$$H_{\text{I-B}} = \sum_{\mathbf{k} \neq 0} V_{\mathbf{k}} \rho_{\text{I}}(\mathbf{k}) (b_{\mathbf{k}} + b_{-\mathbf{k}}^\dagger) \quad (3.21)$$

with the interaction potential $V_{\mathbf{k}} = g_{\text{IB}} \sqrt{\frac{(\xi k)^2}{(\xi k)^2 + 2}}$. Assuming the impurities to be fermions and free in space, i.e. $V_{\text{ext}} = 0$, the model reduces to the well-known Fröhlich model (Fröhlich [1954]),

$$\begin{aligned} H &= H_{\text{B}} + H_{\text{I}} + H_{\text{I-B}} \\ &= \sum_{\mathbf{k}} \frac{\mathbf{k}^2}{2m_{\text{I}}} c_{\mathbf{k}}^\dagger c_{\mathbf{k}} + \sum_{\mathbf{k}} \epsilon_{\mathbf{k}} b_{\mathbf{k}}^\dagger b_{\mathbf{k}} + \sum_{\mathbf{k}, \mathbf{q}} V_{\mathbf{k}} c_{\mathbf{q}+\mathbf{k}}^\dagger c_{\mathbf{q}} (b_{\mathbf{k}} + b_{-\mathbf{k}}^\dagger) \end{aligned} \quad (3.22)$$

where $c_{\mathbf{k}}, c_{\mathbf{k}}^\dagger$ annihilates, creates a particle with momentum \mathbf{k} . The validity of this mapping to the Fröhlich model was extensively discussed in Sacha and Timmermans [2006] and Cucchietti and Timmermans [2006]. The Hamiltonians we have discussed in chapter 2 all had a momentum independent electron-phonon interaction, i.e. the interaction was local in space. This is not the case for the BEC polaron.

Next, the model is mapped to a single particle problem. This is best achieved in a path integral formalism. The action after the Bogoliubov approximation is

$$\begin{aligned} S &= \int d\tau d^3\mathbf{r} \bar{\Psi}(\mathbf{r}, \tau) \left[\partial_\tau - \frac{\nabla^2}{2m_{\text{I}}} + V_{\text{ext}}(\mathbf{r}) + \sum_{\mathbf{k}} V_{\mathbf{k}} e^{i\mathbf{k}\mathbf{r}} (b_{\mathbf{k}}(\tau) + \bar{b}_{-\mathbf{k}}(\tau)) \right] \Psi(\mathbf{r}, \tau) \\ &\quad + \sum_{\mathbf{k}} \int d\tau \bar{b}_{\mathbf{k}}(\tau) (\partial_\tau + \epsilon_{\mathbf{k}}) b_{\mathbf{k}}(\tau). \end{aligned} \quad (3.23)$$

We are mainly interested in the correlation function

$$G(\mathbf{r} - \mathbf{r}', \tau) = \frac{1}{\mathcal{Z}} \int \mathcal{D}[\bar{\Psi}, \Psi, \bar{b}_{\mathbf{k}}, b_{\mathbf{k}}] \Psi(\mathbf{r}, \tau) \bar{\Psi}(\mathbf{r}', 0) e^{-S} \quad (3.24)$$

where \mathcal{Z} is the grand canonical partition function,

$$\mathcal{Z} = \int \mathcal{D}[\bar{\Psi}, \Psi, \bar{b}_{\mathbf{k}}, b_{\mathbf{k}}] e^{-S}. \quad (3.25)$$

Therefore, it is important to introduce the generating functional,

$$\mathcal{Z}[j, \bar{j}] = \frac{1}{\mathcal{Z}} \int \mathcal{D}[\bar{\Psi}, \Psi, \bar{b}_{\mathbf{k}}, b_{\mathbf{k}}] e^{-S - \int d^3\mathbf{r} d\tau [j(\mathbf{r}, \tau)\Psi(\mathbf{r}, \tau) + \bar{j}(\mathbf{r}, \tau)\bar{\Psi}(\mathbf{r}, \tau)]} \quad (3.26)$$

Via the stationary phase method, the functional integration with respect to the impurity fields can be performed. The stationary field Ψ_0 has to fulfill the equation

$$\dot{\Psi}_0(\mathbf{r}, \tau) - \underbrace{\left[\partial_\tau - \frac{\nabla^2}{2m_{\text{I}}} + V_{\text{ext}}(\mathbf{r}) + \sum_{\mathbf{k}} V_{\mathbf{k}} e^{i\mathbf{k}\mathbf{r}} (b_{\mathbf{k}}(\tau) + \bar{b}_{-\mathbf{k}}(\tau)) \right]}_{=:-H_{\text{SP}}(\mathbf{r}, \tau)} \Psi_0(\mathbf{r}, \tau) - \bar{j}(\mathbf{r}, \tau) = 0 \quad (3.27)$$

with the boundary conditions, $\Psi_0(\mathbf{r}, 0) = \bar{\Psi}_0(\mathbf{r}, \beta) = 0$. Formally, the solution can be expressed as

$$\Psi_0(\mathbf{r}, \tau) = \int_0^\tau d\sigma \exp \left[\int_\sigma^\tau d\sigma' H_{\text{SP}}(\mathbf{r}, \sigma') \right] \bar{j}(\mathbf{r}, \sigma). \quad (3.28)$$

Therefore, the generating functional can be rewritten,

$$\mathcal{Z}[j, \bar{j}] = \frac{1}{\mathcal{Z}} \int \mathcal{D}[\bar{b}_{\mathbf{k}}, b_{\mathbf{k}}] e^{-S[\bar{b}_{\mathbf{k}}, b_{\mathbf{k}}] + \int d\tau d\tau' \Theta(\tau - \tau') \langle j(\mathbf{r}, \tau), e^{-\int_{\tau'}^\tau H_{\text{SP}}(\mathbf{r}, \tau)} \bar{j}(\mathbf{r}, \tau') \rangle} \quad (3.29)$$

where the single particle propagator,

$$\langle j(\mathbf{r}, \tau), e^{-\int_{\tau'}^\tau H_{\text{SP}}(\mathbf{r}, \tau)} \bar{j}(\mathbf{r}, \tau') \rangle = \int d^3\mathbf{r} j(\mathbf{r}, \tau) e^{-\int_{\tau'}^\tau H_{\text{SP}}(\mathbf{r}, \tau)} \bar{j}(\mathbf{r}, \tau') \quad (3.30)$$

and the action of the free bosons

$$S[\bar{b}_{\mathbf{k}}, b_{\mathbf{k}}] = \sum_{\mathbf{k}} \int d\tau \bar{b}_{\mathbf{k}}(\tau) (\partial_\tau + \epsilon_{\mathbf{k}}) b_{\mathbf{k}}(\tau) \quad (3.31)$$

have been introduced. Using path integral representation of this propagator, eq. (3.24) can most elegantly be expressed as,

$$G(\mathbf{r} - \mathbf{r}', \tau) = \int \mathcal{D}[\bar{b}_{\mathbf{k}}, b_{\mathbf{k}}] \int_{\mathbf{r}(0)=\mathbf{r}}^{\mathbf{r}(\beta)=\mathbf{r}'} \mathcal{D}\mathbf{r}(\tau) e^{-S_{\text{SP}} - S[\bar{b}_{\mathbf{k}}, b_{\mathbf{k}}]} \quad (3.32)$$

where we have defined the single particle action

$$S_{\text{SP}} = \int d\tau \left[\frac{m_{\text{I}} \dot{\mathbf{r}}^2}{2} + V_{\text{ext}}(\mathbf{r}) + \sum_{\mathbf{k}} V_{\mathbf{k}} e^{i\mathbf{k}\mathbf{r}} (b_{\mathbf{k}}(\tau) + \bar{b}_{-\mathbf{k}}(\tau)) \right]. \quad (3.33)$$

Formally, we can extract the underlying Hamilton formalism of the expression above,

$$H_{\text{SP}} = \frac{\hat{\mathbf{p}}^2}{2m_{\text{I}}} + V_{\text{ext}}(\hat{\mathbf{r}}) + \sum_{\mathbf{k}} \epsilon_{\mathbf{k}} b_{\mathbf{k}}^\dagger b_{\mathbf{k}} + \sum_{\mathbf{k}} V_{\mathbf{k}} e^{i\mathbf{k}\hat{\mathbf{r}}} (b_{\mathbf{k}} + b_{-\mathbf{k}}^\dagger). \quad (3.34)$$

In the following, we will make use of both formulations of the BEC polaron problem. The single particle path integral formalism is very suitable for variational calculations and numerics. The many-impurity formulation is, from the viewpoint of condensed matter physics, more intuitive. Throughout the rest of this chapter, we use units with $\hbar = m_{\text{I}} = \xi = 1$. Hence, energy is measured in units of $\hbar^2 / (m_{\text{I}} \xi^2)$

3.2. Polaron mass, radius and Bragg spectroscopy

In this section we briefly discuss experimentally relevant quantities. Due to interactions with the background BEC, the microscopic properties of an impurity like its mass m_I can be significantly changed. In case of weak interactions, a quasiparticle picture similar to the Fermi liquid theory can be applied (see for example Mahan [2000]). In lowest order perturbation theory, this leads to an effective mass description. In case of strong coupling to the Bogoliubov modes, this picture no longer applies: a polaron is formed. It is still possible to ascribe a mass to it though. In section 3.5 we will identify the polaron mass to a variational parameter. An interesting property of the polaron is its self-trapping, i.e. the phenomenon of its localization. A measure for the localization is the polaron radius R_{Pol} . In terms of correlation functions it is given by (see Tempere et al. [2009])

$$R_{\text{Pol}}^2 = \lim_{\tau \rightarrow 0} \langle \mathbf{r}(\tau) \mathbf{r}(0) \rangle. \quad (3.35)$$

In cold atom physics, Bragg spectroscopy is often used to probe the density-density correlation function, i.e. the two particle correlation functions, of the system of interest. The generic setup is

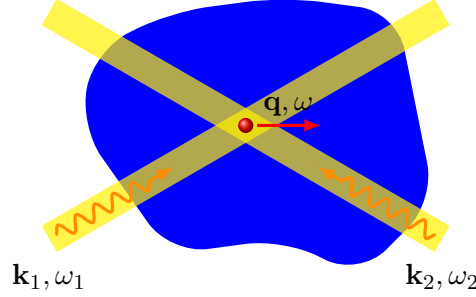


Figure 3.2.: Bragg spectroscopy: two laser beams with momenta $\mathbf{k}_1, \mathbf{k}_2$ and frequencies ω_1, ω_2 are crossed inside the BEC. Then, the impurity can undergo a sequence of absorbing a photon from one laser field and subsequently emitting a photon into the other laser field. The transferred momentum is given by $\mathbf{q} = \mathbf{k}_1 - \mathbf{k}_2$ and transferred energy $\omega = \omega_1 - \omega_2$.

depicted in fig. 3.2: using a set of two laser beams with wave vectors $\mathbf{k}_1, \mathbf{k}_2$ and frequencies ω_1, ω_2 an atom/molecule can undergo a sequence of absorption and emission: first, it can absorb a photon, say from laser beam one with momentum and energy (\mathbf{k}_1, ω_1) , and, subsequently emits a photon with momentum and energy (\mathbf{k}_2, ω_2) into beam two. In terms of a time-dependent perturbation, this can be described by the Hamiltonian

$$H_{\text{Bragg}} = \frac{1}{2} V_0 \rho_{\mathbf{q}} e^{i\omega t} + \text{H.c.} \quad (3.36)$$

where $\mathbf{q} = \mathbf{k}_1 - \mathbf{k}_2$ is the momentum transfer, $\omega = \omega_1 - \omega_2$ the energy transfer, $\rho_{\mathbf{q}}$ particle density in momentum space and V_0 the atom-photon interaction strength. Using linear response theory, the density-density correlation function can be linked to observable quantities like the energy transfer rate (in the limit of large measuring times),

$$\frac{dE(t)}{dt} = \frac{V_0^2}{2} \omega \text{Im} \chi(\omega, \mathbf{q}) \quad (3.37)$$

or the momentum transfer rate

$$\frac{dP(t)}{dt} = \frac{V_0^2}{2} |\mathbf{q}| \text{Im} \chi(\omega, \mathbf{q}) \quad (3.38)$$

with

$$\chi(\omega, \mathbf{q}) = \int dt e^{i\omega t} \Theta(t) \left\langle \left[\rho_{\mathbf{q}}(t), \rho_{\mathbf{q}}^{\dagger}(0) \right] \right\rangle \quad (3.39)$$

which is nothing more than the Fourier transform of the retarded density-density correlation function. For details see for example [Brunello et al. \[2001\]](#). In time-of-flight experiments, the number of particles gaining a momentum $|\mathbf{q}|$ during a Bragg pulse can be measured ([Pitaevskii and Stringari \[2003\]](#)).

3.3. BEC polaron: perturbative approach

As starting point of our perturbative treatment, we use the single particle formalism. We assume the impurity to be confined in a harmonic potential. The action is then

$$S_{\text{SP}} = \int d\tau \left[\frac{\dot{\mathbf{r}}^2}{2} + \sum_{\alpha=x,y,z} \frac{\Omega_{\alpha} r_{\alpha}^2}{2} + \sum_{\mathbf{k}} \epsilon_{\mathbf{k}} b_{\mathbf{k}}^{\dagger} b_{\mathbf{k}} + \sum_{\mathbf{k}} V_{\mathbf{k}} e^{i\mathbf{k}\mathbf{r}} (b_{\mathbf{k}}(\tau) + \bar{b}_{-\mathbf{k}}(\tau)) \right]. \quad (3.40)$$

The bosonic degrees of freedom can easily be integrated out and one finds an effective action,

$$S_{\text{eff}} = \int d\tau \left[\frac{\dot{\mathbf{r}}^2}{2} + \sum_{\alpha=x,y,z} \frac{\Omega_{\alpha} r_{\alpha}^2}{2} \right] + \sum_{\mathbf{k}} \frac{V_{\mathbf{k}}^2}{2} \int d\tau d\tau' G_{\text{Bog}}(\mathbf{k}, \tau - \tau') e^{i\mathbf{k}[\mathbf{r}(\tau) - \mathbf{r}(\tau')]} \quad (3.41)$$

with the Green's function of the Bogoliubov excitations,

$$G_{\text{Bog}}(\mathbf{k}, \tau - \tau') = \frac{\cosh \left[\frac{k\sqrt{\mathbf{k}^2+2}}{4m_{\text{B}}} (2\tau - \beta) \right]}{\sinh \left(\frac{k\sqrt{\mathbf{k}^2+2}}{4m_{\text{B}}} \beta \right)}. \quad (3.42)$$

In units of $\hbar = \xi = k_{\text{B}} = 1$, the interaction potential is $V_{\mathbf{k}}^2 = \alpha \frac{k}{\sqrt{\mathbf{k}^2+2}}$ with $\alpha = \frac{\alpha_{\text{IB}}^2}{\alpha_{\text{BB}}}$. The polaron radius R_{Pol} is given by the limit $\tau \rightarrow 0$ of the Matsubara Green's function,

$$G(\tau) = \langle \mathbf{r}(\tau) \mathbf{r}(0) \rangle = \sum_{i=1}^3 \langle \mathbf{r}_i(\tau) \mathbf{r}_i(0) \rangle_i = \sum_{i=1}^3 G_i(\tau), \quad (3.43)$$

where we have used that the effective action factorizes with respect to spatial dimensions. $\langle \cdot \rangle_i$ is calculated for the 1D problem with trap frequency Ω_i . The polaron radius R_{Pol} can be expanded in the electron-phonon interaction,

$$R_{\text{Pol}}^2 = \lim_{\tau \rightarrow 0} \sum_{i=1}^3 \left[G_i^{(0)}(\tau) + G_i^{(1)}(\tau) \right] + \mathcal{O}(\alpha^2). \quad (3.44)$$

The leading order contribution is given by Matsubara Green's function of the non-interacting system (see eq. (B.9) in the appendix)

$$G_i^{(0)}(\tau) = \frac{1}{2\Omega_i} \frac{\cosh[\Omega_i(|\tau| - \beta/2)]}{\sinh(\Omega_i\beta/2)}. \quad (3.45)$$

The leading order correction $\sum_i G_i^{(1)}$ can best be obtained using the thermal Schwinger functional $W_0[\{\eta_i\}]$ for the free model defined by

$$W_0[\{\eta_i\}] = \left\langle e^{-\sum_{i=1}^3 \int d\tau \eta_i(\tau) \mathbf{r}_i(\tau)} \right\rangle_0. \quad (3.46)$$

We can now decompose the source field η into $\eta_i(\tau) = \tilde{\eta}_i(\tau) + \mathbf{i}\mathbf{k}_i [\delta(\tau - \tau_1) - \delta(\tau - \tau_2)]$. Correlation functions then can be obtained by taking functional derivatives with respect to $\tilde{\eta}(\tau)$. With this in mind, the leading order correction can be calculated to

$$G_i^{(1)}(\tau) = \sum_{\mathbf{k}} V_{\mathbf{k}}^2 \int d\tau_1 d\tau_2 G_{\text{Bog}}(\mathbf{k}, \tau_1 - \tau_2) \frac{\delta^2 W[\{\eta_i\}]}{\delta \tilde{\eta}_i(\tau) \delta \tilde{\eta}_i(0)} \Big|_{\eta_i=0}. \quad (3.47)$$

The functional derivative is evaluated to

$$\begin{aligned} \frac{\delta^2 W[\{\eta_i\}]}{\delta \tilde{\eta}_i(\tau) \delta \tilde{\eta}_i(0)} \Big|_{\eta_i=0} &= -k_i^2 e^{-\sum_j k_j^2 [G_j^{(0)}(0) - G_j^{(0)}(\tau_1 - \tau_2)]} \\ &\times \left[G_i^{(0)}(0 - \tau_2) - G_i^{(0)}(0 - \tau_1) \right] \left[G_i^{(0)}(\tau - \tau_2) - G_i^{(0)}(\tau - \tau_1) \right]. \end{aligned} \quad (3.48)$$

In principle, the time integrations in expression eq. (3.47) can be performed using the Jacobi-Anger expansion. However, the cost is an additional sum the terms of which are weighted by modified Bessel functions. Often, this sum rapidly converges and one has to evaluate a few terms only. In an experimentally relevant regime, the trap frequency is of the order of several 100 Hz ($\Omega \approx 0.001$). In this case, one has to consider many terms. It turns out, that a numerical integration right from the beginning is much more efficient and accurate. In table 3.1, some numerical values of

| | $K_c = 300$ | $K_c = 400$ | $K_c = 500$ |
|---------------|-------------|-------------|-------------|
| $\beta = 5$ | -2.4336 | -2.4343 | -2.4347 |
| $\beta = 10$ | -5.4864 | -5.4867 | -5.4905 |
| $\beta = 20$ | -11.7690 | -11.7830 | -11.7705 |
| $\beta = 50$ | -30.3079 | -30.3434 | -30.2756 |
| $\beta = 100$ | -59.9408 | -60.0306 | -59.7562 |

Table 3.1.: Numerical values for $\sum_i G_i^1$ for different temperatures and frequency cut-off parameters K_c . The trap is chosen to be homogeneous with frequency $\Omega_i = 0.001$ and the mass ratio m_B is fixed to $m_B = 3.8$ (which corresponds to $^{23}\text{Na} - ^6\text{Li}$).

the leading order correction for different but experimentally relevant temperatures and momentum cut-off parameters K_c are given. In case of a sodium-lithium ($^{23}\text{Na} - ^6\text{Li}$), the relative mass is $m_B = 3.8$. A weak dependence on the momentum cut-off is observed.

A perturbative treatment for the density-density correlation function $\chi^R(\mathbf{k}, \omega)$,

$$\chi^R(\mathbf{q}, \omega) = \int_{-\infty}^{\infty} dt \chi(\mathbf{q}, t) e^{i\omega t} = \int_{-\infty}^{\infty} dt \Theta(t) \langle [\rho(\mathbf{q}, t), \rho(-\mathbf{q}, 0)] \rangle e^{i\omega t} \quad (3.49)$$

is much more challenging. The reasons are the following: First, our calculations are based on a finite-temperature Greens function formalism, a.k.a Matsubara Green's functions and they are defined on the imaginary time axis. However, the density-density correlation function is a dynamical quantity and is defined on the real axis. Hence, one has to perform an analytical continuation of the finite-temperature correlation functions. Secondly, the resulting expressions of the perturbation

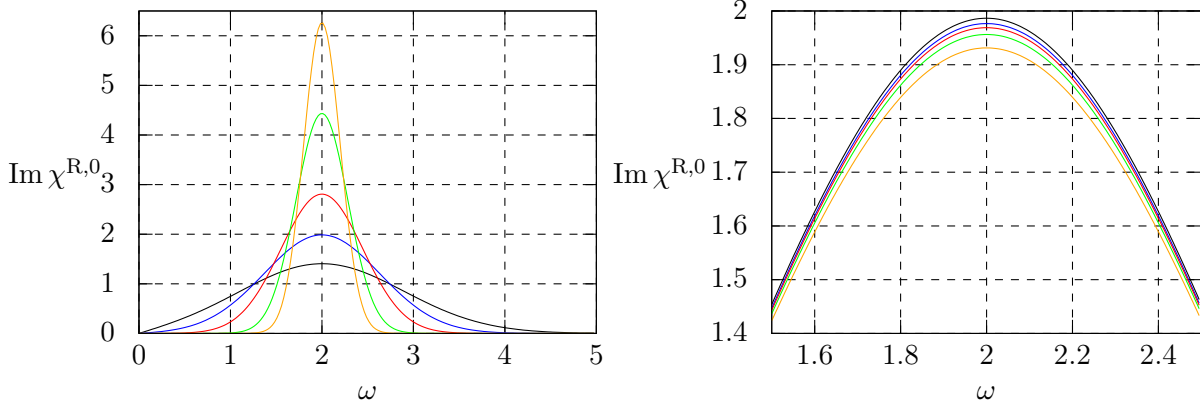


Figure 3.3.: Imaginary part of the density-density correlation function. **Left panel:** The parameters are $q_i = 2$, $\Omega = 0.001$ and $\epsilon_d = 0.001$. The inverse temperatures are $\beta = 5, 10, 20, 50, 100$ (black, blue, red, green and orange curves). **Right panel:** The parameters are $k_i = 2$, $\Omega = 0.001$ and $\beta = 10$. The regularization parameter ϵ_d is $\epsilon_d = 0.001, 0.002, 0.005, 0.01, 0.02$ (black, blue, red, green and orange curves).

expansion contain sequences of δ -peaks (they are positioned at multiples of the trap frequency). This is obvious, because hybridization is a non-perturbative effect. We address this issues in the following. The leading order contribution to the density-density correlation function is

$$\begin{aligned} \chi^{(0)}(\mathbf{q}, \tau) &= \left\langle e^{i\mathbf{q}\mathbf{r}(\tau)} e^{-i\mathbf{q}\mathbf{r}(0)} \right\rangle_0 = e^{-\sum_{i=1}^3 \mathbf{q}_i^2 [G_i^{(0)}(0) - G_i^{(0)}(\tau)]} \\ &= \sum_{\substack{n_i=-\infty \\ i=1,2,3}}^{\infty} \prod_i I_{n_i} \left[\frac{q_i^2}{2\Omega_i \sinh\left(\frac{\Omega_i \beta}{2}\right)} \right] e^{-\frac{q_i^2}{2\Omega_i} \coth\left(\frac{\Omega_i \beta}{2}\right)} e^{n_i \Omega_i (\tau - \beta/2)}. \end{aligned} \quad (3.50)$$

In the second line of eq. (3.50) we have used the Jacobi-Anger relation to rewrite the exponential. The Fourier transform of this expression simply can be found,

$$\chi^{(0)}(\mathbf{q}, i\omega_n) = 2 \sum_{\substack{n_i=-\infty \\ i=1,2,3}}^{\infty} \prod_i I_{n_i} \left[\frac{q_i^2}{2\Omega_i \sinh\left(\frac{\Omega_i \beta}{2}\right)} \right] e^{-\frac{q_i^2}{2\Omega_i} \coth\left(\frac{\Omega_i \beta}{2}\right)} \frac{\sinh\left(\frac{\sum_j n_j \Omega_j \beta}{2}\right)}{\left(\sum_j n_j \Omega_j\right) + i\omega_n}. \quad (3.51)$$

In case of a spherically symmetric trap, i.e. $\Omega_i = \Omega$, $i = 1, \dots, 3$, the expression further simplifies to

$$\chi^{(0)}(\mathbf{q}, i\omega_n) = 2 \sum_{n=-\infty}^{\infty} I_n \left[\frac{\mathbf{q}^2}{2\Omega \sinh\left(\frac{\Omega \beta}{2}\right)} \right] e^{-\frac{\mathbf{q}^2}{2\Omega} \coth\left(\frac{\Omega \beta}{2}\right)} \frac{\sinh\left(\frac{n\Omega \beta}{2}\right)}{n\Omega + i\omega_n}. \quad (3.52)$$

The density-density correlation function eq. (3.49) can then be obtained by analytical continuation, $i\omega_n \rightarrow \omega + i0^+$. The Bragg spectroscopy probes the imaginary part of the retarded density-density correlation function

$$\text{Im} \chi^{\text{R},0}(\mathbf{q}, \omega) = -2\pi \sum_{n=-\infty}^{\infty} I_n \left[\frac{\mathbf{q}^2}{2\Omega \sinh\left(\frac{\Omega \beta}{2}\right)} \right] e^{-\frac{\mathbf{q}^2}{2\Omega} \coth\left(\frac{\Omega \beta}{2}\right)} \sinh\left(\frac{n\Omega \beta}{2}\right) \delta(n\Omega + \omega) \quad (3.53)$$

which is nothing else than a sequence of δ -peaks. Because of interactions with the BEC, dissipation effects lead to a broadening of these peaks. This process is highly non-perturbative. To get a feeling

for the outcome, one can perform a Wigner-Weisskopf (Weisskopf and Wigner [1930]) regularization to model the effects of dissipation. This introduces an artificial time scale τ_d , i.e. a decay time, into the problem. From an experimental point of view, there is an upper bound for this time scale: the measurement time. Using the Wigner-Weisskopf regularization scheme, we can replace the δ -peaks by normalized Lorentz peaks with a width of $\delta_d = 1/\tau_d$. In fig. (3.3), the leading order contribution to the imaginary part of the density-density correlation function is depicted for several temperatures and regularization parameters. As expected, for increasing temperatures the width of the peak decreases while its height increases. The dependence on the regularization parameter ϵ_d is not difficult to understand: with increasing ϵ_d the single Lorentzians tend to overlap more. However, the deviations are small as long as $\Omega < \epsilon_D$ and ϵ_d is much smaller than the other energy scales of the system.

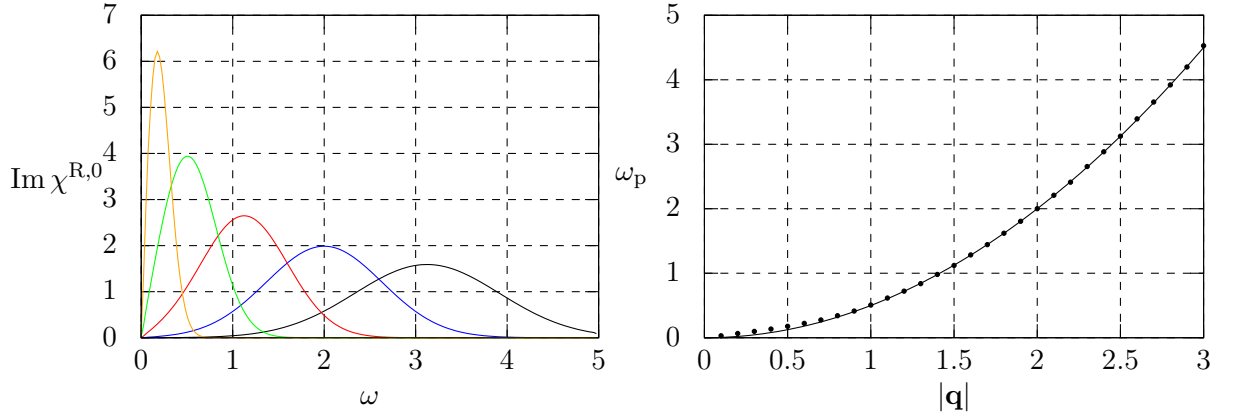


Figure 3.4.: Momentum dependence of the imaginary part of the density-density correlation function. **Left panel:** The parameters are $\epsilon_d = 0.001$ and $\beta = 10$. The transferred momentum is $|\mathbf{q}| = 0.5, 1, 1.5, 2, 2.5$ (black, blue, red, green and orange curves). **Right panel:** The momentum dependence of the peak position ω_p is depicted. The parameters are $\Omega = 0.001$, $\epsilon_d = 0.001$ and $\beta = 10$. The solid line is the function $\mathbf{q}^2/2$.

In fig. 3.4, the momentum dependence of $\text{Im } \chi^{R,0}(\mathbf{q}, \omega)$ is depicted. In case of a flat trapping potential (i.e. $\Omega \ll 1$), the position of the peak $\omega_p(\mathbf{q})$ is given by $\omega_p(\mathbf{q}) \approx \mathbf{q}^2/2$ independent of the temperature

The leading order correction $\chi^{(1)}(\mathbf{q}, \tau)$ is given by

$$\chi^{(1)}(\mathbf{q}, \tau) = \sum_{\mathbf{k}} |V_{\mathbf{k}}|^2 \int d\tau_1 d\tau_2 G_{\text{Bog}}(\mathbf{k}, \tau_1 - \tau_2) \left\langle e^{i\mathbf{q}\mathbf{r}(\tau)} e^{-i\mathbf{q}\mathbf{r}(0)} e^{i\mathbf{k}\mathbf{r}(\tau_1)} e^{-i\mathbf{k}\mathbf{r}(\tau_2)} \right\rangle_0. \quad (3.54)$$

The expectation value of the exponential can be calculated using the thermal Schwinger functional with the source field

$$\eta(\tau') = i\mathbf{q} [\delta(\tau' - \tau) - \delta(\tau')] + i\mathbf{k} [\delta(\tau' - \tau_1) - \delta(\tau' - \tau_2)]. \quad (3.55)$$

In case of an isotropic system, $\Omega_i = \Omega$, one obtains,

$$\begin{aligned} \left\langle e^{i\mathbf{q}\mathbf{r}(\tau)} e^{-i\mathbf{q}\mathbf{r}(0)} e^{i\mathbf{k}\mathbf{r}(\tau_1)} e^{-i\mathbf{k}\mathbf{r}(\tau_2)} \right\rangle_0 &= \exp \left\{ -\mathbf{q}^2 [G^0(0) - G^0(\tau)] - \mathbf{k}^2 [G^0(0) - G^0(\tau_1 - \tau_2)] \right\} \\ &\times \exp \left\{ -\mathbf{q}\mathbf{k} [G^0(\tau_1) - G^0(\tau_2) + G^0(\tau - \tau_2) - G^0(\tau - \tau_1)] \right\}. \end{aligned} \quad (3.56)$$

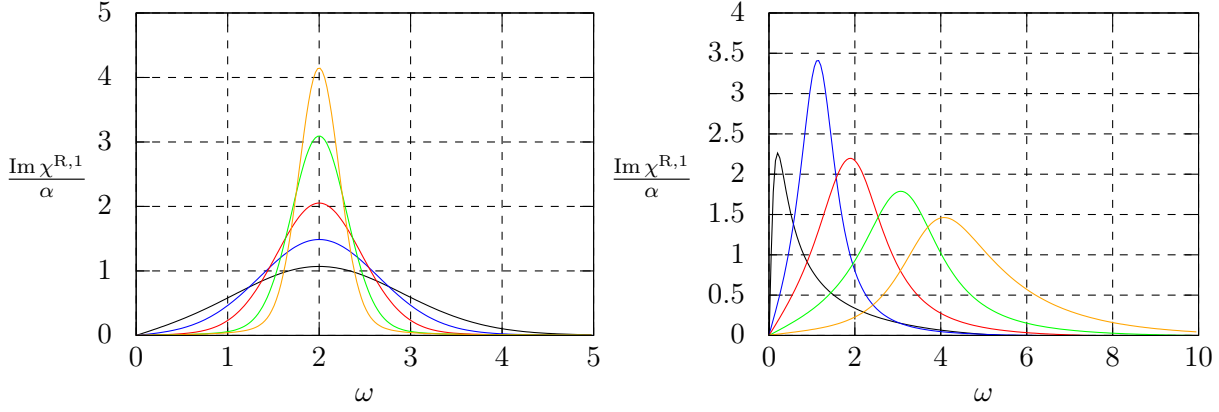


Figure 3.5.: Imaginary part of the leading order correction of the density-density correlation function. **Left panel:** The parameters are $|\mathbf{q}| = 2$, $\Omega = 0.001$ and $\epsilon_d = 0.001$. The inverse temperatures are $\beta = 5, 10, 20, 50, 100$ (black, blue, red, green and orange curves). **Right panel:** The parameters are $\Omega = 0.001$, $\epsilon_d = 0.001$ and $\beta = 10$. The transferred momentum k is varied from $q = 1, 1.5, 2, 2.5, 3$ (black, blue, red, green and orange curves).

The integrals in eq. (3.54) have been evaluated numerically. In fig. 3.3 the leading order correction to the density-density correlation function is depicted. The dependence of the peak properties is similar to that of the non-interacting contribution, $\chi^{R,0}$.

3.4. Imaginary time path integral Monte Carlo simulation

To go beyond perturbation theory, one can employ the imaginary time path integral Monte Carlo method. The starting point is again the action eq. (3.41),

$$S_{\text{eff}} = \int d\tau \left[\frac{\dot{\mathbf{r}}^2}{2} + \sum_{\alpha=x,y,z} \frac{\Omega_\alpha r_\alpha^2}{2} \right] + \sum_{\mathbf{k}} \frac{V_{\mathbf{k}}^2}{2} \int d\tau d\tau' G_{\text{Bog}}(\mathbf{k}, \tau - \tau') e^{i\mathbf{k}[\mathbf{r}(\tau) - \mathbf{r}(\tau')]} \quad (3.57)$$

The interaction potential $V_{\mathbf{k}}$ only depends on the modulus of \mathbf{k} , therefore, in the thermodynamic limit $\sum_{\mathbf{k}} \rightarrow \frac{V}{(2\pi)^3} \int d\mathbf{k}$, the angular integration can easily be performed,

$$\sum_{\mathbf{k}} \frac{V_{\mathbf{k}}^2}{2} \int d\tau d\tau' G_{\text{Bog}}(\mathbf{k}, \tau - \tau') e^{i\mathbf{k}[\mathbf{r}(\tau) - \mathbf{r}(\tau')]} = V \int \frac{dk}{4\pi^2} \frac{\sin k |\mathbf{r}(\tau) - \mathbf{r}(\tau')|}{k |\mathbf{r}(\tau) - \mathbf{r}(\tau')|} k^2 V_{\mathbf{k}}^2 G_{\text{Bog}}(\mathbf{k}, \tau - \tau'). \quad (3.58)$$

In our system of units, the effective action is,

$$S_{\text{eff}} = \int d\tau \left[\frac{\dot{\mathbf{r}}^2}{2} + \sum_{\alpha=x,y,z} \frac{\Omega_\alpha r_\alpha^2}{2} \right] + \int d\tau d\tau' \int \frac{dk}{8\pi} \frac{k^2 \alpha G_{\text{Bog}}(k, \tau - \tau')}{\sqrt{k^2 + 2}} \frac{\sin k |\mathbf{r}(\tau) - \mathbf{r}(\tau')|}{k |\mathbf{r}(\tau) - \mathbf{r}(\tau')|}. \quad (3.59)$$

The coupling constant α has been introduced in the previous section, $\alpha = \frac{\alpha_{\text{IB}}^2}{\alpha_{\text{BB}}}$. It is crucial to notice, that in this representation, the action is obviously a real (and positive) quantity and hence the Boltzmann factor $p[\mathbf{r}(\tau)] = e^{-S_{\text{eff}}[\mathbf{r}(\tau)]}/\mathcal{Z}$ has all the properties of a probability distribution

function. Therefore, stochastic methods like Monte Carlo simulations are very suitable for the calculations of expectation values of observables \mathcal{O} ,

$$\langle \mathcal{O} \rangle = \int \mathcal{D}[r(\tau)] p[r(\tau)] \mathcal{O}[r(\tau)] \quad (3.60)$$

or more general correlations functions. In the following section, we introduce the basic principles of path integral Monte Carlo simulations. We are not aiming for a comprehensive introduction and would like to refer to a number of textbooks (for example [Landau and Binder \[2005\]](#), [Pang \[2006\]](#)) and review articles ([Ceperley \[1995\]](#), [Foulkes et al. \[2001\]](#)).

3.4.1. Monte Carlo integration, Markov processes and importance sampling

The underlying method of path integral Monte Carlo simulations is the Monte Carlo integration scheme. In the framework of high dimensional integration, the need for stochastic methods arises quite naturally. For example, the error estimate of the d -dimensional integral

$$I = \int d^d x f(x) \quad (3.61)$$

using Simpson's rule scales like $N^{-2/d}$ where N is the total number of sampling points (see [Freund and Hoppe \[2007\]](#)). For large d , the evaluation using standard quadratures is very time-consuming from a numerical point of view. Stochastic methods are often less sensitive to the dimension of the integral. For example, the integral

$$I = \int d^d x f(x) = \int d^d x g(x) p(x), \quad (3.62)$$

where $p(x)$ is a probability density, i.e. $\int d^d x p(x) = 1$ and $p(x) \geq 0$, can be estimated by

$$I \approx \bar{g} = \frac{1}{N} \sum_{\substack{i=1 \\ x_i \in p(x)}}^N g(x_i) \quad (3.63)$$

where the x_i are drawn randomly according to the probability density $p(x)$. Due to the central limit theorem, for large N , the average \bar{g} approaches the exact value of the integral I . More precisely, the random variable \bar{g} converges to a Gaussian distribution with mean value $I = \langle g \rangle := \int d^d x g(x) p(x)$ and variance

$$\sigma_g^2 = \frac{1}{N} \langle (g - \langle g \rangle)^2 \rangle. \quad (3.64)$$

As a consequence, the purely statistical error of the estimate \bar{g} scales as $N^{-1/2}$ and is therefore independent of d .

The representation of the integrand $f(x)$ in eq. (3.62) as a product of a new function $g(x)$ and a probability density $p(x)$ is by no means unique. For example, in case of a finite support of f , say $[a, b]$, a suitable density might be $p(x) = \frac{1}{b-a}$. In this case, one trivially finds $g(x) = f(x)$ and the random numbers x_i are uniformly drawn from $[a, b]$. However, this choice might be very inefficient, for instance if the function $f(x)$ is sharply peaked around a value x' . Therefore, the probability density should account as best as possible for the structure of $f(x)$. This is known as importance sampling. There is little to say about a generic method to find a good probability density for

arbitrary $f(x)$. Luckily, in the framework of path integral Monte Carlo there are candidates arising quite naturally: the Boltzmann factors.

However, there is an issue using Boltzmann factors $p[r(\tau)] = e^{-S[r(\tau)]}/\mathcal{Z}$ as probability densities. In general, the partition function \mathcal{Z} is unknown, hence, $p[r(\tau)]$ is known up to proper normalization, $p[r(\tau)] = \alpha p'[r(\tau)]$. Therefore, it is not directly possible to use standard transformation rules (see [Press et al. \[2007\]](#)) to create random numbers according to the probability density p using uniformly distributed random numbers. In the following, we describe a method to generate appropriate samples using a Markov process together with the Metropolis algorithm.

A sequence of configurations (x_1, x_2, \dots) is called a Markov chain, if the $(n+1)$ -th element can be determined from its predecessor x_n according to a transition probability $M_{n \rightarrow n+1}$. Using a Markov chain, the problem of drawing samples according to a given probability is translated to a stochastic dynamical process: the transition from a configuration x_n to a configuration x_{n+1} is given with a probability $M_{n \rightarrow n+1}$. One can show that under the assumptions of ergodicity and detailed balance the elements of the Markov chain indeed are drawn according to the probability distribution p . Loosely speaking, ergodicity is the property, that for each pair of configurations x, x' there exists a finite sequence y_1, \dots, y_n with

$$M_{x \rightarrow y_1} M_{y_1 \rightarrow y_2} \cdots M_{y_{n-1} \rightarrow y_n} M_{y_n \rightarrow x'} > 0, \quad (3.65)$$

i.e. there is a finite probability of a transition $x \rightarrow x'$ with a finite number of intermediate steps. Detailed balance is the property

$$p(x) M_{x \rightarrow x'} = p(x') M_{x' \rightarrow x} \quad (3.66)$$

for each pair x, x' of configurations. For more details on Markov chains see for example [Bremaud \[2001\]](#). The Metropolis algorithm ([Metropolis et al. \[1953\]](#)) is a procedure for constructing a Markov chain with a given (not necessarily normalized) probability density $p = \alpha p'$. From a configuration x , using a stochastic transformation rule $T_{x \rightarrow x'}$ a new configuration x' is proposed. The only restriction to $T_{x \rightarrow x'}$ is the symmetry property, i.e. $T_{x \rightarrow x'} = T_{x' \rightarrow x}$. The precise prescription of the stochastic transformation rule is problem specific. In case of path integral Monte Carlo, one would randomly change a set of sampling points, i.e. deform the path a little. We specify the stochastic transformation rule later. The proposed configuration x' is accepted according to a probability distribution,

$$A_{x \rightarrow x'} = \begin{cases} 1 & \text{if } p(x') > p(x) \\ \frac{p(x')}{p(x)} & \text{if } p(x') < p(x) \end{cases}, \quad (3.67)$$

i.e. $A_{x \rightarrow x'}$ is the probability that the proposed configuration x' is accepted given a configuration x . It is important that these probabilities can be determined without the knowledge of the proper normalization of the probability density p . It is easy to verify, that the transition probability defined as $M_{x \rightarrow x'} = T_{x \rightarrow x'} A_{x \rightarrow x'}$ fulfills the conditions of detailed balance. For example if $p(x') > p(x)$ one obtains,

$$p(x) M_{x \rightarrow x'} = p(x) T_{x \rightarrow x'} = p(x') \frac{p(x)}{p(x')} T_{x' \rightarrow x} = p(x') M_{x' \rightarrow x}. \quad (3.68)$$

From a theoretical point of view, ergodicity is not an issue. Under the assumption that there is a process generating arbitrarily many random numbers, say uniformly in an interval $[0, 1]$, the configuration space can be sampled using random walks. However, from a practical point of view, ergodicity is not achieved that simply. There is the issue of generating random numbers. Although

there are random number generators based on randomness due to quantum physical effects (see for example [Erber and Putterman \[1985\]](#), [Martino and Morris \[1991\]](#), [Ren et al. \[2011\]](#)), they are far from being state-of-the-art.¹ Therefore, one has to draw on to pseudo random number generators. A nice introduction to this subject can be found in the textbook [Gentle \[2010\]](#). For our simulations, we used a 32-bit Mersenne twister (period length $2^{19937} - 1$, equi-distributed in 623 dimensions, passes Diehard tests) described in [Matsumoto and Nishimura \[1998\]](#)

3.4.2. Error analysis and correlations

Most numerical data are only available with limited accuracy. In general, there are two sources for numerical uncertainties. First, there are systematic errors. For example, the representation of numbers is always limited by certain hardware constraints. This can be an issue if one has to deal with very large and very small numbers at the same time. This should (and often can) be avoided in the design of algorithms. Another systematic error stems from the discretization of continuous expressions. In path integral Monte Carlo, these are the finite Trotter decompositions (a.k.a Trotter error) and the restriction to a finite set of Matsubara frequencies. They can be systematically analyzed, see for example [Fye \[1986\]](#). However, it is much more convenient to investigate the dependence of the outcome with respect to the discretization and cut-off parameters. In simulations with short or medium runtime, good control of the systematic errors is achieved this way. The second class of uncertainties stems from the stochastic nature of the method. Coming back to the Monte Carlo integration problem, eq. (3.63),

$$\bar{g} = \frac{1}{N} \sum_{\substack{i=1 \\ x_i \in p(x)}}^N g(x_i), \quad (3.69)$$

in case of uncorrelated measurements $g(x_i)$, an estimate of the variance can be obtained by

$$\sigma_g^2 = \frac{1}{N(N-1)} \sum_{i=1}^N (g(x_i) - \bar{g})^2 = \frac{1}{N-1} (\bar{g}^2 - \bar{g}^2). \quad (3.70)$$

Correlations, however, are an intrinsic problem of Markov chain sampling methods. An estimation of the variance in presence of correlation is given by

$$\sigma_g^2 = \frac{1}{N^2} \sum_{i,j=1}^N [\langle g(x_i) g(x_j) \rangle - \langle g(x_i) \rangle \langle g(x_j) \rangle] \quad (3.71)$$

Due to the Markov chain property, two consecutive configurations x_i and x_{i+1} are in general positively correlated. Hence, the expression for the variance not including correlations underestimates the statistical error. This can simply be verified by splitting the sum in expression eq. (3.71) into a diagonal contribution $i = j$ and an off-diagonal contribution $i \neq j$. Then, the diagonal contribution is up to a bias factor $N/(N+1)$ equal to the variance calculated under the assumption of uncorrelated measurements. A measure for correlations is the normalized autocorrelation function,

$$R(k) = \frac{\langle g(x_1) g(x_{1+k}) \rangle - \langle g(x_1) \rangle \langle g(x_{1+k}) \rangle}{\langle g(x_1) g(x_1) \rangle - \langle g(x_1) \rangle \langle g(x_1) \rangle} \quad (3.72)$$

¹Recently, there are commercial brands available, see for example <http://www.idquantique.com>

and the autocorrelation time τ_g ,

$$\tau_g = 1 + 2 \sum_{k=1}^N R(k) \left(1 + \frac{k}{N}\right). \quad (3.73)$$

The autocorrelation function $R(k)$ determines the degree of correlation of a pair of configurations separated by k intermediate samples, i.e. x_i and x_{i+k} . The variance can easily be expressed in terms of the autocorrelation time,

$$\sigma_g^2 = \frac{1}{N^2} \sum_{i=1}^N \left(\langle g(x_i)^2 \rangle - \langle g(x_i) \rangle^2 \right) \tau_g. \quad (3.74)$$

Instead of using every sample in the Markov chain, taking every k -th sample, i.e. restriction to the sub-chain $x_1, x_{1+k}, x_{1+2k}, \dots$, can substantially reduce correlations. k has to be chosen in such a way that the $A(k)$ is sufficiently close to zero. The variance can then be estimated under the assumption of uncorrelated measurements x_i . Another method to account for correlations is binning. Instead of using the measurements $g(x_i)$, one uses block averages,

$$g_{B,i} = \frac{1}{k} \sum_{j=1}^k g(x_{(i-1)k+j}). \quad (3.75)$$

For sufficiently large k , the correlation of the block averages $g_{B,i}$ can be neglected. Then, the variance can be estimated by

$$\sigma_g^2 = \frac{1}{N_B (N_B - 1)} \sum_{i=1}^{N_B} (g_{B,i} - \bar{g}_B)^2, \quad (3.76)$$

where $N = kN_B$ and $\bar{g}_B = \frac{1}{N_B} \sum_{i=1}^{N_B} g_{B,i}$. Continuously keeping track of correlations during a Monte Carlo simulation is quite time consuming. It is convenient to determine the correlation of the measurements in a pre-run. With this information, the Monte Carlo simulation can be optimized using sub-Markov chains or the binning procedure.

3.4.3. Analytical continuation and Padé approximants

Using path integral Monte Carlo approach, correlation functions can be calculated in imaginary time only. However, response functions like the optical conductivity require the knowledge of correlation functions on the real axis. Therefore, we need methods for the analytical continuation of our numerical data. Nowadays, there are several methods to archive this. The most popular are the Padé approximants [Baker \[1975\]](#), [Vidberg and Serene \[1977\]](#), the singular value decomposition [Bertero et al. \[1985\]](#), [Creffield et al. \[1995\]](#) and the maximum entropy method [Jarrell and Gubernatis \[1996\]](#). We will focus on the Padé approximant.

Given the values of a (correlation) function G for a finite, discrete set of frequencies, for example Matsubara frequencies, $G(i\omega_n) = u_n$ for $n = 1, \dots, N$, G can be determined for $z \in \mathbb{C}$ via a continuous fraction,

$$G(z) = \frac{a_1}{(z - i\omega_1) + \frac{a_2}{(z - i\omega_2) + \dots}} \quad (3.77)$$

where the parameters a_1, \dots, a_N have to be chosen in such a way, that $G(i\omega_i) = u_i$ holds. This can be achieved recursively. First, we define a matrix $A_{i,j}$, $A_{1,i} = u_i$, $i = 1, \dots, N$

$$A_{i,j} = \frac{A_{i-1,j-1} - A_{i-1,j}}{(i\omega_j - i\omega_{i-1}) A_{i-1,j}}. \quad (3.78)$$

and a_i lying on the diagonal, $a_i = A_{i,i}$. Alternatively to the continuous fraction, $G(z)$ can be represented as a rational function,

$$G(z) = \frac{A_N(z)}{B_N(z)} \quad (3.79)$$

where the polynomials A_N, B_N are defined recursively, $A_0 = 0, A_1 = a_1, B_0 = B_1 = 1$ and for $n \geq 1$

$$A_{n+1}(z) = A_n(z) + (z - i\omega_n) a_{n+1} A_{n-1}(z) \quad (3.80)$$

$$B_{n+1}(z) = B_n(z) + (z - i\omega_n) a_{n+1} B_{n-1}(z). \quad (3.81)$$

Therefore, the analytical continuation of a Matsubara correlation function can simply be found by calculating the matrix $A_{i,j}$.

3.4.4. QMC simulation for the BEC polaron

In this section, we adapt the general Metropolis Monte Carlo algorithm to the BEC polaron problem. The starting point is the effective action S eq. (3.41) which can be split into a free contribution S_0 ,

$$S_0[\mathbf{r}(\tau)] = \int d\tau \left[\frac{\dot{\mathbf{r}}^2}{2} + \sum_{\alpha=x,y,z} \frac{\Omega_\alpha r_\alpha^2}{2} \right], \quad (3.82)$$

and a contribution including interaction effects,

$$S_I[\mathbf{r}(\tau)] = \int d\tau d\tau' \int \frac{dk k^2}{8\pi} \frac{\alpha k G_{\text{Bog}}(k, \tau - \tau') \sin k |\mathbf{r}(\tau) - \mathbf{r}(\tau')|}{\sqrt{k^2 + 2}} \frac{1}{k |\mathbf{r}(\tau) - \mathbf{r}(\tau')|}. \quad (3.83)$$

In general, we are interested in observables like expectation values $\langle \mathcal{O} \rangle$,

$$\langle \mathcal{O} \rangle = \int \mathcal{D}[\mathbf{r}(\tau)] \mathcal{O}[\mathbf{r}(\tau)] \frac{e^{-S[\mathbf{r}(\tau)]}}{\mathcal{Z}} \quad (3.84)$$

and correlation functions $\langle \mathcal{O}(\tau) \mathcal{O}(0) \rangle$,

$$\langle \mathcal{O}(\tau) \mathcal{O}(0) \rangle = \int \mathcal{D}[\mathbf{r}(\tau)] \mathcal{O}[\mathbf{r}(\tau)] \mathcal{O}[\mathbf{r}(0)] \frac{e^{-S[\mathbf{r}(\tau)]}}{\mathcal{Z}}. \quad (3.85)$$

Formally, the path integrals are expressed as a limit of high dimensional integrals, $\int \mathcal{D}[\mathbf{r}(\tau)] = \lim_{n \rightarrow \infty} \int \prod_{i=1}^n d^3 r_i$ where the Trotter decomposition τ_i ($i = 1, \dots, n$) of the interval $[0, \beta]$ was introduced. This, of course, leads to a discretization of the continuous path $\mathbf{r}(\tau) \rightarrow \{\mathbf{r}_1 \dots \mathbf{r}_n\}$ ($\mathbf{r}_i = \mathbf{r}(\tau_i)$), too. Details about this kind of limit can be found in the mathematical literature (Albeverio et al. [2008], Johnson and Lapidus [2002]). From a numerical point of view, only finite Trotter decompositions are possible, hence, we have to fix N_{trott} . As mentioned before, this leads

to a systematical error which has to be investigated. We do it by monitoring the dependence on N_{trrott} of the outcome.

With N_{trrott} fixed, we reduce the problem to high dimensional integration. We already know how this task can be done efficiently using the Metropolis Monte Carlo algorithm. Next, we have to define a (not necessarily normalized) probability distribution function p . In principle, a discretized version of $p[\mathbf{r}(\tau)] = e^{-S[\mathbf{r}(\tau)]}/\mathcal{Z}$ would suffice. However, evaluating the action contribution S_I for each proposed path configuration is very expensive. Therefore, we define a probability distribution involving only the free action, i.e. $p[\mathbf{r}(\tau)] = e^{-S_0[\mathbf{r}(\tau)]}/\mathcal{Z}_0$, so that

$$\langle \mathcal{O} \rangle = \sum_{\{\mathbf{r}_i\}}^{N_{\text{samp}}} \mathcal{O}\{\mathbf{r}_i\} e^{-S_I\{\mathbf{r}_i\}} / \tilde{\mathcal{Z}} \quad (3.86)$$

with

$$\tilde{\mathcal{Z}} = \sum_{\{\mathbf{r}_i\}}^{N_{\text{samp}}} e^{-S_I\{\mathbf{r}_i\}} \quad (3.87)$$

and where N_{samp} is the total number of samples. With the notation $\{\mathbf{r}_i\}$ we simply mean the discretized path $(\mathbf{r}_i, \dots, \mathbf{r}_{N_{\text{trrott}}})$. Of course, the configurations $\{\mathbf{r}_i\}$ have to be drawn with respect to the distribution function p . The expression for the correlation function can be found analogously. In order to estimate the statistical error of the observable, we have to consider that $\tilde{\mathcal{Z}}$ itself is a statistical quantity and therefore comes with a uncertainty.

Next, we have to specify the method for the generation of configurations $\{\mathbf{r}_i\}$. First, there is the problem of the initial configuration, $\{\mathbf{r}_i^0\}$. In principle, every guess should lead to the same steady-state (due to ergodicity). However, one could choose an initial configuration far away from any configuration substantially contributing to the ensemble average. Hence, many Monte Carlo steps could be necessary to reach the steady-state. In many cases, drawing configurations is numerically less time-consuming than evaluating observables, i.e. performing measurements. Therefore, one would like to reach the important regions of phase space before starting the actual measurements. This is done by a thermalization routine: in a pre-run, the Monte Carlo sampling routine is used to find a configuration close to the steady-state distribution. To check whether the actual configuration is close enough to the steady-state configuration, one has to monitor some easily accessible properties of the model. In steady-state, up to statistical fluctuations, every property of the system remains stationary. After thermalization, one can start to perform measurements.

There are several methods for drawing configurations. It is not our intention to list them all. In the following, we describe the method we use. Given a configuration $\{\mathbf{r}_i\}$, one can randomly choose an index $j \in \{1, \dots, N_{\text{trrott}}\}$ and try to alter the value of the path at this index by an arbitrary amount $\delta\mathbf{r}$, i.e. $\mathbf{r}_j \rightarrow \mathbf{r}_j + \delta\mathbf{r}$. There are two potential problems with this method. First, the new configuration does not necessarily fulfill appropriate boundary conditions, $\mathbf{r}_1 = \mathbf{r}_{N_{\text{trrott}}}$. Of course, this can be taken care of by suitable control routines. The second problem are correlations. Obviously, subsequent paths are highly correlated and hence so are subsequent measurements. This can be avoided by randomly choosing a set of indices at which the path is randomly altered. This, however, is much more expensive and complicated. It is much more convenient to alter the path $\{\mathbf{r}_i\}$ in its Fourier representation $\{\hat{\mathbf{r}}_i\}$. In doing so, we also avoid the problem of the boundary conditions: They are always taken care of. Altering a single sample point $\hat{\mathbf{r}}_j$, ($j \in \{1, \dots, N_{\text{trrott}}\}$) non-trivially (except for the zero mode, which generates just a translation of the whole path) alters the configuration $\{\mathbf{r}_i\}$. In order to numerically perform a Fourier transformation, we have to

introduce a cut-off N_ω for the Matsubara frequencies ω_n ($-N_\omega \leq n \leq N_\omega$). The cost of a Fourier transformation is of the order of $N_{\text{trott}} \times (2N_\omega + 1)$ which is acceptable. In general, N_ω is strongly temperature dependent. The smaller the temperature, the more Matsubara frequencies we have to consider. Again, similarly to N_{trott} , we determine N_ω heuristically.

3.4.5. Test of the Monte Carlo simulation

One should check the correct functioning of the Quantum Monte Carlo algorithm before applying it to a non-trivial problem. For example, one can check the functioning of the path sampling routine. In fig. 3.6, a sample path is depicted. Clearly, the path fulfills the correct boundary conditions. Next, one should look at the acceptance ratio. In case of path sampling in Matsubara

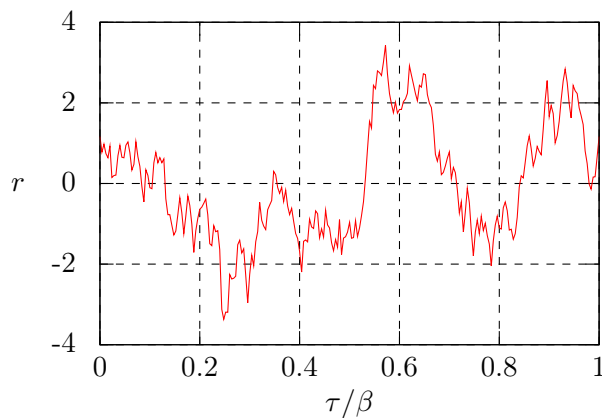


Figure 3.6.: Example of a Monte-Carlo path. The parameters are $\beta = 10$ for the inverse temperature and $\Omega = 0.001$ for the trap frequencies. In total, $2 \times 400 + 1$ sample points in Matsubara space have been used.

space, the acceptance rate is defined by the ration $N_{\text{acc}}(\omega_i) / N_{\text{tot}}(\omega_i)$, where $N_{\text{tot}}(\omega_i)$ is the total number of attempts to change the Fourier component belonging to the Matsubara frequency ω_i and, respectively, $N_{\text{acc}}(\omega_i)$ the number of accepted attempts. If the acceptance rate is close to one, almost every proposed configuration is accepted. As a consequence, one risks to stay too close to the classical solution. On the other hand, if the acceptance rate is close to zero, almost every proposed configuration is rejected. In this case, the configuration space might be sampled very inefficiently. In both cases, convergence of the Monte Carlo simulation might be very bad. As a rule of thumb, one should fix the acceptance rate close to 0.5. In fig. 3.7, the acceptance rate for a system with inverse temperature $\beta = 10$ and trap frequency $\Omega = 0.001$ is depicted. Next, one should check whether the Monte Carlo method is able to reproduce non-interacting results. Obviously, correlations functions are good candidates. We begin with the Green's function,

$$G_i^{(0)}(\tau) = \frac{1}{2\Omega_i} \frac{\cosh[\Omega_i(|\tau| - \beta/2)]}{\sinh(\Omega_i\beta/2)}. \quad (3.88)$$

It is convenient to subtract the contribution coming from the zero mode, i.e.

$$\tilde{G}_i^{(0)}(\tau) = \frac{1}{2\Omega_i} \frac{\cosh[\Omega_i(|\tau| - \beta/2)]}{\sinh(\Omega_i\beta/2)} - \frac{1}{2\Omega_i^2\beta}. \quad (3.89)$$

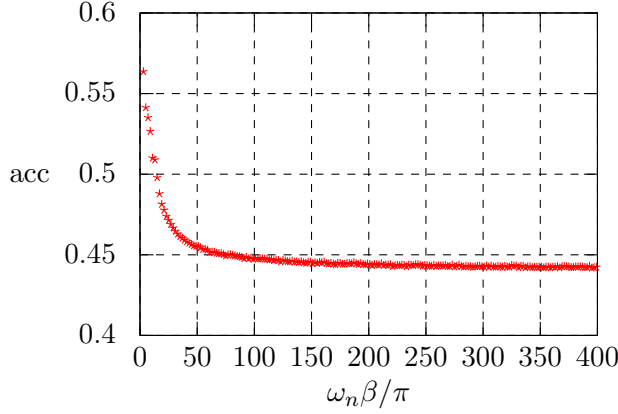


Figure 3.7.: Example of an acceptance rate for a set of Matsubara frequencies. The parameters are $\beta = 10$ for the inverse temperature and $\Omega = 0.001$ for the trap frequencies. In total, $2 \times 400 + 1$ same points in Matsubara space have been used.

Without subtracting a temperature dependent offset, the values of the correlation functions for different temperatures may differ by more than one order of magnitude. In fig. 3.8 (left graph), the Monte Carlo simulation results of the correlation function $\tilde{G}^{(0)}$ are compared with analytical results (see eq. B.9 in the appendix) for several temperatures. The agreement is excellent for all temperatures. Another important quantity are density-density correlation functions (see eq. B.11),

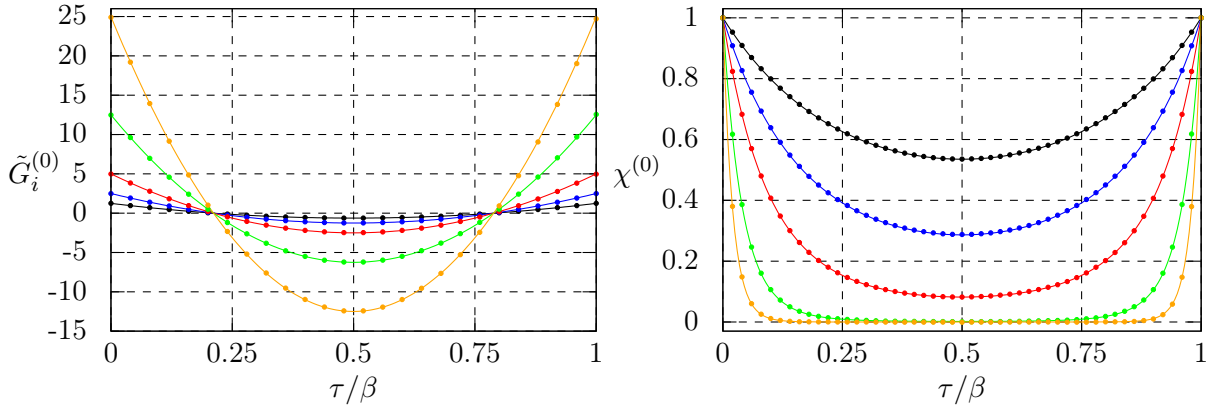


Figure 3.8.: Correlation functions in Matsubara time for the non-interacting model. **Left panel:** the correlation function $\tilde{G}^{(0)}$ (τ) (reduced by the zero-mode contribution) is depicted. The solid lines are the analytic results and the plot points the result of the Monte Carlo simulation. The error bars are of the order of 10^{-2} and are therefore smaller than the size of the plot points. The inverse temperatures β are $\beta = 5, 10, 20, 50, 100$ (black, blue, red, green and orange). **Right panel:** density-density correlation function in Matsubara time for the non-interacting model. The solid lines are the analytic results and the plot points the result of the Monte Carlo simulation. The error bars are of the order of 10^{-3} and are therefore smaller than the size of the plot points. The inverse temperatures are $\beta = 5, 10, 20, 50, 100$ (black, blue, red, green and orange).

$$\chi_i^{(0)}(\mathbf{q}, \tau) = \left\langle e^{iq_i r_i(\tau)} e^{-iq_i r_i(0)} \right\rangle = e^{-q_i^2 [G_i^{(0)}(0) - G_i^{(0)}(\tau)]}. \quad (3.90)$$

In fig. 3.8 (right panel), the Monte Carlo simulation data and the analytical results for $\chi_i^{(0)}(\mathbf{q}, \tau)$ are depicted for several temperatures. Again, the agreement is excellent.

3.4.6. Results and discussion for interacting systems

In this section, we discuss the results from the Monte Carlo simulation. We begin with the polaron radius R_{pol} . It was previously defined in eq. (3.35) and is basically given by a correlation function. Therefore, it is well accessible by our Monte Carlo simulation. For presentational reasons, we calculate a shifted polaron radius,

$$R_s^2 = R_{\text{pol}}^2 - R_{\text{pol}}^2|_{\alpha=0}. \quad (3.91)$$

This makes R_s^2 a negative quantity. In fig. 3.9 (left graph), we compared the Monte Carlo simulation

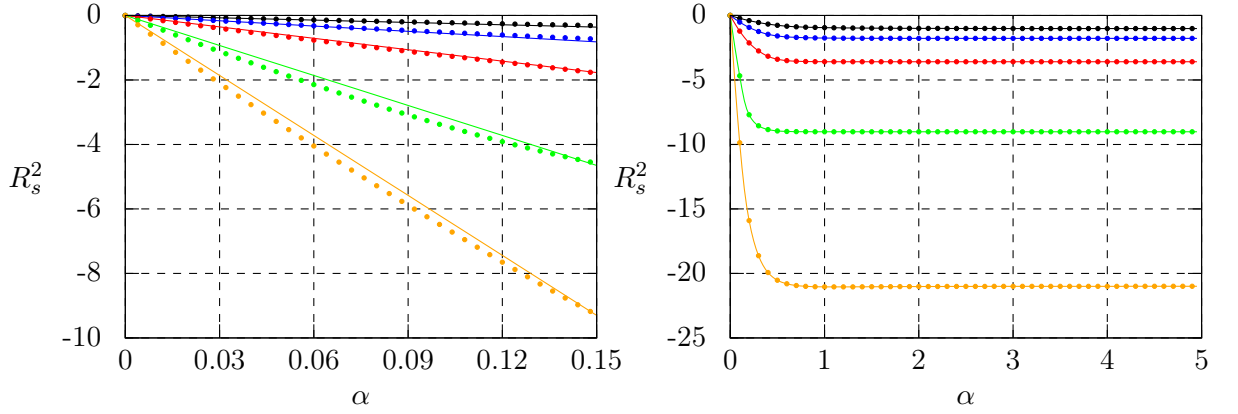


Figure 3.9.: Polaron radius for weak and strong coupling strengths. **Left panel:** the solid lines are the results from perturbation theory to leading order in α . The plot dots are the result of the Monte Carlo simulation. The error bars are of the order of 10^{-1} and are therefore smaller than the size of the plot dots. The inverse temperatures β are $\beta = 5, 10, 20, 50, 100$ (black, blue, red, green and orange). **Right panel:** crossover to arbitrary interaction strengths α . The parameters and the assignments are the same as in the left graph and the solid lines are a guide to the eye.

data with the results from perturbation theory for small coupling strengths α . In case of sufficiently high temperatures, the perturbative results excellently agrees up to coupling constants $\alpha \approx 0.1$. In case of decreasing temperatures, perturbation theory still agrees well with the Monte Carlo simulation. However, the polaron radius is far from being linear up to $\alpha = 0.1$, i.e. perturbation theory is valid for a small range of α , only. In fig. 3.9 (right graph), R_s is depicted over a broad range of interactions α . The lower bound of the polaron radius is set by the contribution coming from the zero mode, $1/\Omega^2\beta$.

The calculation of the density-density correlation function is much more time-consuming from the numerical point of view. The reason is its frequency dependence. The stronger the interaction strength or the lower the temperature, the more Matsubara frequencies are required. Therefore, we concentrate on the experimentally relevant regime. To restore SI units, energy quantities have to be scaled with $\hbar^2/m_I\xi^2$. In case of a sodium condensate with a typical density of $n_0 \approx 7 \times 10^{13} \text{ cm}^{-3}$ and a boson-boson scattering length $a_{\text{BB}} \approx 2.8 \text{ nm}$ (see for example Samuelis et al. [2000]), this corresponds to a factor of 390 nK. The critical temperature for a sodium BEC is approximately $T_c = 220 \text{ nK}$. Using conventional cooling techniques, temperatures up to $T \approx 50 \text{ nK}$ are accessible (see for example Tempere et al. [2009]). Therefore, we can restrict the inverse temperature to $\beta \in [1, 20]$. In sodium-lithium mixtures, the boson-impurity scattering length is of the order of

$a_{\text{IB}} \approx 0.8 \text{ nm}$ (see Gacesa et al. [2008], Schuster et al.) and therefore $\alpha \approx 10^{-3}$. Using Feshbach resonances, this scattering length might be increased.

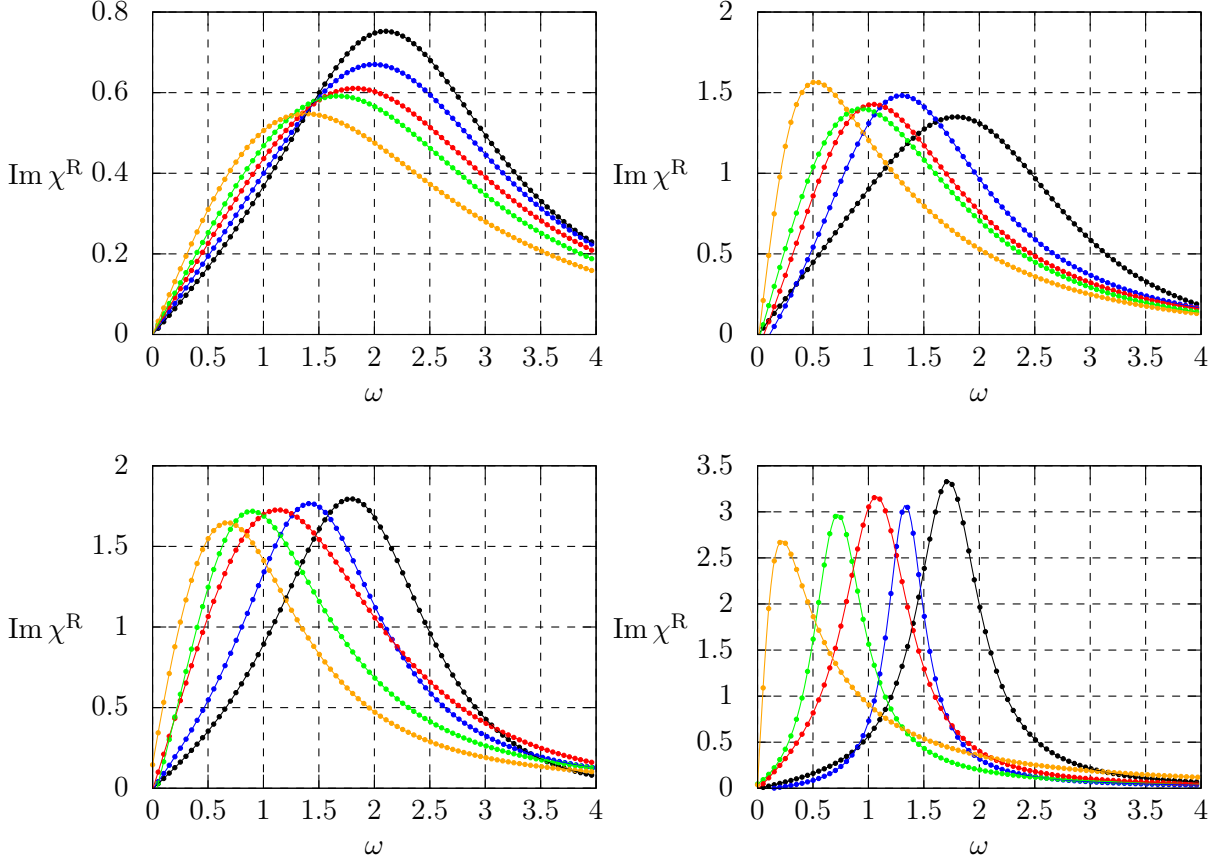


Figure 3.10.: Imaginary part of the density-density correlation function for several interaction strengths and temperatures. The trapping potential is fixed to $\Omega = 0.001$. The interactions strength are $\alpha = 0.05, 0.1, 0.15, 0.2, 0.3$ (black, blue, red, green and orange plot points). The inverse temperatures are $\beta = 1$ (upper left), $\beta = 5$ (upper right), $\beta = 10$ (lower left) and $\beta = 20$ (lower right). Again, the error bars are smaller than the plot points. The solid lines are a guide to the eye.

In fig. 3.10, the imaginary part of the density-density correlation function is depicted for several temperatures and interaction strengths. For increasing coupling strengths, the peak is shifted to lower energies. A similar behaviour is observed in the optical properties of solids and is known as phonon-softening, see for example Koller et al. [2005], Meyer et al. [2002]. One can understand this behaviour in the following way: due to the increasing localization of the quasiparticle, excitations involve a smaller fraction of the background BEC. Therefore, energy can be deposited more easily.

3.5. Variational principle for the BEC polaron

Here we would like to approach the strong-coupling limit by analytical means. One possibility could be the application of the variational method. The main task in variational methods is always to find an appropriate trial model, for example, a trial wave function or a trial action. The rest is an optimization problem: one has to fix the parameters of the trial model in such a way, that a

thermodynamic potential gets extremal. The Jensen-Feynman variational principle is based on the Jensen inequality (Jensen [1906]),

$$\langle f(X) \rangle \geq f(\langle X \rangle) \quad (3.92)$$

where f is a convex function and X a random variable. In combination with his path integral formalism, Feynman used this inequality to construct a powerful variational principle (Feynman [1955]). The key idea is to find an upper bound for the free energy,

$$\begin{aligned} e^{-\beta F} &= \int \mathcal{D}[\mathbf{r}(\tau)] e^{-S[\mathbf{r}(\tau)]} = \int \mathcal{D}[\mathbf{r}(\tau)] e^{-\{S[\mathbf{r}(\tau)] - S_0[\mathbf{r}(\tau)]\}} e^{-S_0[\mathbf{r}(\tau)]} \\ &= e^{-\beta F_0} \langle e^{-(S-S_0)} \rangle_0 \geq e^{-\beta F_0} e^{-\langle S-S_0 \rangle_0} \end{aligned} \quad (3.93)$$

where S_0 is the action of a trial model and $\langle \cdot \rangle_0$ is the expectation value with respect to this trial action. The action S was calculated in eq. (3.41),

$$S = \int d\tau \left[\frac{\dot{\mathbf{r}}^2}{2} + \frac{\Omega \mathbf{r}^2}{2} \right] + \sum_{\mathbf{k}} \frac{|V_{\mathbf{k}}|^2}{2} \int d\tau d\tau' G_{\text{Bog}}(\mathbf{k}, \tau - \tau') e^{i\mathbf{k}[\mathbf{r}(\tau) - \mathbf{r}(\tau')]}, \quad (3.94)$$

where we have chosen the system to be isotropic, i.e. $\Omega_i = \Omega$ ($i = 1, \dots, 3$). Next, we have to model a trial action:

$$S_0 = \int d\tau \left[\frac{\dot{\mathbf{r}}^2}{2} + \frac{\Omega \mathbf{r}^2}{2} \right] + \frac{MW^3}{8} \int d\tau d\tau' \frac{\cosh[W(|\tau - \tau'|) - \beta/2]}{\sinh(W\beta/2)} [\mathbf{r}(\tau) - \mathbf{r}(\tau')]^2, \quad (3.95)$$

where W and M are variational parameters. The underlying model of this action is depicted in

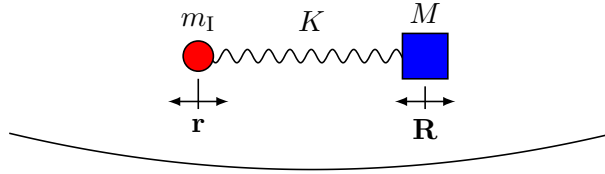


Figure 3.11.: Illustration of the trial model: the impurity is coupled to a fictitious particle with mass M and spring constant K .

fig. 3.11: a second mass M is coupled to the impurity m_I with a spring constant $K = W^2 M$. The trial action is purely quadratic in the field $\mathbf{r}(\tau)$, hence, the expectation values in eq. (3.93) can easily be calculated (see B.2 for some detail). One obtains

$$\begin{aligned} F &\leq \frac{3}{\beta} [\ln(F_+ \beta/2) + \ln(F_- \beta/2) - \ln(W\beta/2)]/2 \\ &+ \frac{3}{\beta} \frac{MW^2}{4} \sum_{\pm} \frac{\pm F_{\pm} \coth(F_{\pm} \beta/2)}{\sqrt{(\tilde{\Omega}^2 + \Omega^2)^2 - 4W^2 \Omega^2}} \\ &- \sum_{\mathbf{k}} |V_{\mathbf{k}}|^2 \int_0^{\beta} d\tau (1 - \tau/\beta) G_{\text{Bog}}(\mathbf{k}, \tau) \mathcal{K}(\mathbf{k}, \tau) \end{aligned} \quad (3.96)$$

where we have introduced $\tilde{\Omega} = W\sqrt{M+1}$,

$$F_{\pm} = \sqrt{\frac{\tilde{\Omega}^2 + \Omega^2}{2} \pm \frac{\sqrt{(\tilde{\Omega}^2 + \Omega^2)^2 - 4W^2 \Omega^2}}{2}} \quad (3.97)$$

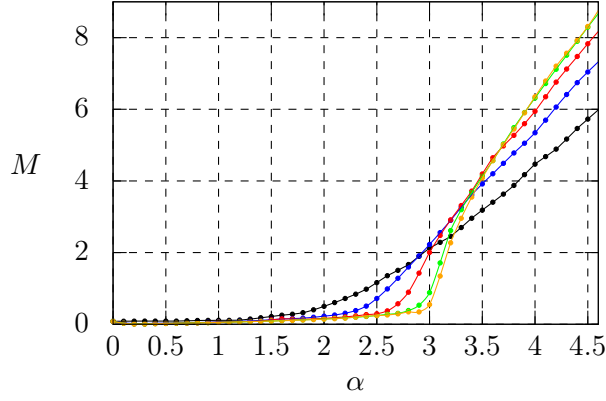


Figure 3.12.: Polaron mass: Depicted is the variational parameter M . The polaron mass is given by $M_{\text{pol}} = M + 1$. The parameters are $\Omega = 0.001$ for the trap frequency. The inverse temperature is $\beta = 5, 10, 20, 50, 100$ (black, blue, red, green, orange plot dots).

and the memory kernel is given by

$$K(\mathbf{k}, \tau) = \exp \left[-\mathbf{k}^2 \left(\tilde{G}(0) - \tilde{G}(\tau) \right) \right]. \quad (3.98)$$

$\tilde{G}(\tau)$ is the Matsubara Green's function $\langle \mathbf{r}_i(\tau) \mathbf{r}_i(0) \rangle_0$ with respect to the trial action S_0 ,

$$\tilde{G}(\tau) = \frac{1}{2\sqrt{(\tilde{\Omega}^2 + \Omega^2)^2 - 4W^2\Omega^2}} \sum_{\pm} \frac{\pm (F_{\pm}^2 - W^2) \cosh [F_{\pm} (|\tau| - \beta/2)]}{\sinh (F_{\pm} \beta/2)}. \quad (3.99)$$

Feynman showed (Feynman [1955]), that the polaron mass M_{pol} can be assigned to the variational parameter M , $M_{\text{pol}} = M + 1$. In fig. 3.12, M is plotted for several temperatures. M remains close to zero for small interaction strengths α . For α approaching $\alpha = 3$, M strongly increases. This behaviour was observed in a BEC impurity without external trap for the impurities in Tempere et al. [2009]. The polaron radius is given by

$$R_{\text{pol}}^2 = \lim_{\tau \rightarrow 0} \tilde{G}(\tau). \quad (3.100)$$

In fig. 3.13, we plotted the shifted polaron radius $R_s^2 = R_{\text{pol}}^2 - R_{\text{pol}}^2|_{\alpha=0}$. Similarly to the polaron mass, its radius almost remains constant for small interaction strengths α . For α approaching $\alpha = 3$, the radius strongly decreases. This behaviour is not in agreement with our path integral Monte Carlo simulation data where the polaron radius strongly decreases even for small α . The reason for this discrepancy is still unknown. One should keep in mind, that contrary to the continual 3D system, which is considered in Tempere et al. [2009], ours includes a finite trapping potential, which is always present in experimental realizations. The arising finite energy level spacing might be the reason for the strong suppression of the polaron radius.

3.6. Cherenkov radiation in ultracold binary mixtures

It is well-known, that charged particles moving in a dispersive background medium emit electromagnetic radiation, if the particles velocity exceeds the phase velocity of light in the medium. This is

$$\Sigma^{3D}(\mathbf{p}, \epsilon) = i\lambda^2 \int \frac{d^3\mathbf{k}}{(2\pi)^3} \int \frac{d\omega}{2\pi} \sqrt{\frac{(\xi k)^2}{(\xi k)^2 + 2}} G_0(\epsilon - \omega, \mathbf{p} - \mathbf{k}) D_0(\omega, \mathbf{k}), \quad (3.102)$$

where the retarded free Green's function for the impurity is

$$G_0(t - t', \mathbf{p}) = -i\Theta(t - t') \left\langle \left\{ c_{\mathbf{p}}(t), c_{\mathbf{p}}^\dagger(t') \right\} \right\rangle, \quad (3.103)$$

$$G_0(\omega, \mathbf{p}) = \frac{1}{\omega - \frac{p^2}{2m} + i\eta} \quad (3.104)$$

and the retarded free Green's functions for the Bogoliubov excitations

$$D_0(t - t', \mathbf{k}) = -i\Theta(t - t') \left\langle \left[b_{\mathbf{k}}(t) + b_{-\mathbf{k}}^\dagger(t), b_{\mathbf{k}}^\dagger(t') + b_{-\mathbf{k}}(t') \right] \right\rangle, \quad (3.105)$$

$$D_0(\omega, \mathbf{k}) = \frac{1}{\omega - \omega_{\mathbf{k}} + i\eta} - \frac{1}{\omega + \omega_{\mathbf{k}} - i\eta}. \quad (3.106)$$

The real part of the self-energy can be related to the mass renormalization α and the polaron shift energy ϵ_0 ,

$$\text{Re } \Sigma^{3D} = -\epsilon_0 - \alpha \frac{p^2}{2m_I} + \dots, \quad (3.107)$$

and with $\Sigma^{3D} - G_0^{-1} = 0$ the relative mass $\frac{m^*}{m_I}$ can be calculated

$$\frac{m^*}{m_I} = 1 + \frac{M_{\text{pol}}}{m_I} = 1 + \frac{\alpha}{6}. \quad (3.108)$$

The imaginary part can be used to calculate the energy loss per unit time [Sollfrey and Yura \[1965\]](#), i.e.

$$\frac{dE_{\text{loss}}}{dt} = \int_0^\infty \omega d\Gamma = \int_0^\infty \omega \frac{d\Gamma}{d\omega} d\omega \quad (3.109)$$

where the decay rate $\Gamma(\omega)$ is given by

$$\Gamma(\omega) = -2\text{Im } \Sigma^{3D}(\omega, \mathbf{p}). \quad (3.110)$$

The ω -integration in the expression of the self-energy can easily be performed using residua,

$$\Sigma^{3D}(\mathbf{p}, \epsilon) = -\lambda^2 \int \frac{d^3\mathbf{k}}{(2\pi)^3} \sqrt{\frac{(\xi k)^2}{(\xi k)^2 + 2}} \frac{1}{\epsilon - \omega_{\mathbf{k}} - \frac{(\mathbf{p}-\mathbf{k})^2}{2m_I} + i\eta}. \quad (3.111)$$

Fixing the z -axis of the integration variable \mathbf{k} along the direction of \mathbf{p} one can integrate over the modulus $|\mathbf{k}| = k$ and the cosine of the angle $\angle(\mathbf{p}, \mathbf{k})$ which we denote by x , and subsequently $d^3\mathbf{k} = k^2 dk d\phi dx$. Introducing momentum transfer $q^2 = |\mathbf{p} - \mathbf{k}|^2 = p^2 + k^2 - 2pkx$ and changing integration variable $x \rightarrow q$, i.e. $q dq = -pk dx$, one finds

$$\Sigma^{3D}(\mathbf{p}, \epsilon) = \lambda^2 \int_0^{k_D} \frac{dk k}{4\pi^2} \sqrt{\frac{(\xi k)^2}{(\xi k)^2 + 2}} \int_{|p-k|}^{|p+k|} \frac{dq}{2\pi} \frac{q}{\epsilon - \omega_{\mathbf{k}} - \frac{q^2}{2m_I} + i\eta} \quad (3.112)$$

where for reasons of regularizations, the Debye cut-off frequency k_D was introduced. Corresponding to the frequency cut-off in solid state systems, there is a cut-off in cold atom systems governed by

the inverse of the Van der Waals radius (see for example [Tempere et al. \[2009\]](#)). Using the Dirac relation, $\frac{1}{\omega+i\eta} = P\frac{1}{\omega} + i\pi\delta(\omega)$ we obtain,

$$\begin{aligned} \text{Re } \Sigma^{3\text{D}}(\mathbf{p}, \epsilon) &= \frac{m_{\text{I}}\lambda^2}{4\pi^2 p} \int_0^{k_{\text{D}}} dk k \sqrt{\frac{(\xi k)^2}{(\xi k)^2 + 2}} \ln \left| \frac{\epsilon - \omega_k - (p+k)^2/2m_{\text{I}}}{\epsilon - \omega_k - (p-\omega_k)/2m_{\text{I}}} \right| \\ \text{Im } \Sigma^{3\text{D}}(\mathbf{p}, \epsilon) &= -\pi \frac{m_{\text{I}}\lambda^2}{4\pi^2 p} \int_0^{k_{\text{D}}} dk k \sqrt{\frac{(\xi k)^2}{(\xi k)^2 + 2}} \int_{(p-k)^2/2m_{\text{I}}}^{(p+k)^2/2m_{\text{I}}} dq \delta(\epsilon - \omega_k - q). \end{aligned} \quad (3.113)$$

The imaginary part is only non-zero, if p fulfills the inequality,

$$\frac{(p-k)^2}{2m_{\text{I}}} < \frac{p^2}{2m_{\text{I}}} - ck\sqrt{1 + (\xi k)^2/2} < \frac{(p+k)^2}{2m_{\text{I}}} \quad (3.114)$$

which is equivalent to the constraint

$$k < 2p - 2m_{\text{I}}c\sqrt{1 + (\xi k)^2/2}. \quad (3.115)$$

Here, we assumed energies close to the mass shell, i.e. $\epsilon \approx p^2/2m_{\text{I}}$. In case of $v = p/m_{\text{I}} > v$, there is always a finite region for k around zero where the inequality holds, hence, the condition for Cherenkov radiation in an immersed BEC is similar to ordinary metals.

In case of a 2D Bose gas with 2D impurities, we proceed similar to the 3D case. Obviously, one immediately finds for the self-energy the expression (see eq. (3.111)),

$$\Sigma^{2\text{D}}(\mathbf{p}, \epsilon) = -\lambda^2 \int \frac{d^2\mathbf{k}}{(2\pi)^2} \sqrt{\frac{(\xi k)^2}{(\xi k)^2 + 2}} \frac{1}{\epsilon - \omega_{\mathbf{k}} - \frac{(\mathbf{p}-\mathbf{k})^2}{2m_{\text{I}}} + i\eta}. \quad (3.116)$$

Using spherical coordinates, the integration significantly simplifies,

$$\Sigma^{2\text{D}}(\mathbf{p}, \epsilon) = -\lambda^2 \int \frac{dk k d\phi}{(2\pi)^2} \sqrt{\frac{(\xi k)^2}{(\xi k)^2 + 2}} \frac{1}{\epsilon - \omega_{\mathbf{k}} + -\frac{p^2+k^2}{2m_{\text{I}}} + pk \cos(\phi)/m_{\text{I}} + i\eta}, \quad (3.117)$$

and hence,

$$\begin{aligned} \text{Re } \Sigma^{2\text{D}}(\mathbf{p}, \epsilon) &= \frac{m_{\text{I}}\lambda^2}{\pi^2} \int_0^{k_{\text{D}}} dk \frac{k \sqrt{\frac{(\xi k)^2}{(\xi k)^2 + 2}} \ln \left(\frac{\epsilon - \omega_k - (p+k)^2/2m_{\text{I}}}{\epsilon - \omega_k - (p-\omega_k)/2m_{\text{I}}} \right)}{\sqrt{-\left[2m_{\text{I}}(\epsilon - \omega_k) - (p+k)^2\right] \left[2m_{\text{I}}(\epsilon - \omega_k) - (p-\omega_k)\right]}} \\ \text{Im } \Sigma^{2\text{D}}(\mathbf{p}, \epsilon) &= -\frac{\lambda^2}{\pi} \int_0^{k_{\text{D}}} dk k \sqrt{\frac{(\xi k)^2}{(\xi k)^2 + 2}} \int d\phi \delta(\epsilon - \omega_k - (k^2 + p^2)/2m_{\text{I}} + kp \cos(\phi)/m_{\text{I}}). \end{aligned} \quad (3.118)$$

Again, considering energies close to the mass shell and using $|\cos \phi| \leq 1$, one obtains the constraint

$$k < 2p - 2m_{\text{I}}c\sqrt{1 + (\xi k)^2/2m_{\text{I}}} \quad (3.119)$$

which is identical to the requirement eq. (3.115) we have found in the 3D case.

In case of a 1D Bose background and fermionic impurities in 1D one finds for the self-energy,

$$\Sigma^{1D}(p, \epsilon) = -\lambda^2 \int \frac{dk}{2\pi} \sqrt{\frac{(\xi k)^2}{(\xi k)^2 + 2}} \frac{1}{\epsilon - \omega_k - \frac{(p-k)^2}{2m_I} + i\eta}. \quad (3.120)$$

Here, a non-zero imaginary part is only possible if the expression in the denominator of the second fraction has real zeros, i.e. $\epsilon - \omega_k - \frac{(p-k)^2}{2m_I} = 0$. For energies near the mass shell, this translates to $pk/m_I - \omega_k - k^2/2m_I = 0$. The existence of a solution of this equation requires that

$$p \geq m_I c \sqrt{\left(1 - \frac{1}{2(m_I c \xi)^2}\right)} \quad (3.121)$$

holds. This makes the 1D case different from the higher dimensional ones. In case of a large healing length $\xi \gg 1/m_I c$ the dissipation condition again is the same as for ordinary metals $v > c$. However, a decreasing ξ sets a smaller critical velocity. Especially, the latter becomes zero for $\xi = 1/(\sqrt{2}m_I c)$ (this is the case for $m_B/m_I = 1$). The metallic case is realized for $m_B/m_I \ll 1$.

The remaining integral in the expressions of the imaginary part of the self-energy can be calculated in the regimes $\xi k_D \ll 1$ and $\xi k_D \gg 1$ at least for the 1D and 3D case. In these limits, we may use the approximations,

$$\sqrt{\frac{(\xi k)^2}{(\xi k)^2 + 2}} \approx \begin{cases} \xi k / \sqrt{2} & \xi k \ll 1 \\ 1 & \xi k \gg 1 \end{cases}. \quad (3.122)$$

One obtains for the imaginary part of eq. (3.113) in the 3D case,

$$\text{Im } \Sigma^{3D}(\epsilon, \mathbf{p}) \approx -\frac{m_I \lambda^2}{\pi p} \begin{cases} \sqrt{2} \xi (p - m_I c)^3 / 3 & \xi k_D \ll 1 \\ [p / (1 + \sqrt{2} m_I \xi)]^2 / 2 & \xi k_D \gg 1 \end{cases}, \quad (3.123)$$

and in the 1D case (see eq. (3.120)),

$$\text{Im } \Sigma^{1D}(\epsilon, \mathbf{p}) \approx -\lambda^2 \begin{cases} \xi \sqrt{2} p^2 / (p/m_I - c) & \xi k_D \ll 1 \\ 2m_I / (p \sqrt{|1 - 2m_I c \xi|}) & \xi k_D \gg 1 \end{cases}. \quad (3.124)$$

In sodium, the cut-off momentum k_D can be estimated to be $\xi k_D \approx 200$ (see [Tempere et al. \[2009\]](#)).

3.6.2. Experimental fingerprint of Cherenkov radiation

One of the best signatures of Cherenkov radiation is its threshold, i.e. the existence of a critical velocity. Using Dyson's equation, the single particle retarded Green's function

$$G^R(\mathbf{p}, t) = i\theta(t) \left\langle \left\{ c_{\mathbf{p}}(t), c_{\mathbf{p}}^\dagger(0) \right\} \right\rangle \quad (3.125)$$

can be obtained. In the frequency domain

$$G^R(\mathbf{p}, \omega) = \left[(G_0^R(\mathbf{p}, \omega))^{-1} - \Sigma(\mathbf{p}, \omega) \right]^{-1} \quad (3.126)$$

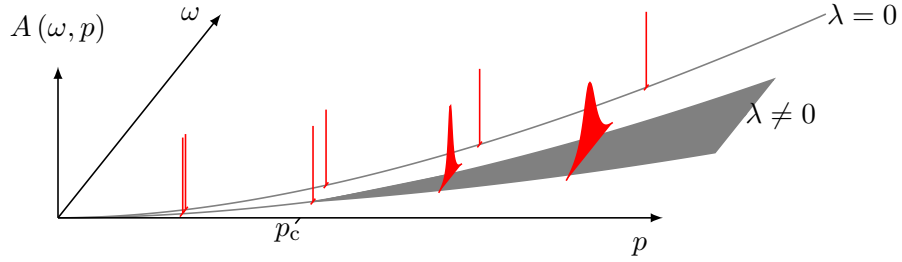


Figure 3.15.: Sketch of the spectral function $A(\mathbf{p}, \omega)$ of the interacting and non-interacting model. In case of the non-interacting system $\lambda = 0$, the spectral function is a δ -function on the mass shell. For the interacting case, $\lambda \neq 0$, the spectral function is δ -peak like for momenta smaller than the critical momentum p_c and a Lorentzian for $p > p_c$. The width is given by the imaginary part of the self-energy. The real part leads to a mass renormalization.

where $G_0^R(\mathbf{p}, \omega)$ is the retarded Green's function of the non-interacting system. The retarded Green's function is related to the spectral function, $A(\mathbf{p}, \omega) = -2\text{Im} G^R(\mathbf{p}, \omega)$ which is an experimentally accessible quantity. For example, angle resolved photoemission spectroscopy (ARPES) can probe the spectral function. The signature of the Cherenkov effect in the spectral function is very clear: in case of momenta smaller than p_c , the spectral function is proportional to a δ -peak on the mass shell. In case of $p > p_c$, the peak is smeared out, i.e. the quasiparticle is allowed to decay. To leading order, the peak is given by a Lorentzian with a width proportional to the imaginary part of the self-energy. An interesting fingerprint of Cherenkov radiation in immersed quantum gases is the energy deposition in the background BEC: while dragging an impurity through the BEC with a velocity smaller than the critical one, no dissipation is observed. However, if the velocity of the particle exceeds the critical velocity, the background BEC absorbs energy. In principle, this is measurable in time-of-flight experiments. The dragging can be realized either by varying the trapping potential or by shooting impurities through the BEC.

4. Conclusions and outlook

In this thesis, the effect of electron-phonon interaction in mesoscopic systems was investigated. We have chosen two perspectives: first, we looked at quantum impurities with internal vibrational degrees of freedom with special emphasis on non-equilibrium transport phenomena. During the last decades, these systems have gained more and more attention. On the one hand, they are very suitable to investigate the nature of electron-phonon interaction on electron transport in a controlled way. On the other hand, they are perfect candidates for future transistors on the nanoscale, so-called single electron devices. Secondly, we looked at immersed ultracold quantum gases. In case of a two-component mixture with a bosonic majority and a fermionic minority species, the system is suitable to model electrons in a crystal lattice interacting with phonons. Due to the high cleanliness and the ability to tune the scattering properties of such systems, they are in many aspects superior to experiments with solids.

In molecular electronics, one is basically interested in transport properties like electric conductance, current and noise. The full counting statistics (FCS) provides a method to characterize the transport properties of mesoscopic systems beyond this. By definition, the FCS is the probability distribution to transfer a certain amount of charge during a fixed measurement time. Therefore, every moment of the distribution is accessible by simple derivation, especially current and noise. But the FCS contains even more information: the structure allows to distinguish the specific processes participating in transport, e.g. transport of correlated pairs. This makes the FCS perfect for correlated systems such as the fractional quantum Hall effect, (s-,p-,d-,... wave) superconductivity or Tomonaga-Luttinger liquids.

Electric conductance and current have already been investigated for a huge class of models to the very detail in the literature. In case of molecular transistors, much work has been done for the case of weak electron-phonon interaction; especially there are several papers available discussing the FCS for such systems. The case of strong electron-phonon interaction is more involved. Work has been done using rate equations/quantum master equations, $P(E)$ theory, diagrammatic Monte Carlo methods and methods combining Keldysh-Green's functions with the Lang-Firsov transformation. Most of them are used to calculate the linear conductance or the electric current, only. Apart from diagrammatic Monte Carlo simulations, they all involve certain approximations.

In this manuscript, we investigated the Anderson-Holstein model in case of strong electron-phonon coupling. Using an extended Keldysh-Green's function technique, we were able to obtain explicit expressions for the FCS in certain approximations. One approximation is the single-particle approximation valid in the strong coupling regime with an additional constraint: the time scale of tunneling processes has to be significantly smaller than the phonon relaxation time, i.e. the hybridization Γ has to be larger than the electron-phonon coupling constant, g . The physical picture behind this approximation is the following: an electron tunneling from the leads to the dot excites a phonon cloud. The electron can then undergo a series of real and virtual tunneling processes before de-exciting the vibrational modes. In the opposite limit, we proposed the polaron tunneling approximation. Here, an electron leaving the quantum dot always completely de-excites the vibra-

tional modes. Both approximation schemes use a many-particle description of the phonon degree of freedom and are not perturbative in the interaction. A comparison with diagrammatic Monte Carlo data showed, that our analytic results are able to describe the basic physical properties. In the regime $g/\Gamma \lesssim 1$, the single particle approximation describes the diagrammatic Monte Carlo data quite well. For increasing g/Γ , i.e. $g/\Gamma > 1$, the single particle approximation significantly deviates from the numerical data. In this regime, the polaron tunneling approximation is much more suitable to describe the numerical data.

If one further decreases the width of the electric leads, they effectively become one-dimensional. It is well known that for 1D field theories, the electron-electron interaction is crucial. Especially, the Fermi liquid theory is no longer accurate and one has to deal with strongly correlated systems described by Tomonaga-Luttinger liquids. The effect of electron-phonon interaction on strongly correlated systems in molecular transistors is barely investigated. Mainly, this is due to the lack of methods to accurately describe these kinds of problems. We looked at a quantum dot with a vibrational degree of freedom tunneling and capacitively coupled to strongly correlated electric leads. It is well known that certain carbon nanotubes represent such kinds of electric leads. Without the vibrational degree of freedom, we solved the non-equilibrium problem in the Toulouse point using bosonization techniques and the Emery-Kivelson rotation. This procedure results in the Majorana resonant level model. The low-energy behaviour of this model is quite interesting: the system is either perfectly transmitting or non-transmitting at all. Especially, this is reflected in the non-monotonic dependence of the effective transmission coefficient on the dot level position Δ_0 . In case of a resonant setup, $\Delta_0 = 0$, the transmittance is perfect. An arbitrarily small detuning away from the resonant case changes the situation completely: the system becomes completely opaque. We incorporated the electron-phonon interaction perturbatively. In the off-resonant case, all corrections remain finite. In current and noise, elastic and inelastic effects of the interaction with the phonon were identified. The low-energy behaviour can be understood in terms of phonon-mediated tunneling. At resonance, the homogeneous propagator develops an infrared singularity. This leads to logarithmic divergences in the perturbation expansion. We performed an RPA-like resummation of the diverging contributions. This yielded the conclusion that the low-energy behaviour can be explained by phonon-suppressed tunneling.

Interestingly, some aspects of the electron-phonon interaction can be understood by interference effects in multi-level systems. These systems can be treated as a generalization of a single level quantum dot to one with multiple energy levels. The simplest example is a double quantum dot setup in parallel arrangement. We investigated the effect of interference on the electron transport by calculating its FCS. We find similar resonance/anti-resonance phenomena as in the case of the strongly coupled Anderson-Holstein model. Moreover, it turned out that the transmission properties of the double quantum dot setup for certain parameter constellations is the same as in the Majorana resonant level model. We proposed to use the tunable anti-resonance to implement a highly efficient spin filter. Using a scattering matrix approach, we showed that our setup is stable against intra-dot interactions. Also, we discussed the stability with respect to finite temperature.

In the BEC polaron problem, we are more interested in thermodynamic or linear response properties rather than in a full non-equilibrium description. Especially interesting from the experimental point of view are quantities which are measurable with the help of time-of-flight experiments and spectroscopy. Using Matsubara Green's functions and imaginary time path integral Monte Carlo simulations, the polaron radius and the density-density correlation function have been obtained. In order to create benchmarks for the numerical procedure we generated perturbation theory results first. Using the quantum Monte Carlo method, we were able to get numerically exact results for the full range of the coupling strength. The polaron radius behaves as expected: for weak couplings,

the radius is set by the properties of the trapping confinement. An increase of the couplings leads to a rapid decrease of the radius. In contrast to the untrapped system, the minimum radius is set by the zero mode and is therefore always finite. For small couplings, we observe a peak at $\omega \approx \mathbf{k}^2/2$ in the imaginary part of the density-density correlation function. Mainly, this is due to the harmonic trapping potential. For increasing interaction strengths, the peak in the density-density correlation function is shifted towards small energies. This can be understood as a phonon-softening effects known from optical properties in solids.

In the next step, we tried to understand the strong coupling regime with the help of analytic approaches. The Feynman-Jensen variational principle allows for a calculation of the polaron mass. For small values of the interaction strength α , the polaron mass remains close to the mass of the isolated impurity. For interaction strengths approaching $\alpha = 3$, the polaron mass strongly increases. This behaviour is in agreement with calculations without an external trap for the impurity. The dependence of the polaron radius is similar to the mass: for small coupling strengths, the radius basically is set by the trap. Near $\alpha = 3$, the radius strongly decreases. This behaviour is not in agreement with the results from the path integral Monte Carlo simulation. The origin of this discrepancy is still unknown and should be investigated in future works. The arising finite energy level spacing might be the reason for the strong suppression of the polaron radius.

In a many-particle description, the BEC polaron has similar properties as charged particles in a dispersive medium: Cherenkov radiation is emitted. We investigated the analog of this effect in a BEC-mixture. Using leading order self-energy expressions, we were able to determine the threshold of the occurrence of Cherenkov radiation. In a BEC, this should be observed by looking at the rate of energy loss. In case of two and three dimensions, the threshold is the same as in the case of ordinary metals, $p \geq m_1c$. In one dimension, this is only true for a sufficiently large healing length of the condensate. For decreasing healing lengths, the threshold can be arbitrarily small.

“There’s Plenty of Room at the Bottom”¹ for future works. The effect of electron-phonon coupling in nanostructures as well as in ultracold quantum gases is still not understood in all of its details. In case of nanostructures, there is still the question about the role of vertex corrections in higher order cumulants. Therefore, an efficient method to cure the divergences in the tunneling expansion is needed. This might be an application for the non-equilibrium renormalization group. Also of interest is the structure the electron-phonon interaction appears in the polaron (Lang-Firsov) picture: in some sense, the phonon can be understood as a modification of the zero mode of the electrode’s fermion fields. This could be investigated with boundary conformal field theory. In case of ultracold quantum gases, most of our calculations based on the single particle picture. It could be interesting to look at the many-impurity BEC. Especially the effect of self-trapping (in the polaron picture) might lead to structures with novel order phenomena. For strong interactions, the effective model of atoms interacting with Bogoliubov modes has to be modified: three or more particle collisions have to be considered and the s-wave scattering approach has to be extended.

¹R. P. Feynman, see [Feynman \[1992\]](#)

Publications

- J. P. Dahlhaus, S. Maier, and A. Komnik. Spin-polarized current generation and detection by a double quantum dot structure. *Phys. Rev. B*, 81(7):075110, 2010
- S. Maier and A. Komnik. Transport properties of a molecular quantum dot coupled to one-dimensional correlated electrons. *Phys. Rev. B*, 82(16):165116, 2010
- S. Maier, T. L. Schmidt, and A. Komnik. Charge transfer statistics of a molecular quantum dot with strong electron-phonon interaction. *Phys. Rev. B*, 83(8):085401, 2011
- S. Maier and A. Komnik. A quantum Monte Carlo approach to the BEC polaron problem. *in preparation*

A. Non-equilibrium formalism for quantum impurity systems

A.1. Non-equilibrium Green's functions: The Keldysh-Schwinger formalism

This section gives a short introduction to the non-equilibrium Green's function formalism. However, it does not claim to be exhaustive in all detail. There are many excellent textbooks, e.g. [Haug and Jauho \[2008\]](#), [Mahan \[2000\]](#), [Rammer \[2007\]](#), dealing with this topic in more detail. For an introduction using functional integration techniques, see for example the review article [Kamenev and Levchenko \[2009\]](#). In the following, we will always assume, that we can divide the Hamiltonian \mathcal{H} in a equilibrium part H and the non-equilibrium contribution H_{neq} ,¹

$$\mathcal{H} = H + H_{\text{neq}}. \quad (\text{A.1})$$

In the operator formalism, Green's functions are introduced as (anti-)time ordered correlation functions of two field operators $\psi(x)$, $\phi(x)$,

$$G(x, x', t, t') = -i \langle T \psi_{\text{H}}(x, t) \phi_{\text{H}}(x', t') \rangle \quad (\text{A.2})$$

where T is the (anti-)time ordering operator, $\langle \cdot \rangle$ is either an expectation value of a pure state or a density matrix (canonical, grand canonical) and the time dependence is defined in the Heisenberg picture. First, we would like to do the math for the system at initial time t_0 in a pure state $|\Phi\rangle$ and later on generalize the results for a generic density matrix ρ ,

$$\rho = \sum_n p_n |\Phi_n\rangle \langle \Phi_n|. \quad (\text{A.3})$$

We begin the calculation by transforming the Green's function into the interaction picture,

$$G(x, x', t, t') = -i \langle \Phi | T S(t_0, t) \psi(x, t) S(t, t') \phi(x', t') S(t', t_0) | \Phi \rangle \quad (\text{A.4})$$

where we have introduced the S -matrix,

$$S(t, t') = T \exp \left[-i \int_t^{t'} d\tau H_{\text{neq}}(\tau) \right] \quad (\text{A.5})$$

and the time evolution of the field operators is taken into the interaction picture, i.e.

$$\psi(x, t) = e^{iHt} \psi(x) e^{-iHt}. \quad (\text{A.6})$$

At this point, introducing the Schwinger contour \mathcal{C}_{S} ([Craig \[1968\]](#), [Schwinger \[1961\]](#)) as depicted in [fig. A.1](#) is appropriate. Formally, the Schwinger contour depends on the two time parameters t , t' ,

¹In our case, this is often a tunneling Hamiltonian and/or a particle-particle interaction. In principle, this contribution can be diagonalizable, too.

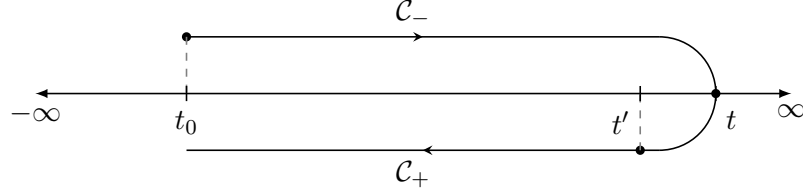


Figure A.1.: Sketch of the Schwinger contour. Both times t_0 and t are chosen to lie on the \mathcal{C}_- branch of the contour, t' lies on the \mathcal{C}_+ branch. In the usual sense of time ordering $t' < t$, in the Keldysh time ordering t is earlier than t' .

but we would like to keep notation simple and do not use a label to indicate this. The contour itself consists of a closed loop in time, starting from the initial time t_0 going to $\max(t, t')$ and back again to t_0 . Next, we introduce an order relation $<_{\mathcal{C}}$ on the contour,

$$t <_{\mathcal{C}} t' \Leftrightarrow \begin{cases} \text{true} & t \in \mathcal{C}_-, t' \in \mathcal{C}_+ \\ t < t' & t, t' \in \mathcal{C}_- \\ t > t' & t, t' \in \mathcal{C}_+ \end{cases}. \quad (\text{A.7})$$

We say $t =_{\mathcal{C}} t'$ if and only if $t = t'$ and both times lie on the same contour. With this in mind, we can define a contour ordering operator $T_{\mathcal{C}}$ analogously to the usual time ordering operator T . Next, we define a generalized S -matrix on the Schwinger contour,

$$S_{\mathcal{C}}(t_0) = T_{\mathcal{C}} \exp \left[-i \int_{\mathcal{C}_S} d\tau H_{\text{neq}}(\tau) \right] \quad (\text{A.8})$$

where the contour integral

$$\int_{\mathcal{C}_S} d\tau \dots := \int_{t_0}^{\max(t, t')} d\tau \dots + \int_{\max(t, t')}^{t_0} d\tau \dots, \quad (\text{A.9})$$

was introduced. The Green's function eq. (A.4) can now be extended to the non-equilibrium Green's function,

$$G(x, x', t, t') = -i \langle \Phi | T_{\mathcal{C}} S_{\mathcal{C}}(t_0) \psi(x, t) \phi(x', t') | \Phi \rangle. \quad (\text{A.10})$$

It is an extension, because the time parameters t, t' can lie on different branches of the contour. Obviously, a similar result holds for a system in a mixed state ρ at t_0 ,

$$G(x, x', t, t') = -i \text{Tr} \{ \rho T_{\mathcal{C}} [S_{\mathcal{C}}(t_0) \psi(x, t) \phi(x', t')] \}. \quad (\text{A.11})$$

We are two more steps away from recovering the Keldysh formalism (Keldysh [1965]). The first step simply extends the Schwinger contour to $+\infty$ by inserting the product $\mathbb{1} = S(t_{\text{max}}, \infty) S(\infty, t_{\text{max}})$ with $t_{\text{max}} = \max(t, t')$ inside the correlation function. The second step is more crucial; it involves the switching procedure of the non-equilibrium contribution. The idea is basically the same as in the equilibrium formalism, i.e. adiabatically switching from the infinite past. The only difference is that we do not switch it off again. In doing this, we arrive at the Keldysh function

$$G(x, x', t, t') = -i \text{Tr} \{ \rho(-\infty) T_{\mathcal{C}} [S_{\mathcal{C}} \psi(x, t) \phi(x', t')] \} =: -i \langle T_{\mathcal{C}} S_{\mathcal{C}} \psi(x, t) \phi(x', t') \rangle \quad (\text{A.12})$$

where we have introduced the Keldysh S -Matrix $S_{\mathcal{C}} = S_{\mathcal{C}}(-\infty)$ and $\rho(-\infty)$ being the pure or mixed state in absence of the non-equilibrium contribution H_{neq} . The time contour is now the well-known Keldysh contour which is depicted in fig. A.2. We will always choose $\rho(-\infty)$ to be the canonical

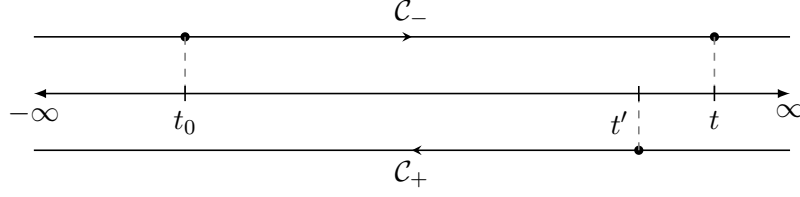


Figure A.2.: Sketch of the Keldysh contour. Both the times t_0 and t lie on the \mathcal{C}_- branch of the contour, t' lies on the \mathcal{C}_+ branch.

$$\rho = \frac{e^{-\beta H}}{\mathcal{Z}} \quad (\text{A.13})$$

or grand canonical density matrix,

$$\rho = \frac{e^{-\beta(H-\mu N)}}{\mathcal{Z}}. \quad (\text{A.14})$$

There is still a major task we have to handle: in general, we do not know the full interacting density matrix ρ . We can overcome this problem by introducing the Kadanoff-Baym contour (Kadanoff and Baym [1962]). We introduce the Kadanoff-Baym contour as an extension of the Schwinger contour

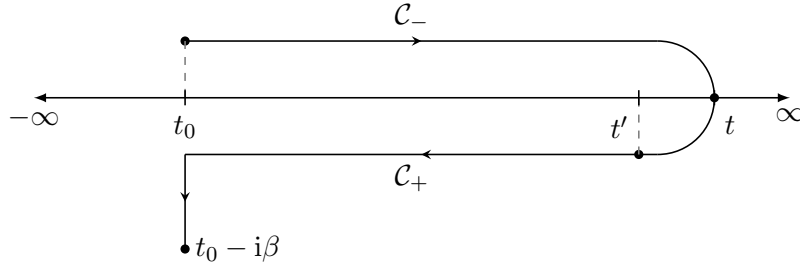


Figure A.3.: Sketch of the Kadanoff-Baym contour.

rather than the Keldysh contour, i.e. we have to reintroduce an initial time t_0 . But first, we have to do some preliminaries. We divide the Hamiltonian H into a non-interacting part, H_0 , and an interaction contribution, H_I ,

$$H = H_0 + H_I. \quad (\text{A.15})$$

Using the interaction picture for this decomposition, the density matrix can be rewritten

$$\frac{e^{-\beta H}}{\mathcal{Z}} = \frac{e^{-\beta H_0}}{\mathcal{Z}} S_I(t_0 - i\beta, t_0) \quad (\text{A.16})$$

where S_I is the S -matrix

$$S_I(t, t') = T \exp \left[-i \int_{t'}^t d\tau H_I(\tau) \right]. \quad (\text{A.17})$$

Together with eq. (A.11) one finds

$$G(x, x', t, t') = -i \text{Tr} \left\{ \frac{e^{-\beta H_0} S_I(t_0 - i\beta, t_0)}{\mathcal{Z}} T_C [S_C(t_0) \psi(x, t) \phi(x', t')] \right\}. \quad (\text{A.18})$$

The time evolution of the field operators is still in the interaction picture with respect to the previous decomposition, $\mathcal{H} = H + H_{\text{neq}}$, i.e. the fields evolve in time with respect to H . To be consistent, the fields have to be transformed to the new interaction picture,

$$\psi(x, t) = S_I(t_0, t) \psi_I(x, t) S_I(t, t_0). \quad (\text{A.19})$$

One obtains

$$G(x, x', t, t') = -i \text{Tr} \left\{ \frac{e^{-\beta H_0} S_I(t_0 - i\beta, t_0)}{Z} T_{\mathcal{C}} [S_{\mathcal{C}}(t_0) S_I(t_0, t) \psi_I(x, t) S_I(t, t') \phi_I(x', t') S_I(t', t_0)] \right\}. \quad (\text{A.20})$$

Defining the Kadanoff-Baym contour $\mathcal{C}_{\text{KB}} := \mathcal{C}_{\text{S}} \cup [t_0 - i\beta, t_0]$, together with an appropriate time ordering operator $T_{\mathcal{C}}$ and a S -matrix,

$$S_{\text{IC}}(t_0 - i\beta, t_0) = T_{\mathcal{C}} \exp \left[-i \int_{\mathcal{C}_{\text{KB}}} d\tau H_I(\tau) \right] \quad (\text{A.21})$$

we end up with an expression

$$G(x, x', t, t') = -i \frac{\text{Tr} \{ e^{-\beta H_0} T_{\mathcal{C}} [S_{\text{IC}}(t_0 - i\beta, t_0) S_{\mathcal{C}}(t_0) \psi(x, t) \phi(x', t')] \}}{\text{Tr} \{ e^{-\beta H_0} T_{\mathcal{C}} [S_{\text{IC}}(t_0 - i\beta, t_0) S_{\mathcal{C}}(t_0)] \}}, \quad (\text{A.22})$$

where we have omitted the label I of the field operators. In the following, we will always assume the time evolution to be according to H_0 . In the limit of $t_0 \rightarrow -\infty$, initial correlation often can be neglected. Therefore, in this limit, the Keldysh contour is recovered and (A.22) becomes

$$G(x, x', t, t') = -i \text{Tr} \rho_0 T_{\mathcal{C}} [S_{\text{IC}} S_{\mathcal{C}} \psi(x, t) \phi(x', t')] = -i \langle T_{\mathcal{C}} [S_{\text{IC}} S_{\mathcal{C}} \psi(x, t) \phi(x', t')] \rangle \quad (\text{A.23})$$

where $\rho_0 = \frac{e^{-\beta H_0}}{Z_0}$. We introduced the second equation to indicate, that the calculation not only holds for the canonical ensemble. It holds for pure states and the grand canonical ensemble, too. Again, the time parameters t, t' lie on the two branches of the Keldysh contour independently of each other. This leaves us with four possible combinations of arranging them. It is convenient to introduce the notion of Keldysh matrices,

$$\mathbf{G}(t, t') = \begin{pmatrix} G^{--}(t, t') & G^{-+}(t, t') \\ G^{+-}(t, t') & G^{++}(t, t') \end{pmatrix}, \quad (\text{A.24})$$

where the meaning of the superscripts is obvious, $G^{ss'}(t, t')$ for $t \in \mathcal{C}_s$ and $t' \in \mathcal{C}_{s'}$. To close this section, we would like to relate the contour ordered Green's function to the real-time Green's function,

$$\begin{aligned} \begin{pmatrix} G^{--}(x, x', t, t') & G^{-+}(x, x', t, t') \\ G^{+-}(x, x', t, t') & G^{++}(x, x', t, t') \end{pmatrix} &= \begin{pmatrix} G^{\text{t}}(x, x', t, t') & G^{<}(x, x', t, t') \\ G^{>}(x, x', t, t') & G^{\bar{\text{t}}}(x, x', t, t') \end{pmatrix} \\ &= \begin{pmatrix} -i \langle T[\psi_{\text{H}}(x, t) \phi_{\text{H}}(x', t')] \rangle & \pm i \langle \phi_{\text{H}}(x', t') \psi_{\text{H}}(x, t) \rangle \\ -i \langle \psi_{\text{H}}(x, t) \phi_{\text{H}}(x', t') \rangle & -i \langle \tilde{T}[\psi_{\text{H}}(x, t) \phi_{\text{H}}(x', t')] \rangle \end{pmatrix} \end{aligned} \quad (\text{A.25})$$

where the upper sign holds for fermions and the lower for bosons. \tilde{T} denotes the anti-time ordering operator. From this relation, one immediately finds that not all of the four components of the contour ordered Keldysh functions are independent. In fact, they satisfy the equation

$$G^{-+} + G^{+-} = G^{--} + G^{++}. \quad (\text{A.26})$$

There are situations where eq. (A.26) does not hold. For example, this is the case for the λ -dependent operator H_{λ} introduced in the definition of the full counting statistics (see eq. (2.16)). This is due to the explicit Keldysh time dependence of the counting field λ .

A.2. Important Keldysh functions

In this section we provide the basic Keldysh functions of the isolated components of quantum impurity systems which are extensively used in chapter 2. We start with the Keldysh functions of the free leads.

A.2.1. Keldysh function of the electronic leads

For the moment, we omit the index to distinguish the left and right reservoirs, because they differ only by the chemical potential $\mu_{L,R}$. At the end of the calculation, we can easily restore our original notation. The Hamiltonian of the isolated electrode is given by

$$H_{\text{lead}} = \int \frac{dk}{2\pi} \epsilon_k c_k^\dagger c_k \quad (\text{A.27})$$

where ϵ_k denote the single particle energies and c_k^\dagger, c_k the creation and annihilation operators of an electron with momentum k . The time dependence of this operators is quite simple. We use Heisenberg's equation of motion to find a differential equation for c_k ,

$$\dot{c}_k(t) = -i \left[H_{\text{lead}}(t), c_k(t) \right] = -i \epsilon_k c_k(t). \quad (\text{A.28})$$

The solution of this equation is simple,

$$c_k(t) = c_k e^{-i\epsilon_k t}. \quad (\text{A.29})$$

An analogous expression holds for the creation operator, $c_k^\dagger(t) = c_k^\dagger e^{i\epsilon_k t}$. The field operator $\Psi(x, t)$ of the lead can be constructed the following way,

$$\Psi(x, t) = \int \frac{dk}{2\pi} e^{ikx} c_k(t). \quad (\text{A.30})$$

Similarly, we can define $\Psi^\dagger(x, t)$. Then, the Keldysh function of the lead

$$g(x - x', t - t') = -i \left\langle T_{\mathcal{C}} \left[\Psi(x, t) \Psi^\dagger(x', t') \right] \right\rangle \quad (\text{A.31})$$

can be expressed in terms of Keldysh functions of the single modes, i.e.

$$g(x - x', t - t') = -i \int \frac{dk dk'}{(2\pi)^2} e^{i(kx - k'x')} \left\langle T_{\mathcal{C}} \left[c_k(t) c_k^\dagger(t') \right] \right\rangle =: \int \frac{dk dk'}{(2\pi)^2} e^{i(kx - k'x')} g_{kk'}(t - t'). \quad (\text{A.32})$$

Using the definition of Keldysh time ordering one immediately finds

$$g_{kk'}(t - t') = -2\pi i \delta(k - k') e^{-i\epsilon_k(t-t')} \begin{pmatrix} \Theta(t - t') - n_k & -n_k \\ 1 - n_k & \Theta(t' - t) - n_k \end{pmatrix} \quad (\text{A.33})$$

where the occupation number $n_k = \langle c_k^\dagger c_k \rangle$ was introduced. Therefore, the Keldysh function for the leads is

$$g(x, t) = -i \int \frac{dk}{2\pi} e^{ikx - i\epsilon_k t} \begin{pmatrix} \Theta(t) - n_k & -n_k \\ 1 - n_k & \Theta(-t) - n_k \end{pmatrix}. \quad (\text{A.34})$$

Most of the time, we are only interested in the case of $x = 0$. Therefore, to keep notation simple, we will omit the coordinate label, $g(t) = g(0, t)$. Using the density of states for a one-dimensional electron gas, $\rho(E)$, one can rewrite eq. (A.34),

$$g(t) = -i \int \frac{dE}{2\pi} \rho(E) e^{-iEt} \begin{pmatrix} \Theta(t) - n_F(E) & -n_F(E) \\ 1 - n_F(E) & \Theta(-t) - n_F(E) \end{pmatrix}, \quad (\text{A.35})$$

where $n_F(E)$ is the Fermi-Dirac distribution function. In the wide flat band limit one obtains

$$g(t) = -i\rho_0 \int \frac{dE}{2\pi} e^{-iEt} \begin{pmatrix} \Theta(t) - n_F(E) & -n_F(E) \\ 1 - n_F(E) & \Theta(-t) - n_F(E) \end{pmatrix}, \quad (\text{A.36})$$

where $\rho_0 = \rho(E_F)$ denotes the density of states at the Fermi energy. Using contour integration techniques one finds

$$g(t) = \rho_0 e^{-i\mu t} \begin{pmatrix} \frac{-1}{\frac{\beta}{\pi} \sinh \left[\frac{\pi}{\beta} (t - i\sigma\eta) \right]} & \frac{1}{\frac{\beta}{\pi} \sinh \left[\frac{\pi}{\beta} (-t - i\eta) \right]} \\ \frac{-1}{\frac{\beta}{\pi} \sinh \left[\frac{\pi}{\beta} (t - i\eta) \right]} & \frac{1}{\frac{\beta}{\pi} \sinh \left[\frac{\pi}{\beta} (t - i\sigma\eta) \right]} \end{pmatrix} \xrightarrow{T \rightarrow 0} i\rho_0 e^{-i\mu t} \begin{pmatrix} \frac{-1}{t - i\sigma\eta} & \frac{1}{-t - i\eta} \\ \frac{-1}{t - i\eta} & \frac{1}{-t - i\sigma\eta} \end{pmatrix}, \quad (\text{A.37})$$

where the infinitesimal (cut-off) parameter η , the sign $\sigma = \text{sgn}(t)$ and the chemical potential μ have been introduced. In frequency space, the Keldysh function for the leads is given by

$$g(\omega) = 2\pi i \rho_0 \begin{pmatrix} n_F(\omega) - \frac{1}{2} & n_F(\omega) \\ n_F(\omega) - 1 & n_F(\omega) - \frac{1}{2} \end{pmatrix}. \quad (\text{A.38})$$

The Keldysh functions of the left and right lead can be found by setting $\mu = \mu_{L,R}$.

A.2.2. Keldysh function for the quantum dot

In molecular electronics, a quantum dot consists of a few fermionic levels. A single level is described by the Hamiltonian,

$$H_{\text{QD}} = \Delta_0 d^\dagger d \quad (\text{A.39})$$

where Δ_0 is the dot level energy and d, d^\dagger the annihilation and creation operator for the states of the quantum dot. Clearly, the time dependence of the dot operator d is given by

$$d(t) = d e^{-i\Delta_0 t}. \quad (\text{A.40})$$

A similar expression holds for the creation operator. The Keldysh function of the quantum dot is then

$$d_0(t, t') = -i \left\langle T_C \left[d(t) d^\dagger(t') \right] \right\rangle = -i e^{-i\Delta_0(t-t')} \begin{pmatrix} \Theta(t-t') - n_d & -n_d \\ 1 - n_d & \Theta(t'-t) - n_d \end{pmatrix}, \quad (\text{A.41})$$

where $n_d = \langle d^\dagger d \rangle$ is the occupation number of the dot level. Assuming a completely uncoupled dot, i.e. no hybridization with a reservoir, $n_d \in \{0, 1\}$. In frequency space, we find

$$d_0(\omega) = \begin{pmatrix} \frac{1}{\omega - \Delta_0 + i\eta} + 2\pi i n_d \delta(\omega - \Delta_0) & 2\pi i n_d \delta(\omega - \Delta_0) \\ 2\pi i (n_d - 1) \delta(\omega - \Delta_0) & \frac{-1}{\omega - \Delta_0 - i\eta} + 2\pi i n_d \delta(\omega - \Delta_0) \end{pmatrix}. \quad (\text{A.42})$$

In most cases, the steady-state of the system does not depend on the initial occupation n_d of the quantum dot. Therefore, one can set $n_d = 0$. It is an easy exercise to show that the Keldysh function of a hybridized quantum dot (coupled to a reservoir) does not depend on n_d .

A.2.3. Keldysh function of the bosonic degree of freedom

The dynamics of a single bosonic mode is described by the Hamiltonian

$$H_B = \Omega \left(B^\dagger B + \frac{1}{2} \right) \quad (\text{A.43})$$

where Ω is the frequency of the bosonic mode and B, B^\dagger are the annihilation resp. creation operators of the bosonic mode. Again, we have $B(t) = B e^{-i\Omega t}$ and $B^\dagger(t) = B^\dagger e^{i\Omega t}$ for the time evolution. The Keldysh function of the boson can be calculated to

$$\tilde{b}_0(t, t') = -i \left\langle T_C \left[B(t) B^\dagger(t') \right] \right\rangle = -i e^{-i\Omega(t-t')} \begin{pmatrix} \Theta(t-t') + n_b & n_b \\ n_b + 1 & \Theta(t'-t) + n_b \end{pmatrix}. \quad (\text{A.44})$$

n_B is the initial occupation of the bosonic mode, $n_B = \langle B^\dagger B \rangle$. More often we are interested in the Keldysh function

$$\begin{aligned} b_0(t, t') &= -i \left\langle T_C \left[B(t) + B^\dagger(t) \right] \left[B^\dagger(t') + B(t') \right] \right\rangle \\ &= -i \begin{pmatrix} e^{-i\Omega|t-t'|} (1 + n_b) + n_b e^{i\Omega|t-t'|} & n_b \left(e^{-i\Omega|t-t'|} + e^{i\Omega|t-t'|} \right) + e^{i\Omega(t-t')} \\ (n_b + 1) \left(e^{-i\Omega|t-t'|} + e^{i\Omega|t-t'|} \right) + e^{-i\Omega(t-t')} & e^{i\Omega|t-t'|} (1 + n_b) + n_b e^{-i\Omega|t-t'|} \end{pmatrix} \\ &= -i (2n_b + 1) \begin{pmatrix} \cos(\Omega|t-t'|) & \cos[\Omega(t-t')] \\ \cos[\Omega(t-t')] & \cos(\Omega|t-t'|) \end{pmatrix} + \begin{pmatrix} -\sin(\Omega|t-t'|) & \sin[\Omega(t-t')] \\ -\sin[\Omega(t-t')] & \sin(\Omega|t-t'|) \end{pmatrix}. \end{aligned} \quad (\text{A.45})$$

A.3. Functional integral formalism for the resonant level model

This section is dedicated to the functional integral treatment of the resonant level model. It is one of the simplest models in mesoscopic transport theory which is still exactly solvable. The Keldysh action for the model is

$$S = S_0 + S_T[\lambda] \quad (\text{A.46})$$

where S_0 describes the isolated leads and the single level quantum dot,

$$\begin{aligned} S_0 &= \int dx dx' \int_C d\tau d\tau' \left[\sum_{\alpha=L,R} \bar{\psi}_\alpha(x, \tau) g_\alpha^{-1}(x-x', \tau-\tau') \psi_\alpha(x', \tau') \right] \\ &\quad + \int_C d\tau d\tau' \bar{d}(\tau) d_0^{-1}(\tau-\tau') d(\tau') \end{aligned} \quad (\text{A.47})$$

and the tunneling action $S_T[\lambda]$,

$$S_T[\lambda] = i\gamma \sum_{\alpha=L,R=\pm} \int_C d\tau \left[e^{\frac{i\alpha\lambda(\tau)}{4}} \bar{d}(\tau) \psi_\alpha(x=0, \tau) + e^{-\frac{i\alpha\lambda(\tau)}{4}} \bar{\psi}_\alpha(x=0, \tau) d(\tau) \right]. \quad (\text{A.48})$$

Up to proper normalization, the full counting statistics is given by the Keldysh partition function (see [Kamenev and Levchenko \[2009\]](#) for details),

$$\mathcal{Z}[\lambda] = \int \frac{\mathcal{D}[\psi_L, \psi_R, d]}{Z_0} \exp \{ -S_0 - S_T[\lambda] \}. \quad (\text{A.49})$$

Using the functional delta distribution,

$$\delta [\psi_\alpha (x = 0, \tau) - \psi_\alpha (0, \tau)] := \int \mathcal{D} [\lambda (\tau)] e^{-i \int_{\mathcal{C}} d\tau \lambda (\tau) [\psi_\alpha (x=0, \tau) - \psi_\alpha (0, \tau)]} \quad (\text{A.50})$$

with $\alpha = \text{L, R}$, the bulk degrees of freedom can easily be integrated out and one is left with an effective zero-dimensional problem,

$$S_{\text{eff}} = S'_0 + S'_T [\lambda] \quad (\text{A.51})$$

with

$$S'_0 = \int_{\mathcal{C}} d\tau d\tau' \left[\sum_{\alpha=\text{L,R}} \bar{\psi}_\alpha (\tau) g_\alpha^{-1} (\tau - \tau') \psi_\alpha (\tau') \right] + \int_{\mathcal{C}} d\tau d\tau' \bar{d} (\tau) d_0^{-1} (\tau - \tau') d (\tau') \quad (\text{A.52})$$

$$S'_T [\lambda] = i\gamma \sum_{\alpha=\text{L,R}=\pm} \int_{\mathcal{C}} d\tau \left[e^{\frac{i\alpha\lambda(\tau)}{4}} \bar{d} (\tau) \psi_\alpha (\tau) + e^{-\frac{i\alpha\lambda(\tau)}{4}} \bar{\psi}_\alpha (\tau) d (\tau) \right]. \quad (\text{A.53})$$

where we omitted the label "0" to keep notation simple. Introducing auxiliary fields $\eta_\alpha (\tau)$, $\bar{\eta}_\alpha (\tau)$ such that

$$\bar{\psi}_\alpha (\tau) = \bar{\eta}_\alpha (\tau) - i \int_{\mathcal{C}} d\sigma \gamma e^{\frac{i\alpha\lambda(\sigma)}{4}} \bar{d} (\sigma) g_\alpha (\sigma - \tau) \quad (\text{A.54})$$

$$\psi_\alpha (\tau) = \eta_\alpha (\tau) - i \int_{\mathcal{C}} d\sigma \gamma e^{-\frac{i\alpha\lambda(\sigma)}{4}} g_\alpha (\tau - \sigma) d (\sigma) \quad (\text{A.55})$$

the lead degrees of freedom can be integrated out and one is left with the effective action of the quantum dot,

$$S_{\text{QD,eff}} [\lambda] = \int d\tau d\tau' \bar{d} (\tau) \left[d_0^{-1} (\tau - \tau') - \sum_{m=\text{L,R}=\pm} \gamma e^{\frac{i\alpha\lambda(\sigma)}{4}} g_m (\tau - \tau') \gamma e^{\frac{-i\alpha\lambda(\sigma)}{4}} \right] d (\tau'). \quad (\text{A.56})$$

After introducing Keldysh vectors $\vec{d} = (d_+, d_-)$, one can Fourier transform

$$\vec{d}_\omega = \int_{-\infty}^{\infty} dt e^{i\omega t} \vec{d} (t) \quad (\text{A.57})$$

and the system becomes diagonal up to Keldysh blocks. The Fourier transformed action is

$$S_{\text{QD,eff}} [\lambda] = \sum_{\omega} \vec{d}_\omega \left[d_0^{-1} (\omega) - \sum_{m=\text{L,R}=\pm} \hat{\gamma}_m g_m (\omega) \hat{\gamma}_m^* \right] \vec{d}_\omega \quad (\text{A.58})$$

where we have introduced the matrix

$$\hat{\gamma}_m = \gamma \sigma_3 \begin{pmatrix} e^{im\lambda_-/4} & 0 \\ 0 & e^{im\lambda_+/4} \end{pmatrix}, \quad (\text{A.59})$$

and its complex conjugate $\hat{\gamma}_m^*$. Because of its block diagonal structure, the Keldysh partition function is just given by

$$\mathcal{Z} [\lambda] = \prod_{\omega} \det \left[d_0^{-1} (\omega) - \sum_{m=\text{L,R}=\pm} \hat{\gamma}_m g_m (\omega) \hat{\gamma}_m^* \right]. \quad (\text{A.60})$$

For the CGF, we obtain

$$\begin{aligned} \ln \chi(\lambda) &= \sum_{\omega} \frac{\mathcal{Z}[\lambda]}{\mathcal{Z}[\lambda=0]} = \mathcal{T} \int \frac{d\omega}{2\pi} \frac{\mathcal{Z}[\lambda]}{\mathcal{Z}[\lambda=0]} \\ &= \mathcal{T} \int \frac{d\omega}{2\pi} \ln \left\{ 1 + T(\omega) \left[(e^{i\lambda} - 1) n_L (1 - n_R) + (e^{-i\lambda} - 1) n_R (1 - n_L) \right] \right\} \end{aligned} \quad (\text{A.61})$$

which has the well known Levitov-Lesovik structure with the transmission coefficient of the resonant level model,

$$T(\omega) = \frac{\Gamma^2}{(\omega - \Delta_0)^2 + \Gamma^2}. \quad (\text{A.62})$$

The hybridization Γ is defined by $\Gamma = \pi \rho_0 \gamma^2$ (wide flat band limit). In order to derive Dyson's equation or Dyson-like equations, one has to introduce source fields into the action. We start with the Keldysh action

$$S = S_{\text{leads}} + S_{\text{QD}} + S_{\text{T}} + S_{\text{SF}}[\xi_{\text{L,R}}, \eta] \quad (\text{A.63})$$

where we now allow interactions on the quantum dot. The single contributions are

$$S_{\text{leads}} = \int_{\mathcal{C}} d\tau d\tau' \left[\sum_{m=\text{L,R}} \bar{\psi}_m(\tau) g_m^{-1}(\tau - \tau') \psi_m(\tau') \right] \quad (\text{A.64})$$

$$S_{\text{QD}} = \int_{\mathcal{C}} d\tau d\tau' \bar{d}(\tau) d_0^{-1}(\tau - \tau') d(\tau') + S_{\text{int}} \quad (\text{A.65})$$

$$S_{\text{T}} = i\gamma \sum_{m=\text{L,R}=\pm} \int_{\mathcal{C}} d\tau \left[e^{\frac{im\lambda(\tau)}{4}} \bar{d}(\tau) \psi_m(\tau) + e^{-\frac{im\lambda(\tau)}{4}} \bar{\psi}_m(\tau) d(\tau) \right] \quad (\text{A.66})$$

$$S_{\text{SF}}[\xi_{\text{L,R}}, \eta] = i \int_{\mathcal{C}} d\tau \left[\sum_{m=\text{L,R}=\pm} (\bar{\xi}_m \psi_m + \bar{\psi}_m \xi_m) + \bar{\eta} d + \bar{d} \eta \right] \quad (\text{A.67})$$

Again, we use auxiliary fields $\eta_m(\tau)$, $\bar{\eta}_m(\tau)$ such that

$$\bar{\psi}_m(\tau) = \bar{\eta}_m(\tau) - i \int_{\mathcal{C}} d\sigma \left[\bar{\xi}_m(\sigma) + \gamma e^{\frac{im\lambda(\sigma)}{4}} \bar{d}(\sigma) \right] g_m(\sigma - \tau) \quad (\text{A.68})$$

$$\psi_m(\tau) = \eta_m(\tau) - i \int_{\mathcal{C}} d\sigma g_m(\tau - \sigma) \left[\xi_m(\sigma) + \gamma e^{-\frac{im\lambda(\sigma)}{4}} d(\sigma) \right] \quad (\text{A.69})$$

holds. After integrating out the leads, one obtains the effective action,

$$S_{\text{eff}} = S'_{\text{QD}} + S'_{\text{SF}}[\xi_{\text{L,R}}, \eta] \quad (\text{A.70})$$

with

$$S'_{\text{QD}} = \int_{\mathcal{C}} d\tau d\tau' \bar{d}(\tau) \left[d_0^{-1}(\tau - \tau') - \sum_{m=\text{L,R}=\pm} \gamma e^{\frac{im\lambda(\tau)}{4}} g_m(\tau - \tau') \gamma e^{-\frac{im\lambda(\tau')}{4}} \right] d(\tau') + S_{\text{int}} \quad (\text{A.71})$$

and

$$\begin{aligned} S'_{\text{SF}}[\xi_{\text{L,R}}, \eta] &= i \int_{\mathcal{C}} d\tau [\bar{\eta} d + \bar{d} \eta] - \int_{\mathcal{C}} d\tau d\tau' \sum_{m=\text{L,R}=\pm} \left[\bar{\xi}_m(\tau) g_m(\tau - \tau') \xi_m(\tau) \right. \\ &\quad \left. + \bar{d}(\tau) \gamma e^{\frac{im\lambda(\tau)}{4}} g_m(\tau - \tau') \xi_m(\tau') + \bar{\xi}_m(\tau) \gamma e^{-\frac{im\lambda(\tau)}{4}} g_m(\tau - \tau') d(\tau') \right]. \end{aligned} \quad (\text{A.72})$$

Although, in presence of interactions, the quantum dot degrees of freedom can in general not be integrated out, one can still get interesting relations. Using functional derivatives, one easily obtains

$$G_{dm}(t, t') = \gamma \int_C d\tau D(t, \tau) g_m(\tau, t') e^{-im\lambda(\tau)/4} \quad (\text{A.73})$$

where D is the full Keldysh functions of the quantum dot including interactions.

A.4. Polarization loop for the TLL

In this section of the appendix we list the lengthy expressions for the polarization loop eq. (2.166). The calculation of the single contributions is quite cumbersome. For the parallel contribution of the polarization loop we have introduced the quantities,

$$\begin{aligned} \Upsilon_{m,n}^{\lambda,\nu}(y) &= \frac{1}{2\kappa} (\alpha_{0,\nu,m} - \alpha_{y,\lambda,n}) \left[\ln \left(\frac{y^2 + \alpha_{0,\nu,m}y + \beta_{0,\nu,m}^2}{y^2 + \alpha_{\omega,\lambda,n}y + \beta_{\omega,\lambda,n}^2} \right) \right] \\ &+ \frac{\alpha_{0,\nu,m} (\alpha_{0,\nu,m} - \alpha_{\omega,\lambda,n}) - 2(\beta_{0,\nu,m} - \beta_{\omega,\lambda,n})}{\kappa \sqrt{4\beta_{0,\nu,m} - \alpha_{0,\nu,m}^2}} \tan^{-1} \left(\frac{2y + \alpha_{0,\nu,m}}{\sqrt{4\beta_{0,\nu,m} - \alpha_{0,\nu,m}^2}} \right) \\ &+ \frac{\alpha_{\omega,\lambda,n} (\alpha_{\omega,\lambda,n} - \alpha_{\omega,\lambda,n}) - 2(\beta_{\omega,\lambda,n} - \beta_{0,\nu,m})}{\kappa \sqrt{4\beta_{\omega,\lambda,n} - \alpha_{\omega,\lambda,n}^2}} \tan^{-1} \left(\frac{2y + \alpha_{\omega,\lambda,n}}{\sqrt{4\beta_{\omega,\lambda,n} - \alpha_{\omega,\lambda,n}^2}} \right) \end{aligned} \quad (\text{A.74})$$

with $\alpha_{\omega,\lambda,\pm} = 2\omega \pm i\Gamma e^{i\lambda/2}$, $\beta_{\omega,\lambda,\pm} = -\Delta_0^2 \pm i\Gamma\omega e^{i\lambda/2}$ and

$$\kappa = (\beta_{0,\nu,m} - \beta_{\omega,\lambda,n})^2 + (\alpha_{y,\lambda,n}\beta_{0,\nu,m} - \alpha_{0,\nu,m}\beta_{\omega,\lambda,n}) (\alpha_{\omega,\lambda,n} - \alpha_{0,\nu,m}). \quad (\text{A.75})$$

For the orthogonal contribution we introduced the expressions,

$$\begin{aligned} \Upsilon_{1,m,n}^{\lambda,\nu}(y) &= \frac{(\alpha_{0,\nu,m} + 2\omega) (\alpha_{0,\nu,m} - \alpha_{\omega,\lambda,n}) - 2(\beta_{0,\nu,m} - \beta_{\omega,\lambda,n})}{\kappa \sqrt{4\beta_{0,\nu,m} - \alpha_{0,\nu,m}^2}} \tan^{-1} \left(\frac{2y + \alpha_{0,\nu,m}}{\sqrt{4\beta_{0,\nu,m} - \alpha_{0,\nu,m}^2}} \right) \\ &+ \frac{-\alpha_{0,\nu,m}^2\omega (\alpha_{0,\nu,m} - \alpha_{\omega,\lambda,n}) + \alpha_{0,\nu,m}\omega (\beta_{0,\nu,m} - \beta_{\omega,\lambda,n})}{\kappa\beta_{0,\nu,m}\sqrt{4\beta_{0,\nu,m} - \alpha_{0,\nu,m}^2}} \tan^{-1} \left(\frac{2y + \alpha_{0,\nu,m}}{\sqrt{4\beta_{0,\nu,m} - \alpha_{0,\nu,m}^2}} \right) \\ &+ \frac{(\alpha_{\omega,\lambda,n} + 2\omega) (\alpha_{\omega,\lambda,n} - \alpha_{0,\nu,m}) - 2(\beta_{\omega,\lambda,n} - \beta_{0,\nu,m})}{\kappa \sqrt{4\beta_{\omega,\lambda,n} - \alpha_{\omega,\lambda,n}^2}} \tan^{-1} \left(\frac{2y + \alpha_{\omega,\lambda,n}}{\sqrt{4\beta_{\omega,\lambda,n} - \alpha_{\omega,\lambda,n}^2}} \right) \\ &+ \frac{-\alpha_{\omega,\lambda,n}^2\omega (\alpha_{\omega,\lambda,n} - \alpha_{0,\nu,m}) + \alpha_{\omega,\lambda,n}\omega (\beta_{\omega,\lambda,n} - \beta_{0,\nu,m})}{\kappa\beta_{\omega,\lambda,n}\sqrt{4\beta_{\omega,\lambda,n} - \alpha_{\omega,\lambda,n}^2}} \tan^{-1} \left(\frac{2y + \alpha_{\omega,\lambda,n}}{\sqrt{4\beta_{\omega,\lambda,n} - \alpha_{\omega,\lambda,n}^2}} \right) \\ &+ \frac{(\alpha_{0,\nu,m}\omega - \beta_{0,\nu,m}) (\alpha_{0,\nu,m} - \alpha_{\omega,\lambda,n}) - \omega (\beta_{0,\nu,m} - \beta_{\omega,\lambda,n})}{2\kappa\beta_{0,\nu,m}} \ln \left(\frac{y^2 + \alpha_{0,\nu,m}y + \beta_{0,\nu,m}}{y^2 + \alpha_{\omega,\lambda,n}y + \beta_{\omega,\lambda,n}} \right) \\ &+ \frac{\omega}{2\beta_{0,\nu,m}\beta_{\omega,\lambda,n}} \ln \left(\frac{y^2}{y^2 + \alpha_{\omega,\lambda,n}y + \beta_{\omega,\lambda,n}} \right), \end{aligned} \quad (\text{A.76})$$

$$\begin{aligned}
 \Upsilon_{2,m,n}^{\lambda,\nu}(y) &= \frac{\omega(\alpha_{0,\nu,m} - \alpha_{\omega,\lambda,n}) - (\beta_{0,\nu,m} - \beta_{\omega,\lambda,m})}{2\kappa} \ln \left(\frac{y^2 + \alpha_{0,\nu,m}y + \beta_{0,\nu,m}}{y^2 + \alpha_{\omega,\lambda,n}y + \beta_{\omega,\lambda,n}} \right) \\
 &+ \frac{(\alpha_{0,\nu,m}\omega - \beta_{0,\nu,m} - \beta_{\omega,\lambda,n})(\alpha_{0,\nu,m} - \alpha_{\omega,\lambda,n}) - (2\omega - \alpha_{\omega,\lambda,n})(\beta_{0,\nu,m} - \beta_{\omega,\lambda,n})}{\kappa\sqrt{4\beta_{0,\nu,m} - \alpha_{0,\nu,m}^2}} \\
 &\times \tan^{-1} \left[(2y + \alpha_{0,\nu,m}) / \sqrt{4\beta_{0,\nu,m} - \alpha_{0,\nu,m}^2} \right] \\
 &+ \frac{(\alpha_{\omega,\lambda,n}\omega - \beta_{\omega,\lambda,n} - \beta_{0,\nu,m})(\alpha_{\omega,\lambda,n} - \alpha_{0,\nu,m}) - (2\omega - \alpha_{0,\nu,m})(\beta_{\omega,\lambda,n} - \beta_{0,\nu,m})}{\kappa\sqrt{4\beta_{\omega,\lambda,n} - \alpha_{\omega,\lambda,n}^2}} \\
 &\times \tan^{-1} \left[(2y + \alpha_{\omega,\lambda,n}) / \sqrt{4\beta_{\omega,\lambda,n} - \alpha_{\omega,\lambda,n}^2} \right], \tag{A.77}
 \end{aligned}$$

$$\begin{aligned}
 \Upsilon_{3,m,n}^{\lambda,\nu}(y) &= \frac{-\beta_{0,\nu,m}(\alpha_{0,\nu,m} - \alpha_{\omega,\lambda,n}) + (\alpha_{0,\nu,m} - \omega)(\beta_{0,\nu,m} - \beta_{\omega,\lambda,n})}{2\kappa} \ln \left(\frac{y^2 + \alpha_{0,\nu,m}y + \beta_{0,\nu,m}}{y^2 + \alpha_{\omega,\lambda,n}y + \beta_{\omega,\lambda,n}} \right) \\
 &+ \frac{[\alpha_{0,\nu,m}\beta_{0,\nu,m} - \omega(\beta_{0,\nu,m} + \beta_{\omega,\lambda,n})](\alpha_{0,\nu,m} - \alpha_{\omega,\lambda,n})}{\sqrt{4\beta_{0,\nu,m} - \alpha_{0,\nu,m}^2}} \tan^{-1} \left(\frac{2y + \alpha_{0,\nu,m}}{\sqrt{4\beta_{0,\nu,m} - \alpha_{0,\nu,m}^2}} \right) \\
 &+ \frac{(2\beta_{0,\nu,m} - \alpha_{0,\nu,m}^2 + \alpha_{\omega,\lambda,n}\omega)(\beta_{0,\nu,m} - \beta_{\omega,\lambda,n})}{\sqrt{4\beta_{0,\nu,m} - \alpha_{0,\nu,m}^2}} \tan^{-1} \left(\frac{2y + \alpha_{0,\nu,m}}{\sqrt{4\beta_{0,\nu,m} - \alpha_{0,\nu,m}^2}} \right) \\
 &+ \frac{[\alpha_{\omega,\lambda,n}\beta_{\omega,\lambda,n} - \omega(\beta_{\omega,\lambda,n} + \beta_{0,\nu,m})](\alpha_{\omega,\lambda,n} - \alpha_{0,\nu,m})}{\sqrt{4\beta_{\omega,\lambda,n} - \alpha_{\omega,\lambda,n}^2}} \tan^{-1} \left(\frac{2y + \alpha_{\omega,\lambda,n}}{\sqrt{4\beta_{\omega,\lambda,n} - \alpha_{\omega,\lambda,n}^2}} \right) \\
 &+ \frac{(2\beta_{\omega,\lambda,n} - \alpha_{\omega,\lambda,n}^2 + \alpha_{0,\nu,m}\omega)(\beta_{\omega,\lambda,n} - \beta_{0,\nu,m})}{\sqrt{4\beta_{\omega,\lambda,n} - \alpha_{\omega,\lambda,n}^2}} \tan^{-1} \left(\frac{2y + \alpha_{\omega,\lambda,n}}{\sqrt{4\beta_{\omega,\lambda,n} - \alpha_{\omega,\lambda,n}^2}} \right). \tag{A.78}
 \end{aligned}$$

A.5. Functional integral treatment of the double quantum dot

In this section we provide details to the calculation of the CGF of the double quantum dot setup using functional integration. The starting point is the Keldysh action

$$S = S_{\text{leads}} + S_{\text{QD}} + S_{\text{T}} \tag{A.79}$$

with

$$S_{\text{leads}} = \int_{\mathcal{C}} d\tau d\tau' \sum_{\substack{m=L,R \\ \sigma=\uparrow,\downarrow}} \bar{\psi}_{m,\sigma}(\tau) g_{m,\sigma}^{-1}(\tau - \tau') \psi_{m,\sigma}(\tau') \tag{A.80}$$

where we have already integrated out the bulk degrees of freedom. $g_{m,\sigma}$ is the usual Keldysh function used before except, for an additional spin index. The action of the quantum dots is

$$S_{\text{QD}} = \int_{\mathcal{C}} d\tau d\tau' \sum_{\substack{i=1,2 \\ \sigma=\uparrow,\downarrow}} \bar{d}_{i,\sigma}(\tau) d_{i,\sigma}^{(0)-1}(\tau - \tau') d_{i,\sigma}(\tau') + i \int_{\mathcal{C}} d\tau \sum_{\sigma=\uparrow,\downarrow} [t_{12}\bar{d}_{1,\sigma}d_{2,\sigma} + t_{12}^*d_{2,\sigma}\bar{d}_{1,\sigma}] \tag{A.81}$$

where $d_{i,\sigma}^{(0)}$ is the Keldysh function of the uncoupled quantum dot i with spin σ and is just d_0 from the resonant level model with $\Delta \rightarrow \Delta_i + h_i\sigma$ (see eq. (A.42)). The tunneling amplitudes γ_{12} describe hopping processes between the quantum dots. Tunneling between the leads and the quantum dots is described by the contribution

$$S_T = i \int_{\mathcal{C}} d\tau \sum_{m=R,L=\pm} \sum_{\substack{i=1,2 \\ \sigma=\uparrow,\downarrow}} \left[\gamma_{m,i} e^{im\lambda(\tau)/4} \bar{d}_{i,\sigma}(\tau) \psi_{m,\sigma}(\tau) + \gamma_{m,i}^* e^{-im\lambda(\tau)/4} \bar{\psi}_{m,\sigma}(\tau) d_{i,\sigma}(\tau) \right]. \quad (\text{A.82})$$

In fig. A.4, the double quantum dot setup is depicted. We allowed for magnetic fluxes Φ_L, Φ_R pen-

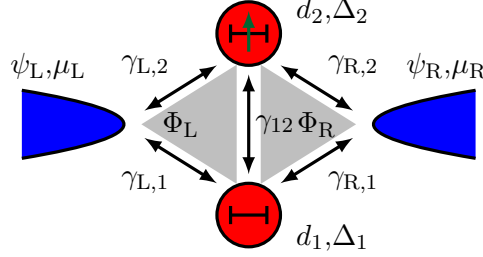


Figure A.4.: Sketch of the double quantum dot interferometer: the interferometer is penetrated by magnetic fluxes Φ_L and Φ_R .

etrating the interferometer. In case of non-vanishing γ_{12} , the model strongly depends on geometric details. We assume a symmetric system, i.e. $\Phi_L = \Phi_R = \Phi/2$. The effect of the magnetic flux can be accounted for by introducing Peierls phases (Peierls [1933]) into the tunneling couplings, i.e. $\gamma_{\alpha,i} \rightarrow \gamma_{\alpha,i} e^{i\phi_{\alpha,i}}$ where $\phi_{\alpha,i}$ is the phase a particle collects while moving from the lead α to the dot i . In the end, the result only depends on a single AB phase (Aharonov-Bohm phase), $\phi = 2\pi\Phi/\Phi_0$, where $\Phi_0 = h/e$ is the magnetic flux quantum and Φ to total magnetic flux penetrating the interferometer.

We integrate out the leads by using auxiliary fields,

$$\bar{\psi}_{m,\sigma}(\tau) = \bar{\eta}_{m,\sigma}(\tau) - i \sum_{i=1,2} \int_{\mathcal{C}} d\sigma \gamma_{m,i} e^{\frac{im\lambda(\sigma)}{4}} \bar{d}_{i,\sigma}(\sigma) g_{m,\sigma}(\sigma - \tau) \quad (\text{A.83})$$

$$\psi_{m,\sigma}(\tau) = \eta_{m,\sigma}(\tau) - i \sum_{i=1,2} \int_{\mathcal{C}} d\sigma g_{m,\sigma}(\tau - \sigma) \gamma_{m,i}^* e^{-\frac{im\lambda(\sigma)}{4}} d_{i,\sigma}(\sigma). \quad (\text{A.84})$$

This leads to an effective coupling of the two quantum dots. We introduce the Keldysh vectors in frequency space, $\vec{d}_{\sigma,\omega} = (d_{1,\sigma,-}, d_{1,\sigma,+}, d_{2,\sigma,-}, d_{2,\sigma,+})$ and $\vec{\bar{d}}_{\sigma,\omega} = (\bar{d}_{1,\sigma,-}, \bar{d}_{1,\sigma,+}, \bar{d}_{2,\sigma,-}, \bar{d}_{2,\sigma,+})$. For sake of clarity, we omit frequency labels at the single components of the vectors. Then, we obtain for the effective action,

$$S_{\text{QD,eff}} = \sum_{\omega} \sum_{\sigma=\uparrow,\downarrow} \vec{d}_{\sigma,\omega} \mathfrak{D}_{\sigma}^{-1}(\omega) \vec{\bar{d}}_{\sigma,\omega} \quad (\text{A.85})$$

where we have introduced the 4×4 matrix

$$\mathfrak{D}_{\sigma}^{-1}(\omega) = \begin{pmatrix} d_{1,\sigma}^{(0)-1}(\omega) - \sum_{m=L,R=\pm} \hat{\gamma}_{m,1} g_{m,\sigma}(\omega) \hat{\gamma}_{m,1}^* & i\gamma_{12}\sigma_3 - \sum_{m=L,R=\pm} \hat{\gamma}_{m,1} g_{m,\sigma}(\omega) \hat{\gamma}_{m,2}^* \\ i\gamma_{12}^*\sigma_3 - \sum_{m=L,R=\pm} \hat{\gamma}_{m,2} g_{m,\sigma}(\omega) \hat{\gamma}_{m,2}^* & d_{2,\sigma}^{(0)-1}(\omega) - \sum_{m=L,R=\pm} \hat{\gamma}_{m,2} g_{m,\sigma}(\omega) \hat{\gamma}_{m,2}^* \end{pmatrix}. \quad (\text{A.86})$$

This yields for the Keldysh partition function

$$\mathcal{Z}[\lambda] = \prod_{\omega} \det \mathfrak{D}_{\sigma}^{-1}(\omega) \quad (\text{A.87})$$

and therefore for the CGF,

$$\ln \chi(\lambda) = \ln \left(\frac{\mathcal{Z}[\lambda]}{\mathcal{Z}[\lambda=0]} \right) \quad (\text{A.88})$$

which has the Levitov-Lesovik form

$$\ln \chi(\lambda) = \mathcal{T} \int \frac{d\omega}{2\pi} \ln \left\{ 1 + T(\omega) \left[\left(e^{i\lambda} - 1 \right) n_L (1 - n_R) + \left(e^{-i\lambda} - 1 \right) n_R (1 - n_L) \right] \right\}. \quad (\text{A.89})$$

The transmission coefficient of the double quantum dot has the structure $T(\omega) = N(\omega)/D(\omega)$ where

$$\begin{aligned} N(\omega) &= 4\gamma_{12} (\Gamma_{R,1}\Gamma_{L,2} + \Gamma_{L,1}\Gamma_{R,2}) + 4\bar{\Gamma}_1 (\omega - \Delta_2)^2 + 4\bar{\Gamma}_2 (\omega - \Delta_1)^2 + 2\bar{\Gamma}^2 (\omega - \Delta_1) (\omega - \Delta_2) \\ &\quad + 8\gamma_{12}^2 \cos(\phi/2) \left[(\bar{\Gamma}_L\Gamma_{R,2} + \bar{\Gamma}_R\Gamma_{L,2}) (\omega - \Delta_1) + (\bar{\Gamma}_L\Gamma_{R,1} + \bar{\Gamma}_R\Gamma_{L,1}) (\omega - \Delta_2) \right] \\ &\quad + 8\gamma_{12}^2 \cos(\phi) \bar{\Gamma}^2 \end{aligned} \quad (\text{A.90})$$

and

$$\begin{aligned} D(\omega) &= 8\gamma_{12}^2 \Gamma_1 \Gamma_2 + 4 \left[\Gamma_1 (\omega - \Delta_1) + \Gamma_2 (\omega - \Delta_2) \right]^2 \\ &\quad + \left[\gamma_{12}^2 - (\omega - \Delta_1) (\omega - \Delta_2) \right]^2 - 2 (\Gamma_{L,1}\Gamma_{R,2} + \Gamma_{L,2}\Gamma_{R,1}) (\omega - \Delta_1) (\omega - \Delta_2) + 4\bar{\Gamma}^4 \\ &\quad + 2 (\bar{\Gamma}_1^4 + \bar{\Gamma}_2^4) + 4\gamma_{12}^2 \sqrt{\bar{\Gamma}^4} + 2 \cos(2\phi) \bar{\Gamma}^4 \\ &\quad + \cos(\phi) \left\{ 4\sqrt{\bar{\Gamma}^4} [(\omega - \Delta_1) (\omega - \Delta_2) - \Gamma_{L,1}\Gamma_{R,2} - \Gamma_{L,2}\Gamma_{R,1}] + 2\gamma_{12}^2 (\bar{\Gamma}_L^2 + \bar{\Gamma}_R^2) \right\} \\ &\quad + 8\gamma_{12} \cos(\phi/2) (\bar{\Gamma}_L + \bar{\Gamma}_R) [(\omega - \Delta_1) \Gamma_2 + (\omega - \Delta_2) \Gamma_1] \end{aligned} \quad (\text{A.91})$$

with the geometric means of the couplings $\bar{\Gamma} = \sqrt[4]{\Gamma_{L,1}\Gamma_{R,1}\Gamma_{L,2}\Gamma_{R,2}}$, $\bar{\Gamma}_{\alpha} = \sqrt{\Gamma_{\alpha,1}\Gamma_{\alpha,2}}$ ($\alpha = L, R$) and $\bar{\Gamma}_n = \sqrt{\Gamma_{L,n}\Gamma_{R,n}}$ ($n = 1, 2$) and the arithmetic means $\Gamma_1 = (\Gamma_{L,1} + \Gamma_{R,1})/2$ and $\Gamma_2 = (\Gamma_{L,2} + \Gamma_{R,2})/2$. A generic property of the double quantum dot system is the existence of distinct anti-resonances. Except for some artificial parameter constellations (height symmetry), there are real roots for ω (i.e. solutions of the equation $T(\omega) = 0$), where the transmission is exactly zero.

In fig. A.5, we depicted the transmission coefficient for a symmetrically tunneling coupled system, i.e. $\Gamma_{m,i} = \Gamma$ for $m = L, R$ and $i = 1, 2$ with no interdot coupling and for a zero AB phase. In case of $\Delta_1 = \Delta_2$ the transmission coefficient just resembles a Lorentzian line shape. But for arbitrary detuning from this situation, a very sharp anti-resonance establishes. The transmission coefficient for this kind of constellations simplifies to

$$T(\omega) = \frac{4\Gamma^2}{4\Gamma^2 + [1/(\omega - \Delta_1) + 1/(\omega - \Delta_2)]^{-2}}. \quad (\text{A.92})$$

In case of a symmetrically coupled setup (again all tunneling couplings are equal to Γ) with $\Delta_1 = \Delta_2 = \Delta$ interdot tunneling just leads to a shift of the transmission coefficient,

$$T(\omega) = \frac{16\Gamma^2}{16\Gamma^2 + (\omega - \Delta - \gamma_{12})^2}. \quad (\text{A.93})$$

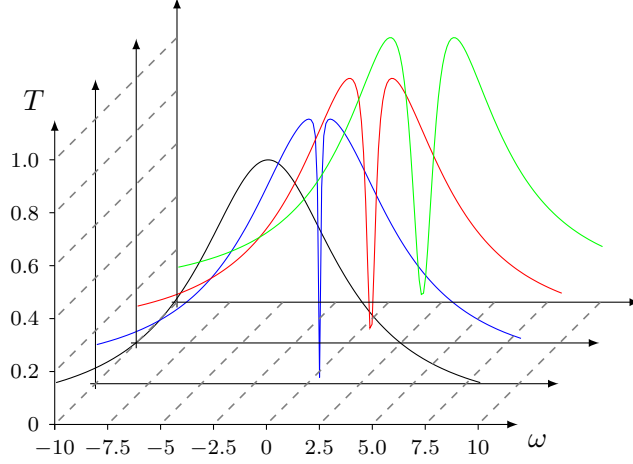


Figure A.5.: Transmission coefficient for the double quantum dot. The system is symmetric in the couplings, i.e. $\Gamma_{m,i} = \Gamma$ with $m = L, R$ and $i = 1, 2$. The interdot tunneling γ_{12} and the AB phase is set to zero. The dot level $\Delta_1/\Gamma = 0$ is fixed. The dot level of the second quantum dot is varied: $\Delta_2/\Gamma = 0, 1, 2, 3$ (black, blue, red, green).

To find a more interesting dependence on the interdot tunneling, we have to allow for an additional asymmetry. In fig. A.6, we depicted the effect of finite interdot tunneling coupling. We have chosen equal tunneling couplings to the leads and an asymmetry in the energy levels of the quantum dots, $\Delta_1 \neq \Delta_2$ and varied the interdot tunneling constant γ_{12} . The transmission coefficient in this case is

$$T(\omega) = \frac{4\Gamma^2}{4\Gamma^2 + [(\omega - \Delta_2)(\omega - \Delta_2) - \gamma_{12}^2]^2 / [(\omega - \Delta_1 + \gamma_{12}) + (\omega - \Delta_2 + \gamma_{12})]^2}. \quad (\text{A.94})$$

If we allow for a finite AB phase, we find for the transmission coefficient

$$T(\omega) = \frac{4\Gamma^2}{4\Gamma^2 + \left[\frac{(\omega - \Delta_1)(\omega - \Delta_2) - \gamma_{12}^2 + 2\Gamma^2(\cos(\phi) - 1)}{(\omega - \Delta_1 + \cos(\phi/2)) + (\omega - \Delta_2 + \cos(\phi/2))} \right]^2}. \quad (\text{A.95})$$

The oscillatory behaviour of similar interferometers, for example the effect of windings, was investigated in Maier [2008]. The Keldysh functions for the quantum dots in case of $\gamma_{m,i} = \gamma$, $\gamma_{12} = 0$, $\phi = 0$ and $\Delta_1 = -\Delta_2 = \Delta$,

$$\mathcal{D}_\lambda D_1^{--} = 2i\Gamma(\omega + \Delta)^2(n_L + n_R - 1) - (\omega - \Delta)(\omega + \Delta)^2 - 8\Gamma^2\omega(1 + \mathcal{F}_{\lambda+}) \quad (\text{A.96})$$

$$\mathcal{D}_\lambda D_1^{-+} = 2i\Gamma(\omega + \Delta)^2[(n_L + n_R)\cos(\lambda/2) + i(n_L - n_R)\sin(\lambda/2)] \quad (\text{A.97})$$

$$\mathcal{D}_\lambda D_1^{+-} = 2i\Gamma(\omega + \Delta)^2[(n_L + n_R - 2)\cos(\lambda/2) - i(n_L - n_R)\sin(\lambda/2)] \quad (\text{A.98})$$

$$\mathcal{D}_\lambda D_1^{++} = 2i\Gamma(\omega + \Delta)^2(n_L + n_R - 1) + (\omega - \Delta)(\omega + \Delta)^2 + 8\Gamma^2\omega(1 + \mathcal{F}_{\lambda+}). \quad (\text{A.99})$$

with

$$\mathcal{F}_{\lambda+} = (e^{i\lambda} - 1)n_L(1 - n_R) + (e^{-i\lambda} - 1)n_R(1 - n_L). \quad (\text{A.100})$$

and

$$\mathcal{D}_\lambda = (\Delta^2 - \omega^2)^2 + 16\Gamma^2\omega^2(1 + \mathcal{F}_{\lambda+}). \quad (\text{A.101})$$

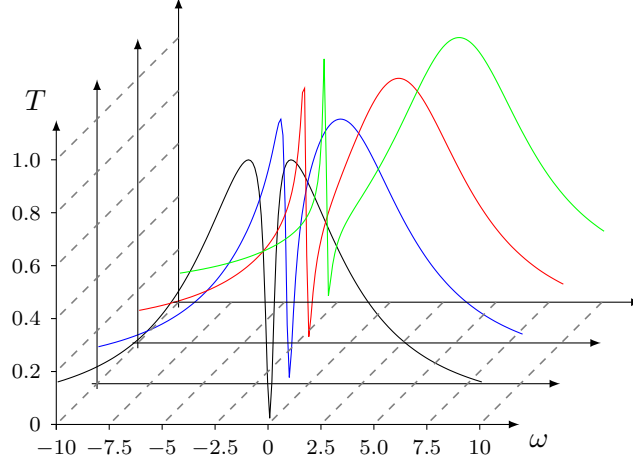


Figure A.6.: Transmission coefficient for the double quantum dot. The system is symmetric in the couplings, i.e. $\Gamma_{m,i} = \Gamma$ with $m = L, R$ and $i = 1, 2$. The dot level energies are $\Delta_1/\Gamma = -\Delta_2/\Gamma = 1$. The AB phase is set to zero. The interdot tunneling coupling is varied: $\gamma_{12}/\Gamma = 0, 1, 2, 3$ (black, blue, red, green curve).

The Keldysh function D_2 is obtained from D_1 by the replacement $\Delta \rightarrow -\Delta$. The mixed Keldysh function D_{12} is given by

$$\mathcal{D}_\lambda D_{12}^{--} = 2i\Gamma (\omega^2 - \Delta^2) (n_L + n_R - 1) + 8\Gamma^2 \omega (1 + \mathcal{F}_{\lambda+}) \quad (\text{A.102})$$

$$\mathcal{D}_\lambda D_{12}^{-+} = 2i\Gamma (\omega^2 - \Delta^2) [(n_L + n_R - 2) \cos(\lambda/2) - i(n_L - n_R) \sin(\lambda/2)] \quad (\text{A.103})$$

$$\mathcal{D}_\lambda D_{12}^{+-} = 2i\Gamma (\omega^2 - \Delta^2) [(n_L + n_R) \cos(\lambda/2) + i(n_L - n_R) \sin(\lambda/2)] \quad (\text{A.104})$$

$$\mathcal{D}_\lambda D_{12}^{++} = 2i\Gamma (\omega^2 - \Delta^2) (n_L + n_R - 1) - 8\Gamma^2 \omega (1 + \mathcal{F}_{\lambda+}) \quad (\text{A.105})$$

and the second mixed Keldysh function D_{21} is obtained from D_{12} via $\Delta \rightarrow -\Delta$.

B. BEC polaron: partition functions and Green's functions

B.1. Matsubara Green's functions for a harmonically confined particle

In this part of the appendix, Matsubara correlation functions used in the BEC polaron problem are provided. We start with a particle in an external potential $V(r)$. The Hamiltonian is given by,

$$H = \frac{p^2}{2} + V(r) \quad (\text{B.1})$$

where r and p are position and momentum operators. We set the mass of the particle $m = 1$ and assume the spatial dimension to be $d = 1$. As long as the potential is separable in the spatial components, i.e. $V(x) = V_1(x_1) + \dots + V_d(x_d)$, the generalization is obvious. Partition functions and correlation functions can best be obtained using path integrals. For example, the partition function is given by

$$\mathcal{Z} = \int_{r(0)=r(\beta)} \frac{\mathcal{D}r \mathcal{D}p}{2\pi} e^{-\int_0^\beta d\tau \left\{ \frac{p^2(\tau)}{2} - ip(\tau)\dot{x}(\tau) + V[x(\tau)] \right\}} \quad (\text{B.2})$$

where we have chosen a "symbolic" continuous representation. The integration with respect to the momentum variable p simply can be performed (canonical action \rightarrow Lagrangian action, see [Kleinert \[2009\]](#)),

$$\mathcal{Z} = C \int_{r(0)=r(\beta)} \mathcal{D}r e^{-\int_0^\beta d\tau \left\{ \frac{1}{2} \left(\frac{dr}{d\tau} \right)^2 + V[x(\tau)] \right\}} \quad (\text{B.3})$$

where C is a constant depending on the underlying Trotter decomposition, i.e. the number N of sampling points. In the limit $N \rightarrow \infty$, this constant tends to diverge. At the end, this is not a problem: C contains no dynamical information and \mathcal{Z} is only interesting compared to a reference system. For details, consult for example [Kleinert \[2009\]](#), [Negele and Orland \[1998\]](#). In the following, we omit the constant C in our notation. The external potential of our interest is harmonic,

$$V(r) = \frac{1}{2} \Omega^2 r^2. \quad (\text{B.4})$$

Next, we calculate the Green's function

$$G(\tau) = \langle r(\tau) r(0) \rangle \quad (\text{B.5})$$

where $0 < \tau < \beta$ and the expectation value is defined by

$$\langle \dots \rangle = \frac{1}{\mathcal{Z}} \int_{r(0)=r(\beta)} \mathcal{D}r \dots e^{-\int_0^\beta d\tau \left[\frac{1}{2} \left(\frac{dr}{d\tau} \right)^2 + \Omega r^2(\tau) \right]}. \quad (\text{B.6})$$

There are several methods to find $G(\tau)$, for example one can use the thermal Schwinger functional defined by the action,

$$S[\eta] = \int_0^\beta d\tau \frac{1}{2} \left[\left(\frac{dr}{d\tau} \right)^2 + \Omega^2 r^2(\tau) \right] - \int_0^\beta d\tau r(\tau) \eta(\tau), \quad (\text{B.7})$$

where $\eta(\tau)$ is a source field. It is not difficult to see that the Green's function is given as the symmetric Dirichlet Green's function of the differential operator

$$D = -\frac{d^2}{d\tau^2} + \Omega^2. \quad (\text{B.8})$$

One obtains

$$G(\tau) = \frac{1}{2\Omega} \frac{\cosh[\Omega(|\tau| - \beta/2)]}{\sinh(\Omega\beta/2)}. \quad (\text{B.9})$$

Another important correlation function appearing in the context of density-density correlation functions is defined by

$$\chi(k, k', \tau) = \left\langle e^{ikr(\tau)} e^{ik'r(0)} \right\rangle. \quad (\text{B.10})$$

Again, the calculation can be done easily using the thermal Schwinger functional. One just has to choose $\eta(\tau') = ik\delta(\tau' - \tau) + ik'\delta(\tau')$ as a source field, Finally

$$\chi(k, k', \tau) = e^{\frac{1}{2} \int d\tau' d\tau'' \eta(\tau') G(\tau' - \tau'') \eta(\tau'')} = e^{-(k^2 + k'^2)G(0)/2 + kk'G(\tau)} \quad (\text{B.11})$$

is obtained.

B.2. Variational principle: partition function and Matsubara Green's functions

In this section, we provide the partition function and Matsubara Green's function for the trial model defined by the action (see eq. 3.95),

$$S_0 = \int d\tau \left[\frac{\mathbf{r}^2}{2} + \frac{\Omega \mathbf{r}^2}{2} \right] + \frac{MW^3}{8} \int d\tau d\tau' \frac{\cosh[W(|\tau - \tau'|) - \beta/2]}{\sinh(W\beta/2)} [\mathbf{r}(\tau) - \mathbf{r}(\tau')]^2. \quad (\text{B.12})$$

Despite of the retardation, the action S_0 is diagonal in Fourier space,

$$S_0 = \frac{1}{2\beta} \sum_n r_n \bar{r}_n \left(\omega_n^2 + \Omega^2 + MW^2 - \frac{MW^4}{W^2 + \omega_n^2} \right) \quad (\text{B.13})$$

where $\omega_n = 2\pi n/\beta$. Then, the partition function \mathcal{Z}_0 can be obtained by

$$\mathcal{Z}_0 = C \frac{\sqrt{2\beta\pi}}{\Omega} \prod_{n>0} \frac{\pi\beta}{\omega_n^2 + \Omega^2 + MW^2 - \frac{MW^4}{W^2 + \omega_n^2}}. \quad (\text{B.14})$$

Choosing the free particle as a reference system, the constant C can be determined,

$$C = \frac{1}{\sqrt{2\pi\beta^3}} \prod_{n>0} \frac{\omega_n^2}{\pi\beta}. \quad (\text{B.15})$$

The partition function then is

$$\mathcal{Z}_0 = \frac{1}{2} \frac{\sinh(W\beta/2)}{\sinh(F_+\beta/2) \sinh(F_-\beta/2)} \quad (\text{B.16})$$

with

$$F_{\pm} = \sqrt{\frac{\Omega^2 + \tilde{\Omega}^2}{2} \pm \frac{\sqrt{(\Omega^2 + \tilde{\Omega}^2)^2 - 4W^2\Omega^2}}{2}} \quad (\text{B.17})$$

where $\tilde{\Omega}$ is defined as $\tilde{\Omega} = W\sqrt{M+1}$. The Matsubara Green's function $\tilde{G}(\tau) = \langle r(\tau) r(0) \rangle_0$ is given by

$$\tilde{G}(\tau) = \frac{1}{\beta} \sum_n \frac{e^{i\omega_n \tau}}{\omega_n^2 + \Omega^2 + MW^2 - \frac{MW^4}{W^2 + \omega_n^2}} \quad (\text{B.18})$$

which is

$$\tilde{G}(\tau) = \frac{1}{2\sqrt{(\Omega^2 + \tilde{\Omega}^2)^2 - 4W^2\Omega^2}} \sum_{\pm} \frac{\pm(F_{\pm}^2 - W^2)}{F_{\pm}} \frac{\cosh[F_{\pm}(|\tau| - \beta/2)]}{\sinh(F_{\pm}\beta/2)}. \quad (\text{B.19})$$

In the limit $\tau \rightarrow 0$, $\tilde{G}(\tau)$ can be defined as polaron radius squared.

Bibliography

- S. Albeverio, R. Höegh-Krohn, and S. Mazzucchi. *Mathematical theory of Feynman path integrals: an introduction*. Lecture notes in mathematics. Springer, 2008.
- M. H. Anderson, J. R. Ensher, M. R. Matthews, C. E. Wieman, and E. A. Cornell. Observation of Bose-Einstein Condensation in a Dilute Atomic Vapor. *Science*, 269(5221):198, 1995.
- P. W. Anderson. Localized Magnetic States in Metals. *Phys. Rev.*, 124(1):41, 1961.
- R. Avriller. Unified description of charge transfer mechanisms and vibronic dynamics in nanoscale junctions . *J. Phys. Cond. Mat.*, 23(10):105301, 2011.
- R. Avriller and A. Levy Yeyati. Electron-phonon interaction and full counting statistics in molecular junctions. *Phys. Rev. B*, 80(4):041309, 2009.
- G. A. Baker. *Essentials of Padé Approximants*. Academic Press, 1975.
- M. Bertero, C. Del Mol, and E. R. Pike. Linear inverse problems with discrete data. I. General formulation and singular system analysis. *Inv. Probl.*, 1:301, 1985.
- I. Bloch, J. Dalibard, and W. Zwerger. Many-body physics with ultracold gases. *Rev. Mod. Phys.*, 80(3):885, 2008.
- M. Bockrath, D. H. Cobden, J. Lu, A. G. Rinzler, R. E. Smalley, L. Balents, and P. L. McEuen. Luttinger-liquid behaviour in carbon nanotubes. *Nature*, 397:598, 1999.
- C. C. Bradley, C. A. Sackett, and R. G. Hulet. Bose-Einstein Condensation of Lithium: Observation of Limited Condensate Number. *Phys. Rev. Lett.*, 78(6):985, 1997.
- S. Braig and K. Flensberg. Vibrational sidebands and dissipative tunneling in molecular transistors. *Phys. Rev. B*, 68(20):205324, 2003.
- B. Bremaud. *Markov Chains: Gibbs Fields, Monte Carlo Simulation, and Queues*. Springer, Berlin, 2001.
- D. Breyel. Diploma thesis: Eigenschaften des Ladungstransportes in parallelen Doppelquantenpunkten und dem SU(4)-Kondo Problem. Heidelberg University, 2010.
- C. Bruder, R. Fazio, and H. Schoeller. Aharonov-Bohm Oscillations and Resonant Tunneling in Strongly Correlated Quantum Dots. *Phys. Rev. Lett.*, 76(1):114, 1996.
- A. Brunello, F. Dalfovo, L. Pitaevskii, S. Stringari, and F. Zambelli. Momentum transferred to

- a trapped Bose-Einstein condensate by stimulated light scattering. *Phys. Rev. A*, 64(6):063614, 2001.
- M. Büttiker, Y. Imry, and M. Ya. Azbel. Quantum oscillations in one-dimensional normal-metal rings. *Phys. Rev. A*, 30(4):1982, 1984.
- P. A. Čerenkov. Visible emission of clean liquids by action of v-radiation. *Doklady Akad. Nauk. SSSR*, 2:451, 1934.
- P. A. Čerenkov. Visible Radiation Produced by Electrons Moving in a Medium with Velocities Exceeding that of Light. *Phys. Rev.*, 52(4):378, 1937.
- D. M. Ceperley. Path integrals in the theory of condensed helium. *Rev. Mod. Phys.*, 67(2):279, 1995.
- C. Chin, R. Grimm, P. Julienne, and E. Tiesinga. Feshbach resonances in ultracold gases. *Rev. Mod. Phys.*, 82(2):1225, 2010.
- R. A. Craig. Perturbation Expansion for Real-Time Green's Functions. *J. Math. Phys.*, 9(4):605, 1968.
- C. E. Creffield, E. G. Klepfish, E. R. Pike, and S. Sarkar. Spectral Weight Function for the Half-Filled Hubbard Model: A Singular Value Decomposition Approach. *Phys. Rev. Lett.*, 75:517, 1995.
- S. M. Cronenwett, T. H. Oosterkamp, and L. P. Kouwenhoven. A Tunable Kondo Effect in Quantum Dots. *Science*, 281:540, 1998.
- F. M. Cucchietti and E. Timmermans. Strong-Coupling Polarons in Dilute Gas Bose-Einstein Condensates. *Phys. Rev. Lett.*, 96(21):210401, 2006.
- J. P. Dahlhaus. Diploma thesis: Interaction effects in the charge transfer statistics of double quantum dot nanostructures. Heidelberg University, 2009.
- J. P. Dahlhaus, S. Maier, and A. Komnik. Spin-polarized current generation and detection by a double quantum dot structure. *Phys. Rev. B*, 81(7):075110, 2010.
- F. Dalfovo, S. Giorgini, L. P. Pitaevskii, and S. Stringari. Theory of Bose-Einstein condensation in trapped gases. *Rev. Mod. Phys.*, 71(3):463, 1999.
- K. B. Davis, M. O. Mewes, M. R. Andrews, N. J. van Druten, D. S. Durfee, D. M. Kurn, and W. Ketterle. Bose-Einstein Condensation in a Gas of Sodium Atoms. *Phys. Rev. Lett.*, 75(22):3969, 1995.
- L. de la Vega, A. Martín-Rodero, N. Agraït, and A. Levy Yeyati. Universal features of electron-phonon interactions in atomic wires. *Phys. Rev. B*, 73(7):075428, 2006.
- R. de Picciotto, M. Reznikov, M. Heiblum, V. Umansky, G. Bunin, and D. Mahalu. Direct observation of a fractional charge. *Nature*, 389:162, 1997.

- D. Djukic, K. S. Thygesen, C. Untiedt, R. H. M. Smit, K. W. Jacobsen, and J. M. van Ruitenbeek. Stretching dependence of the vibration modes of a single-molecule Pt-H₂-Pt bridge. *Phys. Rev. B*, 71(16):161402, 2005.
- B. Dong, H. Y. Fan, X. L. Lei, and N. J. M. Horing. Counting statistics of tunneling through a single molecule: Effect of distortion and displacement of vibrational potential surface. *J. Appl. Phys.*, 105(11):113702, 2009.
- B. Doyon and N. Andrei. Universal aspects of nonequilibrium currents in a quantum dot. *Phys. Rev. B*, 73(24):245326, 2006.
- R. Egger and A. O. Gogolin. Effective Low-Energy Theory for Correlated Carbon Nanotubes. *Phys. Rev. Lett.*, 79(25):5082, 1997.
- R. Egger and A. O. Gogolin. Vibration-induced correction to the current through a single molecule. *Phys. Rev. B*, 77(11):113405, 2008.
- V. J. Emery and S. Kivelson. Mapping of the two-channel Kondo problem to a resonant-level model. *Phys. Rev. B*, 46(17):10812, 1992.
- T. Erber and S. Putterman. Randomness in quantum mechanics—nature’s ultimate cryptogram? *Nature*, 318(6041):41, 1985.
- B. D. Esry, C. H. Greene, J. P. Burke, Jr., and J. L. Bohn. Hartree-Fock Theory for Double Condensates. *Phys. Rev. Lett.*, 78(19):3594, 1997.
- M. Fabrizio and A. O. Gogolin. Interacting one-dimensional electron gas with open boundaries. *Phys. Rev. B*, 51(24):17827, 1995.
- H. Fehske, G. Wellein, J. Loos, and A. R. Bishop. Localized polarons and doorway vibrons in finite quantum structures. *Phys. Rev. B*, 77(8):085117, 2008.
- R. P. Feynman. Slow Electrons in a Polar Crystal. *Phys. Rev.*, 97(3):660, 1955.
- R. P. Feynman. There’s plenty of room at the bottom. *J. Microelectromech. Syst.*, 1(1):60, 1992.
- K. Flensberg. Tunneling broadening of vibrational sidebands in molecular transistors. *Phys. Rev. B*, 68(20):205323, 2003.
- W. M. C. Foulkes, L. Mitas, R. J. Needs, and G. Rajagopal. Quantum Monte Carlo simulations of solids. *Rev. Mod. Phys.*, 73(1):33, 2001.
- R. W. Freund and R. H. Hoppe. *Stoer/Bulirsch: Numerische Mathematik 1*. Springer Berlin, 2007.
- H. Fröhlich. Electrons in lattice fields. *Adv. Phys.*, 3(11):325, 1954.
- A. Furusaki. Resonant tunneling through a quantum dot weakly coupled to quantum wires or quantum Hall edge states. *Phys. Rev. B*, 57(12):7141, 1998.

- A. Furusaki and N. Nagaosa. Single-barrier problem and Anderson localization in a one-dimensional interacting electron system. *Phys. Rev. B*, 47(8):4631, 1993.
- R. M. Fye. New results on Trotter-like approximations. *Phys. Rev. B*, 33(9):6271, 1986.
- M. Gacesa, P. Pellegrini, and R. Côté. Feshbach resonances in ultracold $^6,7\text{Li}+^{23}\text{Na}$ atomic mixtures. *Phys. Rev. A*, 78(1):010701, 2008.
- M. Galperin, A. Nitzan, and M. A. Ratner. Inelastic tunneling effects on noise properties of molecular junctions. *Phys. Rev. B*, 74(7):075326, 2006.
- J. E. Gentle. *Random Number Generation and Monte Carlo Methods*. Springer New York, 2010.
- A. O. Gogolin and A. Komnik. Towards full counting statistics for the Anderson impurity model. *Phys. Rev. B*, 73:195301, 2006.
- A. O. Gogolin, A. A. Nersesyan, and A. M. Tsvelik. *Bosonization and Strongly Correlated Systems*. Cambridge University Press, Cambridge, 1998.
- D. Goldhaber-Gordon, H. Shtrikman, D. Mahalu, D. Abusch-Magder, U. Meirav, and M. A. Kastner. Kondo effect in a single-electron transistor. *Nature*, 391:156, 1998.
- H. Haug and A. Jauho. *Quantum Kinetics in Transport and Optics of Semiconductors*. Springer Berlin / Heidelberg, 2008.
- F. Haupt, T. Novotný, and W. Belzig. Phonon-Assisted Current Noise in Molecular Junctions. *Phys. Rev. Lett.*, 103(13):136601, 2009.
- T. Hecht, A. Weichselbaum, Y. Oreg, and J. von Delft. Interplay of mesoscopic and Kondo effects for transmission amplitude of few-level quantum dots. *Phys. Rev. B*, 80(11):115330, 2009.
- Tin-Lun Ho and V. B. Shenoy. Binary Mixtures of Bose Condensates of Alkali Atoms. *Phys. Rev. Lett.*, 77(16):3276, 1996.
- A. W. Holleitner, C. R. Decker, H. Qin, K. Eberl, and R. H. Blick. Coherent Coupling of Two Quantum Dots Embedded in an Aharonov-Bohm Interferometer. *Phys. Rev. Lett.*, 87(25):256802, 2001.
- T. Holstein. Studies of polaron motion : Part I. The molecular-crystal model. *Ann. Phys.*, 8(3):325, 1959.
- B. Horvatić and V. Zlatić. Perturbation Expansion for the Asymmetric Anderson Hamiltonian. *Phys. stat. sol.*, 99:251, 1980.
- M. Jarrell and J. E. Gubernatis. Bayesian inference and the analytic continuation of imaginary-time quantum Monte Carlo data. *Phys. Rep.*, 269:133, 1996.
- J. Jensen. Sur les fonctions convexes et les inégalités entre les valeurs moyennes. *Acta Math.*, 30:175, 1906.

- G. W. Johnson and M. L. Lapidus. *The Feynman integral and Feynman's operational calculus*. Oxford Mathematical Monographs. Oxford University Press, 2002.
- L. P. Kadanoff and G. Baym. *Quantum statistical mechanics*. Benjamin, 1962.
- A. Kamenev and A. Levchenko. Keldysh technique and non-linear σ -model: basic principles and applications. *Adv. Phys.*, 58(3):197, 2009.
- C. Kane, L. Balents, and M. Fisher. Coulomb Interactions and Mesoscopic Effects in Carbon Nanotubes. *Phys. Rev. B*, 79(25):5086, 1997.
- C. L. Kane and Matthew P. A. Fisher. Transmission through barriers and resonant tunneling in an interacting one-dimensional electron gas. *Phys. Rev. B*, 46(23):15233, 1992.
- D. Kast, D. Kecke, and J. Ankerhold. Charge transfer through single molecule contacts: How reliable are rate descriptions? *Beilstein J. Nanotechnol.*, 2:416, 2011.
- L. Keldysh. Ionization in the Field of a Strong Electromagnetic Wave. *JETP Lett.*, 20:1018, 1965.
- H. Kleinert. *Path integrals in quantum mechanics, statistics, polymer physics, and financial markets*. World Scientific, 2009.
- R. G. Knobel and N. C. Andrew. Nanometre-scale displacement sensing using a single electron transistor. *Nature*, 424:291, 2003.
- J. Koch and J. von Oppen. Franck-Condon Blockade and Giant Fano Factors in Transport through Single Molecules. *Phys. Rev. Lett.*, 94(5):206804, 2005.
- W. Koller, A. C. Hewson, and D. M. Edwards. Polaronic Quasiparticles in a Strongly Correlated Electron Band. *Phys. Rev. Lett.*, 95(25):256401, 2005.
- A. Komnik and A. O. Gogolin. Transport, optical properties, and quantum ratchet effects for quantum dots and molecules coupled to Luttinger liquids. *Phys. Rev. B*, 68(23):235323, 2003a.
- A. Komnik and A. O. Gogolin. Resonant Tunneling between Luttinger Liquids: A Solvable Case. *Phys. Rev. Lett.*, 90(24):246403, 2003b.
- B. Kubala and J. König. Aharonov-Bohm interferometry with quantum dots: scattering approach versus tunneling picture. *Phys. Rev. B*, 67(20):205303, 2003.
- D. P. Landau and K. Binder. *A Guide to Monte Carlo Simulations in Statistical physics*. Cambridge University Press, 2005.
- I.G. Lang and Y. A. Firsov. Kinetic Theory of Semiconductors with low mobility. *Sov. Phys. JETP*, 16:1301, 1963.
- A. J. Leggett. *Quantum Liquids: Bose Condensation and Cooper Pairing in Condensed-Matter Systems*. Oxford University Press, 2006.

- R. Leturcq, C. Stampfer, K. Inderbitzin, L. Durrer, C. Hierold, E. Mariani, M. G. Schultz, F. von Oppen, and K. Ensslin. Franck-Condon blockade in suspended carbon nanotube quantum dots. *Nature*, 5:327, 2009.
- L. S. Levitov and G. B. Lesovik. Quantum Measurement in Electric Circuit. *JETP Lett.*, 58:230, 1993.
- L. S. Levitov and A. V. Shytov. *Green's functions. Theory and practice*. FizMatLit-Nauka, 2002.
- L. S. Levitov, G. B. Lesovik, and H. W. Lee. Electron counting statistics and coherent states of electric current. *J. Math. Phys.*, 37:4845, 1996.
- A.W.W. Ludwig and I. Affleck. Exact conformal-field-theory results on the multi-channel Kondo effect: Asymptotic three-dimensional space- and time-dependent multi-point and many-particle Green's functions. *Nucl. Phys. B*, 428(3):545, 1994.
- G.D. Mahan. *Many-Particle Physics*. Springer New York, 2000.
- S. Maier. Diploma thesis: Korrelationseffekte in der Ladungstransferstatistik von Nanostrukturen. Freiburg University, 2008.
- S. Maier and A. Komnik. A quantum Monte Carlo approach to the BEC polaron problem. *in preparation*.
- S. Maier and A. Komnik. Transport properties of a molecular quantum dot coupled to one-dimensional correlated electrons. *Phys. Rev. B*, 82(16):165116, 2010.
- S. Maier, T. L. Schmidt, and A. Komnik. Charge transfer statistics of a molecular quantum dot with strong electron-phonon interaction. *Phys. Rev. B*, 83(8):085401, 2011.
- E. Mariani and F. von Oppen. Electron-vibron coupling in suspended carbon nanotube quantum dots. *Phys. Rev. B*, 80(15):155411, 2009.
- A. J. Martino and G. M. Morris. Optical random number generator based on photoevent locations. *Appl. Opt.*, 30(8):981, 1991.
- M. Matsumoto and T. Nishimura. Mersenne twister: a 623-dimensionally equidistributed uniform pseudo-random number generator. *ACM Trans. Model. Comput. Simul.*, 8:3, 1998.
- V. Meden and F. Marquardt. Correlation-Induced Resonances in Transport through Coupled Quantum Dots. *Phys. Rev. Lett.*, 96(14):146801, 2006.
- Y Meir and N. S. Wingreen. Landauer formula for the current through an interacting electron region. *Phys. Rev. Lett.*, 68(16):2512, 1992.
- N. Metropolis, A. W. Rosenbluth, M. N. Rosenbluth, A. H. Teller, and E. Teller. Equation of State Calculations by Fast Computing Machines. *J. Chem. Phys.*, 21(6):1087, 1953.
- D. Meyer, A. C. Hewson, and R. Bulla. Gap Formation and Soft Phonon Mode in the Holstein Model. *Phys. Rev. Lett.*, 89(19):196401, 2002.

- A. B. Migdal. Interaction between electrons and lattice vibrations in normal metal. *Sov. Phys. JETP*, 34(7):996, 1958.
- T. Mii, S. G. Tikhodeev, and H. Ueba. Spectral features of inelastic electron transport via a localized state. *Phys. Rev. B*, 68(20):205406, 2003.
- A. Mitra, I. Aleiner, and A. J. Millis. Phonon effects in molecular transistors: Quantal and classical treatment. *Phys. Rev. B*, 69(24):245302, 2004.
- K. Mølmer. Bose Condensates and Fermi Gases at Zero Temperature. *Phys. Rev. Lett.*, 80(9):1804, 1998.
- O. Morsch and M. Oberthaler. Dynamics of Bose-Einstein condensates in optical lattices. *Rev. Mod. Phys.*, 78(1):179, 2006.
- L. Mühlbacher and E. Rabani. Real-Time Path Integral Approach to Nonequilibrium Many-Body Quantum Systems. *Phys. Rev. Lett.*, 100(17):176403, 2008.
- C. J. Myatt, E. A. Burt, R. W. Ghrist, E. A. Cornell, and C. E. Wieman. Production of Two Overlapping Bose-Einstein Condensates by Sympathetic Cooling. *Phys. Rev. Lett.*, 78(4):586, 1997.
- C. Nayak, M. P. A. Fisher, A. W. W. Ludwig, and H. H. Lin. Resonant multilead point-contact tunneling. *Phys. Rev. B*, 59(24):15694, 1999.
- Yu. V. Nazarov. Universalities of weak localization. *Ann. Phys.*, Spec. Issue:193, 1999.
- Yu. V. Nazarov and L. I. Glazman. Resonant Tunneling of Interacting Electrons in a One-Dimensional Wire. *Phys. Rev. Lett.*, 91(12):126804, 2003.
- Yu. V. Nazarov and M. Kindermann. Full counting statistics of a general quantum mechanical variable. *Eur. J. Phys. B*, 35:413, 2003.
- J. W. Negele and H. Orland. *Quantum many-particle systems*. Perseus Books, 1998.
- A. Novikov and M. Ovchinnikov. Variational approach to the ground state of an impurity in a Bose-Einstein condensate. *J. Phys. B*, 43(10):105301, 2010.
- A. Oguri. Fermi-liquid theory for the Anderson model out of equilibrium. *Phys. Rev. B*, 64:153305, 2001.
- S. H. Pan, J. P. O'Neal, R. L. Badzey, C. Chamon, H. Ding, J. R. Engelbrecht, Z. Wang, H. Eisaki, S. Uchida, A. K. Gupta, K.-W. Ng, E. W. Hudson, K. M. Lang, and J. C. Davis. Microscopic electronic inhomogeneity in the high-Tc superconductor $\text{Bi}_2\text{Sr}_2\text{CaCu}_2\text{O}_{8+x}$. *Nature*, 413(6853):282, 2001.
- T. Pang. *An Introduction to Computational Physics*. Cambridge University Press, 2006.
- H. Park, J. Park, A. K. L. Lim, E. H. Anderson, A. P. Alivisatos, and P. L. McEuen. Nanomechanical oscillations in a single- C_{60} transistor. *Nature*, 407:57, 2000.

- J. Park, A. N. Pasupathy, J. I. Goldsmith, C. Chang, Y. Yaish, J. R. Petta, M. Rinkoski, J. P. Sethna, H. D. Abruna, P. L. McEuen, and D. C. Ralph. Coulomb blockade and the Kondo effect in single-atom transistors. *Nature*, 417:722, 2002.
- M. Paulsson, T. Frederiksen, and M. Brandbyge. Modeling inelastic phonon scattering in atomic- and molecular-wire junctions. *Phys. Rev. B*, 72(20):201101, 2005.
- R. Peierls. Zur Theorie des Diamagnetismus von Leitungselektronen. *Z. Phys. A*, 80:763, 1933.
- C. J. Pethick and H. Smith. *Bose-Einstein Condensation in Dilute Gases*. Cambridge University Press, 2008.
- L. P. Pitaevskii and S. Stringari. *Bose-Einstein Condensation*. Oxford University Press, 2003.
- D. G. Polyakov and I. V. Gornyi. Transport of interacting electrons through a double barrier in quantum wires. *Phys. Rev. B*, 68(3):035421, 2003.
- W. H. Press, S. A. Teukolsky, W. T. Vetterling, and B. P. Flannery. *Numerical Recipes 3rd Edition: The Art of Scientific Computing*. Cambridge University Press, 2007.
- X. H. Qiu, G. V. Nazin, and W. Ho. Vibronic States in Single Molecule Electron Transport. *Phys. Rev. Lett.*, 92(20):206102, 2004.
- J. Rammer. *Quantum Field Theory of Non-equilibrium States*. Cambridge University Press, 2007.
- M. Ren, E. Wu, Y. Liang, Y. Jian, G. Wu, and H. Zeng. Quantum random-number generator based on a photon-number-resolving detector. *Phys. Rev. A*, 83(2):023820, 2011.
- R. Riwar and T. L. Schmidt. Transient dynamics of a molecular quantum dot with a vibrational degree of freedom. *Phys. Rev. B*, 80(12):125109, 2009.
- K. Sacha and E. Timmermans. Self-localized impurities embedded in a one-dimensional Bose-Einstein condensate and their quantum fluctuations. *Phys. Rev. A*, 73(6):063604, 2006.
- L. Saminadayar, D. C. Glattli, Y. Jin, and B. Etienne. Observation of the $e/3$ Fractionally Charged Laughlin Quasiparticle. *Phys. Rev. Lett.*, 79:2526, 1997.
- C. Samuelis, E. Tiesinga, T. Laue, M. Elbs, H. Knöckel, and E. Tiemann. Cold atomic collisions studied by molecular spectroscopy. *Phys. Rev. A*, 63(1):012710, 2000.
- A. Schiller and S. Hershfield. Toulouse limit for the nonequilibrium Kondo impurity: Currents, noise spectra, and magnetic properties. *Phys. Rev. B*, 58(22):14978, 1998.
- J. Schmid, J. Weis, K. Eberl, and K. von Klitzing. A Quantum Dot in the Limit of Strong Coupling to Reservoirs. *Physica B*, 256:182, 1998.
- T. L. Schmidt and A. Komnik. Charge transfer statistics of a molecular quantum dot with a vibrational degree of freedom. *Phys. Rev. B*, 80(4):041307, 2009.

- F. Schreck, L. Khaykovich, K. L. Corwin, G. Ferrari, T. Bourdel, J. Cubizolles, and C. Salomon. Quasipure Bose-Einstein Condensate Immersed in a Fermi Sea. *Phys. Rev. Lett.*, 87(8):080403, 2001.
- T. Schuster, R. Scelle, and M. K. Oberthaler. Private communications.
- J. Schwinger. Brownian Motion of a Quantum Oscillator. *J. Math. Phys.*, 2(3):407, 1961.
- R. H. M. Smit, Y. Noat, C. Untiedt, N. D. Lang, M. C. van Hemert, and J. M. van Ruitenbeek. Measurement of the conductance of a hydrogen molecule. *Nature*, 419:906, 2002.
- W. Sollfrey and H. T. Yura. Čerenkov Radiation from Charged Particles in a Plasma in a Magnetic Field. *Phys. Rev.*, 139(1A):A48, 1965.
- B. C. Stipe, M. A. Rezaei, and W. Ho. Single-Molecule Vibrational Spectroscopy and Microscopy. *Science*, 280:1732, 1998.
- H. T. C. Stoof, D. B. M. Dickerscheid, and K. Gubbels. *Ultracold Quantum Fields*. Springer Science+Business Media B.V., 2009.
- M. Tahir and A. MacKinnon. Current noise of a resonant tunnel junction coupled to a nanomechanical oscillator. *e-print arXiv: 1005.3713*, 2010.
- S. Takei, Y-B Kim, and A. Mitra. Enhanced Fano factor in a molecular transistor coupled to phonons and Luttinger-liquid leads. *Phys. Rev. B*, 72(7):075337, 2005.
- J. Tempere, W. Casteels, M. K. Oberthaler, S. Knoop, E. Timmermans, and J. T. Devreese. Feynman path-integral treatment of the BEC-impurity polaron. *Phys. Rev. B*, 80(18):184504, 2009.
- E. Timmermans and R. Côté. Superfluidity in Sympathetic Cooling with Atomic Bose-Einstein Condensates. *Phys. Rev. Lett.*, 80(16):3419, 1998.
- A. G. Truscott, K. E. Strecker, W. I. McAlexander, G. B. Partridge, and R. G. Hulet. Observation of Fermi Pressure in a Gas of Trapped Atoms. *Science*, 291(5513):2570, 2001.
- H. J. Vidberg and J. W. Serene. Solving the Eliashberg Equations by Means of N-Point Padé Approximants. *J. Low. Temp. Phys.*, 29:179, 1977.
- J. von Delft and H. Schoeller. Bosonization for beginners & refermionization for experts. *Ann. Phys.*, 7(4):225, 1998.
- G.N. Watson. *A Treatise on the Theory of Bessel Functions*. Cambridge University Press, 1996.
- U. Weiss, R. Egger, and M. Sasseti. Low-temperature nonequilibrium transport in a Luttinger liquid. *Phys. Rev. B*, 52(23):16707, 1995.
- V. Weisskopf and E. Wigner. Berechnung der natürlichen Linienbreite auf Grund der Diracschen Lichttheorie. *Z. Phys. A*, 63:54, 1930.

- U. Wilhelm, J. Schmid, J. Weis, and K. von Klitzing. Experimental evidence for spinless Kondo effect in two electrostatically coupled quantum dot systems. *Physica E*, 14(4):385, 2002.
- K. Yamada. Perturbation Expansion for the Anderson Hamiltonian. IV. *Prog. Theor. Phys.*, 54:316, 1975a.
- K. Yamada. Perturbation Expansion for the Anderson Hamiltonian. II. *Prog. Theor. Phys.*, 53:970, 1975b.
- Z. Yao, H. W. Ch. Postma, L. Balents, and C. Dekker. Carbon nanotube intramolecular junctions. *Nature*, 402:273, 1999.
- K. Yosida and K. Yamada. Perturbation Expansion for the Anderson Hamiltonian. *Prog. Theor. Phys. Supp.*, 46:244, 1970.
- K. Yosida and K. Yamada. Perturbation Expansion for the Anderson Hamiltonian. III. *Prog. Theor. Phys.*, 53:1286, 1975.
- L. H. Yu and D. Natelson. Kondo physics in C₆₀ Single-Molecule Transistors. *Nano Lett.*, 4:79, 2004.
- L. H. Yu, Z. K. Keane, J. W. Ciszek, L. Cheng, M. P. Stewart, J. M. Tour, and D. Natelson. Inelastic Electron Tunneling via Molecular Vibrations in Single-Molecule Transistors. *Phys. Rev. Lett.*, 93(26):266802, 2004.
- V. Zlatić and B. Horvatić. Series expansion for the symmetric Anderson Hamiltonian. *Phys. Rev. B*, 28(12):6904, 1983.

Curriculum Vitae

Personal Information

| | |
|----------------|--------------|
| Name | Stefan Maier |
| Date of birth | 06/05/1981 |
| Place of birth | Rheinfelden |
| Citizenship | german |
| Marital status | single |

School Education

| | |
|-----------|----------------------------|
| 1988-1992 | Primary school, Maulburg |
| 1992-1998 | Secondary school, Maulburg |
| 1998-2001 | Gymnasium, Lörrach |
| 06/2001 | Abitur |

Military Service

| | |
|-------------------|---------------------------------|
| 07/2001 - 10/2001 | Stetten a.k.M. (basic training) |
| 10/2001 - 03/2002 | Sigmaringen |

Academic Studies

| | |
|-------------------|---------------------------------------|
| 10/2002 - 08/2008 | Freiburg University, major in physics |
| 11/2004 | Vordiplom, major in physics |
| 07/2008 | Diplom, major in physics |

Graduate School

| | |
|---------------|--|
| since 09/2008 | PhD student at the Intitute for Theoretical Physics in Heidelberg Supervisor: Prof. Andreas Komnik |
|---------------|--|

October 20, 2011

Acknowledgement

When man would seek his destiny,
Man's help must then be given;
Save for the whole, ne'er labors he,—
Of many drops is formed the sea,—
By water mills are driven;

(J. C. F. von Schiller, The Philosophers)

During the last years I was happy to constantly receive support by my family, friends and colleagues.

I am much obliged to my supervisor Prof. Andreas Komnik for giving me the opportunity of writing my thesis in his research group, for encouraging and challenging me in my research and for sharing his deep insights into the puzzling world of physics with me. I would like to show my sincere gratitude to Prof. Manfred Salmhofer and Dr. Boris Fine for being my co-advisors.

I am particularly grateful for the unique work atmosphere created by countless friends and coworkers at the institute. Special thanks to my friends and colleagues Henning Soller, Kay Uwe Giering, David Breyel and Karsten Joho for many inspiring discussions, the countless amusing moments at the villa and the support I was happy to receive from them.

I am deeply indebted to Julia Zabel and Hans Fritz for their kind and deep friendship, moral support and for being everlasting sources of inspiration.

Deepest gratitude I owe to my sister, my brothers and my parents for their trust and support.